Ontario

Ontario Geological Survey
Open File Report 6159

Geology, Structure, and Gold Mineralization, Kirkland Lake and Larder Lake Areas (Gauthier and Teck Townships): Discover Abitibi Initiative

2005

105-06645/

Ontario

ONTARIO GEOLOGICAL SURVEY

Open File Report 6159

Geology, Structure, and Gold Mineralization, Kirkland Lake and Larder Lake Areas (Gauthier and Teck Townships): Discover Abitibi Initiative

by

V. Ispolatov, B. Lafrance, B. Dubé, M. Hamilton and R. Creaser

2005

Parts of this publication may be quoted if credit is given. It is recommended that reference to this publication be made in the following form:

Ispolatov, V., Lafrance, B., Dubé, B., Hamilton, M. and Creaser, R. 2005. Geology, structure, and gold mineralization, Kirkland Lake and Larder Lake areas (Gauthier and Teck townships): Discover Abitibi Initiative; Ontario Geological Survey, Open File Report 6159, 170p.

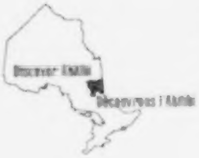

Discover Abitibi
A project of innovation, cooperation and revitalization

Découvrons l' Abitibi
Un projet d'innovation, de coopération et de renouvellement

Discover Abitibi Initiative
The Discover Abitibi Initiative is a regional, cluster economic development project based on geoscientific investigations of the western Abitibi greenstone belt. The initiative, centred on the Kirkland Lake and Timmins mining camps, will complete 19 projects developed and directed by the local stakeholders. FedNor, Northern Ontario Heritage Fund Corporation, municipalities and private sector investors have provided the funding for the initiative.

Initiative Découvrons l'Abitibi
L'initiative Découvrons l'Abitibi est un project de développment économique régional dans une grappe d'industries, projet fondé sur des études géoscientifiques de la ceinture de roches vertes de l'Abitibi occidental. Cette initiative, centrée sur les zones minières de Kirkland Lake et de Timmins, mènera à bien 19 projets élaborés et dirigés par des intervenants locaux. FedNor, la Société de gestion du Fonds du patrimoine du Nord de l'Ontario, municipalités et des investisseurs du secteur privé ont fourni les fonds de cette initiative.

FedNor
Canada

Timmins

KIRKLAND LAKE

Ontario
Northern Ontario Heritage Fund
Fonds du patrimoine du Nord de l'Ontario

© Queen's Printer for Ontario, 2005

©Queen's Printer for Ontario, 2005.

Open File Reports of the Ontario Geological Survey are available for viewing at the Mines Library in Sudbury, at the Mines and Minerals Information Centre in Toronto, and at the regional Mines and Minerals office whose district includes the area covered by the report (see below).

Copies can be purchased at Publication Sales and the office whose district includes the area covered by the report. Although a particular report may not be in stock at locations other than the Publication Sales office in Sudbury, they can generally be obtained within 3 working days. All telephone, fax, mail and e-mail orders should be directed to the Publication Sales office in Sudbury. Use of VISA or MasterCard ensures the fastest possible service. Cheques or money orders should be made payable to the *Minister of Finance*.

Mines and Minerals Information Centre (MMIC)
Macdonald Block, Room M2-17
900 Bay St.
Toronto, Ontario M7A 1C3
Tel: (416) 314-3800

Mines Library
933 Ramsey Lake Road, Level A3
Sudbury, Ontario P3E 6B5
Tel: (705) 670-5615

Publication Sales
933 Ramsey Lake Rd., Level A3
Sudbury, Ontario P3E 6B5
Tel: (705) 670-5691(local)
1-888-415-9845(toll-free)
Fax: (705) 670-5770
E-mail: pubsales@ndm.gov.on.ca

Regional Mines and Minerals Offices:

Kenora - Suite 104, 810 Robertson St., Kenora P9N 4J2

Kirkland Lake - 10 Government Rd. E., Kirkland Lake P2N 1A8

Red Lake - Box 324, Ontario Government Building, Red Lake P0V 2M0

Sault Ste. Marie - 70 Foster Dr., Ste. 200, Sault Ste. Marie P6A 6V8

Southern Ontario - P.O. Bag Service 43, 126 Old Troy Rd., Tweed K0K 3J0

Sudbury - Level B3, 933 Ramsey Lake Rd., Sudbury P3E 6B5

Thunder Bay - Suite B002, 435 James St. S., Thunder Bay P7E 6S7

Timmins - Ontario Government Complex, P.O. Bag 3060, Hwy. 101 East, South Porcupine P0N 1H0

Toronto - MMIC, Macdonald Block, Room M2-17, 900 Bay St., Toronto M7A 1C3

This report has not received a technical edit. Discrepancies may occur for which the Ontario Ministry of Northern Development and Mines does not assume any liability. Source references are included in the report and users are urged to verify critical information. Recommendations and statements of opinions expressed are those of the author or authors and are not to be construed as statements of government policy.

If you wish to reproduce any of the text, tables or illustrations in this report, please write for permission to the Team Leader, Publication Services, Ministry of Northern Development and Mines, 933 Ramsey Lake Road, Level B4, Sudbury, Ontario P3E 6B5.

Cette publication est disponible en anglais seulement.

Parts of this report may be quoted if credit is given. It is recommended that reference be made in the following form:

Ispolatov, V., Lafrance, B., Dubé, B., Hamilton, M. and Creaser, R. 2005. Geology, structure, and gold mineralization, Kirkland Lake and Larder Lake areas (Gauthier and Teck townships): Discover Abitibi Initiative; Ontario Geological Survey, Open File Report 6159, 170p.

Contents

Abstract xvii

Introduction 1

Regional Geologic Setting of the Kirkland Lake–Larder Lake Area 1
  General Geology 1
  Previous Studies of Regional Structural Geology 3
  Definition of the Larder Lake–Cadillac Deformation Zone 3

Gauthier Township Transect 6
  General Geology and Rock Types 6
  Deformation Zones 11
  Deformational Fabrics 11
  Kinematic Indicators in the Larder Lake–Cadillac Deformation Zone 21
  Gold Mineralization 22
    Upper Canada Mine 22
      Rock Types 24
      Hydrothermal Alteration 26
      Structural Geology 26
      Gold Mineralization 34
      Relative Timing of Deformation, Hydrothermal Alteration and Gold Mineralization 38
      Kinematics of the Upper Canada Deformation Zone 39
      Factors Controlling Localization of Mineralization Within the Upper Canada Deformation Zone 40
    Gold Mineralization Along the Larder Lake–Cadillac Deformation Zone 40
      Anoki Property 40
        Anoki Main Zone 42
        Anoki South Zone 46
        Anoki Deep Zone 46
        40 East Zone 47
      McBean 47
      Gold Mineralization Associated with the Larder Lake–Cadillac Deformation Zone in McVittie and McGarry Townships 49
      Characteristics of Gold Mineralization Hosted by the Larder Lake–Cadillac Deformation Zone 51
    Relationships of Gold Mineralization in the Larder Lake–Cadillac and Upper Canada Deformation Zones and Structural Timing of Mineralization 52
    Summary of Factors Controlling the Distribution of Gold Mineralization 53

Teck Township Transect 53
  General Geology 53
  Intrusive Rocks 55
  Deformational Fabrics 61
  Deformation Zones 65
    Larder Lake–Cadillac Deformation Zone 65
    Possible Shear Zone South of the Timiskaming Unconformity 65

Gold Mineralization 66
  Ore-Controlling Faults: Kirkland Lake Fault (Main Break) and '04 Break 66
    Definition of the Kirkland Lake Fault 66
    Camp-Scale Geometry 66
    Surface and Underground Exposures 67
  Plunge of Gold Mineralization 71
  Gold-Bearing Quartz Veins 79
    Geometry and Internal Features 79
    Metallic Minerals 88
    Vein-Filling Types 89
  Post-Ore Veining 90
  Wall Rock Alteration 92
  Sense of Movement Along the Kirkland Lake Fault and '04 Break 93
  Narrows Break Mineralization 93
  D Zone 95
  Intramineral Dikes 95
  Relative Timing of Deformation and Mineralization 106
  Amikougami Creek Fault 107
  U-Pb and Re-Os Geochronology 108
  Geochemistry of Kirkland Lake Gold-Bearing Veins 112
  Origin of Kirkland Lake Gold Mineralization 116

Summary 118
  Deformation History 118
  Gold Mineralization 118

Acknowledgements 119

References 120

Appendix A: Geochemical data 127

Metric Conversion Table 170

FIGURES

1. Regional geology showing positions of map areas 2
2. Generalized geological map of the Gauthier Township transect area 8
3. Total field aerial magnetic map of the Gauthier Township transect area 9
4. AFM and Jensen cation plots of mafic and ultramafic volcanic rocks of the Larder Lake Group 10
5. Relationships between bedding reversals and S2 in Timiskaming turbidites 13
6. Stereonet plots of S2 and L2 14
7. S2 data points from areas 1, 2, and 3 15
8. Stereonet plot of bedding in Timiskaming turbidites 17
9. Stereonet plots of S3, S4, and S5 18
10. Longitudinal section of the Upper Canada Mine 23
11. Location of stripped outcrops west of former Upper Canada shaft #2 25

12. Geological plan of the L stripped outcrop (Upper Canada Mine) .... back pocket
13. Steronet plots of S2, S4, and fold axes from the L stripped outcrop 27
14. Fragment of the L-W stripped outcrop: relationships of S2, S3, and S4 29
15. Stereonet plot of S2, S3, and S4 on the L-W stripped outcrop 29
16. Fragment of the L-NW stripped outcrop: relationships of S2, S3, and S4 30
17. Stereonet plot of S2, S3, and S4 on the L-NW stripped outcrop 30
18. Deep structure of the south flank of the Larder Lake–Cadillac deformation zone in the Anoki area 41
19. Contour lines of the lower contact of Larder Lake basalts corresponding to the "South Splay" 42
20. Anoki Main zone longitudinal section 43
21. Fe/Mg (wt%) ratios of mineralized rocks of the Anoki Main zone, Kerr Addison flow ore and replacement mineralization at the Holloway Mine 46
22. McBean open pit area: contour lines of the south contact of Timiskaming conglomerates (footwall of the McBean mineralized zones) and approximate outlines of the green carbonate mineralized zone 48
23. Schematic depicting location of gold deposits and major occurrences along the Larder Lake–Cadillac deformation zone 49
24. Relationships of the mafic syenite intrusion and stratigraphic units in the central part of the Kirkland Lake camp 60
25. Deformational fabrics of Teck Township transect 61
26. Subsurface position of the Main Break and '04 Break in proximity of Macassa shafts #1 and #2 68
27. Possible fault location south of the Main Break 69
28. Orientation of striations on chloritic slip surfaces of the Main Break, and '04 Break. 70
29. Schematic showing location of the "Mud Break" 73
30. Schematic longitudinal section of the Kirkland Lake camp 76
31. Diagram explaining elements shown in Figure 32 77
32. Stereonets comparing ore plunge to other structural elements 78
33. Location of the Narrows Break stripping and mineralized zone 94
34. Stereonet plots for the Narrows Break stripped outcrop 96
35. Total alkali vs. silica plots of intrusive rocks of the Kirkland Lake camp 101
36. Zr vs. Zr/Y and Zr vs. TiO$_2$ plots for intrusive rocks of the Kirkland Lake camp 102
37. P$_2$O$_5$ vs. V and Zr/TiO$_2$ vs. P$_2$O$_5$ plots for intrusive rocks of the Kirkland Lake camp 103
38. Primitive-mantle-normalized trace element plots for intrusive rocks of the Kirkland Lake camp 104
39. Geological plan of outcrop 004VOI1518 (568572E 5333147N) 105
40. Concordia plot for the U-Pb TIMS (zircon) analysis of the syenite porphyry sample 109
41. Results of in-situ (SHRIMP) analyses of the syenite porphyry sample: concordia plot and distribution of in-situ ages 110
42. Au vs. Te plot for veins of the Kirkland Lake deposit and Narrows Break mineralized zone. Data for samples from this study and previously published data on bulk ore samples and gold-rich grab samples (Kirkland Lake Gold, Teck-Hughes and Lake Shore mines) 113

43. Ternary plot of molecular proportions of combined Au and Ag, Te, and Pb and probable mode of occurrence of gold ... 114

44. Au-Ag-Te ternary plot (wt%) for samples of Kirkland Lake gold veins, Narrows Break mineralization, and mineralized zones of the Gauthier Township transect ... 115

45. Au-As-Te ternary plot (wt%) for samples of Kirkland Lake gold veins, Narrows Break mineralization, and mineralized zones of the Gauthier Township transect ... 115

46. Te-Mo-As ternary plot (wt%) for samples of Kirkland Lake gold veins, Narrows Break mineralization, and mineralized zones of Gauthier Township transect ... 116

PHOTOS

1. Foliation (S2) defined by compositional banding, and stretching lineation (L2) in highly strained Timiskaming conglomerates ... 16

2. F2 fold in Timiskaming turbidites ... 16

3. Stretching lineation (L2) in volcaniclastic breccias east of Dobie townsite ... 17

4. S3 crenulation cleavage overprinting S2, Upper Canada L-W stripping ... 19

5. Crenulation cleavage S4 (northeast-southwest) overprinting S2 in altered felsic dike ... 19

6. Discrete crenulation cleavage S4 in Timiskaming turbidites ... 20

7. Photomicrograph of S4 in Timiskaming siltstone-argillite ... 20

8. Asymmetric pressure shadows on pebbles in highly strained Timiskaming conglomerates ... 21

9. S2 in gold-bearing quartz-sericite-carbonate schists ... 28

10. S3 axial planar to open folds of S2. Upper Canada Mine, L-W stripping ... 28

11. S3 oriented clockwise to S2. Upper Canada Mine, L-NW stripping ... 31

12. Closer view of S3 defined chlorite-rich cleavage bands separating quartz-carbonate-rich microlithons. Upper Canada Mine L-NW stripping ... 31

13. S4 overprinting S3 on the L stripping ... 32

14. Close-up view of the area shown on Photo 13 ... 33

15. S4 axial planar to open folds of S3. Upper Canada Mine, L stripping ... 33

16. Close-up view of L mineralized zone in quartz-sericite-carbonate-altered tuffs ... 35

17. Cut samples from the Upper Canada L mineralized zone (gold-bearing quartz-sericite-carbonate schist near sampling line 11) ... 36

18. Photomicrograph of folded carbonate-rich gold-bearing veinlet transected by S4 cleavage plane ... 37

19. Reflected light photomicrograph of the rectangular area from Photo 18 ... 37

20. Reflected light photomicrograph: intergrowth of native gold with tennantite, and chalcopyrite (Upper Canada Mine, L stripping) ... 38

21. Strongly altered (albite, carbonate, pyrite, quartz) gold-bearing rock, western flanks of the Anoki Main zone ... 44

22. Drill core from western flanks of the Anoki Main zone. Sulphidation halo around a thin quartz stringer . 44

23. Backscattered electron image: veinlet-like segregation of gold in pyrite (Anoki Main zone) ... 45

24. Photomicrograph (reflected light) of the Anoki Main zone mineralization: irregular segregations of chalcopyrite in fractured pyrite 45

25. Drill core from the footwall of the McBean "green carbonate" mineralized zone (hole MB97-19) 48

26. Outcrop of mafic syenite on the Narrows Break stripped outcrop. Magmatic foliation defined by thin feldspathic bands ("felsic ribs") and oriented approximately parallel to the contact of the intrusion 56

27. North wall of stope 4225, Macassa Mine: large leucocratic band ("felsic rib") in mafic syenite. Quartz veins have similar orientation indicating that vein-hosting structures may have been exploiting primary anisotropy of intrusive rocks 57

28. Feldspar-rich syenite porphyry with a chloritic xenolith 58

29. Sparsely porphyritic variety of syenite porphyry 58

30. Pebble-like leucocratic granitoid xenolith in sparsely porphyritic syenite porphyry 59

31. S2 defined by flattened pebbles in Timiskaming conglomerates. Southeastern part of the Teck Township transect area. 62

32. F3 fold with north-south-trending axial plane in carbonate-altered metaultramafic rocks. Southeast of the Teck Township transect area 62

33. Disjunctive cleavage S4 in Timiskaming tuffs. Narrows Break stripped outcrop, roughly 350 m north of the Main Break 63

34. F4 folding in tuffs, Narrows Break stripped outcrop 64

35. S4 defined by pebble flattening in Timiskaming conglomerates 64

36. Main slip plane of the Kirkland Lake fault (Main Break) in the back of the drift, 4500-foot level, Macassa Mine 69

37. Surface exposure of the Main Break east of former Lake Shore shaft 5 72

38. Surface exposure of the "Mud Break" 74

39. Underground exposure of the '04 Break in stope 4528 MCF, Macassa Mine 75

40. Gold-bearing quartz veins associated with the '04 Break; back of stope 4940, Macassa Mine 80

41. Foliation north of a gold-bearing vein hosted by the Main Break (Discovery outcrop) 80

42. Cataclastic band along the margin of the gold-bearing vein (Discovery outcrop) 81

43. Typical textural appearance of a steeply dipping vein associated with the '04 Break (stope 4940, Macassa Mine) 82

44. Close-up view of a stylolite in a break-associated vein ('04 Break, stope 4940, Macassa Mine) 82

45. Cataclasized quartz from Teck-Hughes #1 vein 83

46. Vein 4206-S3 (Macassa Mine) 84

47. Bedding-parallel vein in tuffs (stope 5030, Macassa Mine) 85

48. Close-up view of vein 4206-S3, polished slab from the same part of the vein, and a close-up view illustrating characteristic relationships of white and dark quartz in the same part of the vein 86

49. Fracturing and late vein filling in vein 4206-S3 87

50. Remote view of the Teck-Hughes "E" vein in the proximal hanging wall of the Main Break 88

51. Photomicrographs illustrating vein-filling types in gold-bearing quartz veins 91

52. Narrows Break mineralized zone: sheeted carbonate-quartz veinlets in carbonatized and sulphidized Timiskaming sandstones 97

53. Reflected light photomicrograph of a mineralized veinlet from Narrows Break mineralized zone 97
54. Dike and gold-bearing quartz veins in stope 4529, Macassa Mine 98
55. Dike on the back of stope 4528, Macassa Mine 98
56. Cut sample of the dike-vein contact from stope 4528 (Macassa Mine) 99
57. Surface exposure of an intramineral dike, a close-up view (Macassa property, trench on the north-south powerline, south of the Goldthorpe road) 101
58. Fragment of outcrop 004VOI1518 106

TABLES

1. Overview of structural geological studies of the Kirkland Lake–Larder Lake gold area 4
2. Summary of the Re-Os analytical data 111
A.1. Analytical results for samples from first field season (2003), Gauthier Township: major and trace element geochemistry 128
A.2. Analytical results for samples from second field season (2004), Gauthier and Teck townships: major and trace element geochemistry 141
A.3. Analytical results for samples from mineralized zones other than Upper Canada Mine: trace elements.... 150
A.4. Analytical results for mineralized samples from Upper Canada Mine: trace elements 163
A.5. Analytical results for selected samples from mineralized zones other than Upper Canada Mine: major and selected trace elements 166
A.6. Brief descriptions of geochemical samples from mineralized zones 167

MAPS

Map P.3546–Revised – Precambrian geology of Gauthier Township transect .... back pocket
Map P.3558 – Precambrian geology of Teck Township transect .... back pocket

Abstract

The two-year research project funded under the Discover Abitibi Initiative involved 1:10 000 geologic mapping of regional gold-hosting structures and detailed studies of gold occurrences in Gauthier and Teck townships (Kirkland Lake–Larder Lake area, Abitibi greenstone belt, Ontario). The project focused on gold occurrences along the regional, roughly east-trending Larder Lake–Cadillac deformation zone, the northeast-trending Upper Canada deformation zone, and the brittle to brittle-ductile Kirkland Lake fault (Main Break), which hosts the giant Kirkland Lake gold deposit. Three generations of fabrics formed during post-Timiskaming regional deformation events (D2, D3, and D4). A steeply dipping, east-striking S2 foliation and an east-plunging stretching L2 lineation formed during reverse-dextral slip along the Larder Lake–Cadillac deformation zone. D2 fabrics are overprinted by a north-trending S3 crenulation cleavage which formed during east-west shortening across the deformation zones. A northeast-trending steeply dipping regional S4 foliation axial planar to outcrop-scale Z-shaped F4 folds formed during northwest-southeast compression. Gold mineralization at the Upper Canada Mine along the Upper Canada deformation zone and at several occurrences along the Larder Lake–Cadillac deformation zone (e.g. Anoki and McBean properties) was emplaced during D2 and overprinted by D3 and D4. Kirkland Lake gold mineralization has a distinct metal signature (Te>Au, Mo, Pb, Ag, high Au/Ag, low As) and is probably unrelated to mineralization along the Larder Lake–Cadillac deformation zone and its splays. The gold-bearing veins of the Kirkland Lake deposit could have formed during D4, synchronously with reverse-dextral movement along the Main Break, as hydrothermal fluids associated with deep alkaline magmatism migrated to shallow crustal levels. Gold mineralization of the Narrows Break zone located approximately 350 m north of the Main Break differs in style, alteration, and geochemistry from typical Kirkland Lake gold-bearing veins and probably represents a separate hydrothermal system. Relationships between S4 and sheeted veinlets of the Narrows Break mineralized zone indicate syn-D4 timing of mineralization.

Geology, Structure, and Gold Mineralization, Kirkland Lake and Larder Lake Areas (Gauthier and Teck Townships): Discover Abitibi Initiative

V. Ispolatov[1], B. Lafrance[2], B. Dubé[3], M. Hamilton[4] and R. Creaser[5]
Ontario Geological Survey
Open File Report 6159
2005

---

[1]Mineral Exploration Research Centre, Department of Earth Sciences, Laurentian University, Willet Green Miller Centre, 933 Ramsey Lake Rd., Sudbury, Ontario, P3E 6B5, Canada
vispolatov@laurentian.ca

[2]Department of Earth Sciences, Laurentian University, Sudbury, Ontario, P3E 2C6, Canada
blafrance@laurentian.ca

[3]Geological Survey of Canada Quebec, 490 rue de la Couronne, Québec, QC, G1K 9A9, Canada
bdube@nrcan.gc.ca

[4]Jack Satterly Geochronology Laboratory, University of Toronto, Toronto, Ontario, M5S 3B1, Canada
mahamilton@geology.utoronto.ca

[5]Department of Earth & Atmospheric Sciences, 1-26 Earth Sciences Building, University of Alberta, Edmonton, Alberta, T6G 2E3, Canada
Robert.Creaser@ualberta.ca

Introduction

This report summarizes results of a two-year (2003-2005) research project that was funded under the Discover Abitibi Initiative and aimed to improve understanding of geologic and structural controls of gold mineralization of the Kirkland Lake–Larder Lake gold belt (Thomson 1950). This is a roughly 3-5 km wide, approximately east-west-trending corridor extending from the village of Swastika (west of the town of Kirkland Lake) to Virginiatown (near the Ontario–Quebec border) and including parts of Otto, Teck, Lebel, Gauthier, McVittie and McGarry townships. Geologic mapping constituted the core of this project and concentrated in two areas: 26 km^2 Gauthier Township (2003) transect and 36 km^2 Teck Township transect (2004). Preliminary 1:10 000 scale geological maps P.3546–Revised (Gauthier Township transect) and P.3558 (Teck Township transect) accompany this report. Outside the transect areas, selected key outcrops were examined, and available data on structural geology and gold mineralization were reviewed.

The entire Kirkland Lake–Larder Lake gold belt is covered by high-quality 1:12 000 scale geologic maps produced in the 1930s-1940s (Thomson 1941; Thomson and Griffis 1941; Thomson 1945; MacLean 1944). A number of thematic studies that focused on various aspects of the regional geology and addressed geologic setting of gold mineralization were completed in the 1980s and 1990s. Recent geophysical surveys (e.g., OGS 2002) provided new opportunities for tracing key geologic contacts under overburden and refining regional structure. Continuing exploration for gold has generated valuable geological information, especially on the internal architecture of regional ore-controlling structures. In this report, we integrate new observations and re-evaluated existing geological data, and take into account the results of the most recent geophysical surveys and exploration programs.

The organization of this report is pre-defined by the structure of the project: two major divisions are dedicated to geology of the two transect areas. The final section summarizes main findings of the study. All structural measurements are reported in accordance with the North American right-hand-rule standard. Stereonet plots are based on the equal-area lower hemisphere projections. All location sites are given in UTM zone 17, NAD 83 coordinates.

Regional Geologic Setting of the Kirkland Lake–Larder Lake Area

GENERAL GEOLOGY

The area is part of the southern Abitibi greenstone belt of the Superior Province. The geology and tectonic evolution of the Abitibi belt are discussed in detail in Jackson and Fyon (1991) and Card (1990); only key features of the regional geological framework of the Kirkland Lake–Larder Lake area are briefly summarized here. Supracrustal rocks include submarine komatiitic, tholeiitic and calc-alkaline volcanic sequences of the Blake River (2701-2697 Ma), Kinojevis (2702-2701 Ma) and Tisdale (2710-2703 Ma) assemblages (Figure 1; Ayer et al. 2002). These form a broad east-west-trending synclinorium, the north and south limbs of which are transected by the Destor–Porcupine (north) and Larder Lake (south) regional deformation zones. Belts of clastic sedimentary and alkalic to shoshonitic rocks of the Timiskaming assemblage (2687-2675 Ma) unconformably overlie older sequences along the deformation zones. Felsic and alkalic plutons and dikes (2695-2673 Ma, Ayer et al. 2002) intrude stratified units. The rocks are metamorphosed to prehnite-pumpellyite to greenschist grade; upper greenschist and amphibolite facies rocks are found in contact aureoles of granitoid plutons (Jolly 1978). The Kirkland Lake–Larder Lake gold belt broadly corresponds to the east-west-trending, 3-5 km wide belt of Timiskaming rocks bounded in the south by the Larder Lake–Cadillac deformation zone (Thomson 1950). The belt hosts the Kirkland Lake and Kerr Addison-Chesterville world-class gold deposits and several smaller gold deposits and occurrences. Gold mineralization is spatially associated with the Larder Lake–Cadillac deformation zone (e.g., Kerr Addison-Chesterville, Cheminis, Omega, McBean mines), and with smaller faults and shear zones proximal to the Larder Lake–Cadillac deformation zone (e.g., Kirkland Lake and Upper Canada mines). The largest gold deposit of the area, Kirkland Lake, is associated with the brittle to brittle-ductile Kirkland Lake fault ("Main Break", Todd 1928) roughly 2 km north of the Larder Lake–Cadillac deformation zone. In Québec, world-class Sigma-Lamaque, Malartic, Doyon and Bousquet gold systems and a number of smaller gold deposits occur along the Larder Lake–Cadillac deformation zone (Poulsen et al. 2000; Robert 1989); the largest lode gold deposits are associated with second- and third-order shear zones (Robert 1990).

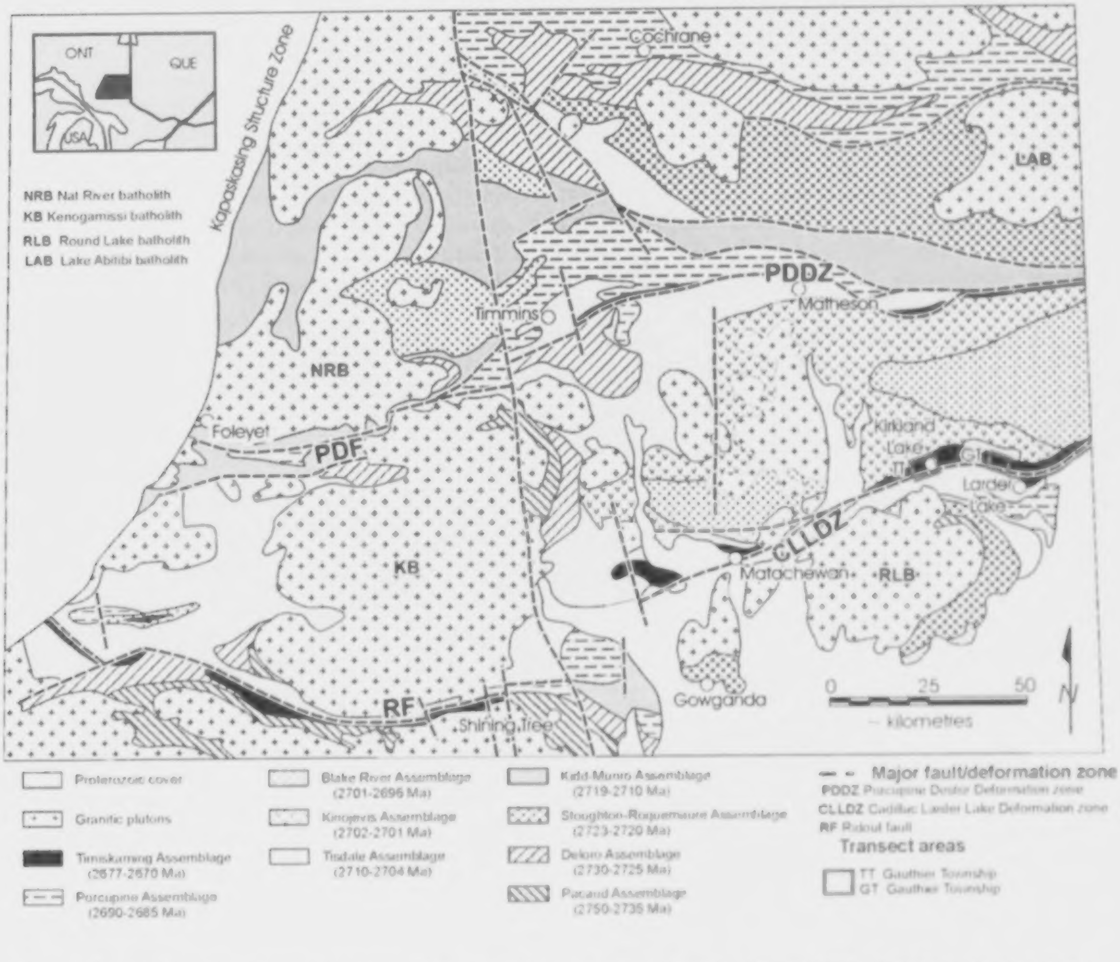
ONT
QUE
USA
Kapuskasing Structure Zone
NRB Nat River batholith
KB Kenogamissi batholith
RLB Round Lake batholith
LAB Lake Abitibi batholith
Cochrane
LAB
PDDZ
Matheson
Timmins
NRB
Foleyet
PDF
Kirkland Lake
TT
GT
Larder Lake
CLLDZ
Matachewan
RLB
KB
Gowganda
RF
Shining Tree
0
25
50
kilometres
N
Proterozoic cover
Granitic plutons
Timiskaming Assemblage (2677-2670 Ma)
Porcupine Assemblage (2690-2685 Ma)
Blake River Assemblage (2701-2696 Ma)
Kinojevis Assemblage (2702-2701 Ma)
Tisdale Assemblage (2710-2704 Ma)
Kidd-Munro Assemblage (2719-2710 Ma)
Stoughton-Roquemaure Assemblage (2723-2720 Ma)
Deloro Assemblage (2730-2725 Ma)
Pacaud Assemblage (2750-2735 Ma)
Major fault/deformation zone
PDDZ Porcupine Destor Deformation zone
CLLDZ Cadillac Larder Lake Deformation zone
RF Ridout fault
Transect areas
TT Gauthier Township
GT Gauthier Township

Figure 1. Regional geology showing positions of map areas (GT - Gauthier Township transect, TT - Teck Township transect; geology modified from Ayer et al. 2002).

PREVIOUS STUDIES OF REGIONAL STRUCTURAL GEOLOGY

Several authors have studied the regional structural geology of the Larder Lake–Kirkland Lake area and addressed the evolution of the Larder Lake–Cadillac deformation zone and its significance for gold mineralization (Hamilton and Hodgson 1984; Toogood and Hodgson 1985, 1986; Toogood 1986a,b; Robert 1989; Hodgson and Hamilton 1989; Hodgson et al. 1991; Smith et al. 1993; Wilkinson 1993; Wilkinson et al. 1999). The major findings and interpretations of these studies are summarized in Table 1. Original nomenclature for deformation events and corresponding fabrics is unchanged; the name Larder Lake–Cadillac deformation zone (LLDZ) is chosen of all the names suggested for this regional structure. All authors identified two major deformational fabrics in Timiskaming assemblage rocks, one of which is linked to the main stage of evolution of the Larder Lake–Cadillac deformation zone. Interpreted shear senses along the Larder Lake–Cadillac deformation zone differ significantly from author to author.

DEFINITION OF THE LARDER LAKE–CADILLAC DEFORMATION ZONE

There is a confusing interchangeable use of names for the regional ore-controlling structure. It is alternatively called the Larder Lake Break (also Kirkland Lake–Larder Lake Break, Kirkland Lake–Larder Lake–Cadillac Break, Cadillac–Larder Lake fault, etc.) or Larder Lake–Cadillac deformation zone (also Cadillac–Larder Lake shear zone, Kirkland Lake–Larder Lake deformation zone, etc.). Originally, the term "Larder Lake Break" (e.g., Thomson 1941; Thomson and Griffis 1941) was applied to a discrete (up to 100-500 feet wide) band of strong shearing and carbonatization at the contact between Timiskaming sedimentary rocks and older mafic volcanics. Weakly carbonatized segments of the Break were documented to contain talc-chlorite schists (Thomson 1941). Most economic gold deposits of the Larder Lake area are spatially associated with the Larder Lake Break (Thomson 1941; Thomson and Griffis 1941).

Hamilton and Hodgson (1984), Hamilton (1986), Toogood and Hodgson (1985) and Toogood (1986b) recognized that deformational fabrics related to this tectonic zone extend over a much wider area (e.g., 2-3 km, Toogood and Hodgson 1985). Hamilton and Hodgson (1984) used the term "Kirkland Lake–Larder Lake deformation zone" to define this wider corridor of variably deformed rocks enveloping the more narrow "Kirkland Lake–Larder Lake Break". Similarly, Robert (1989) defined a 200-750 m wide Cadillac tectonic zone that includes a discrete, up to 50 m wide, Cadillac Break. More recently, Wilkinson et al. (1999) defined the Larder Lake–Cadillac deformation zone as a 10-50 m wide high-strain zone separating the Timiskaming and Hearst assemblages from the older Larder Lake and Boston assemblages, thereby interchanging the original term "Break" with the term "deformation zone".

We recognize that the terms "Break" and "deformation zone" have different meanings and should not be used interchangeably. We use the term "Larder Lake Break" in the original meaning of Thomson (1941) and Thomson and Griffis (1941). Larder Lake Break is a single or branching 10 m to approximately 150 m wide high-strain zone traced from the Kerr Addison-Chesterville deposit (McGarry Township) to the Anoki property (Gauthier Township). It generally corresponds to the contact of Timiskaming and Tisdale assemblages, although local settings of the structure vary. Commonly the Break is marked by bands and lenses (faulted slivers?, Hodgson et al. 1991) of variably carbonatized and locally silicified ultramafic talc-chlorite schists. The Larder Lake–Cadillac deformation zone is a wider structure that is defined by intensity of deformation and development of pervasive fabrics. In the two areas mapped in this project, the Larder Lake–Cadillac deformation zone is 200 to 500 m wide; it commonly encompasses several lithotectonic units and does not have sharp geologic boundaries. The Larder Lake Break (in the original meaning of Thomson 1941) is a major discontinuity within the Larder Lake–Cadillac deformation zone.

Table 1. Overview of structural geological studies of the Kirkland Lake–Larder Lake gold area.

Author	**First generation fabrics/structures**	**Second generation fabrics/structures**	**Regional stress field, LLDZ sense of movement**	**Relative timing of gold mineralization**
Hamilton and Hodgson (1984)	S1: W-NW trending cleavage axial planar to W-NW trending folds (e.g., Spectacle Lake anticline)	S2: NE (040-060)- trending steeply dipping crenulation cleavage.	D1: N-NE (later N-S) compression, oblique sinistral movement on LLDZ D2: NW-SE compression, dextral movement on LLDZ	Late in deformation history
Toogood and Hodgson (1985)	S1: foliation mirrors strike of LLDZ, typical orientation 070-090. Axial planar to steeply plunging isoclinal folds. Stretching lineation (L1) plunging: NE-E, and S-SE, north and south of LLDZ, respectively.	S2: constant 040-070 strike, subvertical dip	LLDZ: early sinistral strike-slip (D1), later transpression with dextral strike-slip	Late in strain history
Toogood and Hodgson (1986)	C-S foliations within the LLDZ	Subvertical NE-trending foliation: result of progressive expansion of LLDZ	Dextral strike-slip movement in LLDZ, expansion in width with progressive displacement	
Toogood (1986a)	C-S foliation within the LLDZ	Subvertical NE-trending foliation overprints C-S fabrics in LLDZ	Dextral strike-slip movement on LLDZ	
Toogood (1989)	Early E-NE to SE trending fabric parallel to LLDZ, common S-C fabrics	Steep NE-trending foliation axial planar to M and Z-folds. Gradual change into subparallel orientation with the earlier fabric in LLDZ. Related to dextral strike-slip movement in a laterally expanding shear zone.	Dextral strike-slip movement, progressive lateral expansion of LLDZ	Upper Canada gold deposit within the Upper Canada deformation zone: 3 penetrative fabrics; the earliest correlates to the early regional fabric. Gold mineralization postdated the earliest fabric, and was modified (structurally and hydrothermally) during the latest deformation phase.
Hodgson and Hamilton (1989)	Pre-Timiskaming D0: folds with no foliation. Post-Timiskaming D1: foliation axial planar to WNW-ESE trending folds, parallel to LLDZ and rotated to LLDZ	D2: typically Z-asymmetric folds, axial planar foliation overprinting D1 fabrics. D2 foliation rotates into parallelism with D1 fabric near LLDZ	D1: NNE-SSW compression, oblique thrusting (N over S), no major strike-slip D2: NW-SE compression, S over N backthrusting	Gold mineralization related to final stages of D2

Author	**First generation fabrics/structures**	**Second generation fabrics/structures**	**Regional stress field, LLDZ sense of movement**	**Relative timing of gold mineralization**
Robert (1989) (Cadillac Tectonic zone, Val d'Or area, Québec)	S1 striking 070-090, oblique to EW-striking Cadillac Tectonic Zone	S2: NE-SW to E-W -trending spaced crenulation cleavage axial planar to Z-asymmetric folds	EW-striking segment of the Cadillac Tectonic Zone: zone of dextral transpression. D1: N-S shortening, subvertical stretching, local dip-slip movements, synchronous dextral shearing. D2: dominantly transcurrent dextral shear, some shortening.	
Hodgson et al. (1991)	S1: E-W to WNW-ESE striking foliation axial planar to upright, tight to isoclinal folds. Parallels the orientation of LLDZ, variably overprinted by S2	S2: E-W to ENE-WSW trending, steeply dipping foliation. Gauthier Township: in about 100 m north of LLDZ bends into parallelism to LLDZ.	LLDZ in Gauthier Township: pre-D1 normal fault (?) D1: thrust fault; D2: oblique reverse-dextral movement (S side up).	Gold mineralization is closely associated with D2 structures (e.g., Kirkland Lake Main Break is a D2 structure).
Smith et al. (1993)	Similar to Hamilton and Hodgson (1984)	Similar to Hamilton and Hodgson (1984)	Sense of movement varies along the LLDZ depending on an orientation of a given segment relative to principal compression direction (D1: N-S to NNE-SSW; D2 : NNW-SSE to NW-SE).	Gold mineralization at Kerr Addison Mine is synchronous to late phases of ductile deformation in LLDZ (i.e., syn-D2).
Wilkinson et al. (1999)	S2 parallels the LLDZ: strike varies from 090 (east-west striking segments) to 085 (northeast-striking segments), and 110 (southeast-striking segments)	S3: subvertical pervasive NE-striking (055-070) crenulation cleavage axial planar to symmetric to Z-asymmetric folds. Locally deflected into parallelism with S2.	D2: N-S shortening: E-W - trending segments of LLDZ accumulate bulk coaxial strain. NE and SE-trending segments experience sinistral and dextral transpression, respectively. Some reverse (S over N) component. D3: NW-SE shortening, dextral reactivation of SE and EW-oriented segments of LLDZ.	

Gauthier Township Transect

GENERAL GEOLOGY AND ROCK TYPES

The Gauthier Township transect (Figures 2 and 3, Map P.3546–Revised, back pocket) is located west of the town of Larder Lake and north of Highway 66. The area comprises Archean mafic and ultramafic volcanic rocks of the Larder Lake Group of the Tisdale assemblage (Jackson 1995; Ayer et al. 2002), alkalic volcanic rocks and clastic sedimentary rocks of the Timiskaming assemblage, and intermediate to felsic volcanic rocks of the Gauthier Group (Tisdale assemblage; Ayer et al. 2002). Volcanic rocks of the Larder Lake Group are exposed in the southern part of the map area along Highway 66; they also form a 250 m wide band between the McBean open pit and Dobie townsite. Along Highway 66, the Larder Lake Group consists of variolitic massive and pillowed basalts with subordinate ultramafic talc-chlorite and (chlorite)-carbonate-fuchsite schists. This predominantly basaltic sequence contains 0.1 to 15 m thick beds of siliceous, locally graphitic, interflow exhalites. Volcanic rocks host gabbroic intrusions composed of plagioclase and coarse-grained (3 mm to 1-2 cm in length) prismatic amphibole possibly replacing primary pyroxene. The band of Larder Lake volcanic rocks north of the McBean pit probably represents a fault-bounded slice. It consists predominantly of pervasively foliated chlorite-rich rocks with no recognizable primary flow textures, and contains discontinuous lenses of ultramafic carbonate-fuchsite schists. Geochemically, foliated chloritic rocks are similar to pillow basalts from the Anoki area (immediately south of the Larder Lake Break) and most likely represent strained basaltic lavas or tuffs. Both pillowed basalts and chlorite schists plot in the tholeiite field of the AFM diagram and, apart from altered rocks of the gold-bearing Anoki zone, in the high-Fe-tholeiitic basalt field of the Jensen cation plot (Figure 4). High MgO (20-25%), Cr (about 1900-2800 ppm) and Ni (about 800-1300 ppm) contents of talc-chlorite and carbonate-fuchsite schists indicate a komatiitic protolith. Felsic to intermediate tuffs and tuff breccias of the Gauthier Group (Tisdale assemblage of Ayer et al. 2002) underlie the northern part of the map area. A 2700±3 Ma U-Pb age of the Gauthier Group was previously reported by Corfu (1993).

Most of the map area consists of Timiskaming volcanic and sedimentary rocks. The sedimentary rocks include two major units. The first unit (unit 1, Figure 2) is located immediately to the north of the Larder Lake Group in the McBean open pit area. It consists of largely non-graded sandstones, highly strained polymictic conglomerates, and minor interbeds and lenses of chlorite schists. In most surface outcrops in the southeast of the map area, the rocks are carbonate-altered and oxidized. The least altered and unweathered sections are from Queenston Mining Inc. drill core from the area west of the McBean pit. There, the unit consists largely of greenish-grey to green sandstones with chlorite-rich matrix. Strained conglomerates constitute 20 to 60 volume % of the unit. Most pebbles are carbonatized and stretched into ribbons and bands; only clasts of leucocratic granitoids, minor porphyries, chert, jasper and quartz, which are both resistant to carbonatization and rheologically competent, survived the intense deformation.

The second sedimentary unit (unit 2, Figure 2) underlies the east-northeastern portion of the map area. It consists of graded grey to greenish-brownish-grey turbiditic sandstone, siltstone and subordinate argillite interlayered with few 10-60 m wide conglomerate horizons. In general, these conglomerates have a higher clast-to-matrix ratio compared to conglomerates in unit 1, perhaps due to lower strain. Feldsparphyric igneous rocks constitute the most abundant clast type in the conglomerates. A U-Pb detrital zircon sample of turbiditic sandstone analyzed in this study returned a maximum age of 2677.7 ± 3.1 Ma (Ayer et al. 2005). This date indicates that turbidites previously thought to predate Timiskaming sedimentation (e.g., Corfu et al. 1991; Jackson 1995; Mueller et al. 1994) belong to the Timiskaming assemblage. In addition to the two major clastic units, smaller units of volcaniclastic sandstones and polymictic conglomerates are associated with Timiskaming volcanic rocks in the western and northern parts of the map area.

Alkalic volcanic rocks of the Timiskaming assemblage occupy the central and east-northeast parts of the map area. North of the Upper Canada Mine, volcanic rocks are represented mainly by massive plagioclase-amphibole-phyric lavas and breccias. The latter consist of angular to subrounded fragments (1-2 cm to 20-30 cm) of brown, reddish-brown and green feldspar-phyric rocks enclosed in a dark green chloritized matrix. Transitions from breccias to massive and flow-banded feldspar-phyric lavas are observed at several localities. Strongly deformed and hydrothermally altered aphanitic tuff and tuff breccia are exposed in stripped outcrops west of the Upper Canada shaft #2. Between the Upper Canada Mine and Dobie townsite, the volcanic rocks consist of intermingled lavas, tuffs and breccias, including pseudoleucite- and pyroxene-bearing varieties. A sample of massive feldspar-phenocryst-rich lava collected approximately 600 m southeast of the former Upper Canada shaft #1, returned a U-Pb zircon age of 2669.6 ±1.4 Ma (Ayer et al. 2005).

West-northwest of the McBean open pit, the southern contact of the volcanic rocks with Timiskaming clastic rocks was intersected by drill holes and traced for roughly 1000 m along strike by Queenston Mining Inc. At the contact, the volcanic rocks are represented by foliated brown to brownish dark grey, largely aphyric lavas (?), which locally contain thin prismatic to acicular amphibole or, less commonly, feldspar laths that are 1-3 mm long. East of Dobie, a separate unit of volcaniclastic breccia, up to 300 m wide, is bounded by Timiskaming sedimentary rocks on the north, south and east. The breccia consists of rounded and angular clasts of pink and reddish-brown, green and white aphanitic and feldspar-phyric volcanics surrounded by a green to greenish-grey matrix. Drilling by Queenston Mining Inc. west of the McBean open pit intersected narrow horizons of tuffs (?) enclosed in conglomerates and sandstones. In addition to being lithologically distinct, these tuffs are notably more magnetic than the sedimentary rocks. Patterns on aerial magnetic maps show that these horizons may constitute the westward continuation of the Timiskaming volcaniclastic unit exposed east of Dobie.

In the east of the map area, there is another large unit of Timiskaming volcanic rocks consisting of massive aphyric and amphibole-phyric lavas and breccias, which are somewhat similar to those exposed north of the Upper Canada Mine. Hyde (1978) named this unit the Bear Lake Formation. It has a U-Pb zircon age of 2677 ± 2 Ma (Corfu et al. 1991). On previously published maps (Thomson and Griffis 1941; Jackson 1995) this unit terminates abruptly south of Little Larder Lake along an east-west-trending contact with the Gauthier Group. Our mapping does not confirm this. Volcanics exposed immediately south and southwest of Little Larder Lake are Timiskaming amphibole-phyric lavas that differ macroscopically and geochemically from the Gauthier Group volcanic rocks. Further west, the along-strike continuation of this unit under fluvio-glacial overburden is marked by a roughly 300 m wide, west-northwest-trending (approximately 290°) magnetic high that can be traced for about 4 km west of Little Larder Lake on airborne magnetic maps (Figure 3). To the east-southeast, the unit extends to the eastern boundary of McVittie Township (Thomson 1941; Thomson and Griffis 1941).

Several generations of intrusive rocks crop out in the area. They include gabbro stocks and sills spatially associated with the Larder Lake basalts; stocks and dikes of quartz-feldspar porphyry, feldspar porphyry, trachyte and syenite porphyry and biotite lamprophyre of probable Timiskaming age; and Early Proterozoic Matachewan diabase dikes.

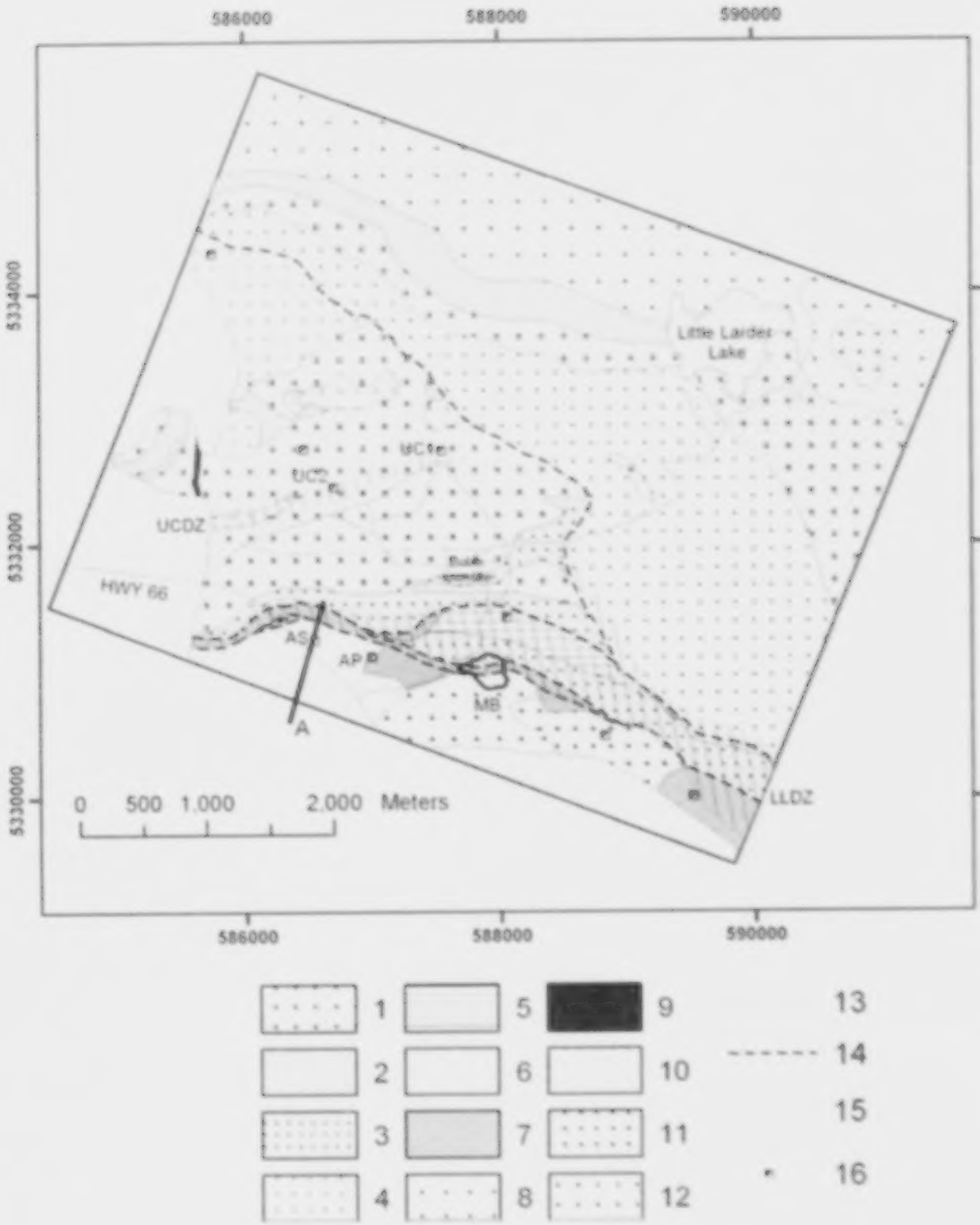
586000
588000
590000
5334000
5332000
5330000
Little Larder Lake
UC1
UC2
UCDZ
HWY 66
AS
AP
MB
A
LLDZ
0 500 1,000 2,000 Meters
1
2
3
4
5
6
7
8
9
10
11
12
13
14
15
16

Figure 2. Generalized geological map of the Gauthier Township transect area. 1-4, Timiskaming assemblage: 1-volcanic rocks, 2-volcaniclastic sandstones and conglomerates, 3-sandstones and conglomerates (unit 1), 4-turbidites (unit 2); 5-7, Larder Lake Group (Tisdale assemblage): 5-mafic volcanic rocks (chlorite schists), 6-mafic volcanic rocks (massive, variolitic and pillowed flows), 7-ultramafic volcanic rocks; 8-Gauthier Group (Tisdale assemblage) felsic to intermediate tuffs and tuff breccias; 9-diabase dikes; 10-syenite porphyries; 11-quartz-feldspar porphyries; 12-gabbro; 13-contacts; 14-faults; 15-deformation zones (LLDZ-Larder Lake–Cadillac; UCDZ-Upper Canada); 16-shafts (UC1,2-Upper Canada shafts 1 and 2; AS and AP-Anoki shaft and ramp portal); MB-McBean open pit. Thick line labeled "A"- approximate location of cross-section shown in Figure 18A.

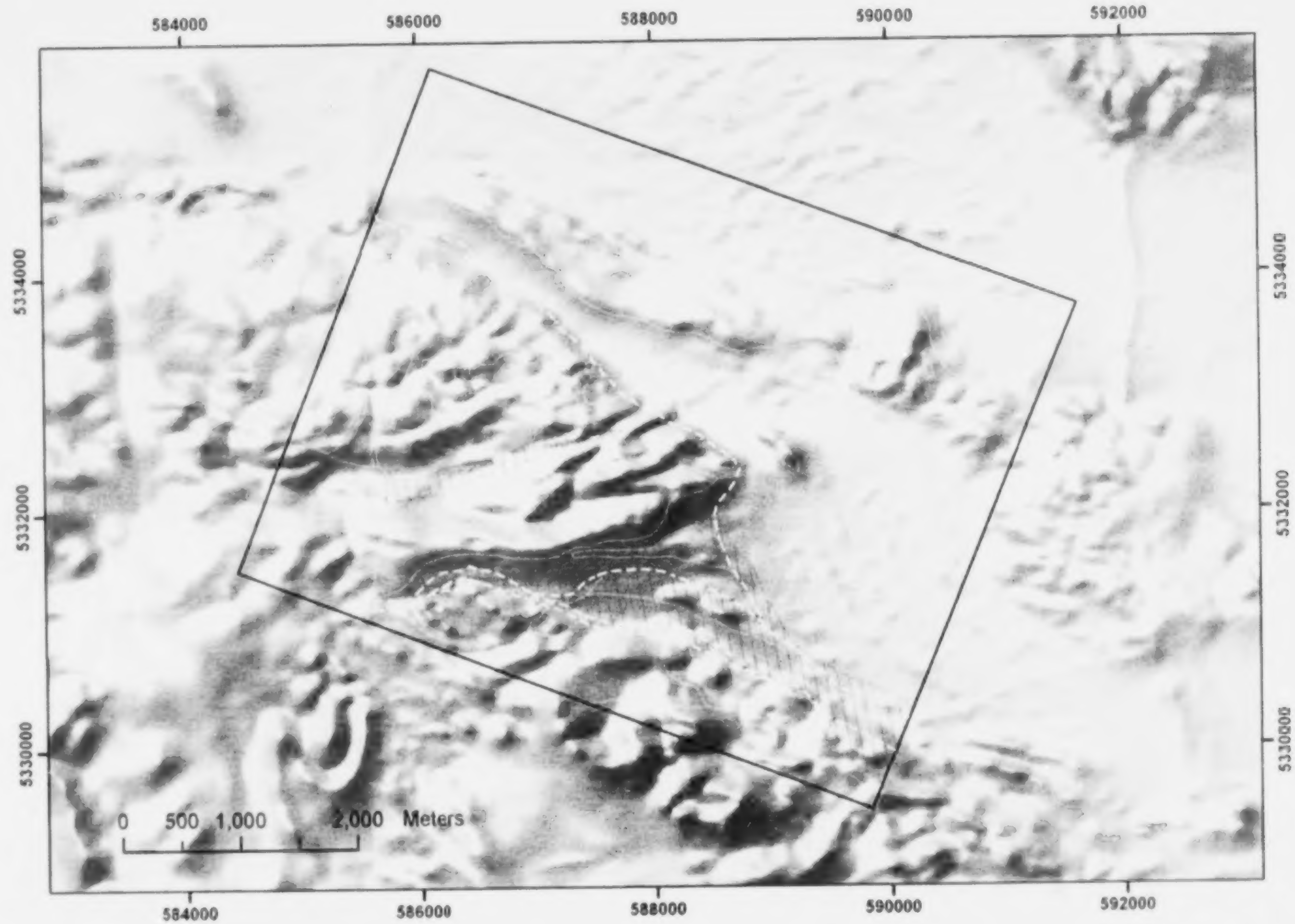
584000
586000
588000
590000
592000
5334000
5332000
5330000
0
500
1,000
2,000
Meters

Figure 3. Total field aerial magnetic map of the Gauthier Township transect area (data from OGS 2004).

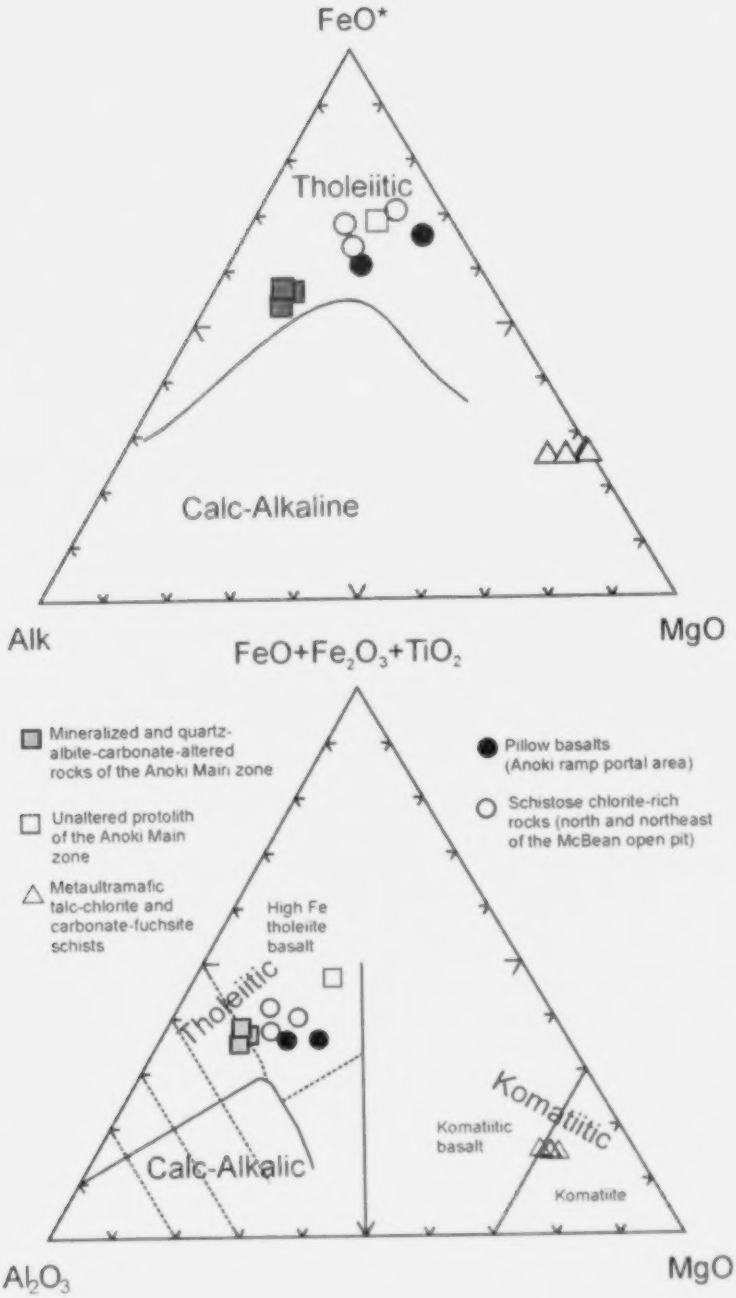

Figure 4. AFM (Irvine and Baragar 1971) and Jensen cation (Jensen 1976) plots of mafic and ultramafic volcanic rocks of the Larder Lake Group.

DEFORMATION ZONES

The most significant structural feature in the area is the southeast-northwest-striking Larder Lake–Cadillac deformation zone, the high-strain zone along the contact between the Timiskaming assemblage and Larder Lake Group (Tisdale assemblage). The zone is defined by the intensity of the deformation and does not have sharp geological boundaries. Near the eastern border of the map area, the estimated width of the high-strain zone is about 500-600 m. Further west, in the poorly exposed area between the McBean pit and Upper Canada Mine, identifying the boundaries of the zone is more difficult, because of rather poor exposure and, perhaps more importantly, because a strong foliation occurs continuously between the Larder Lake–Cadillac and the Upper Canada deformation zones. A 20 to 150 m wide band of highly strained ultramafic talc-chlorite and carbonate-fuchsite schists, traditionally referred to as the Larder Lake Break (Thomson and Griffis 1941), constitutes the southern flank of the Larder Lake–Cadillac deformation zone. Numerous felsic and syenitic dikes intrude the schists. Sketches of the east wall of the McBean open pit by Bell (1987) indicate that texturally variable dikes make up about 50-60% of this unit. Surface mapping and exploration drilling reveal the rather complex internal makeup of the Larder Lake–Cadillac deformation zone. In the McBean pit area, the deformation zone encompasses three lithotectonic units (from south to north): a 50-70 m wide band of ultramafic talc-chlorite and carbonate-fuchsite schists ("Larder Lake Break", Thomson and Griffis 1941); a 150-200 m wide unit of Timiskaming conglomerates and sandstones; and a 250 m wide lens of chlorite schists of the Larder Lake Group. The north contact of this mafic volcanic unit and Timiskaming sedimentary rocks is informally called "the North Break". Immediately to the west, in the Anoki area, the south boundary of the Larder Lake–Cadillac deformation zone broadly corresponds to a northeast-striking (065-070°) and shallowly (approximately 35-40°) dipping fault informally called the "South Splay" by Queenston Mining Inc. geologists (see additional discussion in the "Gold Mineralization" section).

The northeast-striking (approximately 070°) Upper Canada deformation zone is the second largest high-strain zone in the map area; it probably represents a northern splay of the Larder Lake–Cadillac deformation zone (Toogood 1989). The rocks between Upper Canada and Larder Lake–Cadillac deformation zones are pervasively foliated. Further north, the envelope of foliated rocks extends for 400-500 m from the Upper Canada deformation zone. The Upper Canada deformation zone itself is poorly exposed. Strippings west of the former Upper Canada Mine shaft #2 provide a fragmental exposure of the high-strain zone over a distance of about 150 m across strike and roughly 400 m along strike. East and west of this location, the deformation zone is covered by overburden. The western continuation of the deformation zone was reportedly traced by drilling for about 5 km, to its junction with the Larder Lake–Cadillac deformation zone (Toogood 1989). Where it ends to the east is less clear. About 1.5 km east of former shaft #2, the 070° trending deformation zone is expected to transect the magnetically distinct contact between Timiskaming volcanic rocks (west) and turbidites (east). Patterns on aerial magnetic maps do not show major displacement of the contact (Figure 3).

DEFORMATIONAL FABRICS

There are 4 generations of deformational fabrics in the Timiskaming rocks. The earliest post-Timiskaming fabric is designated S2 following Wilkinson et al. (1999). This assignment of the earliest post-Timiskaming fabric to the second deformation event is based on the recognition of an earlier deformational pulse (D1) that produced large-scale folds and thrusts without penetrative fabrics (Wilkinson et al. 1999; Corfu et al. 1991). Wilkinson et al. (1999) and Corfu et al. (1991) interpreted this early event as pre-Timiskaming; our new data suggest otherwise. In the eastern part of the map area, we mapped younging reversals in northwest-striking, northeast-dipping turbidites (Figure 5). The oldest deformational fabric, S2, is consistently oriented counterclockwise to the northeast- and southwest-facing beds. This geometry implies that the rocks were folded during an early event that must be younger than the maximum depositional age of turbidites (2677 Ma).

S2 is the earliest regional fabric, and the main foliation of the Larder Lake–Cadillac and Upper Canada deformation zones. It is defined by flattened clasts in sedimentary and volcanic rocks, and by a penetrative schistosity and compositional banding of secondary chlorite, talc, white mica, fuchsite and carbonate in hydrothermally altered rocks (Photo 1). Figures 6 and 7 illustrate the variations in the orientation of S2. Within the Larder Lake–Cadillac deformation zone (area 1, Figures 6 and 7), S2 generally strikes east-southeast (095-120°) and dips steeply (70-80°) south, roughly parallel to the estimated trend and dip of major lithological contacts in the deformation zone. In the northeast-trending Upper Canada deformation zone, immediately north of it, and between the Upper Canada and Larder Lake–Cadillac deformation zones (area 2, Figures 6 and 7), S2 is steeply dipping and northeast-striking (060-085°). In Timiskaming turbidites (area 3, Figures 6 and 7), S2 strikes 275° to 330° and dips steeply to moderately northeast. It is oriented either parallel to or 5°-20° counterclockwise to bedding (bedding orientation is shown in Figure 8). Relatively rare, open to isoclinal outcrop-scale folds with axial planar S2 occur in turbidites (Photo 2). A well-developed lineation (L2) is associated with S2 throughout the map area. L2 is defined by secondary mineral aggregates (mineral lineation), stretched clasts in conglomerates and volcanic rocks (Photo 2), and varioles in basalts (stretching lineation). L2 plunges moderately to steeply (35°-60°) to the east throughout the map area (Figure 6, Photo 3).

A second foliation, S3, overprints S2 in the Upper Canada deformation zone and several other locations in the map area. S3 is a steeply-dipping, north- and west-northwest-trending, crenulation cleavage (Figure 9) defined by darker, sericite- and chlorite-rich domains (0.5-3 mm wide) separating typically wider (3-10 mm) feldspar-carbonate-quartz domains in which S2 is finely crenulated (Photo 4). The morphology and orientation of S3, as well as its relationships with other fabrics are described in more detail in the section on the geology of the Upper Canada Mine.

S4 is a steeply dipping, northeast-trending (060°-080°, Figure 9) regional cleavage. It is axial planar to outcrop-scale Z-shaped and, more rarely, symmetric folds. Locally, cleavage changes orientation to E-W and even east-southeast, due to deflection along narrow high strain zones. However, on a regional scale, the orientation of S4 is relatively constant, and there is no systematic change in the orientation of S4 with increasing or decreasing distance to the Larder Lake–Cadillac deformation zone. Most typically, S4 is a discrete crenulation cleavage axial planar to microfolded bedding and S2 (Photos 5, 6, and 7). The development of the cleavage was typically accompanied by notable pressure solution removal of material from the limbs of the microfolds (Photo 7).

S5 is a late crenulation cleavage, trending 130° to 170° and dipping 30° to 80° W (Figure 9). It is observed mainly in the Larder Lake–Cadillac deformation zone, in the eastern part of the map area. It overprints all other fabrics, and is commonly axial planar to S-shaped folds of S2. No map-scale structure is associated with this fabric. The regional significance of S5 is at present unclear and it is not further discussed in this report.

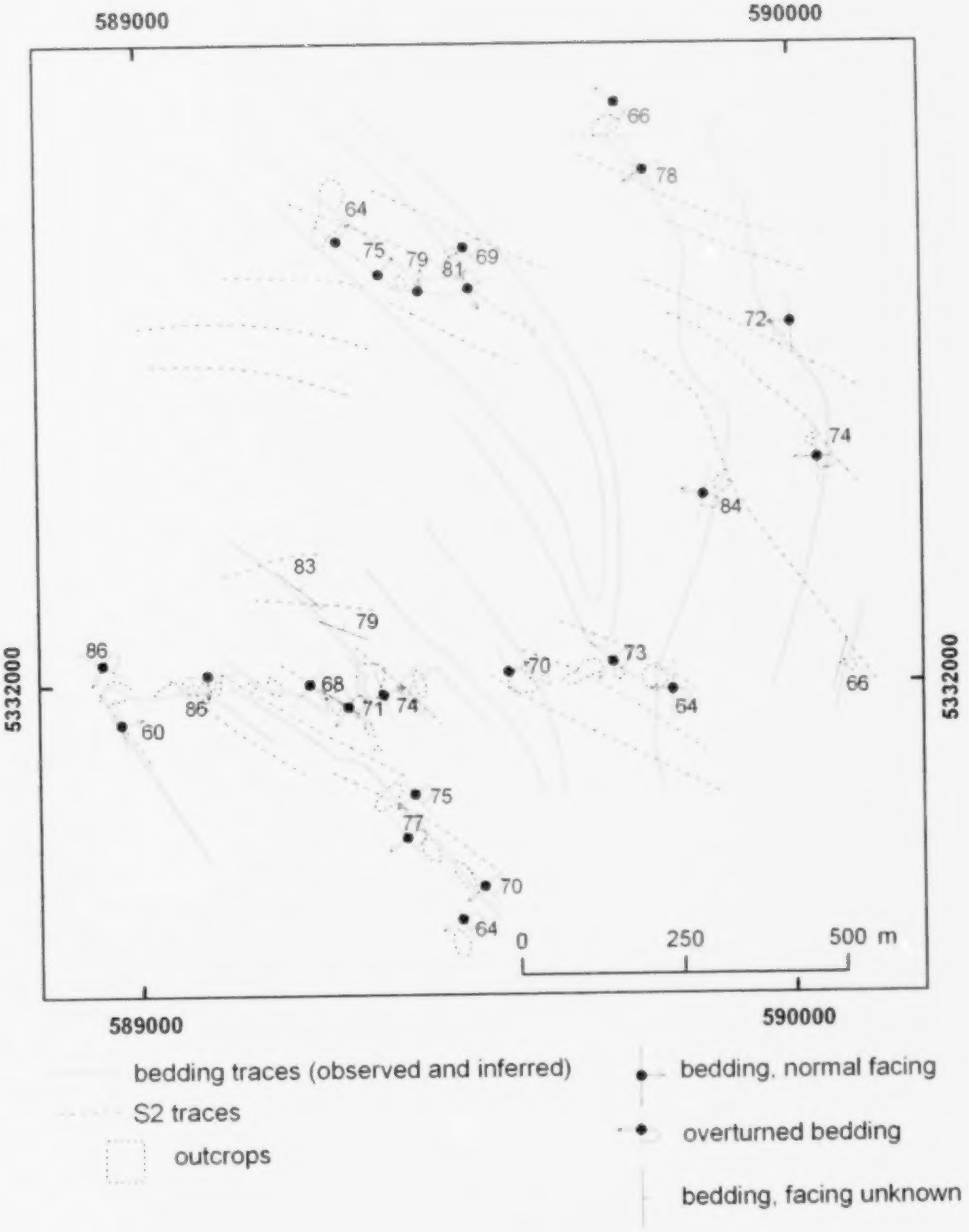
589000
590000
5332000
5332000
66
78
64
75
79
81
69
72
74
84
83
79
86
86
60
68
71
74
70
73
64
66
75
77
70
64
0
250
500 m
589000
590000
bedding traces (observed and inferred)
S2 traces
outcrops
bedding, normal facing
overturned bedding
bedding, facing unknown

Figure 5. Relationships between bedding reversals and S2 in Timiskaming turbidites. Interpreted bedding traces are shown with some generalization. Note consistent counterclockwise orientation of S2 with respect to bedding (regardless of facing direction). This indicates that bedding reversals could not have resulted from D2 folding and probably reflect earlier folding event. (Data shown in this figure were processed after Map P.3546–Revised was finalized, and are not shown on the map.)

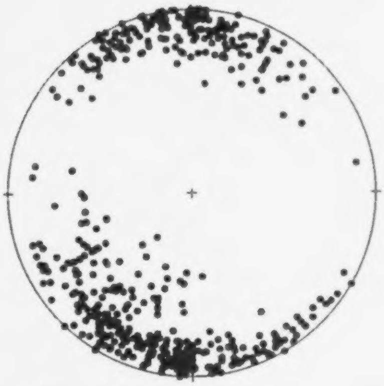

Poles to S2
Entire area, all rock types, N=527

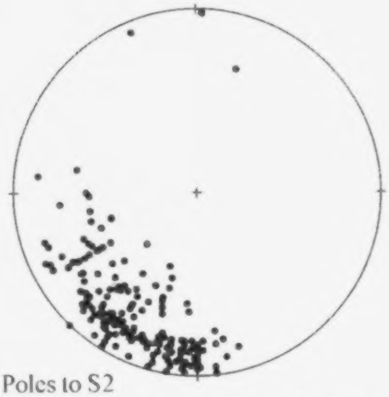

Poles to S2
Area 3, Timiskaming metasedimentary and metavolcanic rocks, N=204

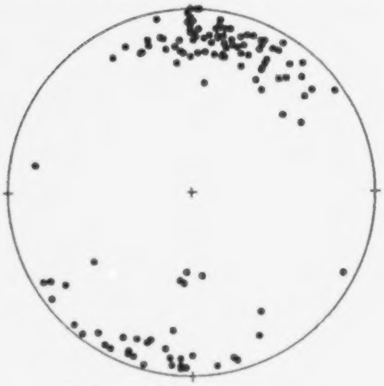

Poles to S2
Area 1, all rock types, N=126

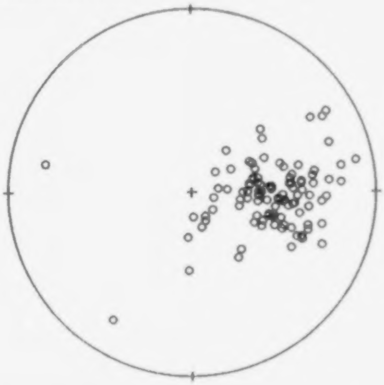

Mineral and stretching lineation (L2)
all locations, all rock types, N=103

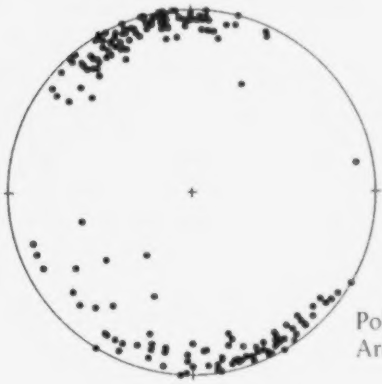

Poles to S2
Area 2, all rock types, N=190

Figure 6. Stereonet plots of S2 and L2 (data collected during detailed mapping of Upper Canada stripped outcrops are not included).

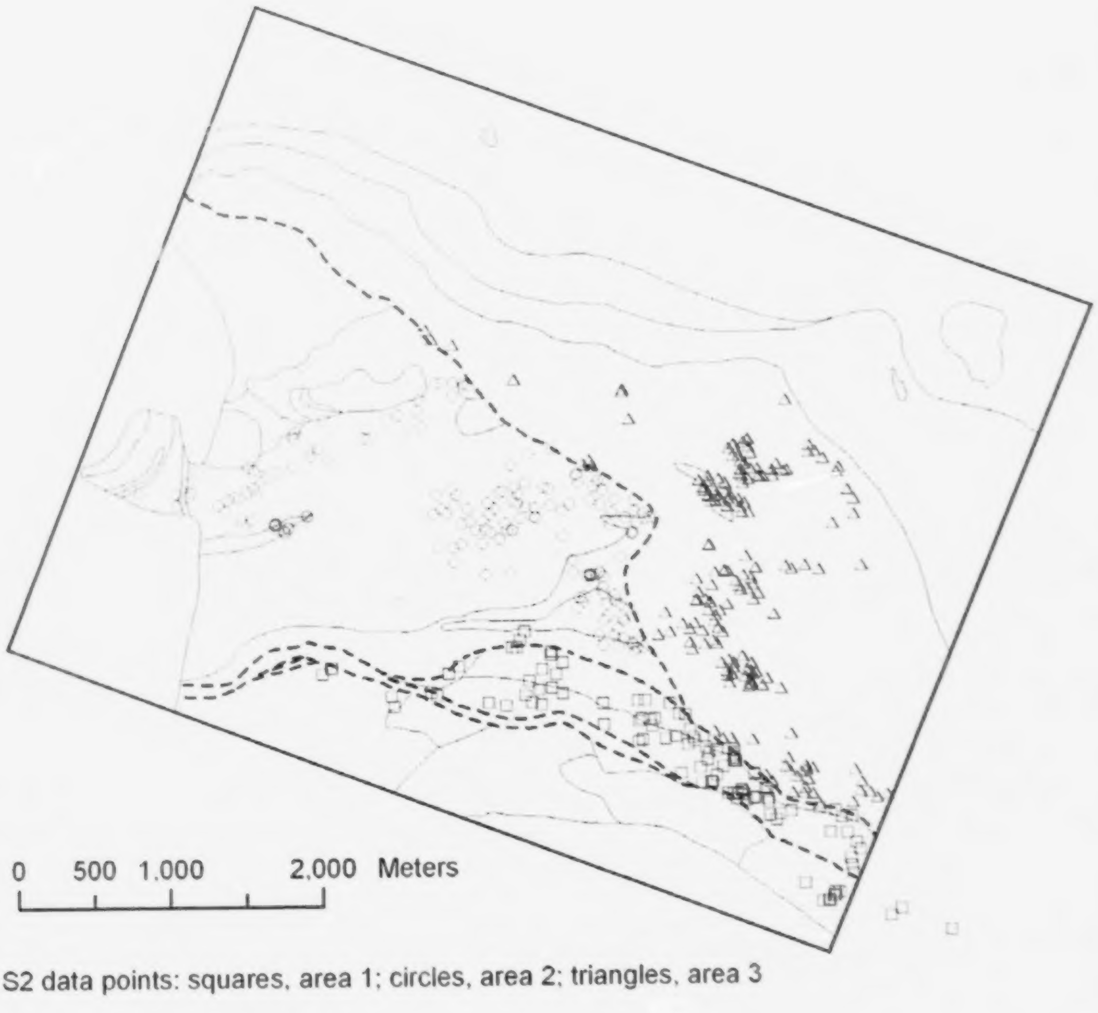
0
500
1,000
2,000
Meters
S2 data points: squares, area 1; circles, area 2; triangles, area 3

Figure 7. S2 data points from areas 1, 2, and 3.

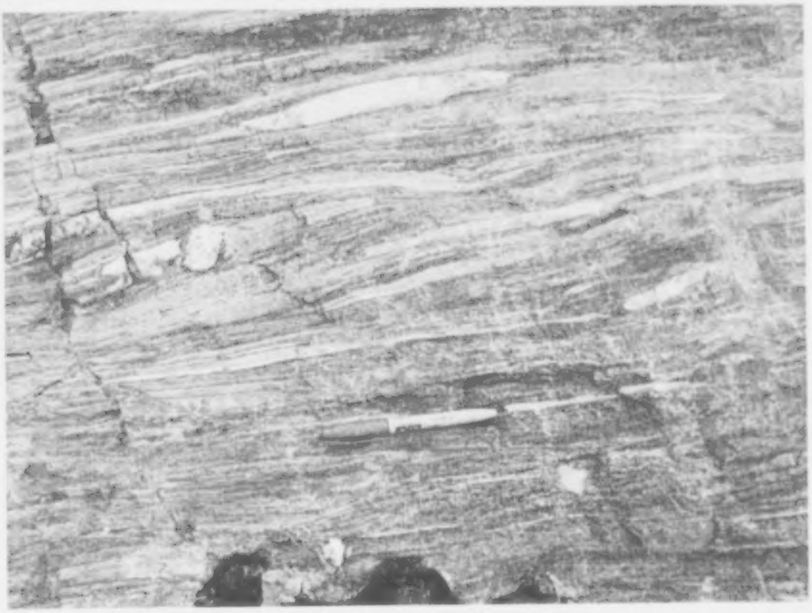

Photo 1. Foliation (S2) defined by compositional banding, and stretching lineation (L2) in highly strained Timiskaming conglomerates. Lineation is marked by pebbles stretched into ribbons (e.g., the upper part of the photo). Plane of view is perpendicular to foliation and approximately parallel to stretching lineation. Marker pen (roughly 15 cm) for scale. North wall of flooded McBean open pit.

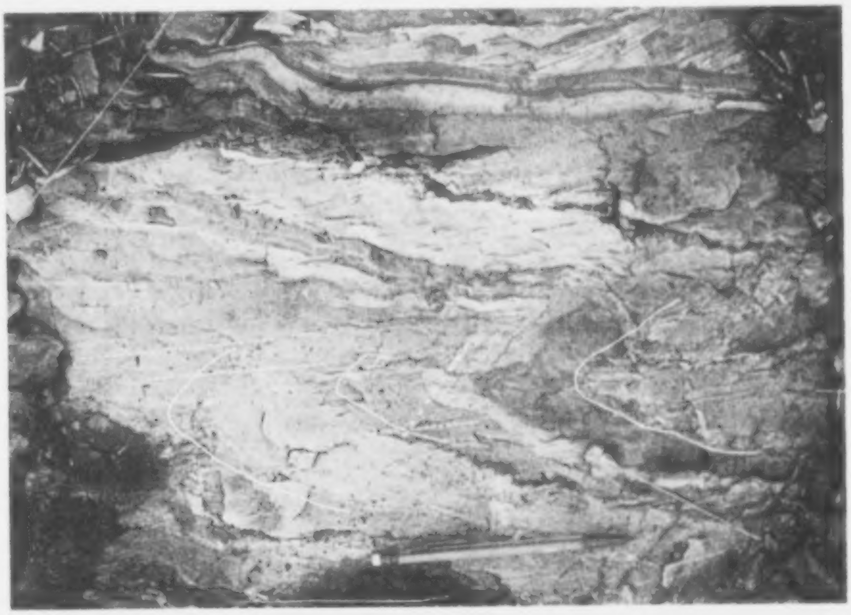

Photo 2. F2 fold in Timiskaming turbidites: bedding (solid line) is folded with axial planar S2 (thin dashed line, east-west) and is overprinted by S4 (thick dashed line, northeast-southwest). Pencil (15 cm) for scale.

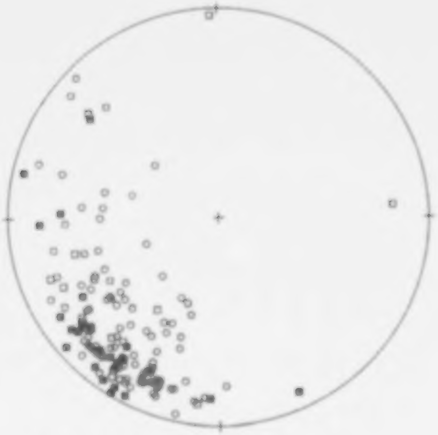

Poles to bedding
Timiskaming turbidites: open circles,
facing unknown (N=102),
open square, normal bedding (N=16),
filled square, overturned bedding (N=25)

Figure 8. Stereonet plot of bedding in Timiskaming turbidites.

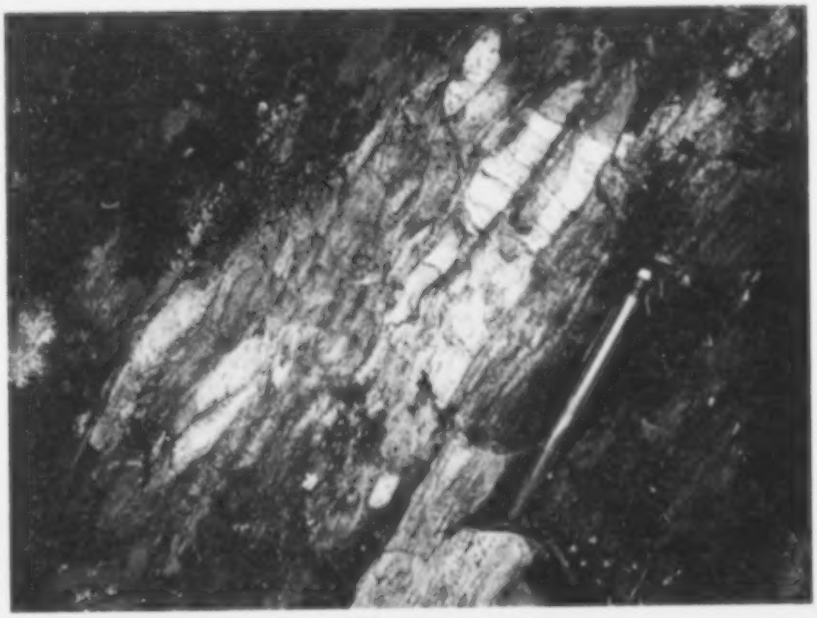

Photo 3. Stretching lineation (L2) in volcaniclastic breccias east of Dobie townsite. Lineation plunges approximately 45-50° east. Pencil (15 cm) for scale.

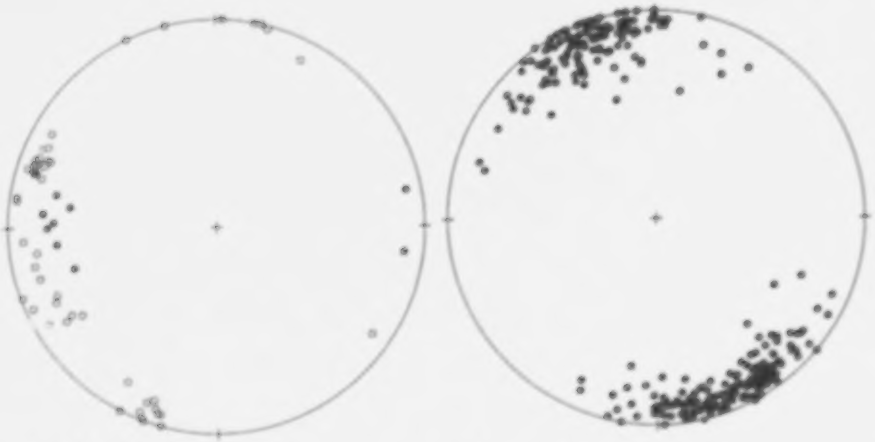

Poles to S3:
open circles, Upper Canada
deformation zone (N=47),
filled circles, other locations (N=10)

Poles to S4:
all locations, all rock types, N=321

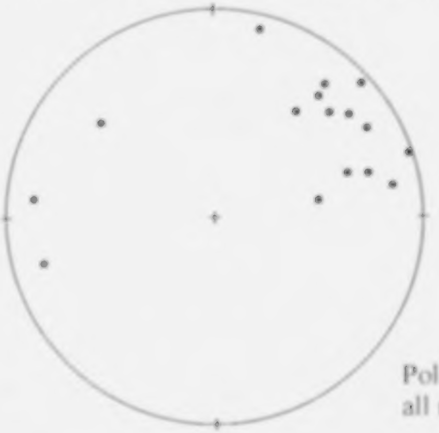

Poles to S5:
all rock types, N=16

Figure 9. Stereonet plots of S3, S4, and S5 (S4 data collected during detailed mapping of Upper Canada stripped outcrops are not included).

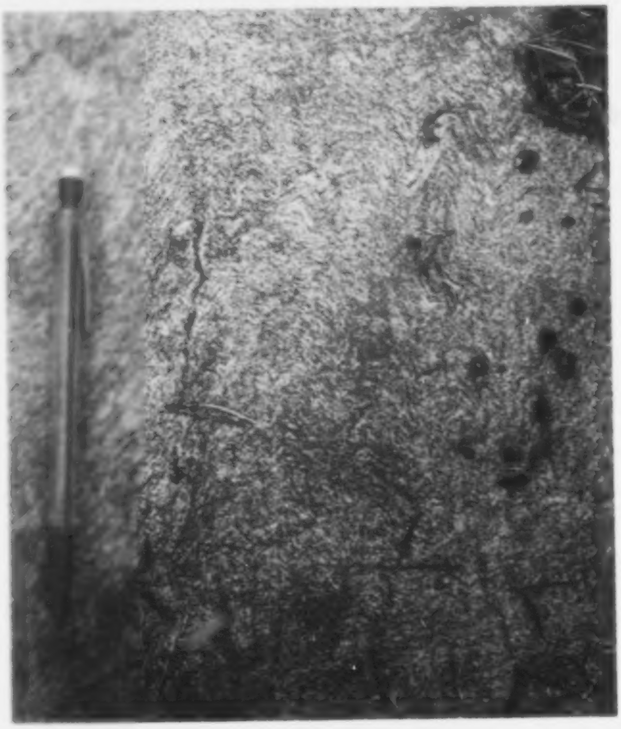

Photo 4. S3 crenulation cleavage (parallel to the pencil) overprinting S2 (oriented approximately east-west, crenulated). Upper Canada L-W stripping. Pencil (15 cm) for scale.

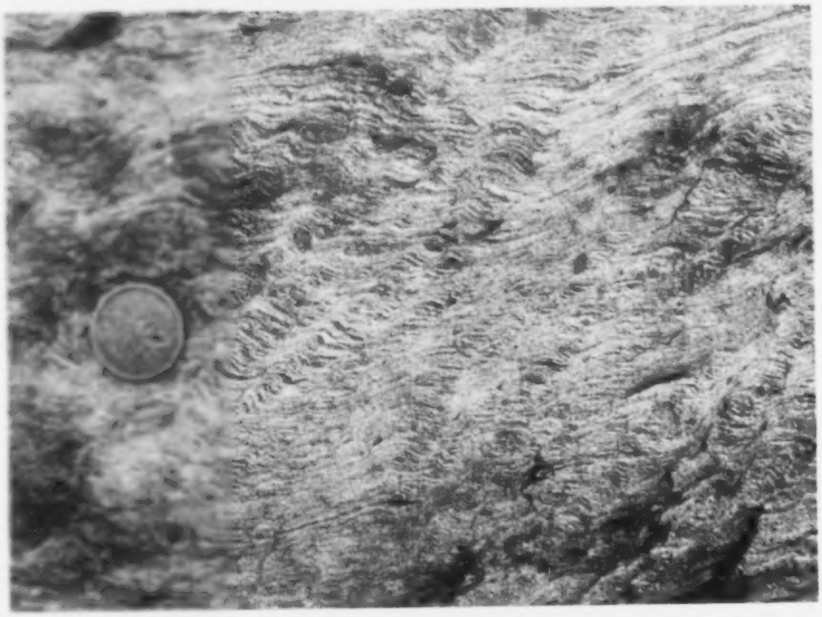

Photo 5. Crenulation cleavage S4 (northeastt-southwest) overprinting S2 in altered felsic dike. Coin diameter 1.8 cm.

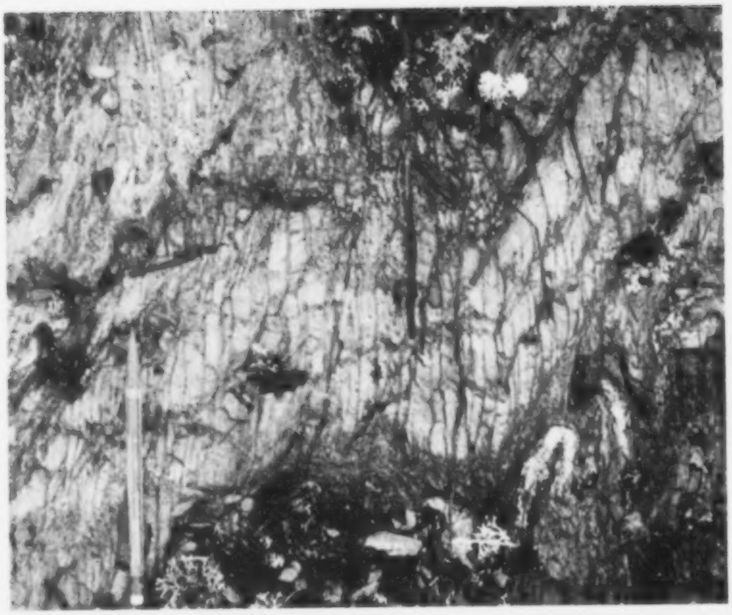

Photo 6. Discrete crenulation cleavage S4 in Timiskaming turbidites.

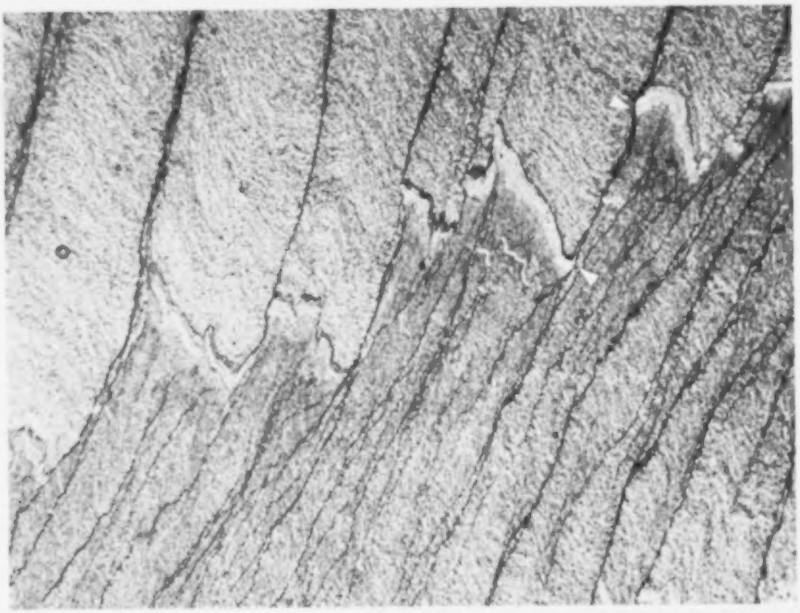

Photo 7. Photomicrograph (plane polarized light, field of view approximately 5 mm) of S4 in Timiskaming siltstone-argillite (darker layer in the bottom half of the photo is finer and more phyllosilicate-rich). Discrete crenulation cleavage S4 (thin dark seams) overprints bedding and bedding-parallel S2. Note tighter spacing of discrete cleavage planes in finer, phyllosilicate-rich rock and an apparent sinistral offset of a thin quartz-rich interbed (marked by white arrows) due to pressure solution along cleavage planes.

KINEMATIC INDICATORS IN THE LARDER LAKE–CADILLAC DEFORMATION ZONE

Asymmetric shear-sense indicators were observed at two localities along the Larder Lake–Cadillac deformation zone. The first location is along the southern flank of the deformation zone at the contact between Timiskaming conglomerate and a band of ultramafic schists that separates Timiskaming clastic rocks from mafic volcanics of the Larder Lake Group and associated gabbroic intrusions (i.e., Larder Lake Break, after Thomson and Griffis 1941). Highly strained Timiskaming conglomerates with well-developed stretching lineation (L2) are exposed in the northern wall of the flooded McBean open pit. On the surface that is parallel to L2 and perpendicular to S2, some of the least strained pebbles show asymmetric pressure shadows indicating oblique reverse-dextral slip (south side over north and to the west) along the direction of stretching lineation (Photo 8).

The second location is at the northern margin of the Larder Lake–Cadillac deformation zone (stripped outcrop at the Princeton Property, eastern part of the area). Here, shear-sense indicators include a combination of dextral Z-shaped drag folds, the clockwise orientation of extensional quartz-carbonate veins with respect to foliation (S2), and offsets of these veins along S2. The interpreted slip direction is similar to that documented at the McBean pit; that is, oblique reverse-dextral slip parallel to the stretching L2 direction.

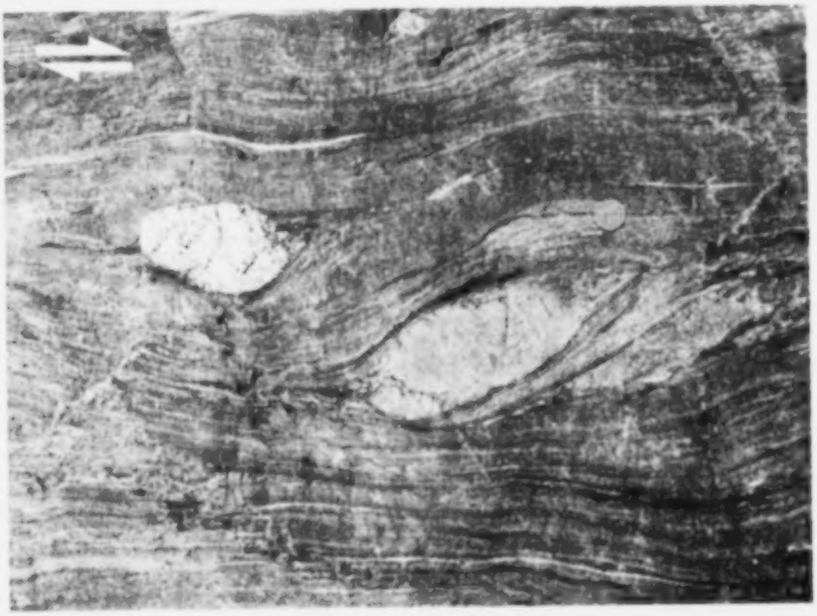

Photo 8. Asymmetric pressure shadows on pebbles in highly strained Timiskaming conglomerates. Plane of view is approximately parallel to stretching lineation L2, north is on the top. Oblique (counterclockwise) alignment of pressure shadows with respect to S2 foliation indicates dextral movement in the direction of stretching lineation, i.e., reverse (south side up)-dextral movement on the Larder Lake deformation zone.

GOLD MINERALIZATION

The accompanying geological map (Map P.3546–Revised, back pocket) shows the location of major gold occurrences. The most important occurrences of gold mineralization are the past-producing Upper Canada Mine and mineralized zones of the McBean and Anoki properties. Recent (1996-present) exploration campaigns of Queenston Mining Inc. and their joint venture partners resulted in the discovery of new significant gold mineralization in the McBean and Anoki areas. All known economic and potentially economic occurrences of gold mineralization are spatially associated with major high-strain zones. Mineralized zones of the McBean Mine and Anoki property (Anoki Main, Anoki South, Anoki Deep, and 40 East) occur within or in close proximity to the Larder Lake–Cadillac deformation zone; mineralization of the Upper Canada Mine is hosted by the Upper Canada deformation zone.

The following section describes the geology of gold occurrences focusing on structural geology and mineralization styles. At present, mineralization can be observed at surface only at the Upper Canada Mine, where the westernmost portion of the most productive L zone is exposed by strippings west of former shaft #2. Mineralization at Anoki and McBean is not exposed and was observed in drill core.

Upper Canada Mine

The Upper Canada Mine operated from 1938 to 1971 and produced 43.49 tonnes of gold at a grade of 10.3 g/t (information of Ontario Ministry of Northern Development and Mines, posted at http://www.mndm.gov.on.ca, downloaded in spring, 2005). Remaining measured and indicated resources are 13.11 t Au at an average grade of 6.9 g/t (Queenston Mining Inc. 2003). The history and general geology of the mine is described by Tully (1963). Most of the ore (66.8% as of 1961) was mined from the L mineralized zone, which is subdivided into the Upper and Lower L zones (Tully 1963). The roughly 600 m long Upper L zone extends from the surface to 575 m depth (the 1750-foot level), whereas the 300-350 m long Lower L zone was developed from 575 m (the 1750-foot level) to 2015 m (the 6150-foot level), the lowest level in the mine. Within the L zone, typical ore bodies are 30 to 60 m long (maximum about 170 m) and are separated by barren or weakly mineralized rocks (Bragg 1967). Other mineralized zones include the B, H, M, Q, and minor C and K zones (Tully 1963). Mineralization is hosted by strongly foliated Timiskaming volcanic rocks and related intrusions within the Upper Canada deformation zone ("Upper Canada Break", Tully 1963). All major mineralized zones strike parallel to the host deformation zone (i.e., east-northeast approximately 075°), dip steeply to vertically, and plunge 40°-60° east. As can be seen on the longitudinal section (Figure 10), the bulk of the ore occurs between the east-plunging stock of leucocratic syenite porphyry ("white spotted porphyry", Tully 1963) (west), and the contact of Timiskaming volcanics and turbidites (east). No ore has been found in turbidites and only the Upper L zone is partially hosted by the leucocratic syenite porphyry (Bragg 1967). Mineralization occurs as silicified zones accompanied by sericite-carbonate alteration; fine native gold is associated with pyrite and less abundant chalcopyrite, arsenopyrite, tennantite-tetrahedrite, galena, altaite, molybdenite and scheelite (Tully 1963). Gold:silver ratio is 2.22:1 (Tully 1963). A series of northeast-trending discrete faults ("mud seams") cut deformed rocks in proximity to the gold mineralization (Tully 1963); these faults are most likely related to late, brittle, overprint of the ductile Upper Canada deformation zone. West of the mine, a post-mineralization diabase dike is dextrally displaced for about 110 m (345 feet) along the "main mud seam" (Tully 1963).

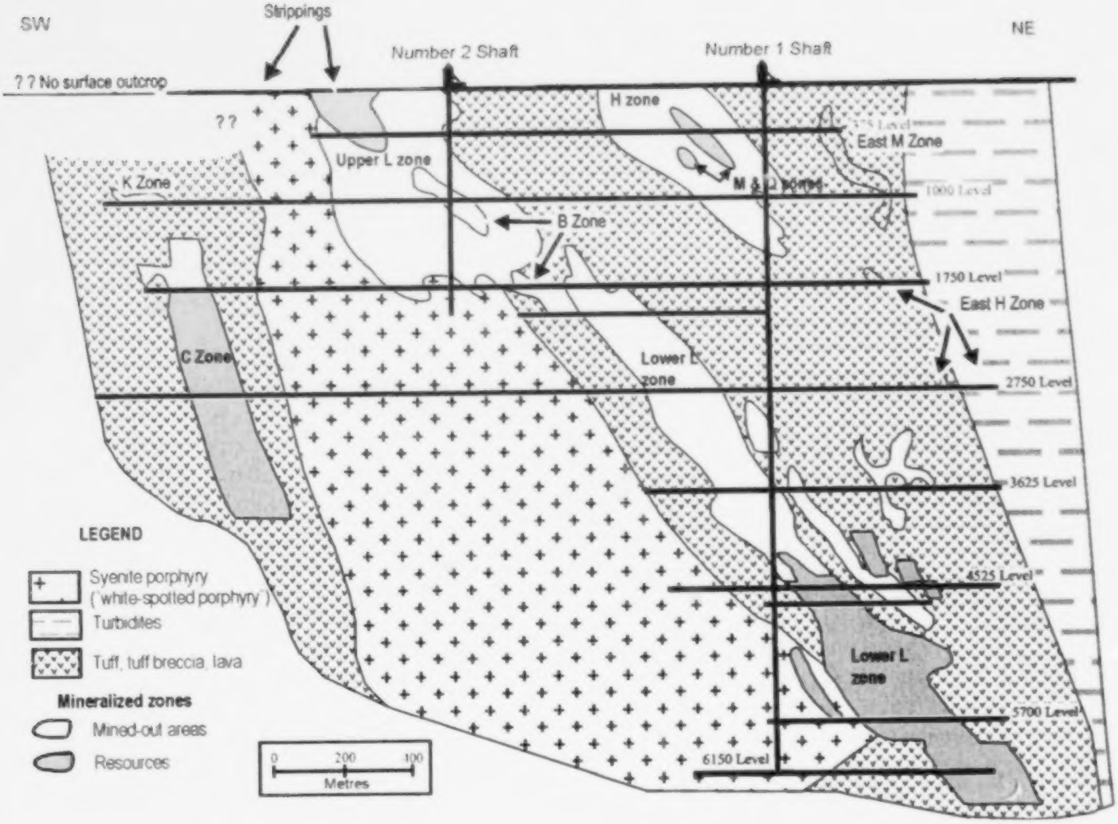
SW
Strippings
NE
Number 2 Shaft
Number 1 Shaft
? ? No surface outcrop
? ?
H zone
East M Zone
Upper L zone
K Zone
M & J zones
1000 Level
B Zone
1750 Level
East H Zone
C Zone
Lower L zone
2750 Level
3625 Level
4525 Level
Lower L zone
5700 Level
6150 Level
LEGEND
Syenite porphyry ("white-spotted porphyry")
Turbidites
Tuff, tuff breccia, lava
Mineralized zones
Mined-out areas
Resources
0
200
400
Metres

Figure 10. Longitudinal section of the Upper Canada Mine, with approximate position of stripped outcrops. Modified from a section posted at Queenston Mining Inc. website, www.queenston.ca and Stevenson et al. (1995).

The westernmost part of the L zone is exposed in stripped outcrops west of the former shaft #2 (Figure 11). Toogood (1989) mapped hydrothermal alteration assemblages and identified 3 generations of penetrative deformational fabrics. He attributed fabrics to dextral strike-slip shear along the Upper Canada deformation zone and concluded that gold mineralization postdated the first deformational fabric and was structurally and hydrothermally overprinted during the formation of the latest fabric. As part of the present project, we mapped the main "L" stripping at a 1:200 scale, and made additional structural observations on other stripped outcrops. Our study confirms several conclusions of Toogood (1989), however there are also important differences. The following sections on the geology of the Upper Canada Mine are based primarily on our new mapping and structural observations. A geologic map of the L stripping is presented in Figure 12 (back pocket). Outlines of stripped outcrops on Figure 12, and gold grade information are from Toogood (1989). Geochemical data for 12 samples from the Upper Canada Mine area are presented in Appendix A; the location of samples from the "L" stripping is shown in Figure 12. Samples were intended primarily for microstructural studies and may not be representative of the gold grades established by the original channel sampling (Toogood 1989).

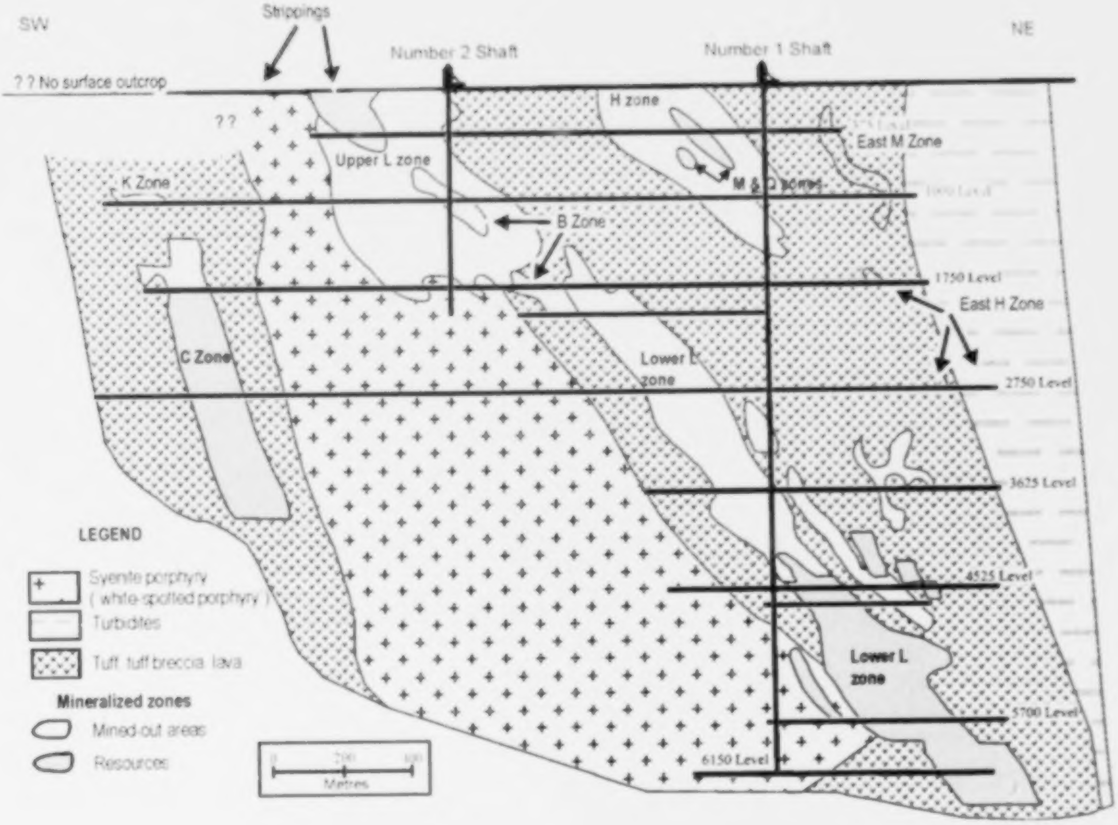
SW
Strippings
NE
Number 2 Shaft
Number 1 Shaft
? ? No surface outcrop
? ?
H zone
East M Zone
Upper L zone
M & Q zones
K Zone
B Zone
1750 Level
East H Zone
C Zone
Lower L zone
2750 Level
3625 Level
LEGEND
Syenite porphyry (white-spotted porphyry)
Turbidites
Tuff, tuff breccia, lava
Mineralized zones
Mined-out areas
Resources
4525 Level
Lower L zone
5700 Level
6150 Level
0
200
400
Metres

Figure 10. Longitudinal section of the Upper Canada Mine, with approximate position of stripped outcrops. Modified from a section posted at Queenston Mining Inc. website, www.queenston.ca and Stevenson et al. (1995).

The westernmost part of the L zone is exposed in stripped outcrops west of the former shaft #2 (Figure 11). Toogood (1989) mapped hydrothermal alteration assemblages and identified 3 generations of penetrative deformational fabrics. He attributed fabrics to dextral strike-slip shear along the Upper Canada deformation zone and concluded that gold mineralization postdated the first deformational fabric and was structurally and hydrothermally overprinted during the formation of the latest fabric. As part of the present project, we mapped the main "L" stripping at a 1:200 scale, and made additional structural observations on other stripped outcrops. Our study confirms several conclusions of Toogood (1989), however there are also important differences. The following sections on the geology of the Upper Canada Mine are based primarily on our new mapping and structural observations. A geologic map of the L stripping is presented in Figure 12 (back pocket). Outlines of stripped outcrops on Figure 12, and gold grade information are from Toogood (1989). Geochemical data for 12 samples from the Upper Canada Mine area are presented in Appendix A; the location of samples from the "L" stripping is shown in Figure 12. Samples were intended primarily for microstructural studies and may not be representative of the gold grades established by the original channel sampling (Toogood 1989).

ROCK TYPES

The rocks exposed in stripped outcrops (Figure 11) include tuff, tuff breccia, and leucocratic feldspar-phyric syenite porphyry ("white spotted porphyry" of Tully 1963). Tuffs are generally strongly altered and consist largely of hydrothermal sericite, fine-grained quartz and carbonate. At the L-NW stripping, (Figure 11), where quartz-sericite-carbonate alteration is weaker then elsewhere, the tuffs contain abundant secondary chlorite. Most tuffs are aphanitic and do not contain identifiable crystals or rock clasts. However, at a few places at the L stripping, sparse (<5-10%) relict feldspar grains (0.5-2 mm) can be seen in tuffs. Tuff breccia consisting of angular (1-5 cm to 7-10 cm) lithic clasts enclosed in a strongly tourmalinized matrix comprises a distinct rock type exposed on the L and L4 strippings.

Leucocratic feldspar-phyric syenite porphyry contains 20-40% ovoid feldspar phenocrysts set in an altered (quartz-sericite ± carbonate) matrix. These rocks form a wedge-like, eastward-tapering body parallel to the general trend of the Upper Canada deformation zone. Between the L-W and L-NW strippings, the width of the intrusion is about 70 m, near the eastern end of the L stripping, the body is only about 5 m wide. The exposed westernmost portion of the L mineralized zone is spatially associated with the narrow "nose" of the syenite body (Figure 11). As can be judged from the block-diagram in Tully (1963) and the longitudinal section of the mine (Figure 10), the wedge-shaped syenite body tends to widen with depth and the line of its eastern termination plunges about 40-50° east. Association of the L zone with the eastern terminus of the intrusion generally persists with depth: the Upper L zone occurs at the contact and is partially hosted by the intrusion and the Lower L zone is located up to roughly 150 m east of the syenite body. In addition to widespread syenite porphyry, there are also pink, reddish-grey or grey fine-grained aphyric rocks that occur as lenses and discontinuous bands (e.g., 0.1 by 1 m to 1 by 4 m). Like all other rock types, these rocks are variably foliated and folded. Most probably, these rocks represent boudinaged small dikes (Toogood 1989) and they are shown as "aphanitic microdikes" on Figure 12.

The L stripping (Figure 12, back pocket) exposes the westernmost part (roughly 70 m) of the L mineralized zone. The main rock type is the leucocratic syenite porphyry, bounded by tuffs and tuff breccias, to the north and south, respectively. The nature of the northern contact of the intrusion varies in the outcrop. West of the channel sampling line 11 where syenite porphyry is bounded by aphanitic tuffs, the contact is sharp and quite distinct in the outcrop, whereas east of this channel sampling line, the contact is more diffuse. The syenite porphyry still has a distinctive porphyritic texture defined by the presence of 30-35% feldspar phenocrysts, but strongly altered and foliated rocks north of the inferred porphyry contact also contain sparse (typically ≤ 5%) relic feldspar grains. Although these feldspar-bearing rocks are interpreted as tuffs, they could represent strongly altered and sheared syenites.

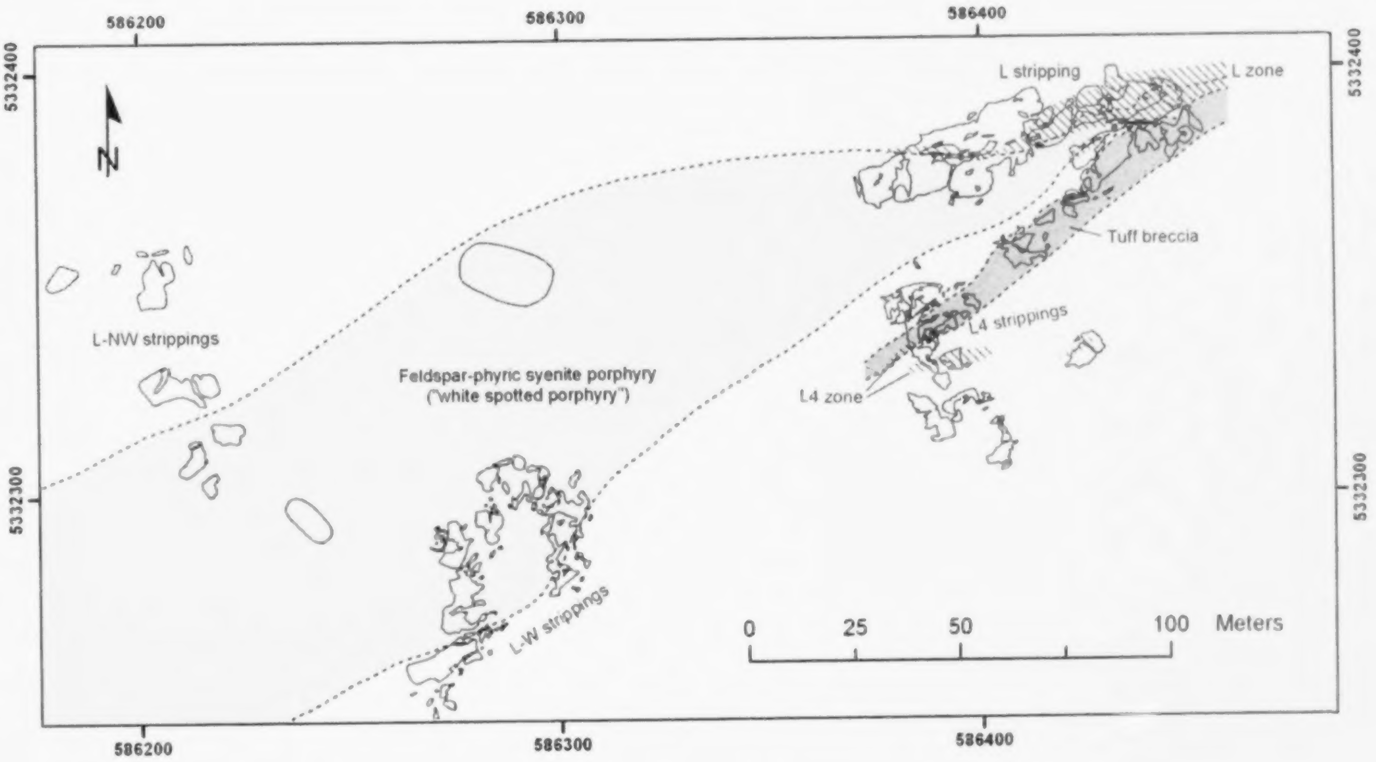
586200
586300
586400
5332400
5332300
N
L stripping
L zone
Tuff breccia
L4 strippings
L4 zone
L-NW strippings
Feldspar-phyric syenite porphyry
("white spotted porphyry")
L-W strippings
0
25
50
100
Meters

Figure 11. Location of stripped outcrops west of former Upper Canada shaft #2, inferred contacts of the leucocratic syenite porphyry ("white-spotted porphyry") intrusion, and location of mineralized zones. Outlines of stripped outcrops are from Toogood (1989).

HYDROTHERMAL ALTERATION

All rocks exposed in the stripped area are hydrothermally altered. There is a ubiquitous quartz-sericite-carbonate alteration characterized by variable carbonate abundance. Distinct carbonate-rich (CO_2 approximately 8-14%) schistose rocks occur along the north contact of the syenite porphyry body and are shown as quartz-sericite-carbonate schists on Figure 12. As discussed below, these carbonate-rich schists constitute the gold-bearing zone between channels 10 and 16. Toogood (1989) identified the carbonate as ankerite or ferroan dolomite based on staining tests. Finely disseminated pyrite is present in quartz-sericite-carbonate-altered rocks throughout the stripping, and the abundance of pyrite does not appear to be related to the intensity of carbonatization. Tourmalinization occurs locally, and tends to be spatially associated with a tuff breccia horizon exposed in the southeast part of the L stripping and on the L4 stripping. In addition to the tuff breccias, weak tourmalinization was also microscopically observed in the syenite porphyry (L stripping, channel 14). The 2-10 cm thick veins of translucent quartz (also containing albite and carbonate) are widespread and belong to two major groups: folded early veins parallel or near parallel to S2 foliation; and late, steep, north-south-trending veins crosscutting all deformational fabrics. Throughout the L stripping, most veins are barren, with the exception of the area of quartz veining sampled by channel 3.

STRUCTURAL GEOLOGY

Three penetrative deformational fabrics are observed in stripped outcrops. They correlate with the regional deformation fabrics described above. The earliest foliation, S2, is steeply dipping and northeast striking (065-085°, in places to 100°; Figures 12, 13, 14, 15, 16, and 17). In the tuffs, S2 is a differentiated foliation defined by domains rich in carbonate, quartz, and feldspar (?) alternating with thinner sericite-rich domains (Photo 9). S2 is also expressed by alignment of individual mica flakes, quartz ribbons, feldspar porphyroclasts in syenite porphyries, and by flattened lithic clasts in tuff breccia. In thin section, trains of fine pyrite and titanite also mark S2 foliation.

S2 is overprinted by a differentiated crenulation cleavage S3. On the L-W stripping, north portion of the L4 stripping, and a few locations on the L stripping, S3 is oriented approximately north-south (340°-020°), at a high angle to S2. On the L-W stripping, in altered syenite porphyry, north-striking S3 is marked by diffuse, 1-2 mm wide sericite-rich cleavage bands oriented at a high angle (60-70° counterclockwise to almost orthogonally) to S2, and axial planar to open folds of S2 (Figures 14 and 15, Photo 10). Under the microscope, sericitic cleavage bands are noted to contain fine pyrite and titanite(?).

In the north part of the L4 stripping, the diffuse S3 cleavage bands trend 330°-340° and are nearly orthogonal to S2. S3 is marked by rosettes and irregular clusters of hydrothermal tourmaline and very fine titanite (?) grains. Tourmaline also occurs along S2. Some euhedral tourmaline crystals are oriented at high angle to S3 planes, indicating that tourmalinization either postdated the formation of S3 or possibly occurred during its final phases. Both tourmaline-bearing fabrics are overprinted by northeast-trending (065°-070°) S4.

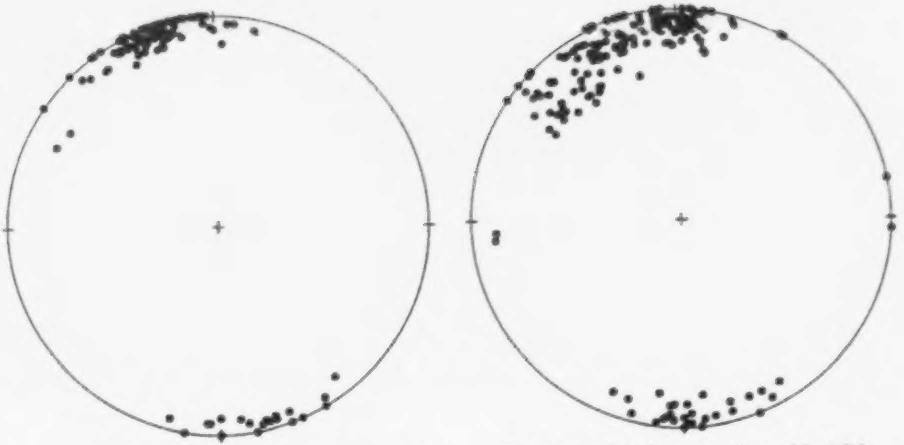

Poles to S4, L stripping, N=131

Poles to S2, L stripping, N=189

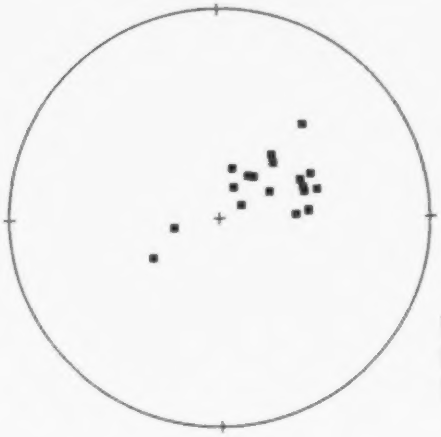

L stripping
Fold axes (F4 folds, folded S2),
N=19

Figure 13. Steronet plots of S2, S4, and fold axes from the L stripped outcrop.

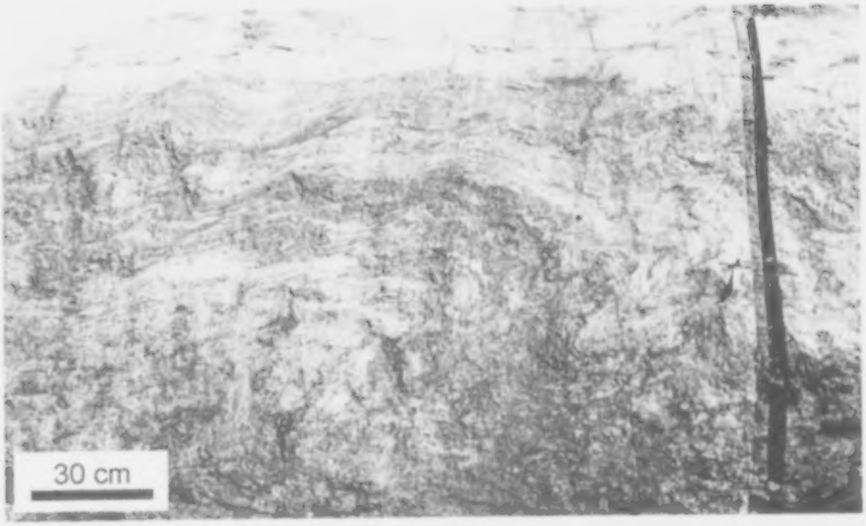

Photo 9. S2 in gold-bearing quartz-sericite-carbonate schists, defined by intercalating bands variably rich in silica, sericite, and carbonate. S2 is folded into Z-asymmetric folds (F4). Upper Canada Mine, L stripping, sampling line 13, looking south. Syenite porphyry (light tones) along the upper margin of the photo.

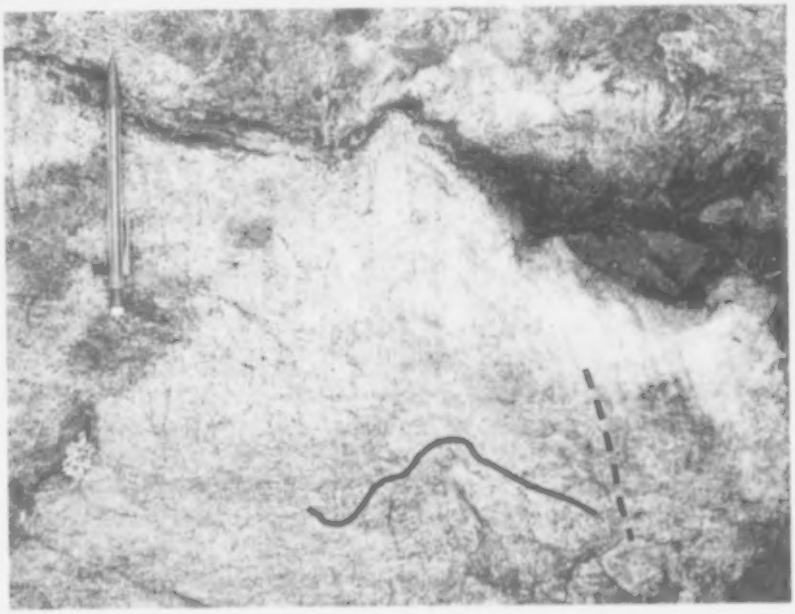

Photo 10. S3 (dashed line) axial planar to open folds of S2 (solid line). Upper Canada Mine, L-W stripping.

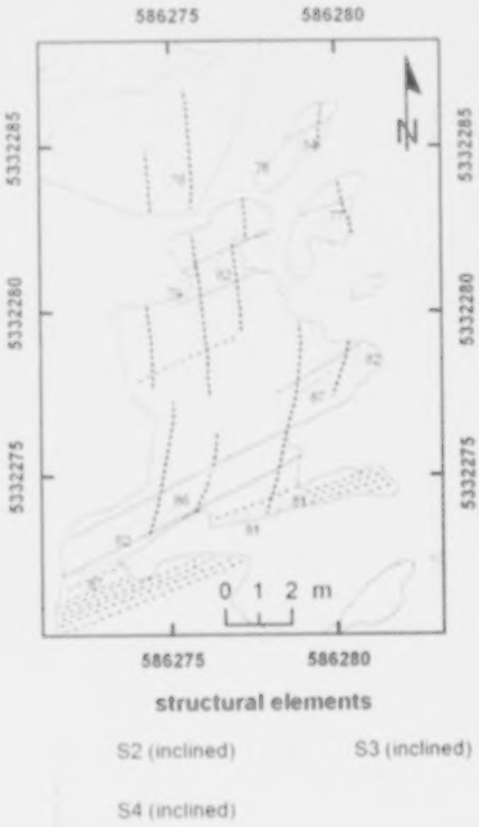
586275
586280
5332285
5332280
5332275
N
0 1 2 m
structural elements
S2 (inclined)
S3 (inclined)
S4 (inclined)

Figure 14. Fragment of the L-W stripped outcrop: relationships of S2, S3, and S4. Solid lines-S2; thick dashed lines-S3; thin dashed lines-S4. Outcrop outlines are from Toogood (1989).

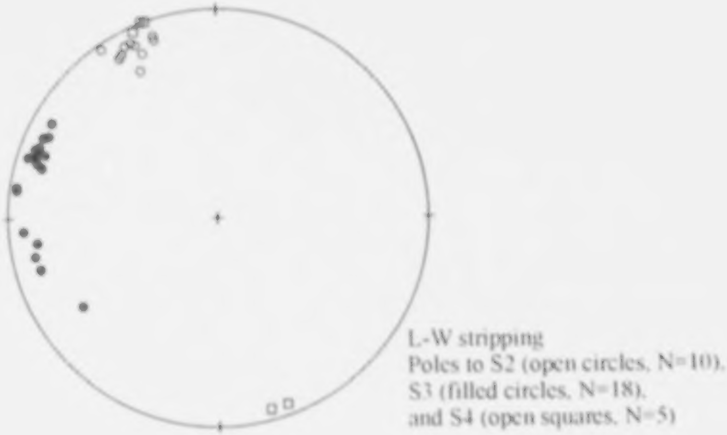

Figure 15. Stereonet plot of S2, S3, and S4 on the L-W stripped outcrop (area shown in Figure 14).

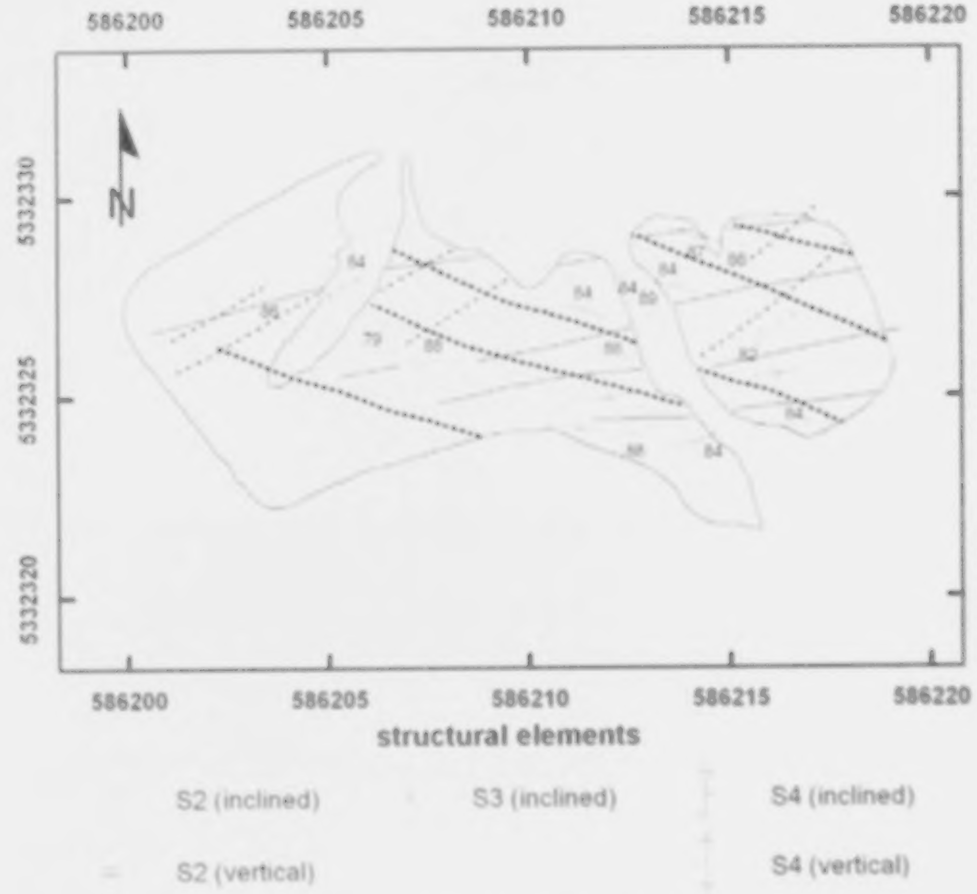
586200
586205
586210
586215
586220
5332330
5332325
5332320
N
84
86
79
88
84
84
89
87
86
84
88
82
84
88
84
structural elements
S2 (inclined)
S3 (inclined)
S4 (inclined)
S2 (vertical)
S4 (vertical)

Figure 16. Fragment of the L-NW stripped outcrop: relationships of S2, S3, and S4. Solid lines-S2; thick dashed lines-S3; thin dashed lines-S4. Outcrop outlines are from Toogood (1989).

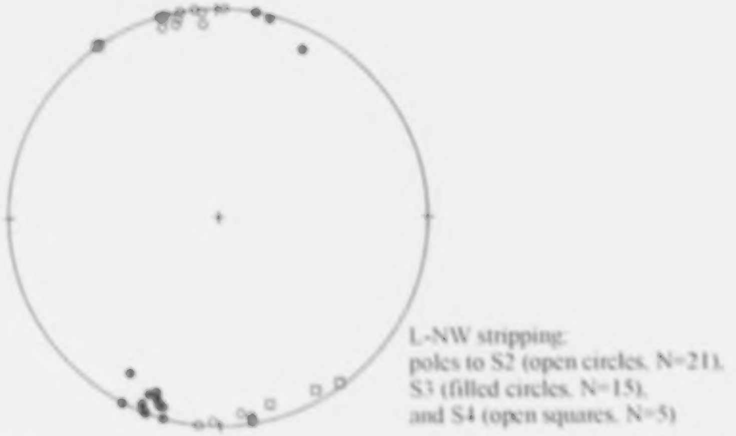

Figure 17. Stereonet plot of S2, S3, and S4 on the L-NW stripped outcrop (area shown on Figure 16).

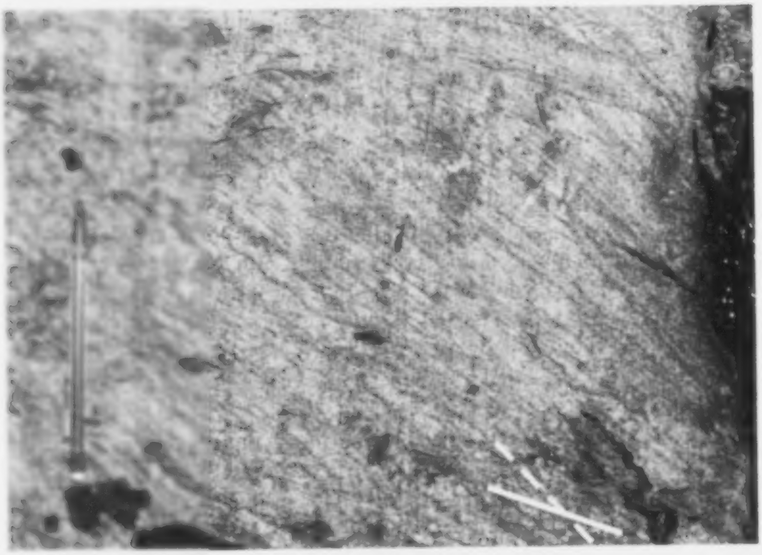

Photo 11. S3 (dashed line) oriented clockwise to S2 (solid line). Upper Canada Mine, L-NW stripping. Pencil is 15 cm.

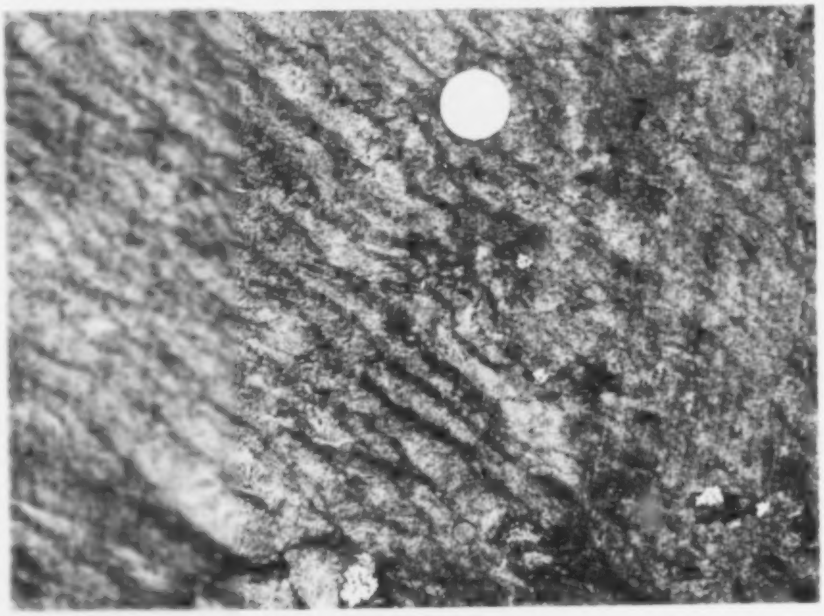

Photo 12. Closer view of S3 defined by dark 1-2 mm wide chlorite-rich cleavage bands separating quartz-carbonate-rich microlithons. Upper Canada Mine, L-NW stripping. Diameter of the coin is 2 cm.

At the L-NW stripped outcrop (Figures 16 and 17, Photos 11 and 12), there is a drastic change in the orientation of S3. S3, defined by 0.5-2 mm wide chlorite-sericite-rich bands, trends southeast (100°-110°) and is oriented approximately 30° clockwise to S2. In quartz-carbonate-rich microlithons, S2 typically shows S-asymmetric crenulation, indicative of dextral slip parallel to S3. In thin section, some sharp S3 planes are marked by trains of very fine-grained brown, near opaque leucoxene (?), probably representing insoluble residue left by pressure solution. Some discrete cleavage planes are noted to offset S2-parallel silica-rich bands, without preserving continuity of the latter.

Both S2 and S3 are overprinted by a steeply dipping, northeast-trending (065-080°), S4 foliation (Photos 13, 14, and 15). At the L-NW stripping, S4 occurs as thin discrete crenulation cleavage of S2 and S3. At the L-W stripping, tightly spaced S4 defines a shear zone in which tightly folded S3 underwent dextral (clockwise) rotation. On the L stripping, the overprint of S2 and S3 by S4 is particularly strong. North of the quartz-sericite-carbonate schist, S2 is isoclinally folded and transposed parallel to S4 with locally preserved intrafolial detached fold hinges. Originally north-trending S3 is also partially or completely transposed parallel to S4. Rotation of S3 into parallelism with S4 does not follow a consistent pattern: cases of both clockwise and counterclockwise rotation are documented on the L stripping. In thin sections from the L stripping, S4 is defined by discrete sericite- and pyrite-rich cleavage planes, transposed S2 and probably S3, and quartz fibres in fringes around pyrite grains. Pyrite trains along S4 planes locally transect pyrite-poor siliceous layers in microfold hinges, which supports at least some hydrothermal re-distribution of pyrite. In thin sections from the L-NW stripping, S4 occurs as a sharp discrete crenulation cleavage that is usually better developed in mica-rich domains and is marked by very fine opaque grains, possibly leucoxene.

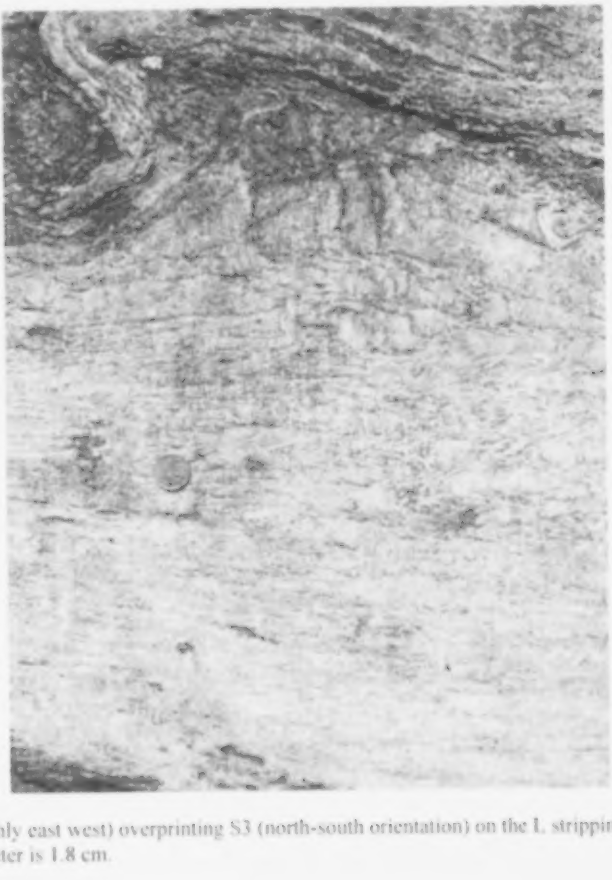

Photo 13. S4 (oriented roughly east west) overprinting S3 (north-south orientation) on the L stripping. Plan view; south is at the top of the photo. Coin diameter is 1.8 cm.

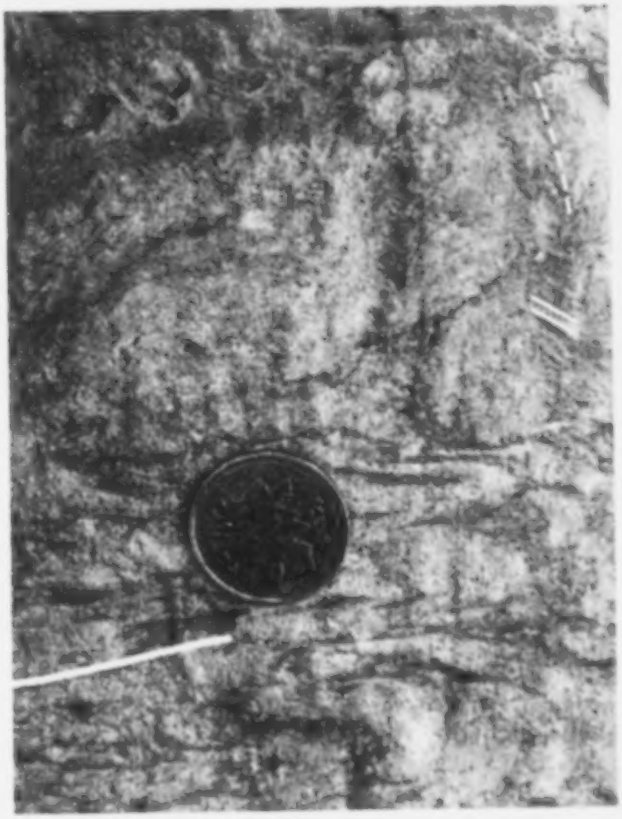

Photo 14. Close-up view of the area shown on Photo 13. S2 (double line) is preserved in S3 microlithons (oriented parallel to the dashed line). S4 (solid line) is axial planar to microfolds of S3.

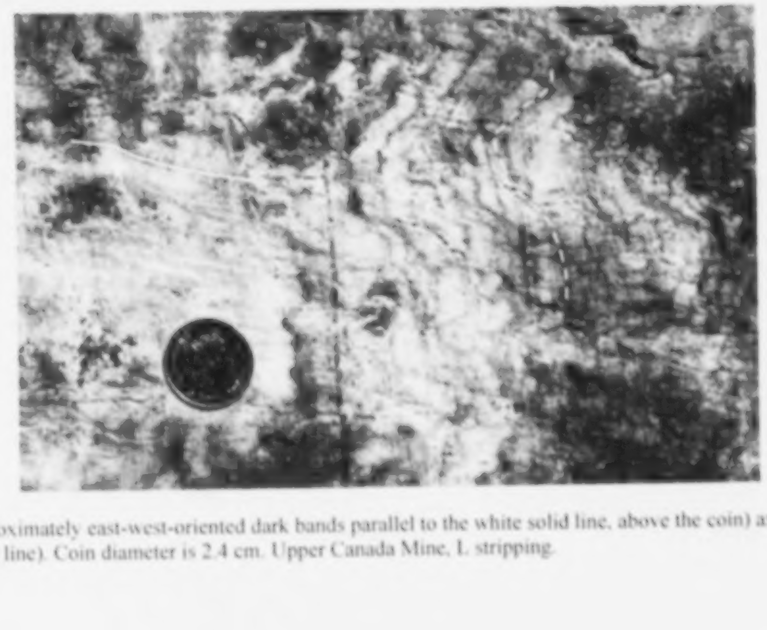

Photo 15. S4 (approximately east-west-oriented dark bands parallel to the white solid line, above the coin) axial planar to open folds of S3 (dashed line). Coin diameter is 2.4 cm. Upper Canada Mine, L stripping.

Within the band of quartz-sericite-carbonate schist, between channels 10 and 13, S2 is folded into northeast-plunging Z-asymmetrical folds with locally developed steep axial planar cleavage striking 030°-045° (Photo 9). In the syenite porphyry immediately south of this schist, Z-asymmetrical to symmetrical folds plunge 60-70° (to almost vertically) northeast and have steep, northeast-striking (about 030°-040°) axial planar cleavage (Figure 12). These folds are interpreted as F4 folds. Their axial planes are oriented counterclockwise with respect to S4 in highly strained tuffs (north of the syenite porphyry), possibly reflecting clockwise rotation of folds during the shear. Although the Z-asymmetry of F4 folds is more typical, it is important to note that east-northeast-plunging symmetrical and S-asymmetrical folds of S2 with axial planar S4 occur in the eastern part of the L stripping.

In addition to the pervasive fabrics described above, a non-pervasive crenulation foliation striking 110-120° is locally observed on the stripped outcrops. It postdates S3 and is overprinted by S4. At present, the significance of this fabric is not clear.

GOLD MINERALIZATION

Information on gold grades for the L stripped outcrop compiled from Toogood (1989) is shown in Figure 12. No quantitative assay data are available; gold grades are illustrated by bar graphs depicting variation from 1 to 10 g/t. The graphs do not differentiate the grades above 10 g/t; however, as evident from the original report, some values exceeded this arbitrary limit, reaching up to 28 and 42 g/t (Toogood 1989).

Toogood (1989) noticed a difference in gold grade distribution west and east of channel sampling line 11. West of this channel, gold occurs within a 0.3-2.0 m wide sharply bounded band of the quartz-sericite-carbonate schist at the north contact of the syenite porphyry body. Gold grades ≥ 10 g/t are fairly common in these carbonate-rich rocks. East of channel 11, the mineralized zone becomes wider. Grades ≥ 1 g/t occur over an 8-10 m wide zone, mostly north of the syenite porphyry body, and limits of mineralization, especially its north boundary, are no longer sharply defined. (A band of the quartz-sericite-carbonate schist can be traced to channel 7; it constitutes the southern flank of the mineralized zone between channels 7 and 10.) The swell of the mineralized zone is accompanied by a decrease in the average gold grade (Figure 12; see also Toogood 1989).

The mineralized zone trends 095° west of channel 13, and 070° east of it. Practically over its entire exposed length, mineralization occurs in pervasively quartz-sericite-carbonate-altered rocks with disseminated fine-grained pyrite. Most typical is a banded to laminated texture defined by intercalated S2-parallel carbonate-, sericite- and silica-rich, 2-5 mm wide bands (Photos 9 and 16). Some of these thin carbonate- and quartz-rich lamellae may be classified as veinlets, but due to their pervasive nature and impossibility to outline discrete veinlet swarms or vein zones, it is more appropriate to consider them as part of the pervasive alteration.

Apart from the quartz-sericite-carbonate schist, it is difficult if not impossible to distinguish gold-bearing from barren rocks in the outcrop. For example, between channels 8 and 11, tuffs exposed north of the assay-defined mineralized zone are strongly sericitized and silicified and contain abundant disseminated pyrite, but their gold grades are less than 1 g/t.

In one locality (channel 3), high gold grades correspond to an area of extensive quartz veining. These veins are macroscopically similar to barren veins seen elsewhere in outcrop. They may be more carbonate- and pyrite-rich (Toogood 1989) but the strong oxidation masks their original mineralogy. The material that was sampled by channel 3 included both veins and host rocks, and high grades may be related to gold contained in mineralized host rocks. Alternatively, the quartz veins in this part of the L zone may be gold bearing and different from barren veins observed in other parts of the outcrop.

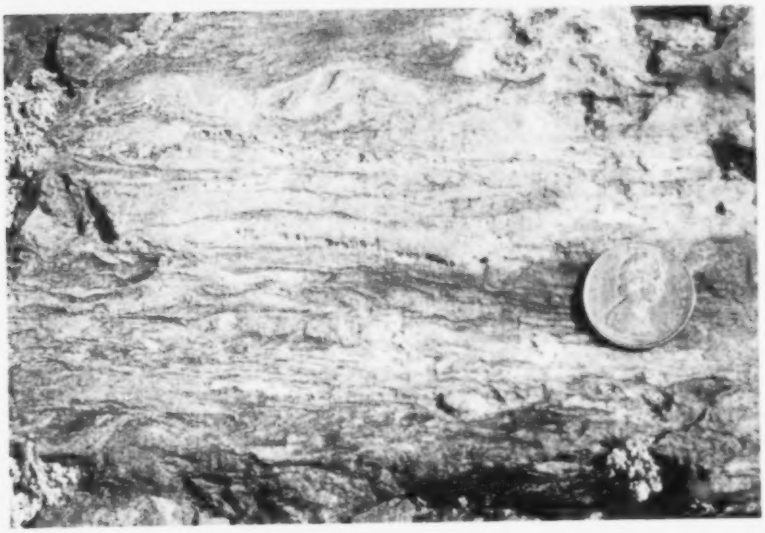

Photo 16. Close-up view of L mineralized zone in quartz-sericite-carbonate-altered tuffs (L stripping, near sampling line 7). Distinct are pervasive quartz-carbonate bands and veinlets (0.3-1 cm thick) separated by darker, sericite-rich bands.

In cut slabs and thin sections of the gold-bearing carbonate-rich schists (channels 10, 11 and 12), mineralized rock consists of interlayered 1-3 mm wide sericite-, carbonate- and silica-rich bands. This compositional banding defines the S2 foliation in altered rocks, along with alignment of individual mica flakes and strained quartz ribbons. Fine-grained (0.1-0.2 mm), largely anhedral pyrite occurs predominantly in sericite-rich layers, sometimes additionally concentrating along their boundaries. Native gold was observed in cut slabs and thin sections collected near channel 11 (sample 11-1, Figure 12, Photos 17 to 20). Gold (0.02-0.1 mm to 0.5 mm) occurs in thin (1-3 mm), carbonate-rich (carbonate>quartz), quartz-carbonate bands or veinlets that are parallel to S2 foliation and are folded with axial planar S4 (Photos 17 and 18). Gold shows no preferential association with S2-S4 –parallel pyrite segregations: gold grains are typically enclosed in quartz-carbonate gangue outside foliation-controlled pyrite clusters (Photos 18 and 19). Tennantite ($(Cu,Fe)_{12}As_4S_{13}$, identification confirmed by SEM) and minor chalcopyrite are associated with gold (Photos 19 and 20). In one location, a cluster of gold grains is accompanied by a few pyrite grains, some of which enclose small gold particles. Scheelite and relatively rare euhedral rhombic arsenopyrite are present in some gold-bearing quartz-carbonate bands or veinlets. Scanning electron microscope imaging of anhedral pyrite grains clustering along S2 foliation planes revealed no detectable gold inclusions in pyrite. Gold-bearing quartz-carbonate bands and veinlets appear less strained than some silica-rich bands defining S2. This may indicate that the veinlets were emplaced relatively late in the D2 deformation.

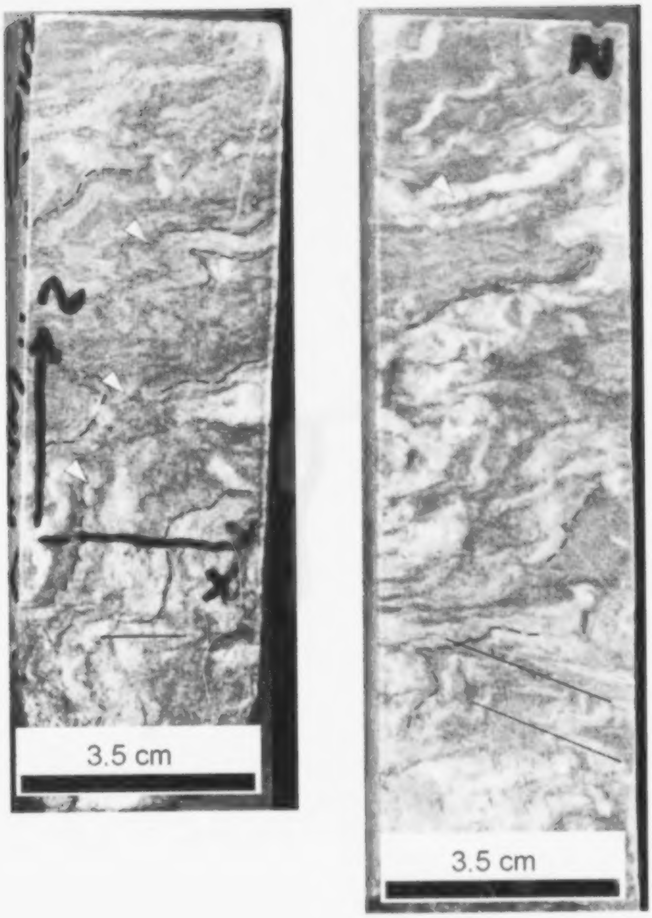

Photo 17. Cut samples from the Upper Canada L mineralized zone (gold-bearing quartz-sericite-carbonate schist near sampling line 11). The rock consists of intercalated sericite (dark)-, silica-, and carbonate (light)-rich bands that define S2. S2 (dashed lines) is folded with locally visible axial planar S4 (solid lines). Note that photographed surfaces are overturned from their actual orientation (as if they were viewed from inside outcrop upwards), as a result, folds show opposite (mirrored) asymmetry. In "normal" plan view, the folds are Z-asymmetric (see Photo 9 for the general outcrop view). Macroscopically visible (0.5-1 mm) native gold occurs in folded, S2-parallel, thin (2-5 mm) quartz-carbonate bands and veinlets (white pointers mark gold grain locations). Folding and S4 postdate gold mineralization.

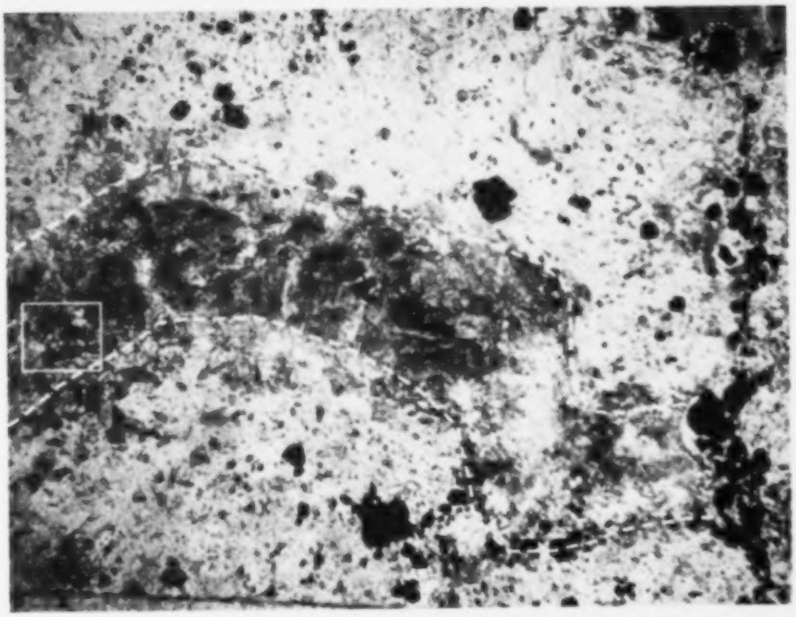

Photo 18. Photomicrograph (plane polarized light) of folded carbonate-rich gold-bearing veinlet transected by S4 cleavage plane ("vertical" train of opaque grains (pyrite) along the right-hand margin of the photo). Field of view is 4 mm. Rectangle corresponds to the area shown on Photo 19.

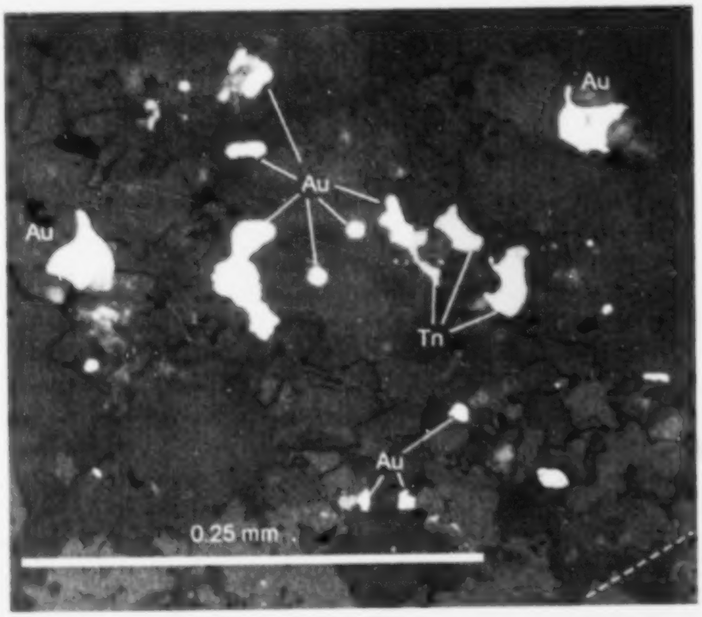

Photo 19. Reflected light photomicrograph of the rectangular area from Photo 18: Au, native gold; Tn, tennantite.

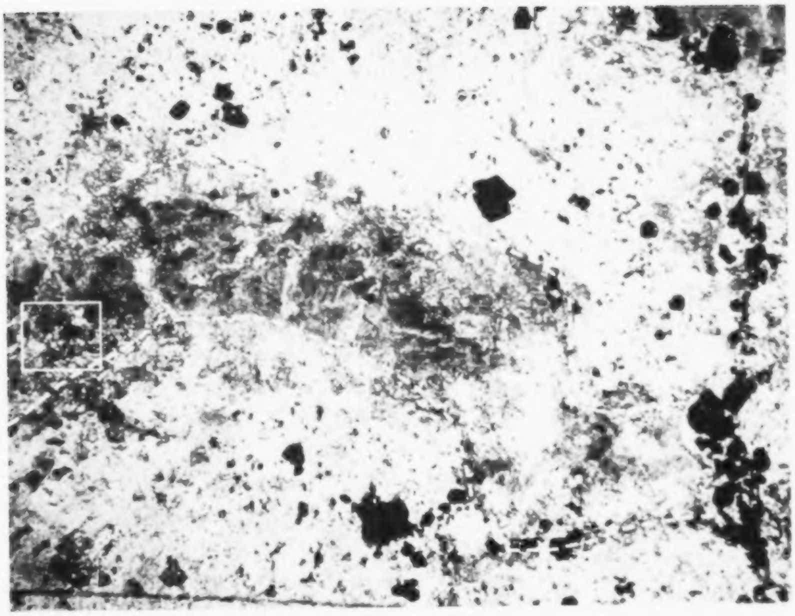

Photo 18. Photomicrograph (plane polarized light) of folded carbonate-rich gold-bearing veinlet transected by S4 cleavage plane ("vertical" train of opaque grains (pyrite) along the right-hand margin of the photo). Field of view is 4 mm. Rectangle corresponds to the area shown on Photo 19.

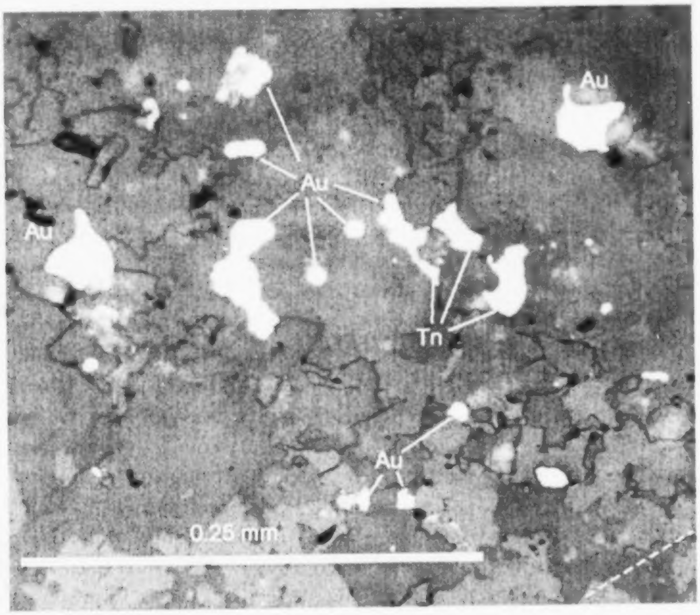

Photo 19. Reflected light photomicrograph of the rectangular area from Photo 18: Au, native gold; Tn, tennantite.

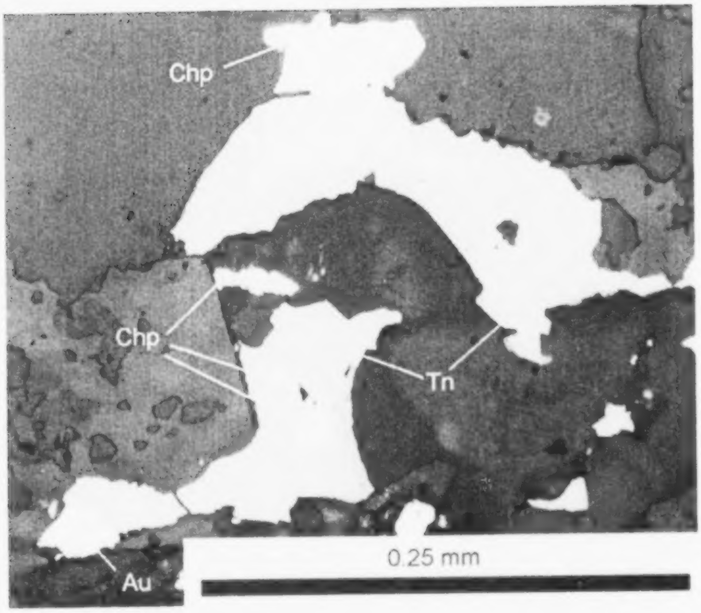

Photo 20. Reflected light photomicrograph: intergrowth of native gold (Au) with tennantite (Tn), and chalcopyrite (Chp) (Upper Canada Mine, L stripping).

RELATIVE TIMING OF DEFORMATION, HYDROTHERMAL ALTERATION AND GOLD MINERALIZATION

Relationships of alteration mineral assemblages and deformation fabrics documented in outcrops and thin sections suggest that there are multiple generations of quartz, sericite, and carbonate. However, the most extensive quartz-sericite-carbonate alteration broadly overlapped with the formation of S2, and possibly partially predated it. All subsequent stages of deformation were imposed on strongly sericitized, silicified and variably carbonatized rocks. This is because S2 is a compositional foliation defined by bands of deformed hydrothermal mineral aggregates. Formation of S2-parallel auriferous quartz-carbonate veinlets and extensive carbonatization within the gold-bearing zone is part of the main syn-D2 alteration event. The fact that gold-bearing quartz-carbonate (carbonate-rich) veinlets are more weakly strained compared to some silica-rich bands suggests that these veinlets could have formed relatively late in the D2 event. Some subordinate carbonatization occurred afterwards (probably episodically throughout the deformation history) as suggested by the presence of euhedral carbonate rhombs, scattered or clustering in small patches and overgrowing S2, S3, and S4. Similarly, apart from S2, sericitization is also associated with S3 (e.g., L-W stripping) and S4. The occurrence of S4-parallel quartz fibres in fringes around pyrite grains indicates at least some deposition (or redistribution) of silica during the latest deformation phase. In addition to these late quartz occurrences, there are barren quartz-carbonate veins that cut across S4. Pyrite is associated with S2; it also occurs along S3 foliation planes (e.g., L-W stripping), and is quite abundant along S4. Pyrite along S4 planes could have partially resulted from transposition of S2-related pyritic bands, and possibly accumulated as an insoluble phase during pressure solution along S4. However, some hydrothermal re-deposition probably took place. The typical anhedral shape of most pyrite grains may reflect their early deposition and subsequent deformation and partial dissolution. Unlike carbonate, sericite, quartz and pyrite, hydrothermal tourmaline was emplaced in a single late event. Relationships of tourmaline and deformational fabrics suggest that tourmalinization occurred after (or was partially

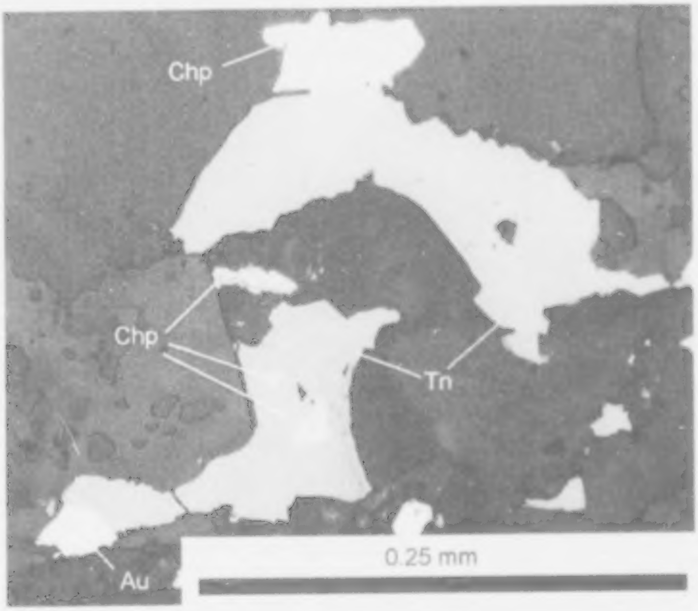

Photo 20. Reflected light photomicrograph: intergrowth of native gold (Au) with tennantite (Tn), and chalcopyrite (Chp) (Upper Canada Mine, L stripping).

RELATIVE TIMING OF DEFORMATION, HYDROTHERMAL ALTERATION AND GOLD MINERALIZATION

Relationships of alteration mineral assemblages and deformation fabrics documented in outcrops and thin sections suggest that there are multiple generations of quartz, sericite, and carbonate. However, the most extensive quartz-sericite-carbonate alteration broadly overlapped with the formation of S2, and possibly partially predated it. All subsequent stages of deformation were imposed on strongly sericitized, silicified and variably carbonatized rocks. This is because S2 is a compositional foliation defined by bands of deformed hydrothermal mineral aggregates. Formation of S2-parallel auriferous quartz-carbonate veinlets and extensive carbonatization within the gold-bearing zone is part of the main syn-D2 alteration event. The fact that gold-bearing quartz-carbonate (carbonate-rich) veinlets are more weakly strained compared to some silica-rich bands suggests that these veinlets could have formed relatively late in the D2 event. Some subordinate carbonatization occurred afterwards (probably episodically throughout the deformation history) as suggested by the presence of euhedral carbonate rhombs, scattered or clustering in small patches and overgrowing S2, S3, and S4. Similarly, apart from S2, sericitization is also associated with S3 (e.g., L-W stripping) and S4. The occurrence of S4-parallel quartz fibres in fringes around pyrite grains indicates at least some deposition (or redistribution) of silica during the latest deformation phase. In addition to these late quartz occurrences, there are barren quartz-carbonate veins that cut across S4. Pyrite is associated with S2; it also occurs along S3 foliation planes (e.g., L-W stripping), and is quite abundant along S4. Pyrite along S4 planes could have partially resulted from transposition of S2-related pyritic bands, and possibly accumulated as an insoluble phase during pressure solution along S4. However, some hydrothermal re-deposition probably took place. The typical anhedral shape of most pyrite grains may reflect their early deposition and subsequent deformation and partial dissolution. Unlike carbonate, sericite, quartz and pyrite, hydrothermal tourmaline was emplaced in a single late event. Relationships of tourmaline and deformational fabrics suggest that tourmalinization occurred after (or was partially synchronous with) S3 and pre-dated S4. Tourmalinization does not appear to bear any significance for gold mineralization at the Upper Canada Mine.

The 0.02-0.1 mm grains of native gold occur in S2-parallel, quartz-carbonate bands or veinlets and are not associated with abundant anhedral pyrite clustering along S2 and S4 planes. The presence of some submicroscopic gold in pyrite is possible, but this gold is unlikely to contribute significantly to the overall grade balance. Although available geochemical data are insufficient for robust statistical analysis, there is no tendency for correlation between gold grades and sulphide abundance expressed as sulphur percentage. Occurrence of gold in carbonate-rich veinlets concurs with the overall nature of the mineralized zone, especially west of channel 11, where gold grades ≥ 1 g/t are confined to a sharply bounded band of particularly carbonate-rich (CO_2 approximately 8-13%) schists. S4 foliation and related folding overprint the mineralized zone as a whole and individual 1-3 mm thick gold-bearing bands and veinlets, as observed on outcrop- and thin-section scales. In summary, the Upper Canada mineralized system experienced protracted (episodic or continouus) hydrothermal activity that spanned 3 deformation events. Gold was introduced during a syn-D2 hydrothermal episode as replacement-style and sheeted veinlets, probably simultaneously with major carbonatization, and all subsequent deformation and alteration stages modified existing mineralization.

The effects of overprinting hydrothermal and deformational events on gold distribution are somewhat difficult to evaluate. Toogood (1989) proposed that larger width and lower gold grade in the eastern part of the L stripping is due to remobilization during the development of the S4. He also suggested that the 40-60° easterly rake of near-linear ore zones is controlled by the intersection of S2 and S4.

We believe that the late deformation and hydrothermal event could have modified mineralization, but presently available data are insufficient to attribute variations in grade distribution to the D4 overprint. Observed grade patterns may, for example, reflect original lateral variation in mineralization style and be completely unrelated to the post-mineralization overprint. Similarly, the apparent parallelism of ore shoots and S2-S4 intersection does not automatically imply structural control imposed by post-mineralization, syn-D4 modification. The moderate easterly plunge of the ore shoots is parallel to L2 stretching lineation, and may represent the original, syn-mineralization geometry.

KINEMATICS OF THE UPPER CANADA DEFORMATION ZONE

No unequivocal syn-D2 asymmetric shear-sense indicators were documented within the stripped part of the Upper Canada deformation zone. The near-vertical dip of the zone and lack of significant displacement of the geophysically distinct contact of turbidites and volcanic rocks east of the Upper Canada Mine suggests a strong component of flattening strain during D2. With respect to D4, conflicting kinematic indicators (e.g., both Z- and S-asymmetric folds, clockwise and counterclockwise rotation of S3 associated with S4 can similarly be interpreted as indicative of largely compressional strain during the late deformation stage.

Previously, Toogood (1989) interpreted the Upper Canada deformation zone as a dextral shear zone, with S2, S3, and S4 (S1, S2, and S4 in Toogood's original nomenclature) representing S, "ecc", and C fabrics, respectively (cf. Platt 1984; Berthe et al. 1979; Lister and Snoke 1984). We disagree with this interpretation for following reasons. S2 orientations range from about 060° to about 100° (Figures 13, 15, and 17), which cannot be considered as systematically counterclockwise to the estimated 070° strike of the deformation zone. The orientation of S3 on the L-NW stripping and predominantly S-asymmetric crenulation pattern match the expected geometry of extensional shear bands. However, as S3 is oriented at a high angle to S2 and is commonly axial planar to folded S2 (L-W stripping), it cannot be interpreted as a dextral shear band fabric. S3 is a crenulation cleavage that overprints S2 and is in turn overprinted by S4, i.e., these fabrics are not contemporaneous. All 3 fabrics also occur outside the Upper Canada deformation zone, and are more probably related to consecutive regional deformation events rather than to the internal evolution of the Upper Canada deformation zone. Consequently, the geometric relationships between the three fabrics cannot be interpreted as shear sense indicators.

FACTORS CONTROLLING LOCALIZATION OF MINERALIZATION WITHIN THE UPPER CANADA DEFORMATION ZONE

Mineralized zones of the Upper Canada Mine occur within a roughly 1500 m long segment of the approximately 6000 m long Upper Canada deformation zone. The L mineralized zone that contributed 67% of gold production (Tully 1963) has a strike length of 300-600 m. On the scale of the deformation zone, gold-bearing rocks comprise an easterly plunging linear feature located close to the northeastern termination of the host structure. Factors controlling this location are not completely clear primarily due to the poor exposure of the area: almost the entire gold-bearing segment of the deformation zone east of former shaft #2 is unexposed. From what we presently know, two factors may potentially have played a role in localization of mineralization. The stock of rheologically more competent feldspar-phyric syenite porphyry ("white spotted porphyry") may have provided a "strain shadow" favourable for focusing fluid flow (e.g., Oliver et al. 2001 and references therein). Also, a northwest-striking turbidite contact discordant to the northeast-trending Upper Canada deformation zone may have acted as an impermeable barrier enhancing fluid focusing. Competency contrast between feldspar-rich syenite porphyry and less competent tuffs may have been a factor in small-scale localization of gold-bearing zones along the contact between the two rock types (e.g., L-stripping, Figure 12).

Gold Mineralization Along the Larder Lake–Cadillac Deformation Zone

ANOKI PROPERTY

Gold mineralization of the Anoki property comprises 4 major mineralized zones (Anoki Main, Anoki South, 40East, and Anoki Deep zones) and several smaller occurrences. All zones are outlined by drilling, and the Anoki Main zone is also developed by a ramp, which is presently flooded. Drill core from representative intersections of mineralized zones was examined as part of the present project. Geology of the Anoki property is shown on the accompanying geological map (P.3546–Revised, back pocket). A band of ultramafic talc-chlorite schists (Larder Lake Break, Thomson and Griffis 1941) separates mafic volcanic rocks of the Larder Lake Group (south) and Timiskaming sandstone-conglomerate sequence (north). Timiskaming alkalic volcanic rocks, expressed as a contrasting magnetic high on aerial magnetic maps, were uncovered by drilling 150-200 m farther north of the Larder Lake Group–Timiskaming contact. Compilation of drilling data of Queenston Mining Inc. revealed a pronounced flexure-like bend of the Timiskaming–Larder Lake Group contact in the western part of the Anoki area. There, the contact, marked by a band of talc-chlorite schists, changes orientation from about 110° to about 070°. The contact between Timiskaming volcanic and sedimentary rocks further north appears to follow the same pattern. Drilling also produced interesting data on deep structure of the south flank of the Larder Lake–Cadillac deformation zone (Figures 18 and 19). Basalts of the Larder Lake Group are underlain by a "South Splay" (Queenston Mining Inc. 2003), a northeast (roughly 070°)-striking and shallowly (35-40°) southeast-dipping fault marked by a sliver of variably carbonatized ultramafic rocks. Below this fault is a wedge-shaped unit of tuffs, sandstones and conglomerates that probably belong to the Timiskaming assemblage, although they are different from typical Timiskaming clastic rocks exposed and uncovered by drilling to the north. The South Splay is discordant to internal stratigraphy of the overlying Larder Lake basalt unit.

as seen from truncation of several interflow exhalite horizons, and of flow unit hosting the Anoki Main zone.

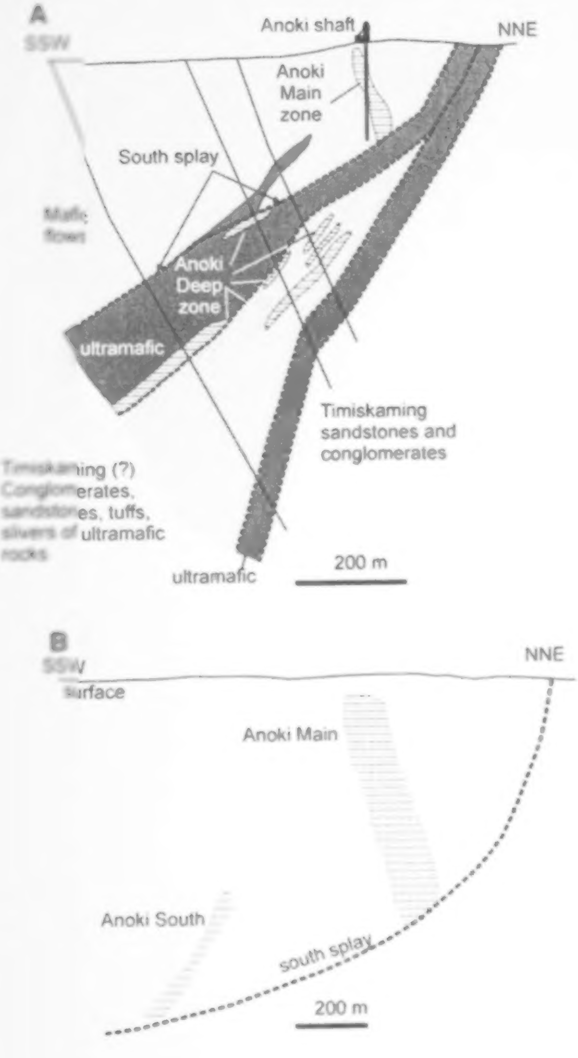
A
SSW
Anoki shaft
NNE
Anoki
Main
zone
South splay
Mafic
flows
Anoki
Deep
zone
ultramafic
Timiskaming
sandstones and
conglomerates
Timiskaming (?)
Conglomerates,
sandstones, tuffs,
slivers of ultramafic
rocks
ultramafic
200 m
B
SSW
NNE
surface
Anoki Main
Anoki South
south splay
200 m

Figure 18. Deep structure of the south flank of the Larder Lake–Cadillac deformation zone in the Anoki area. A) schematic cross-section illustrating geologic setting of the "South Splay", Anoki Main and Anoki Deep mineralized zones (approximate location of the cross-section is shown in Figure 2). Modified from a cross-section posted at Queenston Mining Inc. website (www.queenston.ca), downloaded in spring 2005. B) schematic cross section (located approximately 350 m east of the cross section A), illustrating relationships of Anoki South and Anoki Main zone with the South Splay. Anoki South zone is spatially associated with an interflow exhalite horizon enclosed in mafic volcanic rocks. Modified from Queenston Mining Inc. (2003).

as seen from truncation of several interflow exhalite horizons, and of flow unit hosting the Anoki Main zone.

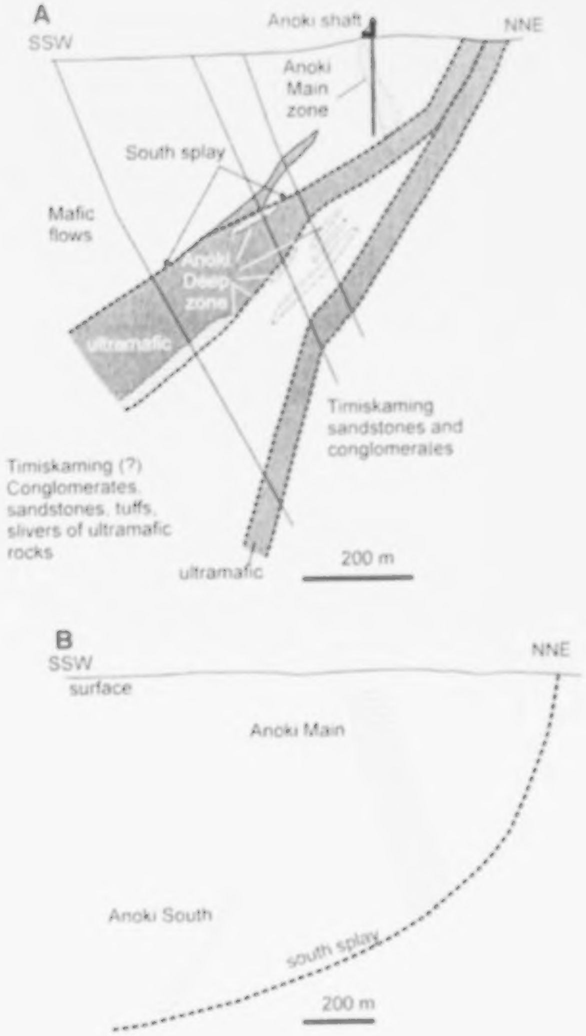
A
SSW
Anoki shaft
NNE
Anoki Main zone
South splay
Mafic flows
Anoki Deep zone
ultramafic
Timiskaming sandstones and conglomerates
Timiskaming (?) Conglomerates, sandstones, tuffs, slivers of ultramafic rocks
ultramafic
200 m
B
SSW
NNE
surface
Anoki Main
Anoki South
south splay
200 m

Figure 18. Deep structure of the south flank of the Larder Lake–Cadillac deformation zone in the Anoki area. A) schematic cross-section illustrating geologic setting of the "South Splay", Anoki Main and Anoki Deep mineralized zones (approximate location of the cross-section is shown in Figure 2). Modified from a cross-section posted at Queenston Mining Inc. website (www.queenston.ca), downloaded in spring 2005. B) schematic cross section (located approximately 350 m east of the cross section A), illustrating relationships of Anoki South and Anoki Main zone with the South Splay. Anoki South zone is spatially associated with an interflow exhalite horizon enclosed in mafic volcanic rocks. Modified from Queenston Mining Inc. (2003).

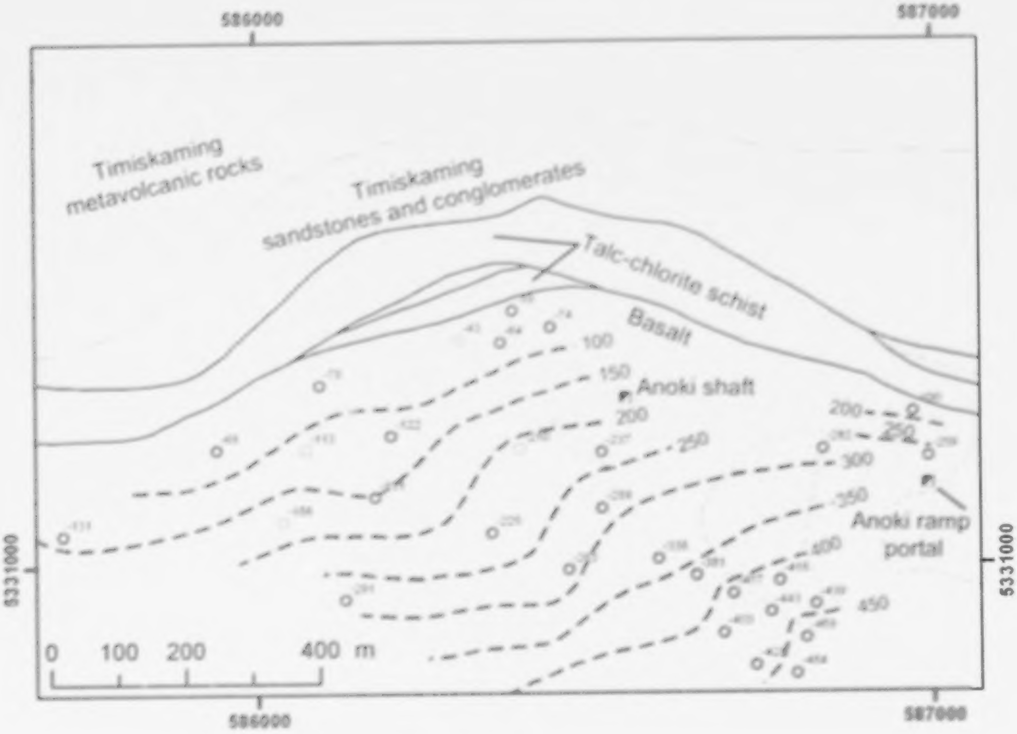
586000
587000
Timiskaming metavolcanic rocks
Timiskaming sandstones and conglomerates
Talc-chlorite schist
Basalt
100
150
Anoki shaft
200
250
200
250
300
350
Anoki ramp portal
400
450
5331000
5331000
0 100 200 400 m
586000
587000

Figure 19. Contour lines (thick dashed lines, numbers depict depth from surface in m) of the lower contact of Larder Lake basalts corresponding to the "South splay" (Anoki area, see accompanying Map P.3546–Revised for general geology). Based on drilling data of Queenston Mining Inc. (squares and circles are drill intersections of the contact).

Anoki Main Zone

The Anoki Main zone is a steeply (approximately 60-65°) north-dipping, east-southeast-striking, mineralized zone hosted in basalts of the Larder Lake Group (Queenston Mining Inc. 2003). The accompanying map (P.3546–Revised, back pocket) depicts the location of the uppermost part of the zone ("Anoki" in the list of gold occurrences). In a longitudinal section view, the mineralized zone has a shape of a 60 by 450 m band, plunging about 30° to the east (Figure 20). The upper surface of the South Splay constitutes the lower limit of mineralization. The mineralized zone consists of seven lens-shaped bodies containing measured and indicated resources of 2.98 t Au with an average grade of 5.7 g/t and inferred resources of 0.2 t Au with an average grade of 5.7 g/t (Queenston Mining Inc. 2003). Mineralization is approximately concordant to the internal stratigraphy of the basaltic sequence: cross section in Figure 4 in Thomson and Griffis (1941) shows near-parallel orientation of the mineralized lens and interflow cherty exhalite beds. In the present study, Anoki Main zone mineralization was examined in drill core (holes AN96-01 and AN03-61, Queenston Mining Inc.). Mineralization is spatially confined to a compositionally and texturally distinct flow unit. The unaltered protolith is a greenish dark grey to very dark green, chlorite-rich, strongly magnetic rock, commonly containing coarse (1-2 mm) magnetite grains and, in places, feldspar phenocrysts and glomeroporphyritic segregations. Pillow-rim textures, fine (hyaloclastitic ?) brecciation and inclusions of interflow cherts are recognized in places. Geochemical data for one relatively unaltered sample are presented in Appendix A (Table A.2); the major element signature of the rock, diagnostic of iron-rich tholeiite, was illustrated earlier (see Figure 4). Altered and mineralized rocks are massive, light grey to brownish light grey, and contain abundant pyrite cubes (1-3 mm, Photo 21). This is clearly a replacement mineralization; only few quartz and quartz-carbonate veinlets (0.3-1 cm thick) are present. Where bulk alteration is relatively weak, distinct 2-3 cm wide bleaching and sulphidation halos around thin quartz stringers are observed (Photo 22). In thin sections, mineralized rocks consist of massive aggregate of variably oriented euhedral to subhedral hydrothermal albite, carbonate, coarse (1-5 mm) pyrite, with minor quartz and relatively sparse sericite. Gold is macroscopically invisible and occurs as very small inclusions in pyrite. In thin section from a relatively high-grade interval (22 g/t), one gold particle 0.04 mm was observed in a fractured pyrite grain. Scanning electron microscopic (SEM) examination revealed the presence of sparse 2-10 µm rounded or veinlet-like gold segregations in pyrite (Photo 23). Perhaps a significant proportion of gold is present in even finer, disseminated or lattice-bound form, undetectable by SEM. Pyrite grains also contain inclusions of chalcopyrite (Photo 24), and more rare sphalerite and galena. In addition to 5-7% sulphur content related to strong pyritization, the Anoki Main zone is characterized by elevated Cu and As (Appendix A).

The sulphide-rich replacement mineralization, where micron-size gold is disseminated in pyrite, is most likely a result of sulphidation of an Fe-rich, high Fe/Mg protolith (e.g., Phillips et al. 1984; Ridley et al. 1996; Böhlke 1988). Similar depositional mechanisms are interpreted to have occurred at the Kerr Addison-Chesterville Mine hosted by the Larder Lake–Cadillac deformation zone (Smith et al. 1993; see also further discussion of Kerr Addison geology) and at the Holloway Mine spatially associated with the Destor–Porcupine deformation zone (Ropchan 2000; Ropchan et al. 2002). The Fe/Mg (weight %) ratio of the Anoki Main zone ranges from about 4.5 to about 7, which approximates or slightly exceeds corresponding ratios of Kerr Addison replacement "flow ore", and is generally below, but still comparable with the very high Fe/Mg values of the Holloway Mine mineralization (Figure 21). High Fe/Mg ratios favour formation of pyrite, whereas at low ratios (initial molar Fe/(Fe+Mg)<0.5) all Fe tends to be incorporated into Mg-rich carbonate, and sulphidation does not occur (Böhlke 1988). Molar Fe/(Fe+Mg) ratio of the Anoki Main zone protolith is approximately 0.65, i.e., the composition of the rock is favourable for sulphidation reactions.

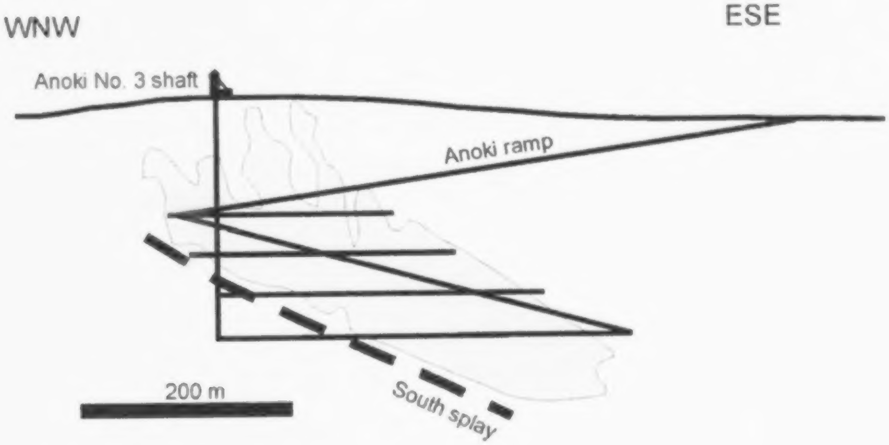

Figure 20. Anoki Main zone longitudinal section (modified from Queenston Mining Inc. 1996).

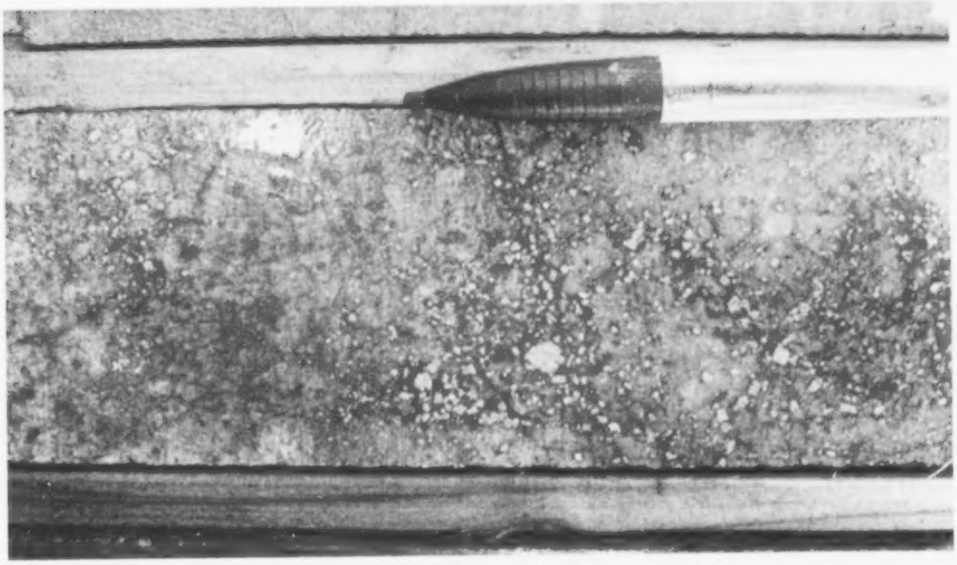

Photo 21. Strongly altered (albite, carbonate, pyrite, quartz) gold-bearing rock, western flanks of the Anoki Main zone.

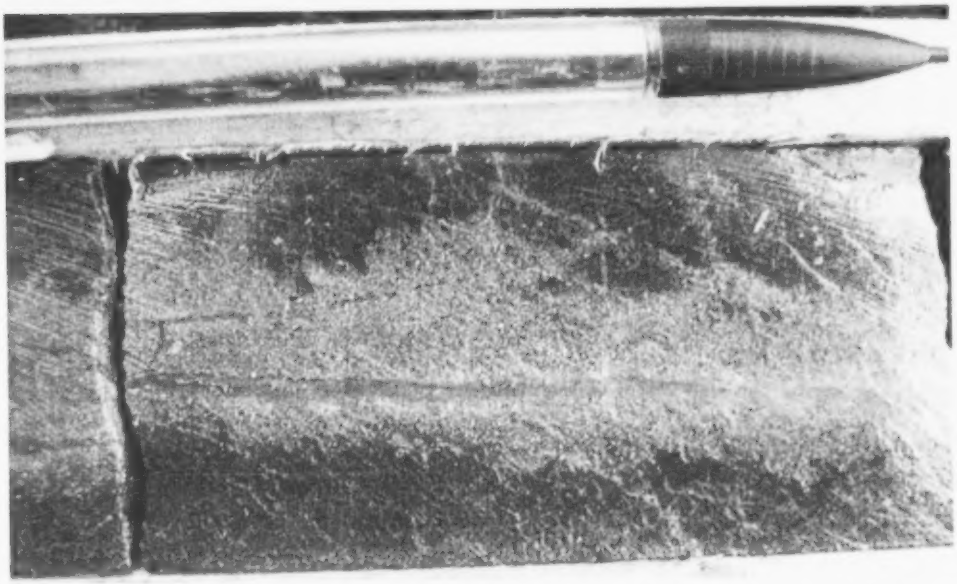

Photo 22. Drill core from western flanks of the Anoki Main zone. Sulphidation (pyrite) halo around a thin (2-3 mm) quartz stringer.

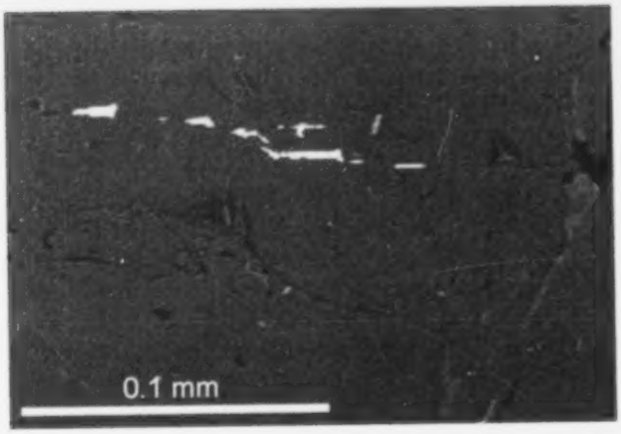

Photo 23. Backscattered electron image: veinlet-like segregation of gold (white) in pyrite (dark grey background) (Anoki Main zone).

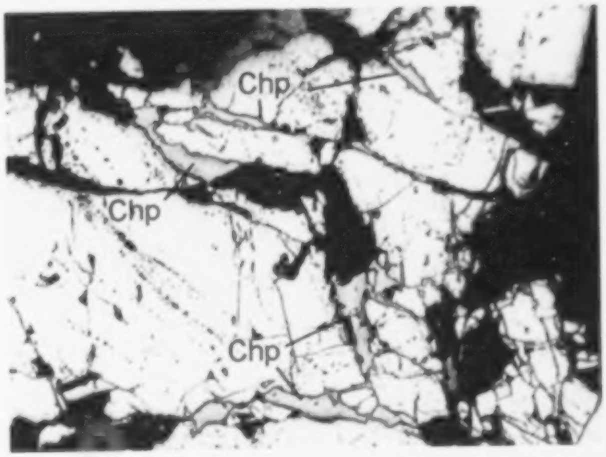

Photo 24. Photomicrograph (reflected light) of the Anoki Main zone mineralization: irregular segregations of chalcopyrite (Chp) in fractured pyrite (field of view is 0.25 mm wide).

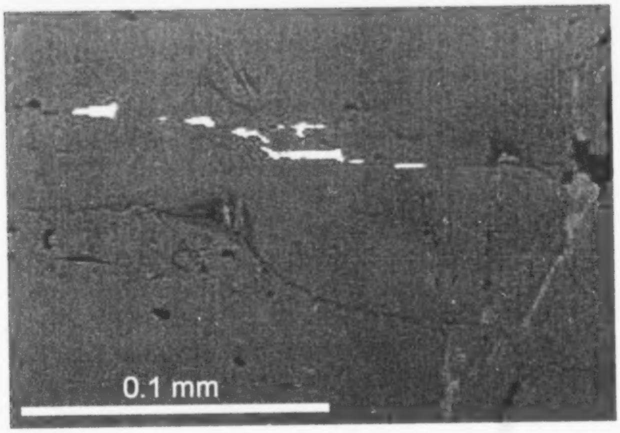

Photo 23. Backscattered electron image: veinlet-like segregation of gold (white) in pyrite (dark grey background) (Anoki Main zone).

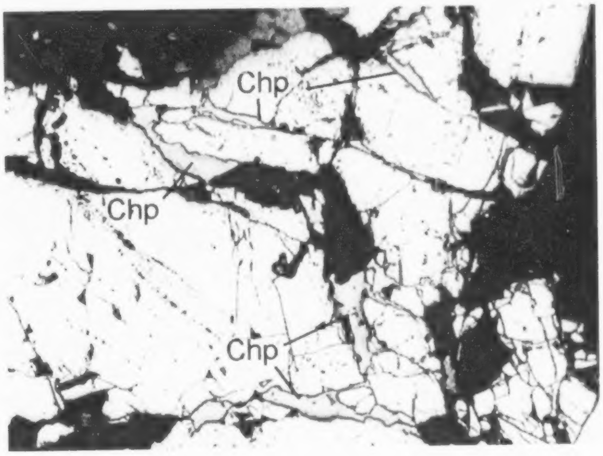

Photo 24. Photomicrograph (reflected light) of the Anoki Main zone mineralization: irregular segregations of chalcopyrite (Chp) in fractured pyrite (field of view is 0.25 mm wide).

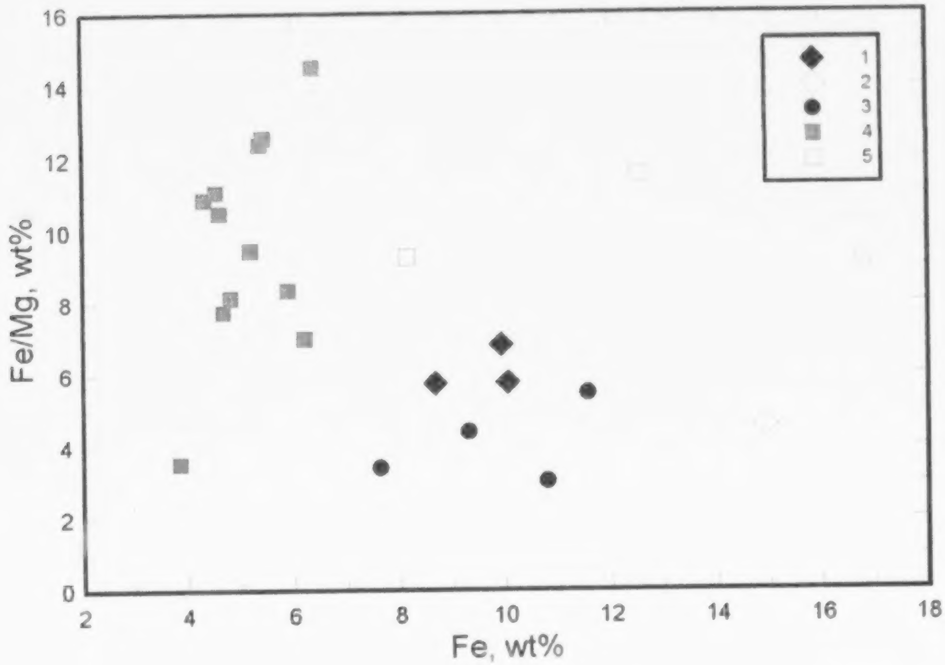

Figure 21. Fe/Mg (wt%) ratios of mineralized rocks of the Anoki Main zone, Kerr Addison flow ore (data from Warwick 1981) and replacement mineralization at the Holloway Mine (data from Ropchan 2000). 1-2, Anoki Main zone (Larder Lake Group, 1-mineralized rocks, 2-unmineralized protolith); 3, Kerr Addison flow ore, Au 19-27 g/t, Larder Lake Group, data from Warwick (1981); 4-5, Holloway Mine (4-mineralized variolitic rocks, Au 1-13 g/t; 5-mineralized Fe-tholeiites, Au 1-12 g/t).

Anoki South Zone

The Anoki South zone is hosted by a unit of siliceous (locally graphitic) interflow exhalites separating massive basalt flows of the Larder Lake Group. The host exhalite horizon strikes east-southeast and dips about 55° south. A 200 m long, 100 m wide and, on average, 3 m thick zone was explored by drilling 250-500 m below surface (Queenston Mining Inc. 2002, 2003). Inferred resources are 0.689 t of gold at an average grade of 6.5 g/t (Queenston Mining Inc. 2003). Mineralization consists of quartz veins and veinlets with visible gold, pyrrhotite, pyrite, chalcopyrite, cubanite and sphalerite. The South Splay constitutes the lower limit of the Anoki South zone (Figure 18). Geochemically, mineralization of the Anoki South zone differs from other gold occurrences of the map area by its distinctly higher base metal (Cu, Zn, Pb, ±Ni) content (Appendix A). This geochemical signature may reflect metal precipitation related to the presence of graphite or carbonaceous matter.

Anoki Deep Zone

The geologic setting of the the Anoki Deep zone is illustrated in Figure 18. Mineralization occurs in a wedge-shaped, south-dipping unit of presumably Timiskaming tuffs, sandstones and conglomerates that are macroscopically different from Timiskaming sandstones and conglomerates exposed further north. Tuffaceous and clastic rocks contain lenses and slivers of ultramafic talc-chlorite and carbonate-fuchsite schists. The South Splay and the Larder Lake Break confine the unit from south and north. Mineralization comprises several intervals of quartz veining enclosed by carbonate-fuchsite-altered ultramafic rocks, or by carbonatized tuffs and clastic rocks with disseminated pyrite. Mineralization is typically low-grade (1-5 g/t); the best intersection is 30.2 g/t over 4.0 m (www.queenston.ca). The upper contact of the Anoki Deep zone (i.e., the South Splay) constitutes the down-dip limit of Anoki Main and Anoki South zones.

40 East Zone

The 40 East zone is hosted in a band of Timiskaming clastic sedimentary rocks flanked by Larder Lake Group mafic-ultramafic rocks to the south and by Timiskaming alkalic volcanic rocks to the north. The northeast-trending, southwest-dipping zone was traced by drilling over a strike length of 600 m (Queenston Mining Inc. 2003). It comprises quartz-carbonate-feldspar veins and veinlets with 1-3% pyrite and visible gold enclosed in altered sandstones, and, at least in some drill intersections, spatially associated with carbonate-sericite-altered feldspar-phyric dikes or sills. The best intersections include 10.5 g/t over 0.9 m, 16.8 g/t over 2.7 m, and 11.5 g/t over 0.7 m (Queenston Mining Inc. 2003). Petrographic observations on one polished thin section of a strongly sulphidized (pyrite), carbonate-sericite-altered feldspar-phyric rock from the 40 East zone revealed the presence of very small (≤ 0.05 mm) gold particles in pyrite grains and carbonate gangue. Pyrite also contains sphalerite inclusions. Geochemical data for one drill intersection of the 40 East zone are presented in Appendix A.

MCBEAN

McBean mineralization is confined to a band of metamorphosed and hydrothermally altered ultramafic rocks at the southern margin of the Larder Lake–Cadillac deformation zone ("Larder Lake Break", Thomson and Griffis 1941). Numerous syenitic and felsic porphyry dikes constitute up to 50-60 volume % of the unit (illustrations in Bell 1987). Meta-ultramafic schists are flanked by gabbros to the south and by Timiskaming conglomerate and sandstone package to the north. Drilling data indicate that mineralization is spatially associated with a distinct bend in the attitude of the host lithologic units. In the mine area, the strike of the south Timiskaming contact changes from about 120° to about 080°-090°. This is accompanied by a change of dip angle from 75°-80° (southwest) to about 60° (south-southeast) (Figure 22). Mineralized zones have a strike length of about 600 m, they dip steeply south approximately parallel to lithological contacts, and plunge about 50° to the east. Mineralization was traced to 600-650 m below the surface and remains open down plunge. The mineralized zones contain measured and indicated resources of 4.26 t of gold with an average grade of 5.1 g/t, and inferred resources of 11.93 t of gold with an average grade of 6.5 g/t (Queenston Mining Inc. 2003). Gold values correspond to zones of quartz veining enveloped by carbonate-fuchsite schists ("green carbonate ore") and zones of variably intensive bulk alteration and sulphidation of syenite dikes (Bell 1987). The bulk of the ore that was mined from the presently flooded McBean open pit came from low-grade mineralized zones in altered syenite with disseminated pyrite (1.71-5.14 g/t, average 2.98 g/t; Bell 1987). The ore contained fine gold largely associated with pyrite that probably formed by sulphidation of primary magnetite in the dikes (Bell 1987). At deeper levels (below about 300 m depth) explored by Queenston Mining Inc., mineralization includes zones of quartz veining in carbonate-fuchsite schists and volumetrically subordinate quartz-carbonate-sericite-altered aphyric dikes with disseminated pyrite and small quartz veinlets. The grades in these deep zones are typically higher than those in the pit; visible gold in quartz veins was reported in several drill holes. In the present study, mineralization was examined in two drill holes (MB96-19 and MB96-12). Two foliations are observed in carbonate-fuchsite schists enveloping gold-bearing veinlets. The main foliation is defined primarily by compositional banding (i.e., intercalation of mica- and carbonate-rich bands) and is overprinted by discrete crenulation cleavage. Although drill core material provides only general orientation constraints, the two foliations likely correspond to S2 and S4 (Photo 25). Emplacement of gold mineralization and related carbonate-fuchsite alteration probably overlapped in time with S2 formation.

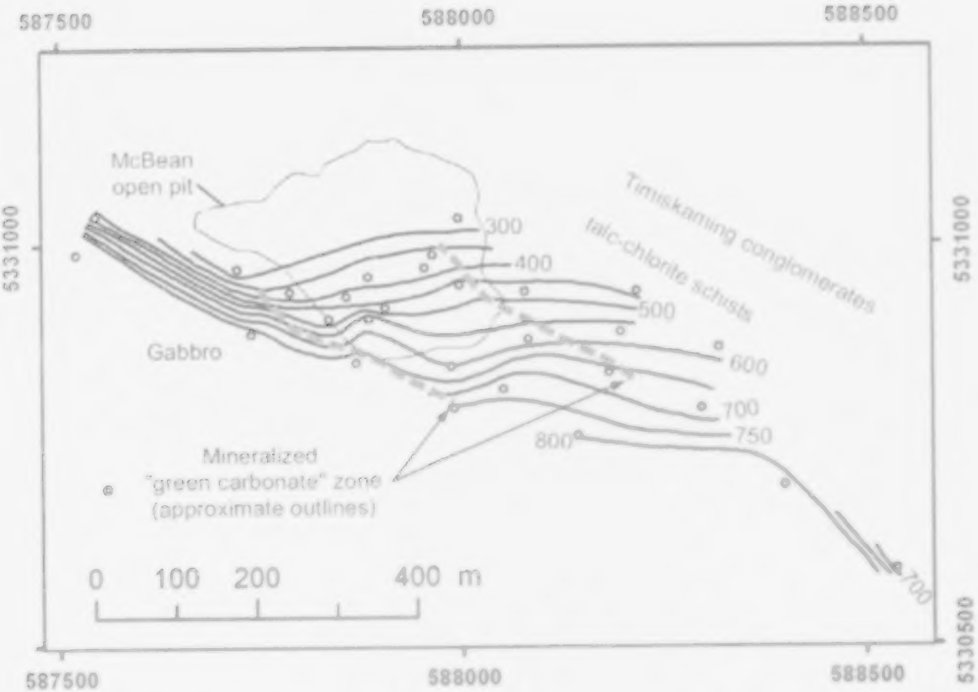
587500
588000
588500
5331000
5330500
McBean open pit
Timiskaming conglomerates
talc-chlorite schists
Gabbro
300
400
500
600
700
750
800
700
Mineralized "green carbonate" zone (approximate outlines)
0
100
200
400 m

Figure 22. McBean open pit area: contour lines of the south contact of Timiskaming conglomerates (footwall of the McBean mineralized zones) and approximate outlines of the green carbonate mineralized zone (depth about 300-700 m). Numbers depict depth (in m), circles correspond to drill intersections of the contact. Based on Queenston Mining Inc. drilling data.

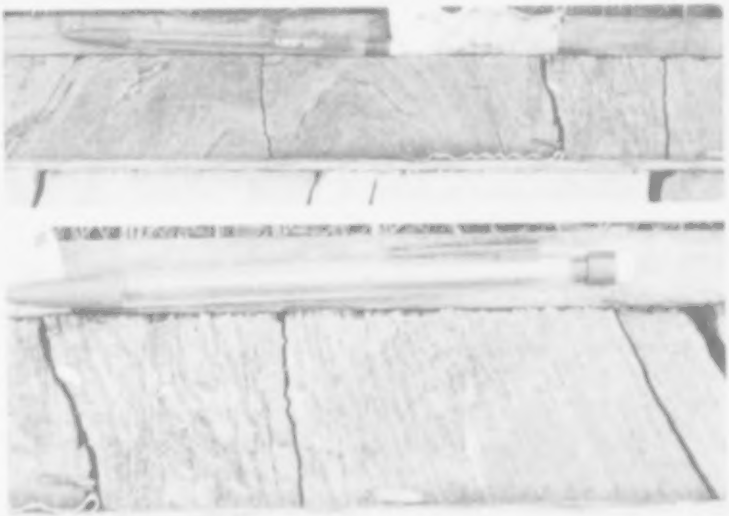

Photo 25. Drill core from the footwall of the McBean "green carbonate" mineralized zone (hole MB97-19). Photographed interval is located about 20 m down hole from the high-grade mineralization and is itself anomalous in gold (approximately 0.45 g/t). Top: fold closure; folded S2 defined by compositional banding of hydrothermal carbonate, fuchsite, and possibly chlorite. Bottom: axial planar discrete crenulation cleavage that is indistinguishable from S4 in surface outcrops. If hydrothermal alteration is directly related to gold mineralization, the relationships imply that mineralization occurred prior to or was broadly synchronous with D2 and was overprinted by D4.

In addition to the described mineralized zones there are several smaller showings, most of which are depicted on the geological map (see Map P.3546–Revised). Interesting are occurrences along the north flank of the Larder Lake–Cadillac deformation zone marked by a unit of mafic-ultramafic volcanic rocks: e.g., Murphy shaft zone and Princeton ("North Break") (see Map P.3546–Revised for locations). In both cases, mineralization appears to be spatially associated with a contact of Larder Lake mafic-ultramafic volcanics (south) and Timiskaming clastic rocks (north). Although these gold occurrences are economically insignificant, the presence of gold indicates that auriferous fluids were migrating along this part of the deformation zone. Better mineralization could possibly be found at more favourable depositional sites along the north flank of the Larder Lake–Cadillac deformation zone.

GOLD MINERALIZATION ASSOCIATED WITH THE LARDER LAKE–CADILLAC DEFORMATION ZONE IN MCVITTIE AND MCGARRY TOWNSHIPS

Thomson and Griffis (1941) recognized that mineralization of the Anoki and McBean (formerly Queenston) properties corresponds to the western continuation of a regional ore-controlling structure ("Larder Lake Break") that also spatially controls the location of the Kerr Addison-Chesterville, Cheminis, and Omega gold deposits, as well as several smaller occurrences in McVittie and McGarry townships (to the east of the Gauthier map area, Figure 23). The geology of the largest gold deposits associated with the Larder Lake–Cadillac deformation zone is briefly reviewed to further compare it with mineralization of the Anoki and McBean properties.

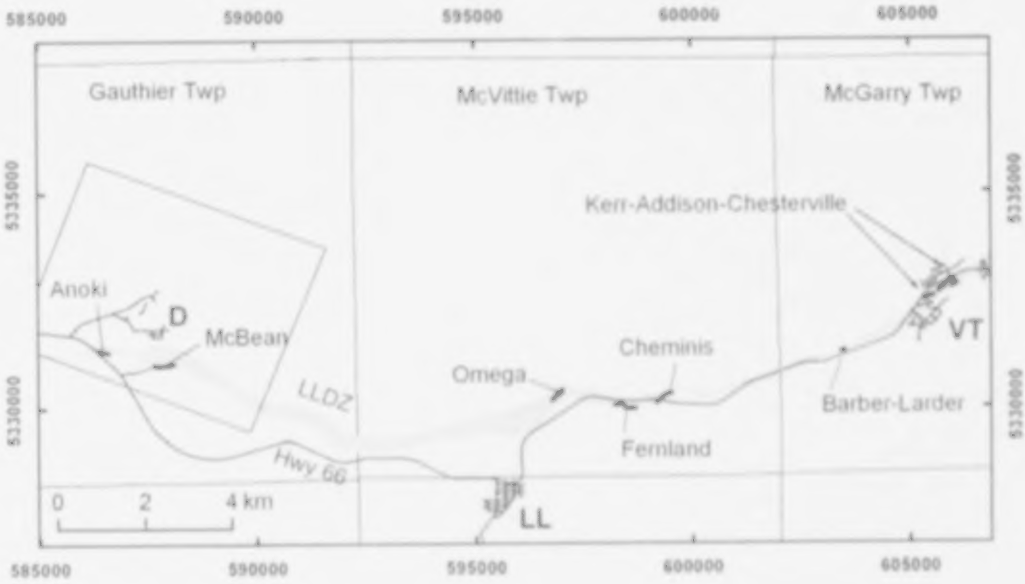

Figure 23. Schematic depicting location of gold deposits and major occurrences along the Larder Lake–Cadillac deformation zone (LLDZ). Abbreviated are town names: D, Dobie; LL, Larder Lake; and VT, Virginiatown. After Thomson (1941) and Smith et al. (1993).

Detailed information is available for the world-class Kerr Addison-Chesterville Mine that produced roughly 332 tonnes of gold (Smith et al. 1993; Kishida and Kerrich 1987). Mineralization is hosted by a mafic-ultramafic sequence of the Larder Lake Group, within the Larder Lake–Cadillac deformation zone. To the north, mineralization is bounded by a sliver of Timiskaming turbidites. The contact of Timiskaming turbidites and Larder Lake Group volcanics trends northeast and dips steeply north (Smith et al. 1993). Gold ore was mined to a depth of 1400 m (Smith et al. 1993). The alteration envelope associated with gold mineralization is tabular, 50-120 m thick, and steeply north dipping. In the longitudinal section view, it has a funnel-like shape, narrowing from 900 m (strike length) at surface to 300 m at a depth of 1700 m, and plunging about 70° to the east (Smith et al. 1993). Most of the gold (230 t Au at 11.0 g/t Au) was produced from replacement-style "flow ore", representing sulphidized, pyrite-rich, Fe-tholeiites and "green carbonate ore" comprised of quartz veins and stockworks in carbonate-fuchsite-altered komatiites (118 t Au at 7.8 g/t; Smith et al. 1993; Kishida and Kerrich 1987). Less significant mineralization types include "albitite ore" consisting of sulphidized dikes, sills and plugs (3 t Au at 3.9 g/t, plus about 5-15% of the green carbonate ore), and "graphitic ore" (sulphidized Fe-tholeiite with graphitic interflow horizons, and mineralized clasts in graphitic gouge of the late-stage Kerr fault, 14.3 t Au at 7.9 g/t; Smith et al. 1993). Mineralization is typically flanked by unmineralized talc-chlorite schists, both along and across the strike (Smith et al. 1993).

The Cheminis and Omega mines are located west of the Kerr Addison Mine, in McVittie Township. Both systems are hosted by the Larder Lake–Cadillac deformation zone, which in that area spatially coincides with a single or branching, 150 to 400 m wide band of intermingled mafic and ultramafic volcanic rocks of the Larder Lake Group, bounded by Timiskaming sedimentary and volcanic rocks to the north and south (Thomson 1941). Mineralized systems are spatially associated with broad S-shaped bends of the mafic-ultramafic belt along the Larder Lake–Cadillac deformation zone. Mineralization occurs along the northeast-trending segments of the mafic-ultramafic band. In both mine areas, lithologic units dip to the south: 70°-80° at Cheminis, and 60° (to 45° at depth) at Omega (Thomson 1941; Clark and Bonnar 1987).

Mineralization at the Cheminis Mine occurs as near-vertically plunging ore shoots, with a strike length of 50-150 m and explored vertical extent of about 1 km (Clark and Bonnar 1987). Based on available descriptions, pyrite-rich replacement of mafic lava and "cherty" tuff comprises the predominant mineralization type (Thomson 1941). Gold occurs as micron-size particles in pyrite; other sulphides include arsenopyrite, sphalerite, pyrrhotite and tetrahedrite (Clark and Bonnar 1987). Variably carbonatized ultramafic talc-chlorite schists flank mineralized zones. Occurrence of less significant "carbonate ore" probably related to quartz veining in carbonatized ultramafic rocks is reported on the website of NFX Gold, present owner of the Cheminis Mine (www.nfxgold.com).

In the Omega Mine, mineralization occurs within a roughly 750 m long zone. Replacement-style mineralization is predominant; gold-bearing quartz stockworks in carbonate-fuchsite-altered ultramafic rocks are minor (Thomson 1941). Pyrite-rich replacement ore is confined to petrographically distinct quartz phenocryst-bearing dacite horizons bordered by sheared and variably carbonatized talc-chlorite schists (Thomson 1941). Subordinate chalcopyrite and arsenopyrite occur in replacement ore along with pyrite. Smaller gold occurrences, e.g., Barber Larder (McGarry Township) and Fernland (McVittie Township), are similarly hosted by the Larder Lake–Cadillac deformation zone and consist mainly of sulphide-bearing replacement zones in volcanic rocks (Thomson 1941).

CHARACTERISTICS OF GOLD MINERALIZATION HOSTED BY THE LARDER LAKE–CADILLAC DEFORMATION ZONE

Gold mineralization at the Anoki and McBean properties is similar to the above-described gold deposits of McVittie and McGarry townships. In particular, the replacement-style, pyrite-rich Anoki Main zone shares strong analogies with the Kerr Addison-Chesterville flow ore, and replacement ores of Cheminis and Omega mines. Gold-bearing quartz stockworks in carbonate-fuchsite schists explored at depth at the McBean deposit and within the Anoki Deep zone are similar to the "green carbonate" ore at Kerr Addison-Chesterville. Mineralized aphyric dikes of the McBean ore zone strongly resemble the albitite ore of the Kerr Addison Mine described by Smith et al. (1993). Mineralization of the Anoki South zone that is hosted by a graphitic exhalite horizon may correlate to the graphite ore of the Kerr Addison-Chesterville Mine. Similarities in mineralization styles as well as analogous structural setting within the Larder Lake–Cadillac deformation zone suggest that gold-bearing zones of the Anoki and McBean properties are likely related to mineralization of Kerr Addison-Chesterville, Cheminis, and Omega mines. All these occurrences of gold mineralization are parts of a single regional hydrothermal system. The most characteristic features of this system are summarized below:

1. Gold mineralization is localized within a first-order structure, that is, the Larder Lake–Cadillac deformation zone (Smith et al. 1993), and (as far as we are aware) there is no tendency for preferential occurrence of larger deposits in second- and third-order structures;

2. Mineralization is commonly associated with gentle S-shaped bends along the Larder Lake–Cadillac deformation zone (Anoki, McBean, Omega, and Cheminis);

3. On the scale of the host deformation zone, mineralization tends to form linear shoots (strike length<dip length) that plunge roughly parallel to the regional stretching lineation (L2): e.g., 40-50° east at McBean (this study); approximately 70° E at Kerr Addison-Chesterville (Smith et al. 1993, p. 30); near vertical at Cheminis (longitudinal section in Clark and Bonnar 1987; structural data in Wilkinson 1993, p.142).

4. At least some mineralized zones are centered on relatively competent lava flow units (e.g., Omega, Cheminis, possibly Kerr Addison) that are flanked by rheologically weak and probably impermeable ultramafic talc-chlorite schists (e.g., Thomson 1941; Smith et al. 1993).

5. There are two principal types of gold mineralization: a) the economically most important style is the pyritic replacement ore where gold is present largely as submicroscopic particles in pyrite (accounts for about 65% of gold at Kerr Addison-Chesterville, most gold at Cheminis and Omega, and Anoki Main zone), and b) the second in importance are quartz stockworks and veins in carbonate-fuchsite-altered ultramafic rocks, where coarser gold is present principally in quartz. The two mineralization types coexist within individual deposits and are probably related to the same hydrothermal episode (e.g., Smith et al. 1993). Localization and shape of individual replacement ore bodies is typically defined by primary or structurally modified geometry of geochemically and rheologically favourable units (Smith et al. 1993; present study of the Anoki Main zone). Volcanic rocks of the Larder Lake Group constitute the most common protolith for replacement ores. Volcanic protoliths of the Anoki Main zone and Kerr Addison-Chesterville flow ore (Warwick 1981; Kishida and Kerrich 1987) are Fe-tholeiites. Carbonate is the major component in both mineralization types, which indicates that ore was generated by carbonic, CO_2 – rich fluids (e.g., Kishida and Kerrich 1987). Sulphidation of the Fe-rich, high Fe/Mg tholeiitic rocks must have constituted the main gold deposition mechanism for pyritic replacement mineralization (Böhlke 1988; Phillips et al. 1984; Smith et al. 1993), whereas relatively coarse gold in quartz veins enclosed in carbonate-fuchsite alteration was most likely deposited through phase separations (e.g., Smith et al. 1993). The latter mechanism agrees well with the rather irregular distribution of gold in "green carbonate

ore" (Smith et al. 1993) and occurrence of gold-barren quartz stockworks in carbonate-fuchsite schists. Both types of mineralization most probably belong to the syn-deformation greenstone-hosted quartz-carbonate vein (mesothermal-orogenic) deposit class.

6. Syn-mineralization hydrothermal alteration likely increased competency of host rocks; ultramafic talc-chlorite schists were modified into carbonate-fuchsite rocks with abundant quartz veining, the largely chloritic flow unit of the Anoki zone was replaced by albite-rich aggregate. In both cases, hydrothermal products are more rigid than the protolith, and are likely to respond more brittley to continuing deformation and maintain or even enhance permeability.

Occurrence of mesothermal gold mineralization in the first order deformation zone is unusual. Within the most economically significant gold camps, the largest gold deposits are typically found in subsidiary second- and third-order structures (e.g., Eisenlohr et al. 1989; Robert 1990; McCuaig and Kerrich 1998). This atypical localization pattern may be due to the nature of the Larder Lake–Cadillac deformation zone in the Larder Lake area. Lithological assemblage of the Larder Lake–Cadillac deformation zone includes competent mafic volcanic units intermingled with or enveloped by incompetent and impermeable ultramafic talc-chlorite schists (Thomson 1941). This combination probably constituted favourable ground for maintaining isolated discrete permeable fluid conduits within the deformation zone. Competent tholeiitic volcanic units responded more brittley, thus enhancing their overall permeability. Rheologically weak talc-chlorite schists enveloped these permeable zones, preventing fluid dispersal and maintaining high fluid/rock ratios within fluid pathways. Some of these competent units were also geochemically favourable for sulphidation (e.g., Fe-tholeitic, high Fe/Mg rocks), and gold deposition occurred.

The location of gold deposits in the Larder Lake–Cadillac deformation zone may (at least in part) reflect biases in exploration strategies, that is, the "Larder Lake Break" has for almost 100 years attracted the most attention from geologists and prospectors alike, and potentially gold-bearing subsidiary structures may have been overlooked. There is no geological factor precluding the occurrence of gold mineralization along subsidiary faults or shear zones that were hydraulically connected to the Larder Lake–Cadillac deformation zone during a regional hydrothermal mineralizing event. The presence of Fe-tholeiites in the Kinojevis assemblage and Larder Lake Group (north and south of the Larder Lake–Cadillac deformation zone) supports the possibility for formation of replacement-style gold mineralization along subsidiary splays of the Larder Lake–Cadillac deformation zone.

Relationships of Gold Mineralization in the Larder Lake–Cadillac and Upper Canada Deformation Zones and Structural Timing of Mineralization

Are the gold deposits along the Larder Lake–Cadillac and Upper Canada deformation zones genetically related? A definite answer to this question requires more detailed knowledge of fluid compositions (e.g., Neumayr and Hagemann 2002). However, our data suggest close relationships between gold occurrences in the two deformation zones. The Upper Canada deformation zone is probably a splay of the Larder Lake–Cadillac deformation zone, both zones are syn-D2 and could be hydraulically connected. In both deformation zones, mineralizing fluids were CO_2 -rich (i.e., carbonic), which resulted in carbonate-rich alteration assemblages at the Upper Canada, Anoki, McBean, and other gold deposits of Larder Lake–Cadillac deformation zone. The plunge of ore zones at the Upper Canada, McBean, Cheminis, and Kerr Addison is approximately parallel to stretching lineation L2. There are differences in the metal inventories of the different mineralized zones (Appendix A), but they are relatively minor and do not preclude a possible linkage between gold occurrences.

Syn-D2 introduction of gold is documented in the "L" mineralized zone of the Upper Canada Mine. For mineralization hosted by the Larder Lake–Cadillac deformation zone, the structural timing data are not so definitive. However, relationships between alteration and deformational fabrics in McBean drill core, and the likelihood of close relationships between mineralization in the two deformation zones, imply that gold mineralization hosted by Larder Lake–Cadillac deformation zone could also be broadly synchronous with D2.

Summary of Factors Controlling the Distribution of Gold Mineralization

All the gold deposits and occurrences discussed above occur in syn-D2 ductile deformation zones. The order of deformation zones does not appear to be a major controlling factor, at least as seen from the distribution of presently known deposits. Most deposits occur in northeast-trending structures, however there are exceptions and, more importantly, there is no indication that a northeast orientation is essential for the localization of gold deposits. In the Larder Lake–Cadillac deformation zone, some gold occurrences are spatially associated with bends along the host structure or lithological contacts within it. The setting of the Upper Canada mineralization may have been partially controlled by the syenite porphyry intrusion and the contact between the volcanic and turbiditic units. Geochemically favourable lithologies, such as Fe-tholeiites in Anoki Main zone and Kerr Addison flow ore, acted as chemical traps for replacement-style gold mineralization via host rock sulphidation. The presence of graphite or carbonaceous matter at the Anoki South zone could have assisted in the deposition of gold by changing the redox conditions of auriferous fluids. For other observed types of gold mineralization, host lithologies are unlikely to have directly controlled the gold deposition.

Teck Township Transect

The 36 km^2 transect includes the town of Kirkland Lake, and the area immediately west of it, south and north of the Highway 66 (Map P.3558, back pocket). The area is underlain from north to south by mafic volcanic rocks of the Kinojevis assemblage, clastic sedimentary rocks and alkalic volcanic rocks of the Timiskaming assemblage, and mafic volcanic rocks of the Tisdale assemblage intruded by the Murdock Creek pluton (Ayer et al. 2002). In this project, major ore-controlling structures were examined underground and mapped at surface at a scale of 1:10 000. Mapping was conducted mainly north of Highway 66 and was focused on Timiskaming assemblage rocks; only a few Tisdale and Kinojevis rock outcrops were examined. In addition, structural data were collected along the southern contact of the Timiskaming assemblage south of the town of Kirkland Lake.

GENERAL GEOLOGY

A description of the geology of the Kirkland Lake area can be found in Todd (1928), Thomson (1950), and Lackey (1990), and more detailed discussion of specific stratigraphic assemblages and units are presented by Hyde (1978, 1980), Lackey (1990), Mueller et al. (1994), and Legault and Hattori (1994a,b). The geology of the Kirkland Lake deposit is described by Todd (1928), Thomson et al. (1950), Charlewood (1964), Watson and Kerrich (1983), Watson (1984), Kerrich and Watson (1984), Lackey (1990), and Still (2001). The following brief description addresses only aspects of the geology that are relevant to the present study.

The Kinojevis assemblage underlies the northern part of the map area and consists of north-facing pillowed basalts and coarser gabbroic or dioritic rocks interpreted as intrusions or coarser flow units (Thomson 1950). North-facing Kinojevis volcanic rocks are unconformably overlain by Timiskaming sedimentary and volcanic rocks that form a 3 km wide northeast-trending band. Thomson (1950) documented the unconformable nature of the lower Timiskaming contact. In this project, the partially exposed unconformable north contact of the Timiskaming assemblage was observed in the newly stripped outcrops on the Marion-Boyce properties north of the town of Kirkland Lake. There, the north-facing pillow basalts of the Kinojevis assemblage are overlain by a roughly 4-5 m thick layer of basal breccias, consisting largely of angular clasts (1-3 cm to 20-75 cm) of the underlying basalts. Large (20-50 cm) pillow fragments can be unequivocally recognized by well-defined pillow rims. The breccias are interlayered with thinly (2-3 mm) laminated siltstones, and further up-section (southward) they are overlain by interlayered sandstone-siltstone.

With the exception of a small area west of Gull Lake, the Timiskaming rocks face south and dip steeply to moderately (approximately 50-70°) to the south (Thomson 1950). Alluvial-fluvial (e.g., Hyde 1980; Mueller et al. 1994) sandstones and conglomerates are volumetrically predominant in the Timiskaming assemblage. Corfu et al. (1991) reported a <2680±3 Ma U-Pb detrital zircon age for Timiskaming sandstone from the central part of the map area. Volcanic rocks include three major alkalic pyroclastic units named (from north to south): Grenfell, Goodfish, and Blanche River formations (Hyde 1978; Lackey 1990). The unit in the middle (Goodfish Formation of Lackey 1990) is disrupted and "duplicated" at surface by the Kirkland Lake fault (e.g., Todd 1928; Thomson 1950; Lackey 1990). To the south, Timiskaming rocks are bounded by the mafic-ultramafic volcanic rocks of the Tisdale assemblage. The latter are intruded by the 2672±2 Ma Murdock Creek pluton (Wilkinson et al. 1999).

The Larder Lake–Cadillac deformation zone corresponds to the southern margin of the Timiskaming assemblage (Wilkinson et al. 1999). About 2 km to the north, syenitic stocks are cut by the Kirkland Lake fault or Main Break, a brittle to brittle-ductile fault that strikes roughly 65° and dips steeply to the south. Gold mineralization of the Kirkland Lake deposit generally occurs along this fault and its immediate splays. Mineralization comprises relatively sulphide-poor quartz veins, with gold and associated tellurides occurring mostly in the veins rather than in the altered host rocks. In the currently active Macassa Mine at the western end of the camp, the main ore-controlling structure is the '04 Break. The '04 Break is a northeast-striking fault, which is parallel to and located 120-140 m north of the Main Break (Charlewood 1964; Still 2001). Ore-controlling faults and auriferous quartz veins are offset by major post-ore faults, including the Amikougami Creek, Tegren, Lake Shore, and Sylvanite faults (Thomson et al. 1950). No economic mineralization has been found to date west of the Amikougami Creek fault. Other significant faults include the northeast-trending Amalgamated Kirkland–Blanche River and Murdock Creek faults. The moderately (approximately 045°) north-dipping No. 5 fault exposed in underground workings of the Wright-Hargreaves Mine and apparently corresponding to the Murdock Creek fault at surface offsets the Main Break with a reverse sense of movement (i.e., north side up, about 125 m horizontal and about 150 m vertical components; Thomson et al. 1950; Hopkins 1940).

The history of gold discovery and production is discussed in detail in Thomson et al. (1950), Charlewood (1964) and Still (2001). Production commenced in 1915, and through the 20th century, the Macassa, Kirkland Lake Gold (later Kirkland Minerals), Teck-Hughes, Lake Shore, Wright-Hargreaves, Sylvanite and Toburn mines collectively produced 758.3 metric tonnes of gold from 49 862 868 tonnes of ore with an average grade of 15.21 g/t (Gosselin and Dube 2005). Gold was mined from one giant Kirkland Lake gold deposit. In the central part of the camp, underground workings extend to about 2.5 km below the surface, and mineralization remains open to depth (Charlewood 1964). Production-based (1913-1962) gold to silver ratio averages 5.4:1 for the entire camp, with the highest, 9.0:1, at Kirkland Lake Gold (Kirkland Minerals) and the lowest, 4.2:1, at Toburn (Charlewood 1964). At present, Kirkland Lake Gold Inc. owns the Macassa, Kirkland Minerals, Teck-Hughes, Lake Shore, and Wright-Hargreaves properties and produces gold from Macassa number 2 and 3 shafts and Lake Shore ramp (www.klgold.com). Operations at Macassa, where most underground observations were made during this project, presently extend from the 3400-foot to the 5000-foot level. The Amikougami Creek fault constitutes the western limit of presently known economic gold mineralization of the Kirkland Lake gold camp. On the east side of the fault mineralization extends vertically for about 1250 m (2900 to 7050-foot levels, M. Sutton and S. Carmichael, Kirkland Lake Gold Inc., personal communication, 2005) and is open at depth.

In addition to the Main Break and '04 Break mineralization (i.e., Kirkland Lake gold deposit), there are several smaller gold deposits and occurrences, including Amalgamated Kirkland (Stevenson et al. 1995), Federal Kirkland, Florena, and Hudson Rand (Kirkland Gold Rand, Thomson 1950). The geology and gold mineralization of these properties are not discussed in this report; most shaft sites are shown on the accompanying geologic map (Map P.3558, back pocket).

INTRUSIVE ROCKS

This section describes igneous rocks of the Kirkland Lake composite stock that hosts gold mineralization, and of smaller bodies intruding the Timiskaming assemblage in the general proximity to the Kirkland Lake fault (Main Break) and in the area north of it. The large Murdock Creek pluton located south of the Larder Lake–Cadillac deformation zone was not examined in this project and is not discussed here.

The petrography of the intrusive rocks was previously described by Todd (1928), Thomson (1950), Watson (1984), Hicks and Hattori (1988), and Hattori and Levesque (1989); the geochemistry was characterized by Watson (1984), and Kerrich and Watson (1984). The descriptions presented below are based on original observations of this study. The geochemistry of the intrusions is briefly illustrated in the section on intramineral dikes.

Alkalic igneous rocks are subdivided into three phases (from the earliest to the latest phase): mafic (augite) syenite; syenite; and syenite porphyry. Mafic (augite) syenite forms the western part of the composite stock transected by the Main Break, and a large, up to 350 m wide, body 500-800 m north of the Main Break. The two bodies apparently join at depth (e.g., Charlewood 1964). Mafic syenite consists of pyroxene (augite), K-feldspar, locally biotite, and minor plagioclase. Visually estimated percentage of augite varies from 25 to 60%. In most locations, pyroxenes are to a variable extent replaced by chlorite and carbonate. Most augite syenites are near equigranular (2-5 mm grain size); porphyritic varieties with augite phenocrysts and fine-grained, feldspar-rich groundmass were observed in small dikes in the northwest part of the area (north of the railway). Hydrothermally altered mafic syenite has a characteristically spotty appearance defined by dull-green to greenish light grey pseudomorphs after pyroxene set in a red, K-feldspar-rich matrix. A distinct characteristic of augite syenite is the presence of 0.5-1 cm to 10-20 cm thick leucocratic band-like inclusions informally called "felsic ribs". Texturally, these inclusions vary from aphanitic to coarse-grained, the latter consisting of long-prismatic K-feldspar (3-5 mm). The constant presence of leucocratic bands marks the originally anisotropic nature of the mafic syenites and existence of primary (magmatic) planar fabrics in the intrusions. An example of such fabric is shown in Photo 26, from the Narrows Break stripped outcrop, where closely spaced (10-15 cm) thin felsic ribs are oriented parallel to the contact of the intrusion. Some gold-bearing quartz veins at the Macassa Mine are oriented approximately parallel to these "felsic ribs" indicating that vein-hosting fractures could have exploited primary anisotropy of the intrusions (Photo 27). Sharp contacts between the mafic syenite intrusions and host sedimentary and pyroclastic rocks were observed in several locations. Although the contacts are undoubtedly intrusive, and bedding is commonly truncated on a small scale, the overall orientation of observed contacts is approximately parallel to bedding in the Timiskaming rocks.

Syenite constitutes a relatively minor rock type, which forms an irregular pipe-like body exposed along the Main Break on the Teck-Hughes and Lake Shore properties. It plunges 30° to 40° southwest. The upper contact of this pipe-like body approximates the upper boundary of the Main Break gold mineralization from the former Kirkland Lake Gold shaft #1 to Macassa shaft #1. Typical syenite is a hollocrystalline rock consisting almost entirely of randomly oriented subhedral to anhedral prismatic K-feldspar; varieties that are transitional to mafic syenite may contain up to 20% pyroxene. In addition to the pipe-like syenite intrusion exposed on the Teck-Hughes property, a narrow body of syenite was mapped roughly 550 m north of the Main Break, along the contact of a large mafic syenite intrusion. Syenite in that location contains approximately 15% pyroxene and probably represents a rock type transitional to mafic syenite. Todd (1928) reported sharp intrusive contacts between syenite and mafic syenite, and Watson (1984) described both sharp and gradational contacts.

Syenite porphyries form a 2 km long by 0.5 km wide body that underlies the northern part of the town of Kirkland Lake and hosts gold mineralization at the former Lake Shore, Wright-Hargreaves, Sylvanite, and Toburn mines. In addition to this large intrusion, syenite porphyries occur as numerous smaller dikes, sills and stocks throughout the map area. Two textural varieties were identified during mapping; for descriptive purposes they are named "feldspar-rich" and "sparsely porphyritic". Apart from rare exceptions, these two varieties are macroscopically distinct, and can be mapped as separate rock types, however they are not distinguished on Map P.3558. This is because systematic re-mapping of intrusive phases was not among the main objectives of this project, and only a few syenite porphyry intrusions were examined.

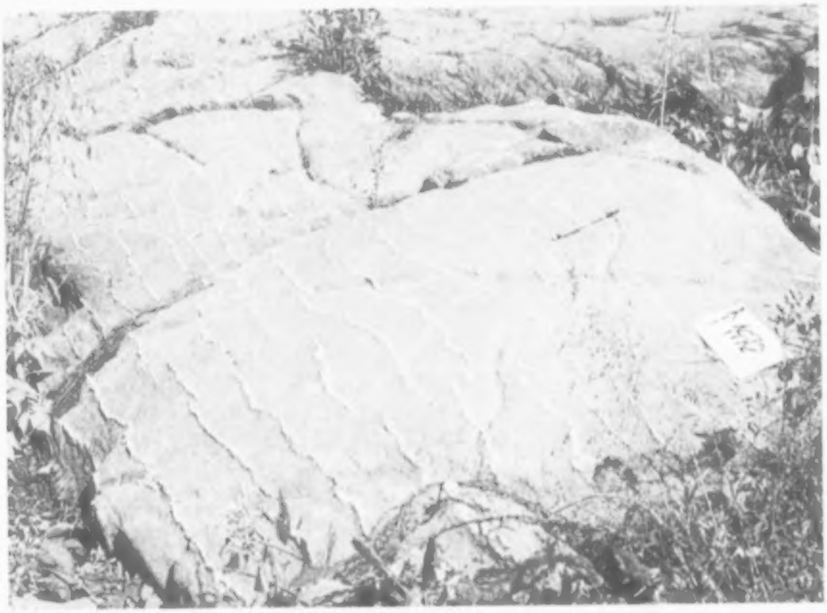

Photo 26. Outcrop of mafic syenite on the Narrows Break stripped outcrop. Magmatic foliation defined by thin (0.5-2 cm) feldspathic bands ("felsic ribs") spaced at 15-30 cm and oriented approximately parallel to the contact of the intrusion.

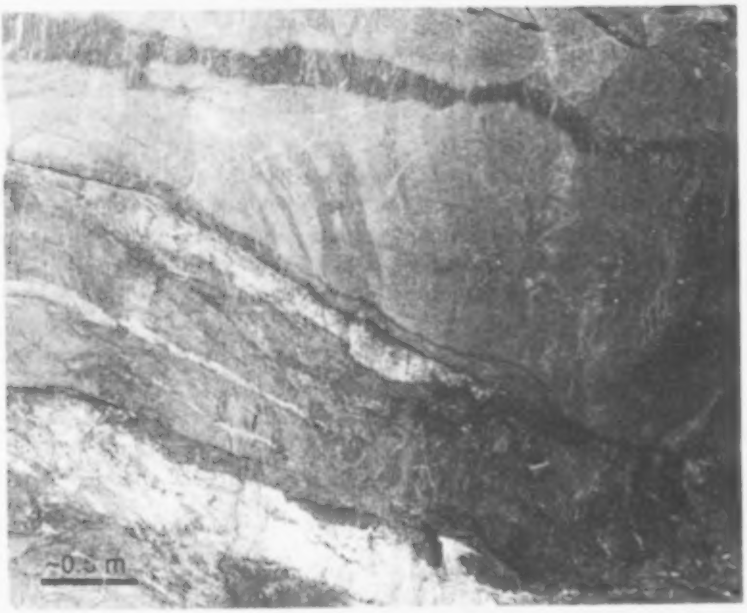

Photo 27. North wall of stope 4225, Macassa Mine. In the upper part of the photograph, note the large leucocratic band ("felsic rib", maximum thickness approximately 30 cm) in mafic syenite. Quartz veins have a similar orientation indicating that vein-hosting structures may have been exploiting primary anisotropy of intrusive rocks.

"Feldspar-rich" syenite porphyry is a massive rock that contains 30-50% fine (1-2 mm to 3-4 mm), short prismatic to subequant plagioclase phenocrysts along with 5-10% biotite, and less commonly amphibole. Also characteristic is the presence of green angular aphanitic xenoliths, presumably of mafic volcanic rocks (Photo 28). The presence of xenoliths is so typical that it is used by mine geologists as a diagnostic feature to distinguish syenite porphyries from syenites in underground workings throughout the camp. Our observations indicate that the main intrusive body of the Kirkland Lake stock (hosting Wright-Hargreaves, Sylvanite and Toburn mineralization), and associated dike-like apophyses probably consist of this rock type, although not all exposures of the main intrusive body were examined. In addition to the main stock, a smaller, 700 by 100 m intrusion immediately west of the former Kirkland Lake, south of the railway and about 400 m north of the Main Break, also consists of this syenite porphyry variety.

Sparsely porphyritic syenite porphyries differ from feldspar-rich varieties by lower feldspar phenocryst contents (5-15 to 20%, Photo 29), their larger size (1-5 mm), and by a significantly higher percentage of mafic minerals (20-35%), represented mainly by amphibole (0.25-1 mm, to 3 mm locally) and subordinate biotite. Very melanocratic syenite porphyries, with up to 50% amphibole and 5-15% feldspar, form a 100-200 m wide elongate intrusive body stretching roughly parallel to and 200-250 m south of the Timiskaming-Kinojevis contact, east and west of the Amikougami Creek fault. In addition to green aphanitic xenoliths, sparsely porphyritic syenite porphyries also contain rounded (pebble- to cobble-like) granitoid xenoliths that are 5 to 20 cm in diameter (Photo 30). Xenoliths of high-grade crystalline schist and vein quartz (1cm by 3 cm) were observed in one locality. Direct relationships between the two varieties of syenite porphyry were not observed. Dikes of "feldspar-rich" syenite porphyry crosscut mafic syenite and syenite bodies.

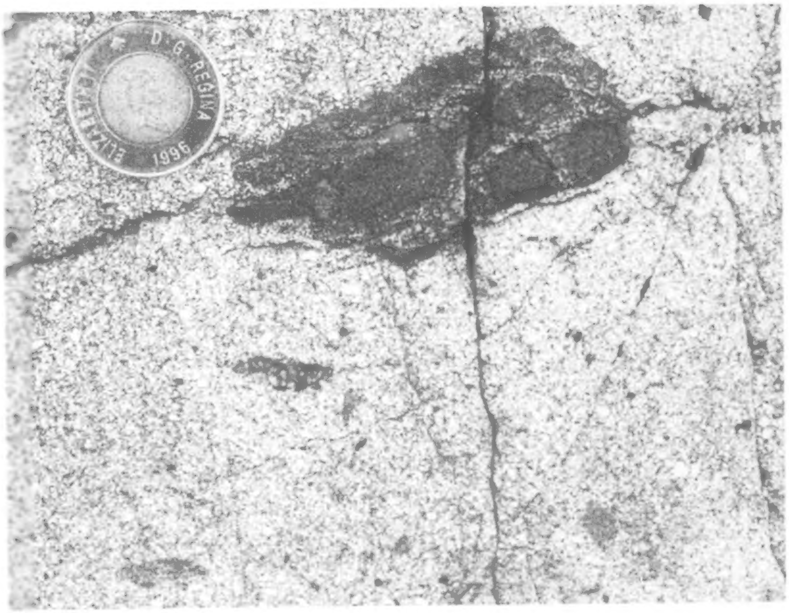

Photo 28. Feldspar-rich syenite porphyry with a chloritic xenolith. Note high percentage of fine-grained feldspar phenocrysts (white). Coin diameter is approximately 2.5 cm.

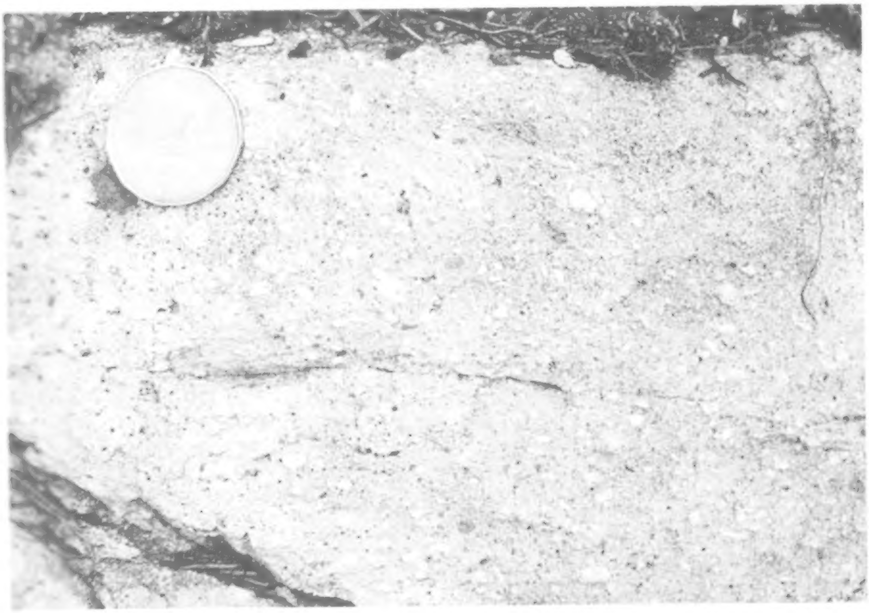

Photo 29. Sparsely porphyritic variety of syenite porphyry, coin diameter is approximately 2.5 cm.

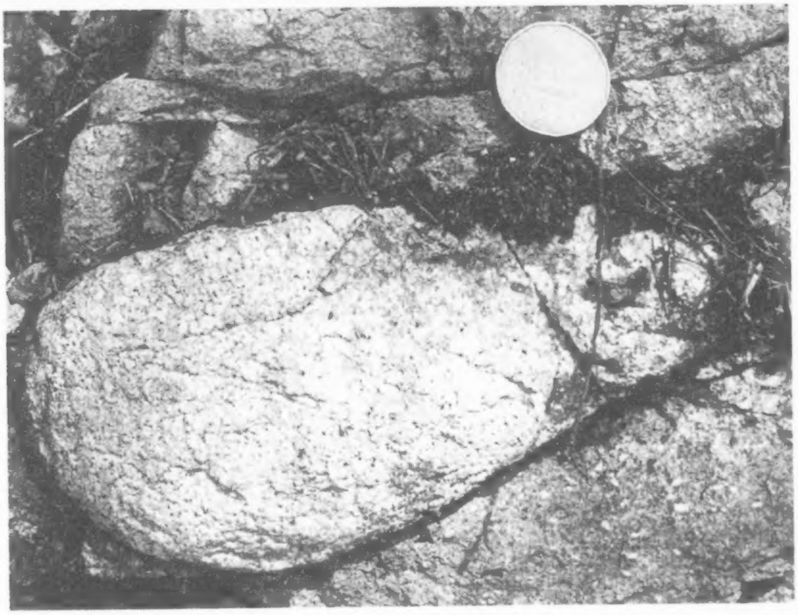

Photo 30. Pebble-like leucocratic granitoid xenolith in sparsely porphyritic syenite porphyry.

A somewhat different variety of feldspar-phyric rocks was observed on a small peninsula along the west shoreline of the former Kirkland Lake, about 450 m north of the railway. The rock has a light green matrix and contains about 20% feldspar phenocrysts (1-5 mm). It is non magnetic, whereas typical syenite porphyries are moderately magnetic. On the map by Hopkins (1949, plate 1) this rock is depicted as granite porphyry. Most exposures of the granite porphyry are to the east of former Kirkland Lake, where the rock forms a 100-200 m wide east-northeast-trending body. It is probably the equivalent of a quartz-feldspar porphyry body uncovered by a long north crosscut at the 3075-foot level at the Lake Shore Mine (Thomson et al. 1950, p.151). Outcrops on the east side of the former Kirkland Lake were not examined in this project. On the accompanying geologic map (Map P.3558), the rocks are shown as syenite porphyries (as compiled from Thomson 1945), however, they almost certainly represent a separate intrusive phase.

A distinct rock type occurs north of Highway 66, immediately west of Amikougami Creek. This porphyritic rock contains prismatic phenocrysts of feldspar and pyroxene set in an aphanitic groundmass. The rocks form a 300 m wide southwest-trending body that reportedly has an intrusive contact with host tuffs (Thomson 1950). On Map P.3558, the rock is described as trachyandesite based on field identification. Geochemically, these rocks are very similar to mafic syenites and may represent their hypabyssal equivalent (see geochemical plots in a section describing intramineral dikes). Other intrusive rocks include coarse biotite lamprophyres, Matachewan diabase dikes and intramineral dikes (the latter are discussed in a separate section).

The shapes of alkalic intrusions were previously discussed by Thomson et al. (1950). The ore-hosting composite intrusion which consists from west to east of mafic syenite, syenite and syenite porphyry is aligned approximately parallel to the host stratified units. Its south contact dips more shallowly than the northern contact, and the body widens with depth (Thomson et al. 1950). Near Macassa shaft #1, the steeply (roughly 75-80°) dipping mafic syenite intrusion crosscuts more shallowly south-dipping tuffs and conglomerates, however the dip of the southern contact becomes more shallow below the 2000-foot level, and the body widens to the south at deeper levels (Thomson et al. 1950). As can be judged from cross sections, Main Break ore does not occur in the upper, narrow and steep portion of the intrusion (e.g., Thomson et al. 1950, sheet A, cross-section 2).

The geometry of a large mafic syenite intrusion that hosts mineralization in the central-western parts of the camp can be interpreted as a combination of a larger (200-250 m wide on surface) approximately concordant part and relatively narrow (50-80 m) northeast-trending (roughly 060-070°), steeply south-dipping (roughly 80°) apophyses that are generally discordant to the host rocks (Figure 24). The western boundary of the syenite pipe-like body corresponds to the base of the discordant apophysis. This geometry is important for the distribution of gold mineralization because the western (i.e., upper in cross-section view) limit of the wider part of the mafic syenite intrusion and of the syenite pipe-like body in the hanging wall of the Main Break approximately coincide with the upper boundary of gold mineralization at the Kirkland Lake Gold Mine and the eastern part of the Macassa Mine. A smaller syenite porphyry body approximately 400 m north of the Main Break in the same area also appears to consist of a near-concordant larger portion and a narrow discordant northeast-trending apophysis (Figure 24).

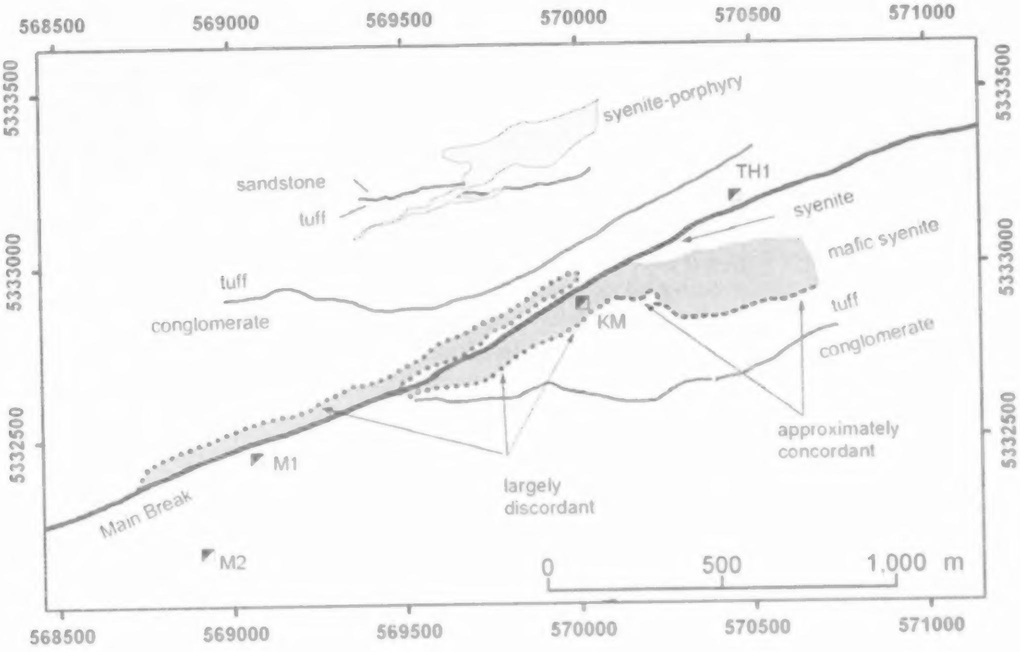

Figure 24. Relationships of the mafic syenite intrusion and stratigraphic units in the central part of the Kirkland Lake camp. The intrusion consists of a larger, approximately concordant portion (note the orientation of south-southwestern contact of the intrusion and tuff-conglomerate contact) and narrow northeast (approximately 070°)-striking apophyses that are discordant (approximately 20-25° counterclockwise) with respect to the roughly east-west-trending stratigraphic contacts. The south-southwest contact of the larger (approximately concordant) part of the intrusion plunges (30-40°) westward. The smaller syenite porphyry intrusion north of the Main Break shows similar geometry: a larger body with near concordant southern contact and a narrow northeast-trending apophysis oriented 20-25° counterclockwise to the stratigraphic contacts. Selected shafts shown for reference: M1 and 2- Macassa #1 and #2: KM-Kirkland Lake Gold Main shaft: and TH1- Teck-Hughes #1 shaft.

DEFORMATIONAL FABRICS

Compared to the Gauthier transect area, rocks in the Teck Township transect are characterized by generally lower strain and weaker development of penetrative deformational fabrics. S2, the earliest deformation fabric present in Timiskaming rocks, is only developed within or in the immediate proximity of the Larder Lake–Cadillac deformation zone at the contact between Timiskaming sedimentary rocks (conglomerates, sandstones, and siltstones) and volcanic rocks (tuffs) and Tisdale assemblage mafic-ultramafic volcanic rocks (south of the map area). S2 strikes 070° to 110°, dips 70° to 80° to the south, and tends to mimic the orientation of the Larder Lake–Cadillac deformation zone (Figure 25). It is a penetrative foliation defined by flattened clasts in conglomerates (Photo 31) and tuffs and by alternating chlorite, sericite (± fuchsite) and carbonate layers in mafic-ultramafic volcanic rocks. A steeply (about 70°) east-dipping stretching lineation is locally associated with S2 in conglomerates.

S3 was documented only in the chlorite-fuchsite-carbonate-altered ultramafic rocks of the Tisdale assemblage. It is expressed as a north-trending (350° to 005°) cleavage dipping moderately to steeply (50° to 80°) to the east and axial planar to east-southeast-plunging symmetric and Z-asymmetric folds of S2 (Figure 25, Photo 32). Many of these folds do not have an axial-planar cleavage. No unequivocal overprinting relationships with S4 were documented in the Teck Township map area, and the north-south-trending fabric was assigned to S3 based on similarity in orientation with the S3 foliation of the Gauthier Township transect.

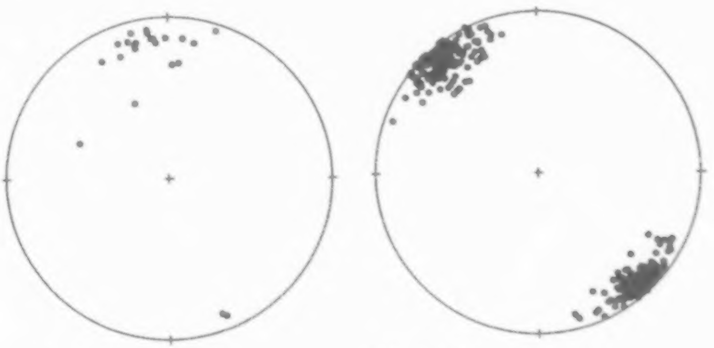

Poles to S2 (N=23)

Poles to S4
All locations, all rock types N=317

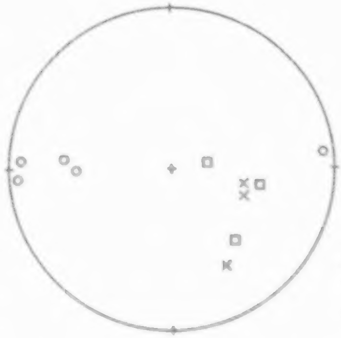

Poles to S3 (circles, N=5),
S2-S3 intersection lineation ("X", N=3),
and F3 fold axes (squares, N=3)

Figure 25. Deformational fabrics of Teck Township transect: S2 (along the Larder Lake–Cadillac deformation zone), S3 (+S2-S3 intersection lineation and F3 fold axes), and S4.

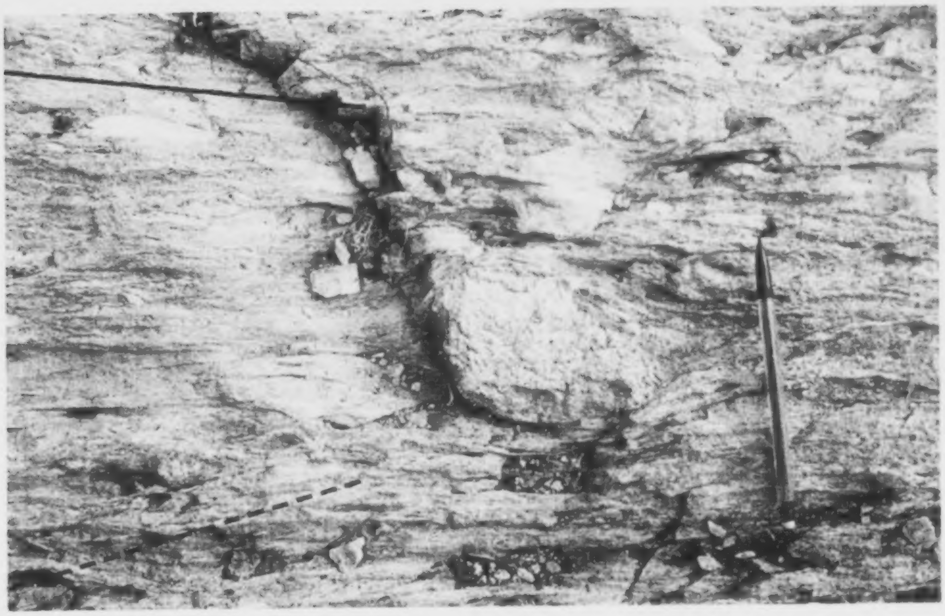

Photo 31. S2 (parallel to the solid line) defined by flattened pebbles in Timiskaming conglomerates (elongate white lenses in the upper part of the photograph) and overprinted by weakly developed S4 (parallel to the dashed line). Southeastern part of the Teck Township transect area (station 004VOI1590). Pencil (15 cm) for scale.

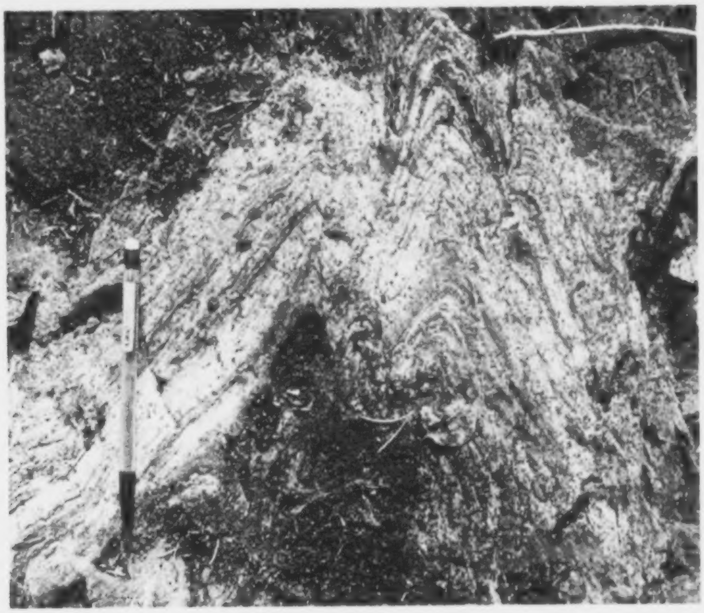

Photo 32. F3 fold with north-south-trending axial plane in carbonate-altered meta-ultramafic rocks. Southeast of the Teck Township transect area (station 004VOI1589). Pencil (15 cm) for scale.

S4 is the most common deformation fabric in the Timiskaming rocks. It consistently strikes 040 to 065° and dips steeply southeast or northwest (Figure 25). Along the Larder Lake–Cadillac deformation zone, S4 is a spaced crenulation cleavage overprinting S2 (Photo 31). North of the deformation zone, development of S4 is uneven. In the center of the map area (i.e., from about 200 m south of the Kirkland Lake fault to the Blanche River–Amalgamated Kirkland–Murdock Creek faults), S4 is relatively weakly developed. Further north, S4 is present again. In bedded tuffs, S4 occurs as spaced disjunctive cleavage, in places axial planar to poorly developed, southwest-plunging folds (Photo 33). Well-developed folds are only rarely observed. Most commonly, there is a long (northwest-trending) limb transected by counterclockwise-oriented S4, and a hinge portion with near orthogonal S4. Instead of the second, southwest-trending limb, the hinge is disrupted (Photo 34) and offset by a single or several tightly spaced shear surfaces parallel to S4 or trending roughly 020°. This pattern is again followed by northwest-trending bedding and counterclockwise-oriented S4. Bedding-S4 intersection lineation plunges moderately southwest, except in the area near the railroad – Goldthorpe road intersection, where the plunge becomes more shallow (15°-20°), and opposite (northeast) plunge directions are noted locally. In conglomerates, S4 is defined by weak to moderate pebble flattening (Photo 35). Fe-carbonatized mafic volcanic clasts are typically more strained than other clast types. Weakly to moderately developed S4 is also observed in mafic (augite) syenite, and sparsely porphyritic varieties of syenite porphyry. Based on simple visual comparison, the highest intensity of D4 deformation (compared to other rock types and locations) appears to occur in the band of conglomerates south of the Timiskaming–Kinojevis assemblages contact and north of the large mafic syenite intrusion (north of the railway).

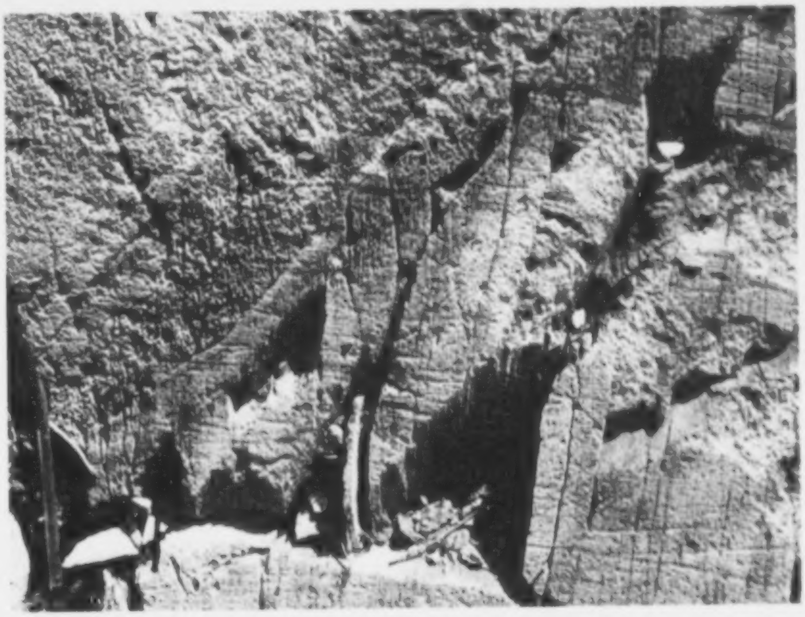

Photo 33. Disjunctive cleavage S4 in Timiskaming tuffs. Pencil (approximately 15 cm, left-hand bottom) for scale. Narrows Break stripped outcrop, about 350 m north of the Main Break (station 004VOI1531).

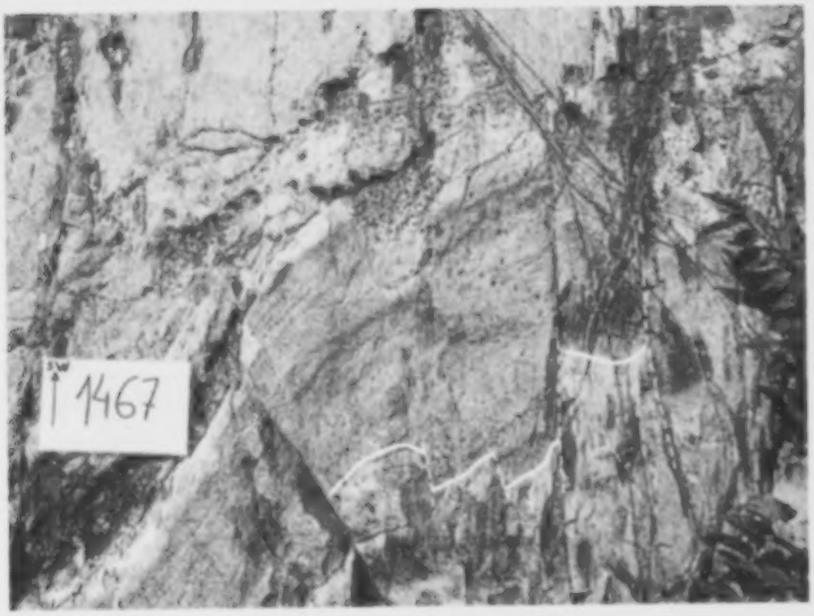

Photo 34. F4 folding in tuffs (plan view, facing southwest). Photographed is a transition from the west-northwest-trending limb (lower left-hand, S4 is oriented counterclockwise to bedding) to the hinge portion (S4 at high angles to bedding). In the hinge, bedding planes (solid white lines) are disrupted by shear surfaces (white dashed line) that are parallel or near parallel to axial planar S4. Further northwest from the photographed hinge portion, bedding planes again trend northwest and are transected by counterclockwise-oriented S4, i.e., there is practically no southwest-trending limb with S4 oriented clockwise to bedding. Narrows Break stripped outcrop, station 004VOI1467.

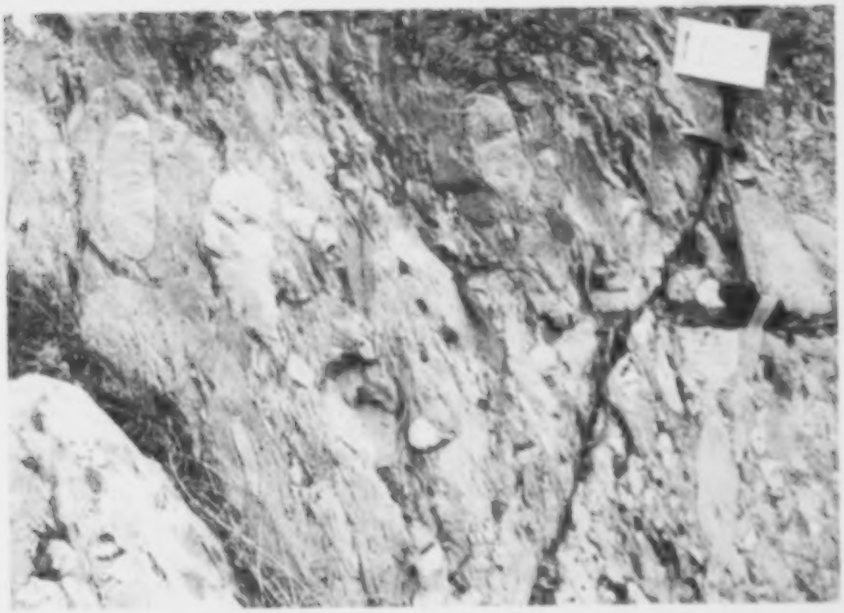

Photo 35. S4 defined by pebble flattening in Timiskaming conglomerates (approximately 1 km north of the Main Break, station 004VOI1562). Cross-section view facing northeast, white tag (upper right-hand) is 17 cm wide.

DEFORMATION ZONES

Larder Lake–Cadillac Deformation Zone

The Larder Lake–Cadillac deformation zone corresponds to the southern contact of Timiskaming sedimentary and pyroclastic rocks with mafic-ultramafic volcanic rocks of the Tisdale assemblage. The deformation zone does not have sharp geological boundaries, and is defined mainly by the intensity of the deformation and occurrence of the S2 foliation. In the present project, structural observations within the Larder Lake–Cadillac deformation zone were made mainly in the southeastern part of the area, where the Timiskaming–Tisdale assemblages contact changes orientation from northeast (near the eastern border of Teck Township) to approximately east-west (western part of Lebel Township). The estimated width of the deformation zone in this area is 400-500 m, although delineating the northern limit of the zone is somewhat difficult, especially in areas where S2 and S4 have similar orientation. The overall intensity of deformation of the Larder Lake–Cadillac deformation zone in Teck Township transect is weaker compared to Gauthier Township. In addition to the development of S2, and similar to the Gauthier Township transect, the deformation zone is marked by bulk carbonatization, especially of ultramafic rocks. Quartz-iron-carbonate veins accompanied by wall-rock carbonatization occur locally in the Timiskaming sandstone-conglomerate package. S2-parallel quartz veins up to roughly 20 cm thick are exposed at the intersection of the powerline and the ATV trail near the southeast corner of the map area. The veins are boudinaged parallel to S2, and subsequently overprinted by S4, implying that they were emplaced before or during D2 deformation. No information on gold grades is available, but the obvious lack of exploration interest indicates that these veins are probably not gold-bearing. No distinct asymmetric shear-sense indicators were observed in the Larder Lake–Cadillac deformation zone in the Teck Township transect area.

Possible Shear Zone South of the Timiskaming Unconformity

Another predominantly ductile deformation zone (possibly a suite of several shear zones) may be located in the north of the map area, between the Timiskaming unconformity and the large mafic syenite intrusion. It occurs mainly in conglomerates and is oriented approximately parallel to the unconformity. Although surface exposures are insufficient to precisely delineate this deformation zone, there are several lines of evidence supporting its existence. Highly strained conglomerates are observed in a fragmental outcrop on the Casakirk property, approximately 70 m northeast of the former Abba shaft. Rocks exposed in stripped outcrops on Marion-Boyce properties (north of the town of Kirkland Lake) and corresponding to the lowermost part of the Timiskaming assemblage are characterized by stronger than average S4 foliation, iron-carbonatization and quartz veining. A long north crosscut at the 3075-foot (approximately 940 m) level at the Lake Shore Mine uncovered a 50 m wide zone of strongly carbonatized and sheared conglomerates, with barren quartz veins about 100-150 m south of the Timiskaming unconformity (Thomson et al. 1950, p.83). Hopkins (1949) reported that this zone was also intersected by surface diamond drilling. Drilling from a long north crosscut at the 3000-foot level at the Macassa Mine also revealed a zone of strongly sheared conglomerates (Thomson et al. 1950). If these occurrences of deformed rocks constitute a single shear zone, most probably it corresponds to D4, since the deformational fabric observed in surface outcrops is indistinguishable from S4 elsewhere.

GOLD MINERALIZATION

Ore-Controlling Faults: Kirkland Lake Fault (Main Break) and '04 Break

DEFINITION OF THE KIRKLAND LAKE FAULT

The Kirkland Lake fault (Main Break; Todd 1928; Thomson 1945; Thomson et al. 1950) is the main ore-controlling structure of the Kirkland Lake camp. Thomson et al. (1950) discussed the two most popular definitions of the Kirkland Lake fault that stem from different interpretations of the relationships between the Main Break and its splays (North and South veins on the Lake Shore and Wright-Hargreaves properties, and their equivalents further east). The first definition assumes the existence of a single-plane Main Break, and all splays of the Break are considered strictly subsidiary (Ward et al. 1948). Under this interpretation, the Main Break coincides with the North (No. 2) vein of the Lake Shore Mine; approximately 100 m east of Lake Shore shaft #5, the North Vein splits in a northeastern direction (050°), while the Main Break continues for about 450 m striking approximately 085-090°, where it intersects with the South vein, and coincides with the latter further east. The east-west-trending segment of the Main Break between the North and South vein is presently informally called the "Mud Break" due to intensive sericitization along it. Thomson et al. (1950) proposed an alternative concept in which the single-plane Main Break going eastward splits into more and more splays with decreasingly less displacement on each of the branches. Although one of the branches is usually stronger and accommodates more displacement than others, all splays are considered part of the same fault system. Although we agree that the second interpretation is more geologically realistic and all splays of Main Break probably constitute a single fault system along with the "parent" fault, the accompanying geologic map (Map P.3558) is based on the first (single-plane Main Break) interpretation (as compiled from Thomson 1945), primarily to reflect the well-known historical names of the most prominent veins and mineralized zones and for general simplicity of description.

CAMP-SCALE GEOMETRY

The main ore-controlling structure of the Kirkland Lake camp is the brittle to brittle-ductile Kirkland Lake fault (Main Break). It was continuously traced at surface and underground for about 4800 m, from the east limit of Kirkland Lake camp to the eastern part of Macassa Mine (e.g., Charlewood 1964). In the eastern and central parts of the camp, where mineralization extends to the surface, the ore-controlling structures were followed by underground workings from the shallowest levels to a maximum of about 2450 m depth (Charlewood 1964). Near the eastern end of the camp (Sylvanite and Toburn mines), the Main Break strikes approximately 080°; further west (the Wright-Hargreaves, Lake Shore, Teck-Hughes, Kirkland Lake Gold properties and the eastern part of the Macassa Mine), the orientation varies between 060° and 070°. The fault dips south; dip angles at the eastern-central part of the camp are generally very steep (roughly 80° to vertical at the Wright-Hargreaves and the eastern part of the Lake Shore Mine; about 70°-80° at the western part of the Lake Shore). Further west, at the Kirkland Lake Gold Mine and the eastern part of the Macassa Mine, the fault typically dips steeply (approximately 80°) to a depth of 1100-1200 m, and becomes more shallowly dipping (60°-65°) at deeper levels (Charlewood 1964). The most important splays of the Kirkland Lake fault in the east-central parts of the camp are the North and South vein structures (Thomson et al. 1950). West of the Teck-Hughes property, gold mineralization along the Main Break starts plunging about 30°-40° southwest, and near the Macassa shaft #1, the upper limit of the Main Break gold mineralization is about 900 m below surface (the 3000-foot level; Thomson et al. 1950).

Further westward, the surface continuation of the Main Break is somewhat ambiguous, because of the branching nature of the fault. In proximity to the Macassa shafts #1 and #2, at depths of 1200-1400 m, the fault splits into north and south branches, and the more persistent and better mineralized north branch connects to another fault, the '04 Break, via several minor crossover structures (e.g., R, R-2 and S breaks; Watson 1984; Watson and Kerrich 1983; Charlewood 1964). At the 4500-foot (1370 m) level of the Macassa Mine, near shaft #2, the '04 Break is approximately parallel to the Main Break, it strikes about 060°, dips 60-65° south and is located approximately 140 m north of the Main Break (Figure 26). Blocks bounded by the '04 Break and Main Break branches host important subsidiary veins (Charlewood 1964). Further west, the '04 Break becomes the main ore-controlling structure; it is also believed to be the main displacement plane in this part of the Kirkland Lake camp.

Underground (at a depth interval of about 1100-2100 m), the '04 Break was traced for approximately 1700 m, from the eastern part of the Macassa property (i.e., about 300 m southeast of Macassa shaft #1) to the Amikougami Creek fault, and a possible continuation of the structure (although unmineralized) was identified on the west side of the Amikougami Creek fault. In underground workings, the '04 Break dips steeply south (typically 65°-70°, rarely 45°-55°), and strikes northeast (055°-065°). At surface, two northeast-striking (050°-060°) near-parallel faults, 100-120 m apart, have been identified in the western part of the Macassa Mine (north of Macassa shaft #3, see Map P.3558): the north fault was previously mapped by Thomson (1945) and examined in the present project, and the south structure was identified by Macassa Mine geologists (unpublished company maps provided by Kirkland Lake Gold Inc.). On the accompanying Map P.3558, the north and south faults are interpreted as the '04 Break and Kirkland Lake fault (Main Break), respectively. Although this interpretation may be not entirely correct (correlation of surface features with structures at depth >1000 m could be uncertain), most probably both faults are related to the Kirkland Lake fault system. Dikes and elongate stocks of the mafic syenite and syenite porphyry are spatially associated with the two faults. In surface exposures north of Macassa shaft #3, the main slip of the northern fault coincides with a contact of a narrow (5 m) strongly deformed, foliated mafic syenite dike.

Surface mapping of this project reveals that there may be another fault, located roughly 350-400 m north of Macassa shaft #3 and striking approximately 050-055°. A rather abrupt decrease in intensity of S4 foliation (north – foliated, south – unfoliated or weakly foliated) in Timiskaming conglomerates was observed north of Macassa shaft #3 (outcrops along Macassa ore haul road) and west of Macassa shaft #2 (outcrops along the powerline). This change in deformation strength may be due to the existence of a fault separating blocks with different strain intensity (Figure 27).

SURFACE AND UNDERGROUND EXPOSURES

The Kirkland Lake fault is exposed underground at the Macassa Mine (eastern sections), and at surface on the Wright-Hargreaves, Lake Shore, and Teck-Hughes properties. Underground, unmineralized portions of the fault were observed at the 4500-foot level of the Macassa Mine, in proximity to shaft #2. At this location, the fault strikes 060°-070°, dips approximately 70° south and consists of a single 7-10 cm wide chlorite gouge band, and, less commonly, of a wider (30-50 cm) zone of breccia and branching chloritic slips. Veins of late, barren translucent quartz, with white and pink carbonate, and rare chlorite rosettes, are hosted by the fault (Photo 36). Along the fault plane, the rocks are typically carbonatized, and deformed into fine-grained cataclasite. The chloritic surface of the main slip plane contains gentle striations (orientation shown in Figure 28). The most common orientations are a) steep (raking approximately 60-90°, both east and west) and b) plunging shallowly to the west (5-30°). Shallowly west-plunging striations are documented to overprint the steeply plunging striations.

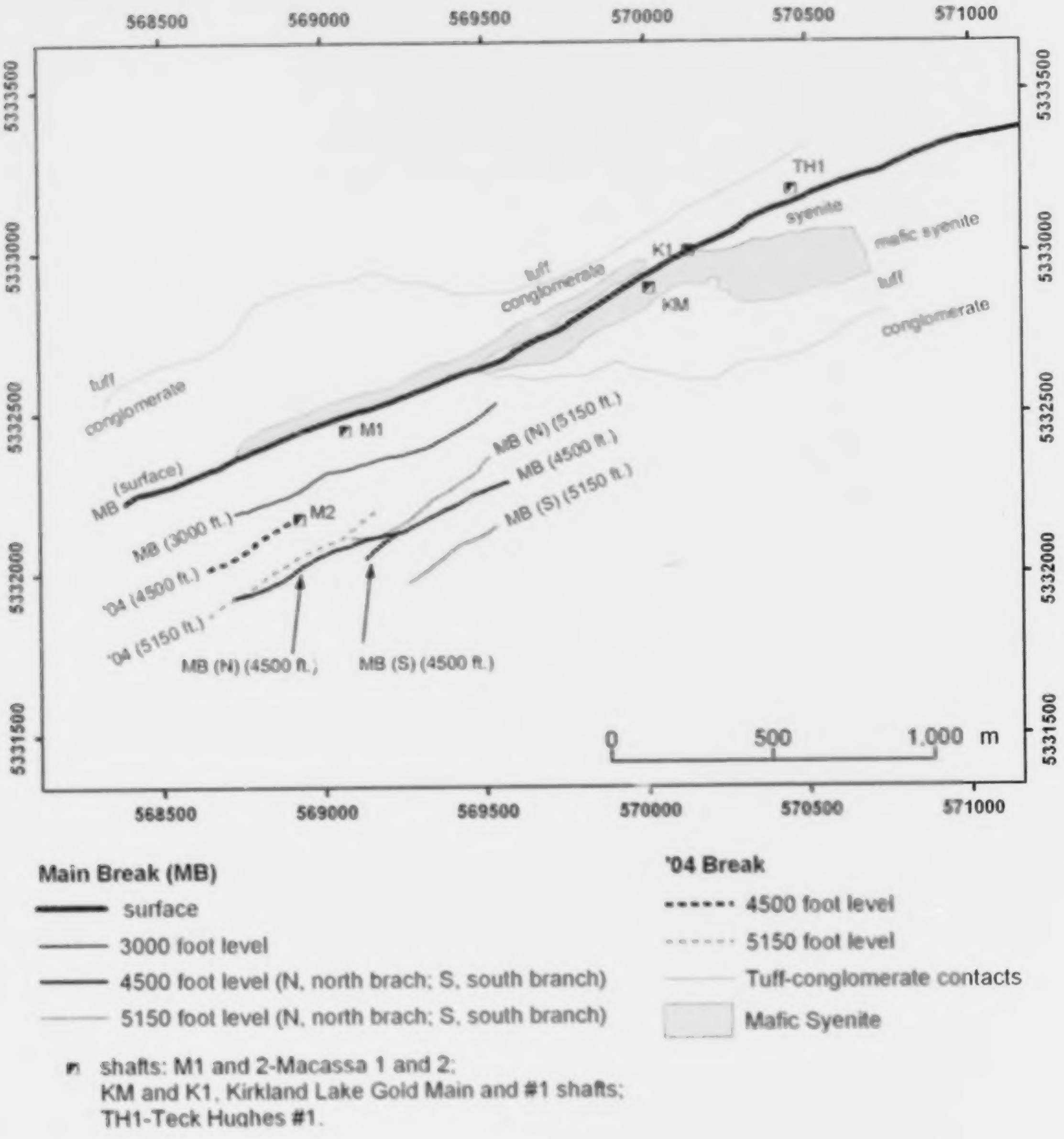
568500
569000
569500
570000
570500
571000
5333500
5333000
5332500
5332000
5331500
TH1
syenite
mafic syenite
K1
tuff
conglomerate
KM
tuff
conglomerate
tuff
conglomerate
M1
MB (surface)
MB (3000 ft.)
M2
MB (N) (5150 ft.)
MB (4500 ft.)
MB (S) (5150 ft.)
'04 (4500 ft.)
'04 (5150 ft.)
MB (N) (4500 ft.)
MB (S) (4500 ft.)
0
500
1,000 m
Main Break (MB)
surface
3000 foot level
4500 foot level (N, north brach; S, south branch)
5150 foot level (N, north brach; S, south branch)
'04 Break
4500 foot level
5150 foot level
Tuff-conglomerate contacts
Mafic Syenite
shafts: M1 and 2-Macassa 1 and 2;
KM and K1, Kirkland Lake Gold Main and #1 shafts;
TH1-Teck Hughes #1.

Figure 26. Subsurface position of the Main Break and '04 Break in proximity to Macassa shafts #1 and #2. (Also shown are surface geological markers: tuff-conglomerate contact and mafic syenite intrusion). The Main Break splits into north and south branches; east of Macassa shaft#1, the north branch of the Main Break reverses dip to the north. At the 4500-foot level, the '04 Break is located about 140 m north of the Main Break (north branch). Further west, the '04 Break becomes the main ore-controlling structure. Data from Thomson et al. (1950) and Charlewood (1964).

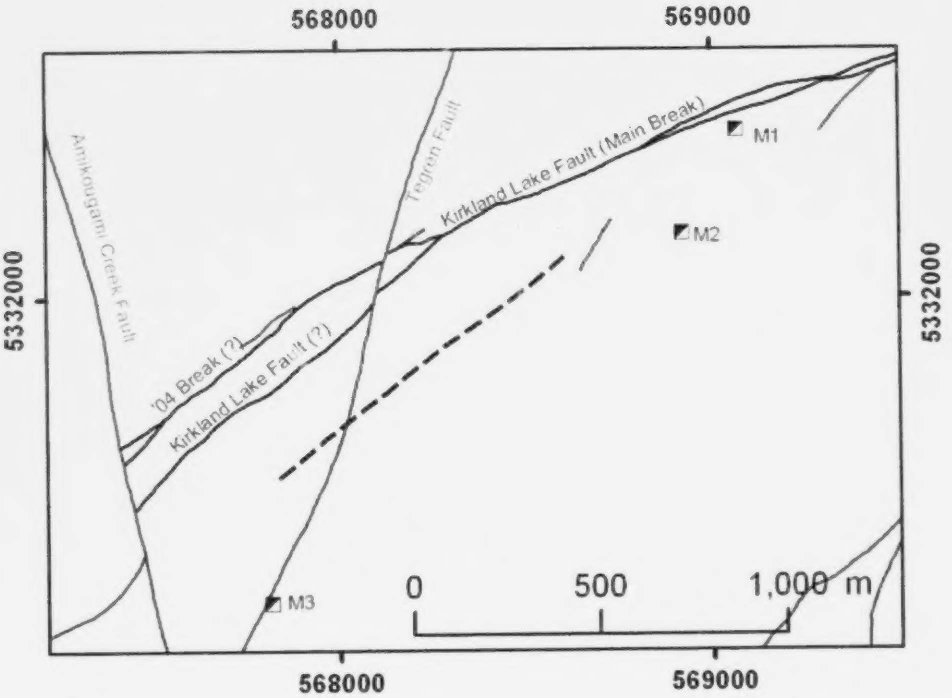
568000
569000
5332000
5332000
568000
569000
Amikougami Creek Fault
Tegren Fault
Kirkland Lake Fault (Main Break)
'04 Break (?)
Kirkland Lake Fault (?)
M1
M2
M3
0
500
1,000 m

Figure 27. Possible fault location south of the Main Break (thick dashed line). Based on abrupt decrease in S4 foliation intensity in Timiskaming conglomerates (from north to south), observed in outcrops along the Macassa ore haulage road (north of shaft #3) and along the powerline (west of shaft #2). M1,2, and 3- Macassa shafts #1, #2, and #3.

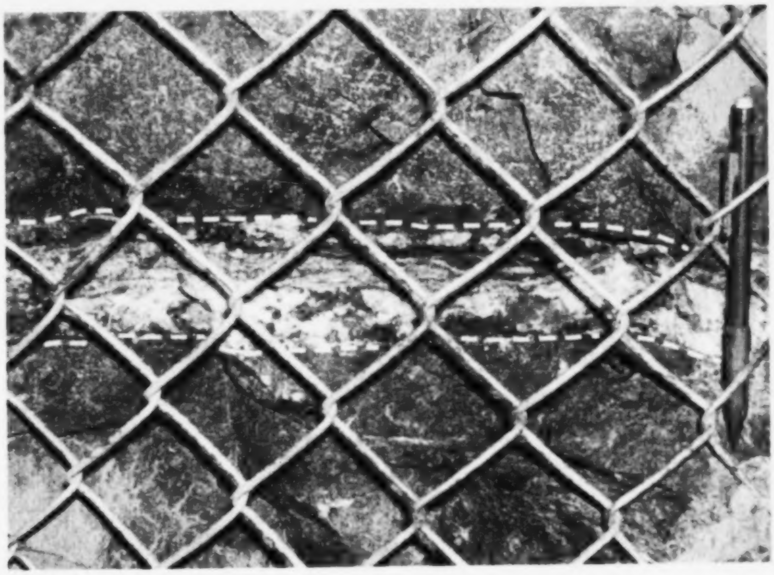

Photo 36. Main slip plane of the Kirkland Lake fault (Main Break) in the back of the drift, 4500-foot level, Macassa Mine. The Main Break hosts post-ore, barren quartz-carbonate-chlorite vein. Pencil is 15 cm long.

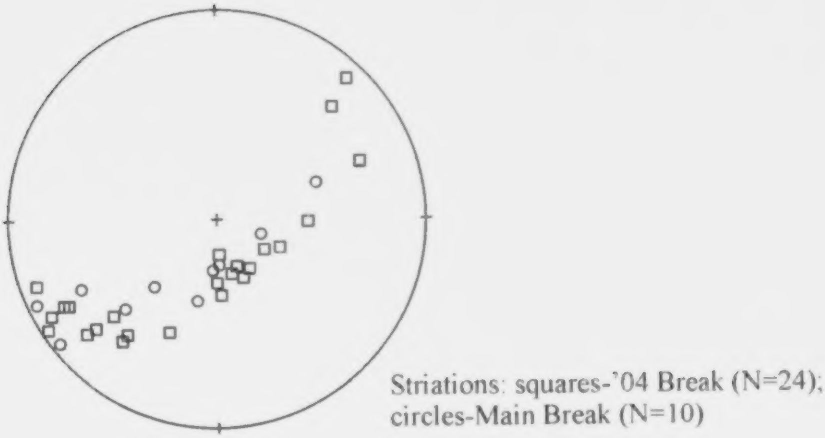

Figure 28. Orientation of striations on chloritic slip surfaces of the Main Break and '04 Break. All data from Macassa underground workings.

At surface, the Main Break is best exposed on the Lake Shore property, east of former shaft #5. It consists of several northeast-striking (060-075), south-dipping (75-80°), 10-25 cm wide deformation bands, characterized by strong sericitic alteration. These bands show an internal foliation oriented oblique to their boundaries, both in plan and cross-section view. In plan view, the foliation is oriented at 15-20° counterclockwise to the boundaries of the bands; in cross-section view, the foliation dips steeper (or even shows vertical orientation or steep north dips) than the deformation bands (Photo 37). The orientation of the foliation suggests reverse-dextral (south side up and to the west) slip along the Main Break.

Another surface exposure of the Main Break is the flooded small open pit, exposing the "Mud Break", i.e., the east-west-trending segment of the Kirkland Lake fault between the North and South veins near the west border of the former Wright-Hargreaves property (Figure 29). Observations in 2002, prior to mining operations, show that this segment of the Main Break is a 3-4 m wide high-strain zone. The zone consists largely of sericite-rich highly foliated syenite porphyry (Photo 38A). The sericite alteration is associated with small quartz veinlets and is symmetrically distributed in the wall-rock selvages (Photo 38B). The foliation trends east-northeast, parallel to the overall orientation of the Mud Break segment and is syn- to post-sericite alteration. The sericite is oriented parallel to or has been transposed by the foliation (Photo 38C). A roughly 20 m wide zone of low-grade (Au ≤ 3-4 g/t) mineralization is associated with the Mud Break. Mineralization comprises a weak quartz stockwork and a strong hydrothermal replacement characterized by silicification and sericite, with 2-10% disseminated pyrite.

The '04 Break was observed underground at the 3825, 4250, 4500, 4750, and 4900-foot levels of the Macassa Mine. It is similar in orientation (northeast strike (055°-065°), south dip (60°-70°)) to the Main Break, and is defined by similar narrow (2-10 cm) single or branching chloritic bands and locally wider (20 cm to 1 m) breccia zones, as in the Main Break. The discrete fault slip surfaces are commonly accompanied by wider (0.5-2.5 m) envelopes of carbonatized fine-grained cataclasite traditionally called "mylonite" in mine terminology. The cataclasite shows a banded texture defined by reddish-brown lenses and discontinuous bands (1-3 cm wide), separated by a darker chloritized matrix, or has a more uniform, greyish light brown color. Typically, cataclasite is aphanitic, however, 1-2 mm feldspar fragments are recognizable in places. Thomson et al. (1950, p.100) described the petrography of these fault rocks, characterizing them as carbonate-rich cataclastic microbreccias consisting primarily of fragmented feldspars and secondary carbonate. Cataclasite bands are commonly bounded by sharp slip surfaces. Foliation in cataclastic bands, if present, is in most cases parallel to the fault boundaries. On the western face of stope 4528 MCF, weakly developed foliation defined by alignment of breccia clasts and diffuse compositional banding is oriented steeper (80°-85° south) than boundaries of the cataclastic band (approximately 55°-60° south), which is compatible with reverse sense of shear (Photo 39). In addition to the oblique foliation observed in stope 4528 MCF, the main '04 Break slip is in places (e.g., stope 4940) accompanied by more shallowly dipping fractures, oriented at about 20° to the slip plane (in cross section view). These can be interpreted as synthetic Riedel fractures compatible with reverse slip. Gentle striations on chloritic slip surfaces of the '04 Break are either steep or moderately to shallowly inclined to the west. East-plunging striations are relatively rare (Figure 28). As discussed below, the striations on chloritic slip surfaces probably record post-mineralization movements.

Other, subsidiary, ore-controlling structures in the Macassa Mine include the South Break, '05 Break, and No. 6 Break (Still 2001). Of these structures, only the No. 6 Break was observed in this study. The No. 6 Break apparently splays from the '04 Break above the 4250-foot level. It strikes about 070°, dips 40°-55° to the south, and diverges from the '04 Break with depth (Still 2001). The wedge-shaped block between the 4250-foot and 4500-foot levels confined by the '04 Break and No. 6 Break is the host of several economically important ore zones (Still 2001). The No. 6 break was briefly examined in stope 4225 (above the 4250 level), where it occurs as a narrow (3-5 cm) chloritic fault separating augite syenite (footwall) and tuff (hanging wall).

Plunge of Gold Mineralization

One of the most notable features of the Kirkland Lake gold camp is the westerly plunge of the Main Break mineralization. It begins approximately from the western boundary of the Teck-Hughes property (close to Kirkland Lake Gold shaft #1) and continues to the Macassa Mine 3000-foot level, between shafts #1 and #2 (Figure 30). Along this plunging interval, the upper boundary of mineralization approximately coincides with the top of the pipe-like syenite body in the hanging wall of the Main Break (e.g., Charlewood 1964). From the 3000-foot level of the Macassa Mine (between shafts 1 and 2), the upper limit of the ore drops steeply to the 4375-foot level, and the '04 Break becomes the main ore-controlling structure at deeper levels and further west (Charlewood 1964). West of Macassa shaft #2, mineralization along the '04 Break does not show a single, clearly defined, plunge. At present, ore hosted by the '04 Break is actively mined at the 3825-foot level at the western part of the Macassa Mine and there are no clear indications for upper limits of mineralization.

The westerly plunge of mineralization between the Teck-Hughes Mine and the eastern part of Macassa shafts #1 and #2 corresponds to the segment of the Main Break that is oriented 20°-30° counterclockwise with respect to the strike of stratified units (tuffs and conglomerates) and to the western contact of larger, near concordant, part of the mafic syenite body (Figure 31). The general plunge of Main Break mineralization from surface to the 3000-foot level at Macassa is approximately parallel to the calculated intersection line between the Main Break and the tuff-conglomerate contact south of the Main Break (Figures 31 and 32). The plunge of the westernmost tip of an irregular pipe-like syenite body in the hanging wall of the Main Break between surface and the 3000-foot level of the Macassa Mine has approximately the same orientation. The intersection of the Main Break and the tuff-conglomerate contact north of the Break is oriented similarly. The end of the plunge at the 3000-foot level of the Macassa Mine corresponds to the area where the general trend of stratified units changes from east-west to northeast, i.e., becoming approximately parallel to the Main Break.

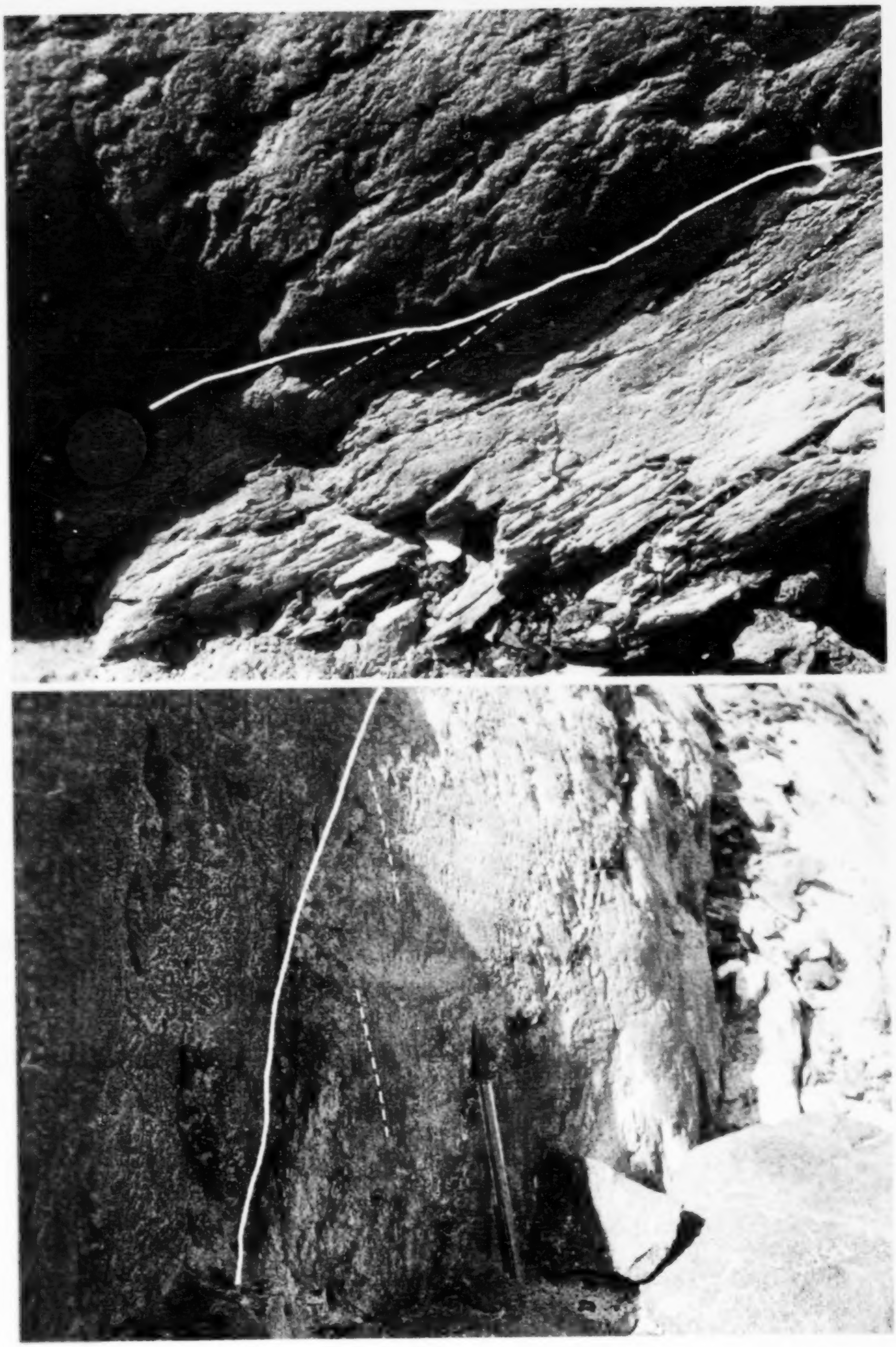

Photo 37. Surface exposure of the Main Break east of the former Lake Shore shaft #5 (top, plan view, west is on the right-hand side; bottom, cross-section view facing west). At this location, the Main Break comprises several sericitic deformation bands; photographed is one of these bands. Oblique (in plan and cross-section view) orientation of internal foliation (dashed lines) with respect to the boundaries of the band (solid lines) implies oblique reverse–dextral (south-side up and to the west) sense of movement.

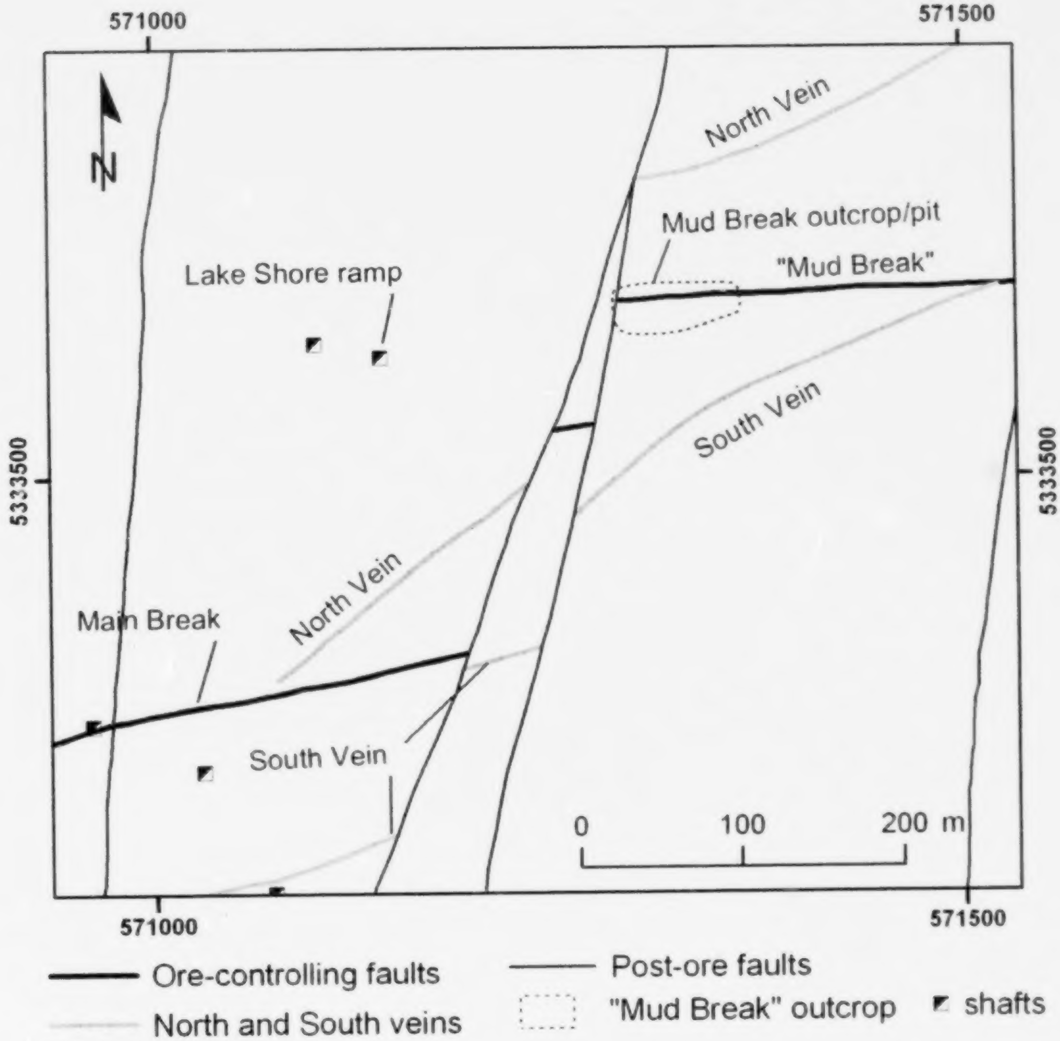
571000
571500
5333500
5333500
N
North Vein
Mud Break outcrop/pit
"Mud Break"
Lake Shore ramp
South Vein
North Vein
Main Break
South Vein
0
100
200 m
571000
571500
Ore-controlling faults
Post-ore faults
North and South veins
"Mud Break" outcrop
shafts

Figure 29. Schematic showing the location of the "Mud Break".

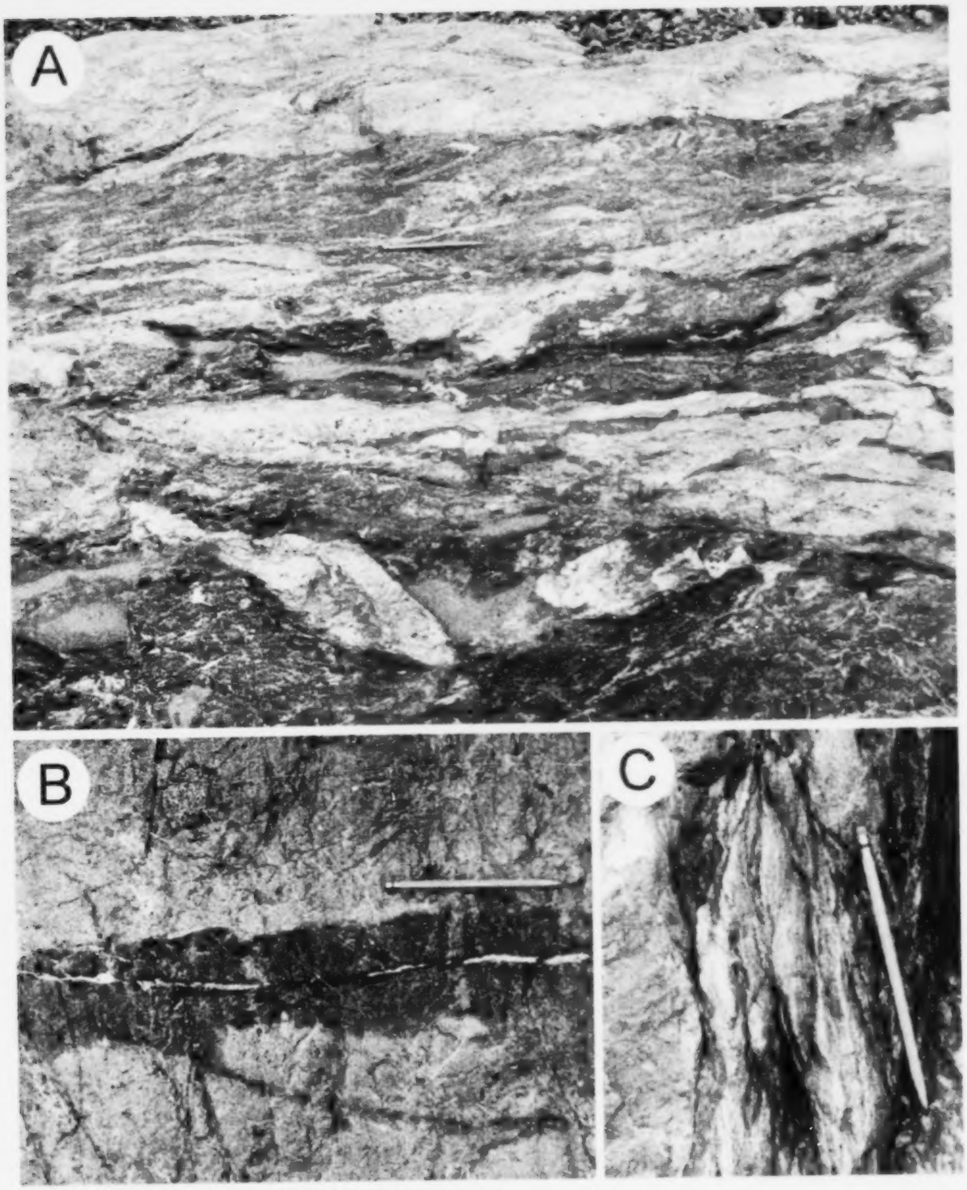

Photo 38. Surface exposure of the "Mud Break" (pencil, approximately 15 cm, for scale). A) General view of the "Mud Break": foliation in strongly sericitized syenite porphyry. B) Sericitization halo (dark) around a thin quartz veinlet. C) Cross-section view of a foliated sericite-rich band.

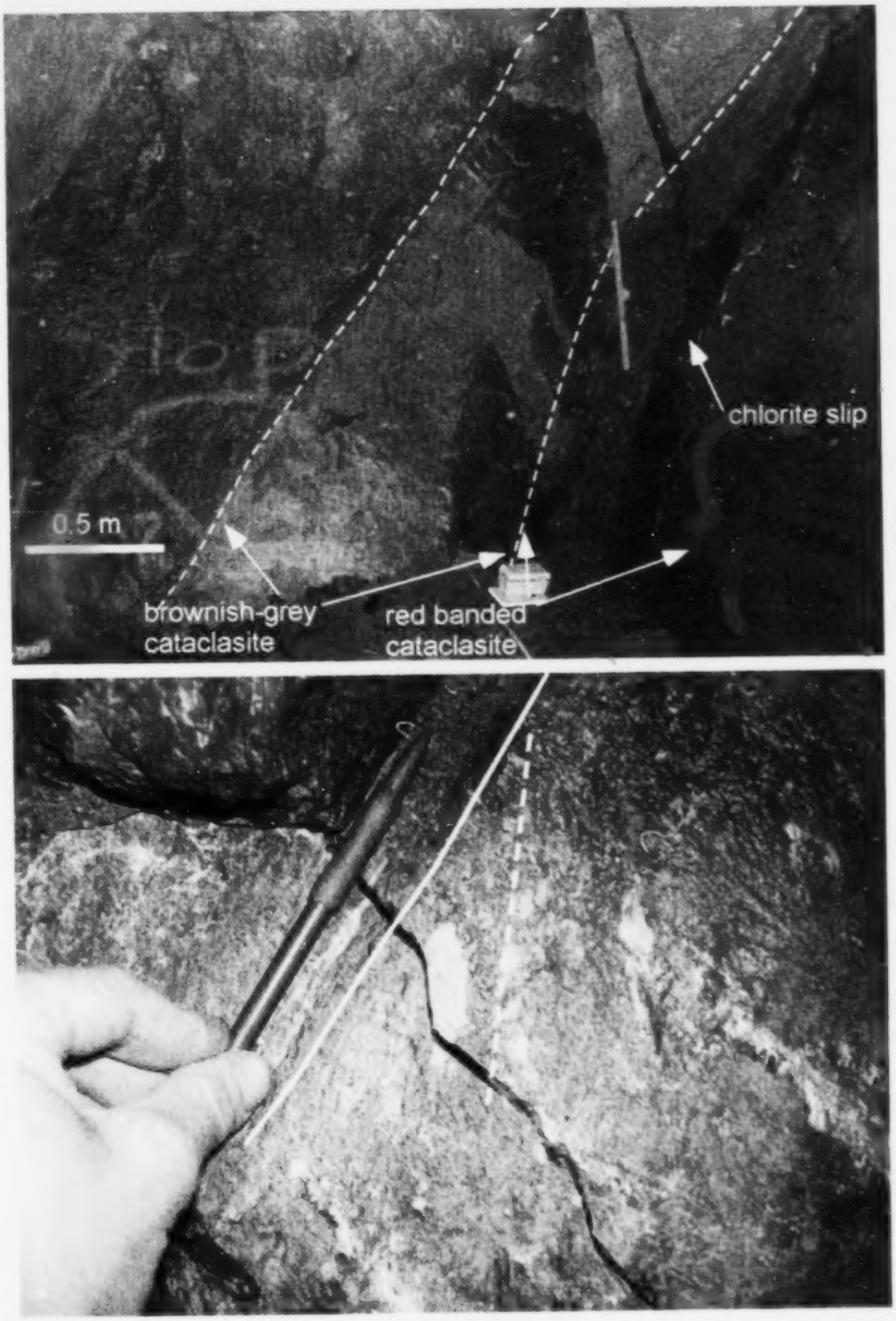
0.5 m
chlorite slip
brownish-grey cataclasite
red banded cataclasite

Photo 39. Underground exposure of the '04 Break in stope 4528 MCF, Macassa Mine. Cross-section view facing west. Top, general view towards west end of the stope. Main chloritic slip of the break is flanked from the south by bands of red and brownish-grey cataclasite. Bottom, a close up view of the southern contact of the brownish grey cataclasite band. Weakly developed internal foliation (dashed line), defined by clast alignment, dips steeper than the contact of the band (solid line), which is compatible with reverse (south over north) sense of shear.

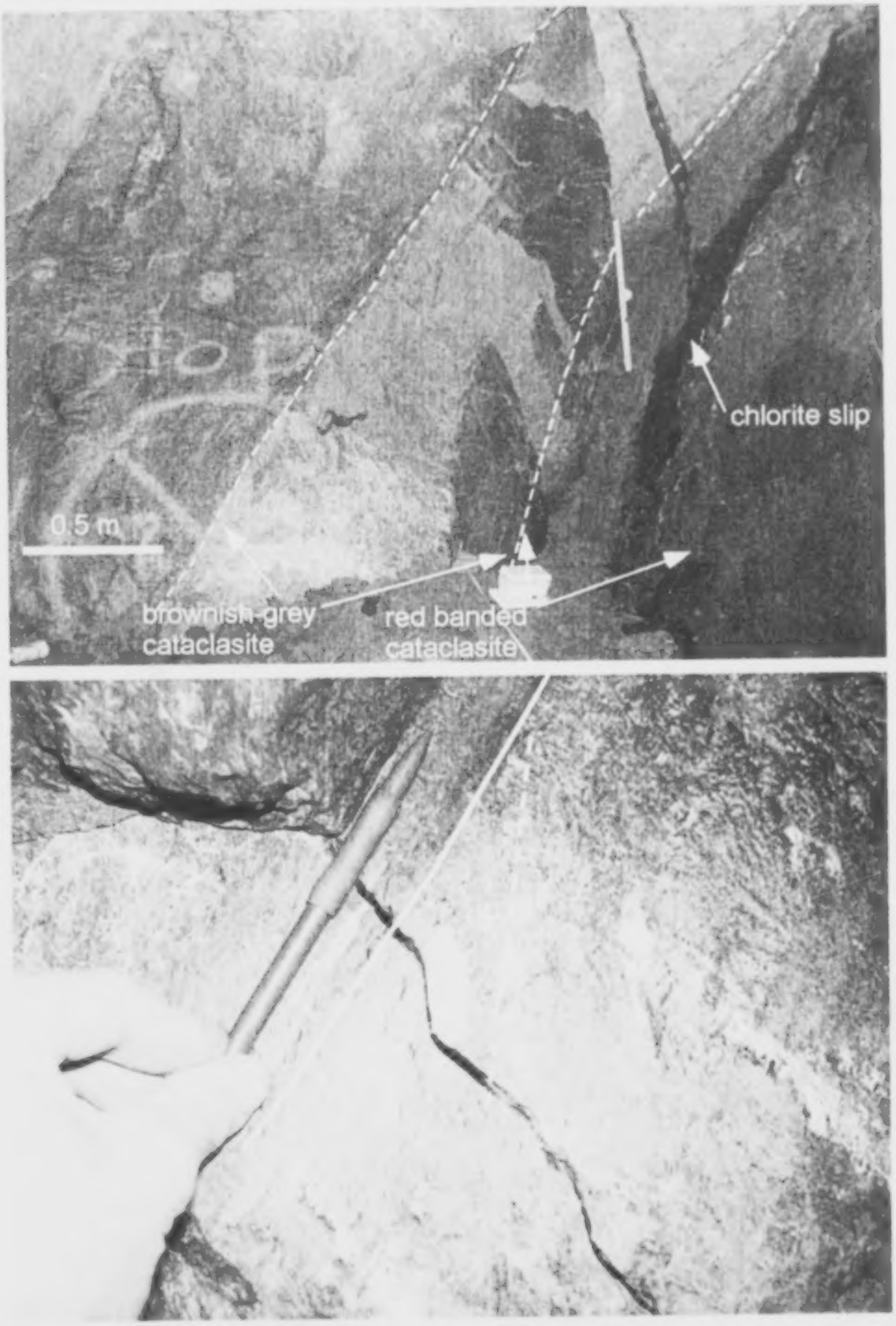
TOP
0.5 m
chlorite slip
brownish-grey cataclasite
red banded cataclasite

Photo 39 Underground exposure of the '04 Break in stope 4528 MCF, Macassa Mine. Cross-section view facing west. Top, general view towards west end of the stope. Main chloritic slip of the break is flanked from the south by bands of red and brownish-grey cataclasite. Bottom, a close up view of the southern contact of the brownish grey cataclasite band. Weakly developed internal foliation (dashed line), defined by clast alignment, dips steeper than the contact of the band (solid line), which is compatible with reverse (south over north) sense of shear.

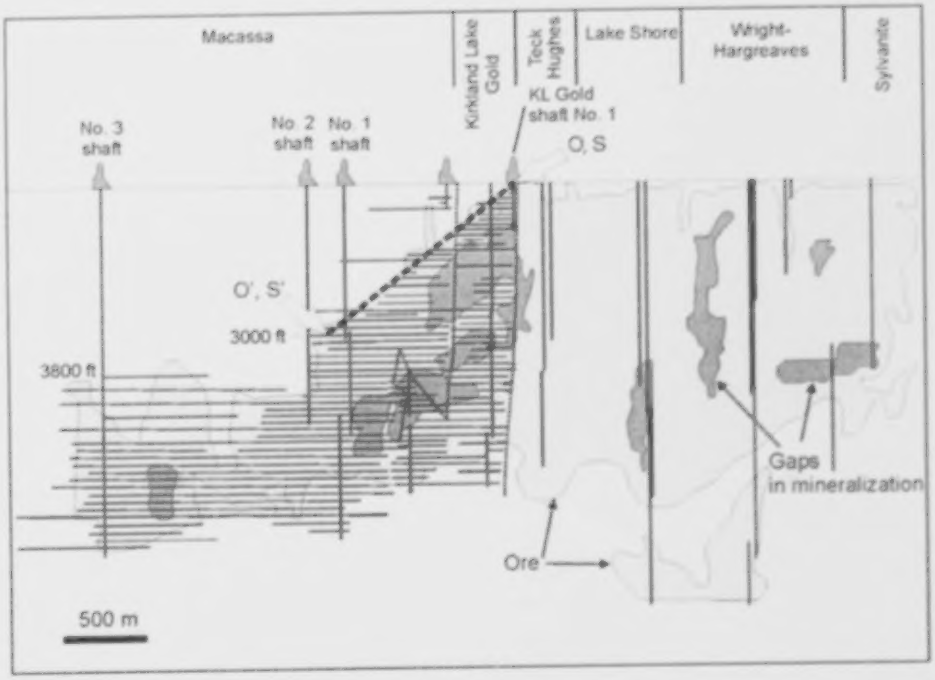
Macassa
Kirkland Lake Gold
Teck Hughes
Lake Shore
Wright-Hargreaves
Sylvanite
KL Gold shaft No. 1
O, S
No. 3 shaft
No. 2 shaft
No. 1 shaft
O', S'
3000 ft
3800 ft
Gaps in mineralization
Ore
500 m

Figure 30. Schematic longitudinal section of the Kirkland Lake camp. Modified from Still (2001) and Ridler (2001). Arrows depict position of points O, S, O', and S' from Figure 31.

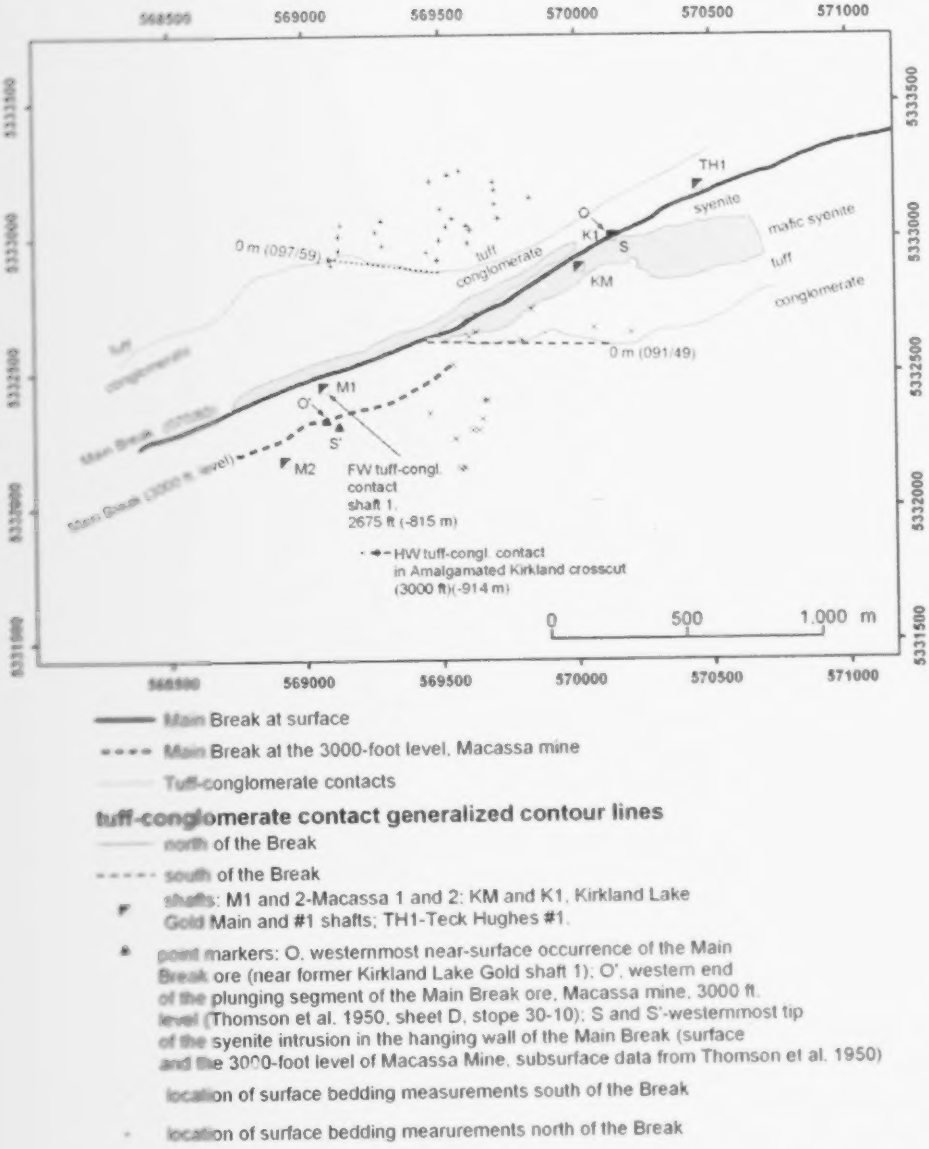
568500
569000
569500
570000
570500
571000
5333500
5333000
5332500
5332000
5331500
TH1
syenite
mafic syenite
O
K1
S
KM
tuff
conglomerate
0 m (097/59)
tuff
conglomerate
0 m (091/49)
tuff
conglomerate
M1
O'
S'
Main Break (070/80)
Main Break (3000 ft. level)
M2
FW tuff-congl. contact shaft 1, 2675 ft (-815 m)
HW tuff-congl. contact in Amalgamated Kirkland crosscut (3000 ft)(-914 m)
0
500
1,000 m
Main Break at surface
Main Break at the 3000-foot level, Macassa mine
Tuff-conglomerate contacts
tuff-conglomerate contact generalized contour lines
north of the Break
south of the Break
shafts: M1 and 2-Macassa 1 and 2; KM and K1, Kirkland Lake Gold Main and #1 shafts; TH1-Teck Hughes #1.
point markers: O, westernmost near-surface occurrence of the Main Break ore (near former Kirkland Lake Gold shaft 1); O', western end of the plunging segment of the Main Break ore, Macassa mine, 3000 ft. level (Thomson et al. 1950, sheet D, stope 30-10); S and S'-westernmost tip of the syenite intrusion in the hanging wall of the Main Break (surface and the 3000-foot level of Macassa Mine, subsurface data from Thomson et al. 1950)
location of surface bedding measurements south of the Break
location of surface bedding mearurements north of the Break

Figure 31. Diagram explaining elements shown in Figure 32. Main Break strikes 070° and dips 80° between surface and the 3000-foot level of Macassa Mine. Straight dotted (north of the Break) and dashed (south of the Break) lines are generalized contour lines of the tuff-conglomerate contact (actual contact is shown as a solid grey line). Orientation of the contact is 097/59 north of the Break and 091/49 south of the Break. Dip angles are calculated based on intersections in Macassa shaft #1 (north of the Main Break, 2675-foot level, data from Charlewood 1964) and in Macassa Amalgamated Kirkland crosscut at the 3000-foot level (data from Lackey 1990), assuming planar geometry. O and O' (triangular symbol) depict the westernmost surface exposure of the Main Break ore (near the former Kirkland Lake Gold shaft #1) and the western end of the plunging segment of the Main Break ore on the 3000-foot level at the Macassa (Thomson et al. 1950, sheet D, stope 30-10). S and S' correspond to positions of the westernmost tip of the pipe-like syenite body in the hanging wall of the Main Break, respectively, at surface and at the 3000-foot level of the Macassa Mine. For legibility, the syenite porphyry intrusions are not shown (see Map P.3558 for details).

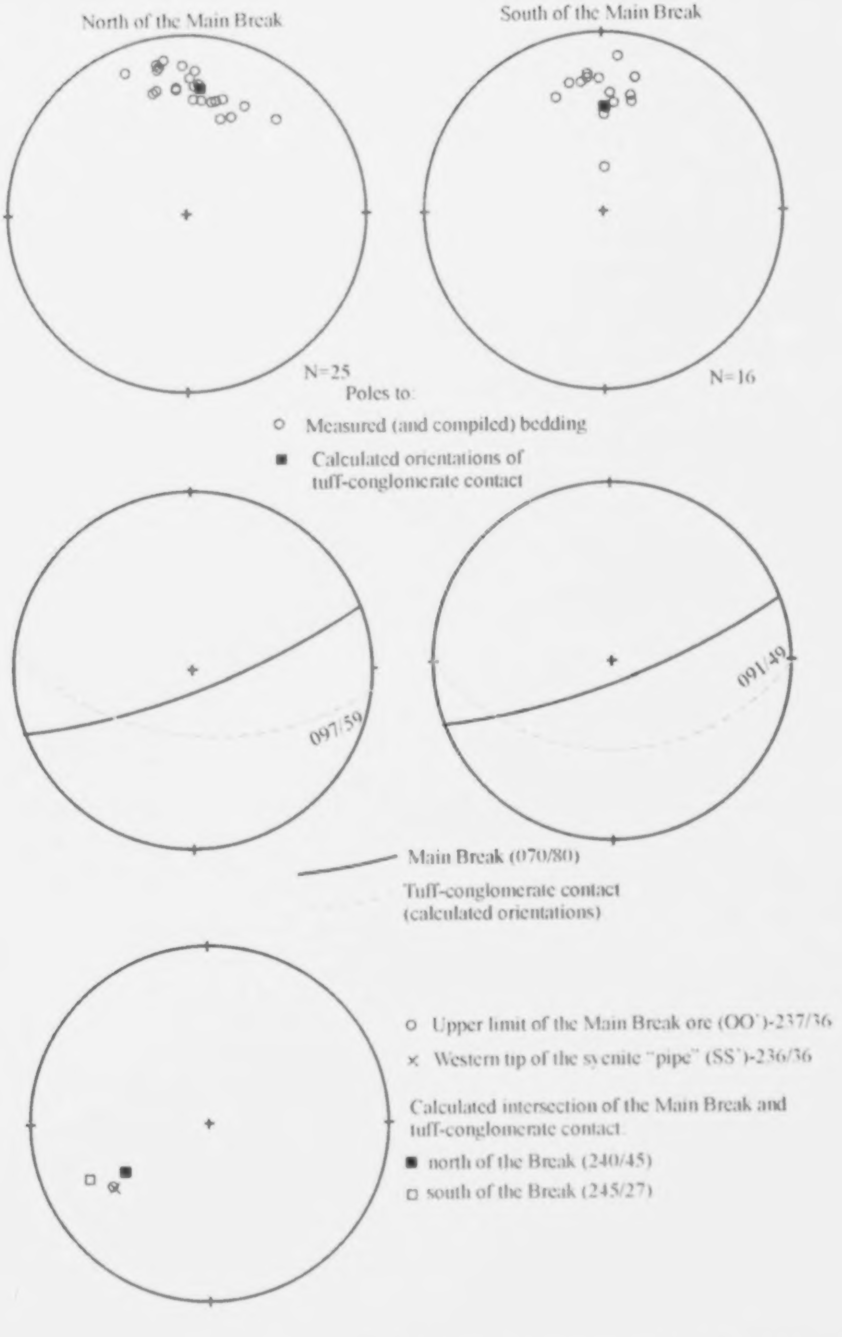
North of the Main Break
South of the Main Break
N=25
N=16
Poles to:
○ Measured (and compiled) bedding
■ Calculated orientations of tuff-conglomerate contact
097/59
091/49
Main Break (070/80)
Tuff-conglomerate contact (calculated orientations)
○ Upper limit of the Main Break ore (OO')-237/36
× Western tip of the syenite "pipe" (SS')-236/36
Calculated intersection of the Main Break and tuff-conglomerate contact:
■ north of the Break (240/45)
□ south of the Break (245/27)

Figure 32. Stereonets comparing ore plunge to other structural elements. The upper row compares calculated orientations of the tuff-conglomerate contact with actual bedding measurements, north and south of the Main Break. The middle row shows angular relationships of the Main Break (between surface and the 3000-foot level of the Macassa Mine) and the tuff-conglomerate contact (north and south of the Break). The lowermost net depicts trends and plunges of the western limit of the Main Break ore (OO' line of Figure 31), of the westernmost tip of the pipe-like syenite body (SS' line of Figure 31), and of calculated intersections between the Main Break and tuff-conglomerate contact (north and south of the Break).

Gold-Bearing Quartz Veins

GEOMETRY AND INTERNAL FEATURES

Auriferous quartz veins were observed mainly underground, at the 3825, 4250, 4500, 4750, and 4900-foot levels of the Macassa Mine, where they are hosted by mafic (augite) syenite, tuff and syenite porphyry. Principal types of gold mineralization in Macassa include "break ore"(gold-bearing quartz veins hosted by or localized in the immediate proximity to the Main Break and the '04 Break), footwall and hanging wall veins, and breccia ore (Still 2001). From these ore types, break ore (break veins) and hanging wall veins were examined in the present project. Breccia ore (i.e., ore confined between major faults, consisting of altered, silicified and strongly fractured rocks, with pods and lenses of quartz; Watson and Kerrich 1983; Still 2001) was not accessible at the time of this study. In addition to veins in the Macassa Mine, observations were made on the Teck-Hughes #1 vein, and veins hosted by the Main Break (east of the former Lake Shore shaft #5, and the Discovery ouctcop vein on the former Wright-Hargreaves property). Due to clear association with major steeply dipping fault structures, these three veins can be classified as "break ore" under Macassa Mine nomenclature.

Veins localized along the '04 break at the Macassa Mine (e.g., stopes 4247, 4940, 3826, 3829) generally dip 60°-80° south (near parallel to the host structure) with local shallower and steeper dips. Veins may be localized along the main slip of the '04 Break or along subsidiary fractures in close proximity to the main slip. Typically, these are clear-cut, planar, roughly 15-50 cm thick veins consisting largely of milky white quartz (see further discussions of vein textures and quartz types). Less common are irregular and discontinuous pockets of grey to dark grey quartz along the '04 Break (stopes 4940 and 4517, Photo 40). Most stoped "break ore" bodies consist of several veins, some of which may be oriented obliquely (up to 30-40°) to the break. Some of these oblique veins terminate abruptly against the main chlorite slip (e.g., stope 3826), probably indicating post-ore movement along the '04 Break. Contacts of break-associated veins with wall rocks are sharp or, less commonly, gradational, through sheeted veinlet zones.

A gold-bearing vein hosted by the Main Break is exposed on the Discovery outcrop (the former Wright-Hargreaves property). Along the north contact of the vein (over about 0.5 m), the host syenite porphyry is distinctly foliated (Photo 41). The foliation is sub-parallel to the vein contact and defines a strain gradient towards the vein. The north margin of the vein is marked by a roughly 5-7 cm wide band of cataclasized quartz (Photo 42). Similar cataclasite is present in the Teck-Hughes #1 vein that is hosted by a subsidiary splay of the Main Break.

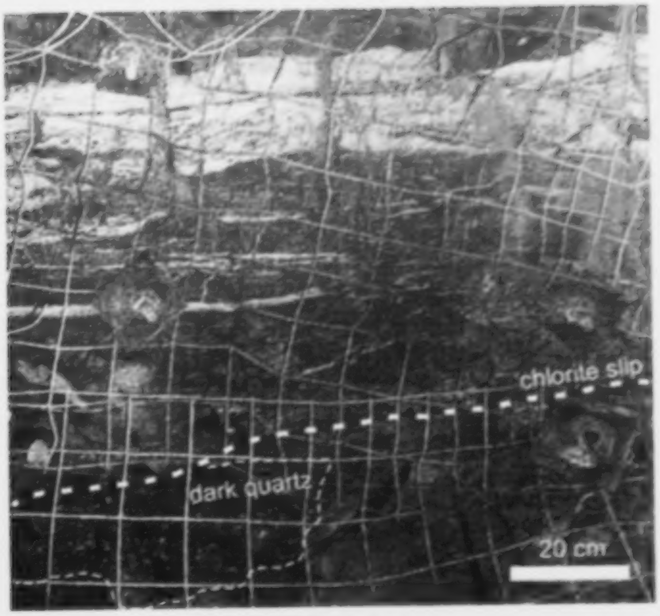

Photo 40. Gold-bearing quartz veins associated with the '04 Break; back of stope 4940, Macassa Mine, west is on the left-hand side. Planar vein 0.5-1 m south of the main chloritic slip of the '04 Break and irregular pod of dark quartz along the slip. Both are gold-bearing (samples 4940-1 and 4940-3, listed in Appendix A are, respectively, from the planar vein and the irregular quartz pod).

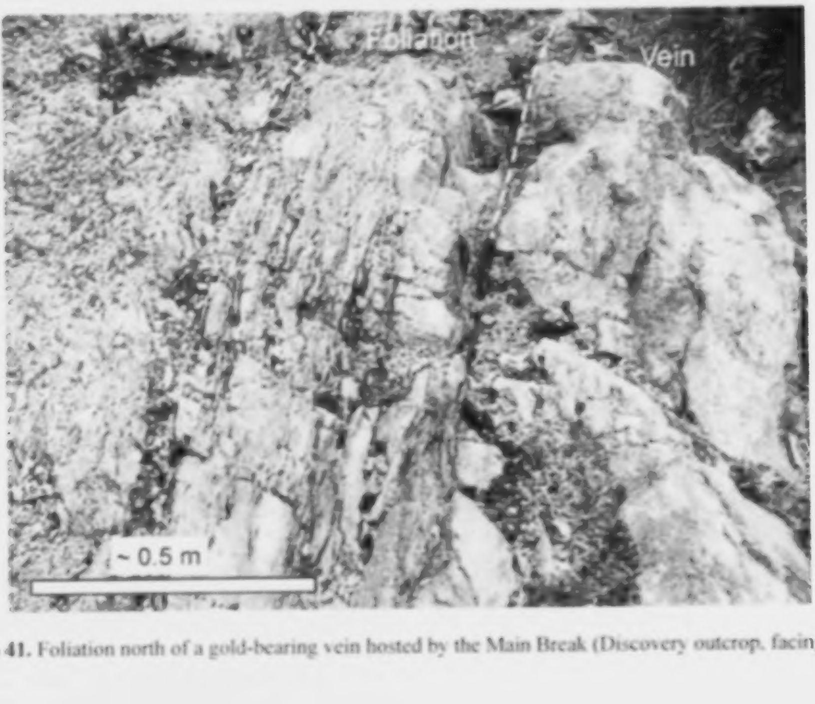

Photo 41. Foliation north of a gold-bearing vein hosted by the Main Break (Discovery outcrop, facing east).

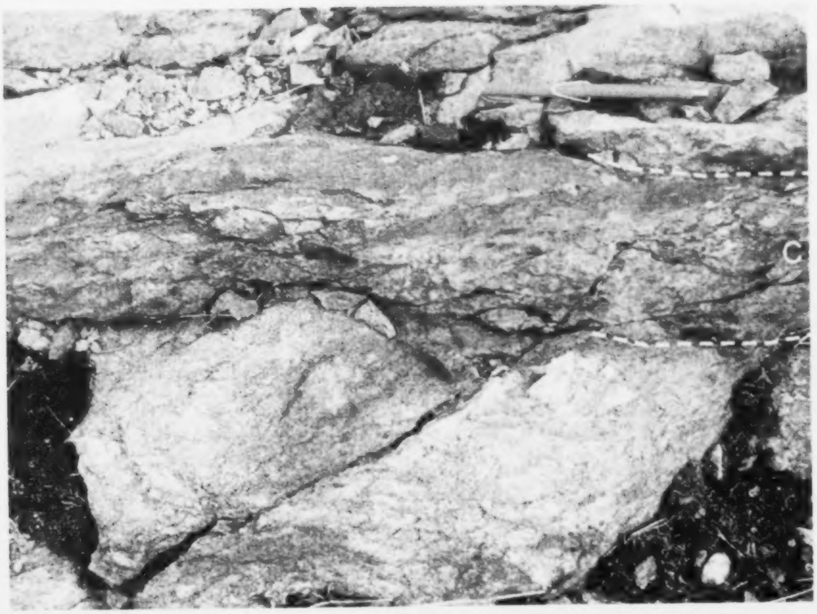

Photo 42. Cataclastic band (C) along the margin of the gold-bearing vein (Discovery outcrop, facing north). Pen magnet (approximately 12 cm) for scale.

The break-associated auriferous veins are characterized by massive, banded and breccia textures, which typically alternate along and across the strike of a single vein. Massive portions of veins consist of uniform white quartz filling. Banded to laminated texture is defined by irregular bands of darker quartz, sharp slip surfaces coated with fine molybdenite and graphite (?), and 0.5 to 3 cm thick slivers of host rocks oriented parallel to vein walls. Also characteristic is the presence of stylolites approximately parallel to the vein boundaries (Photos 43 and 44), with approximately horizontal, northwest-southeast-oriented teeth (cones). Length of stylolite teeth varies from millimetres to 1-1.5 cm. Stylolites are marked by dark films of fine molybdenite-graphite material and locally (e.g., stopes 4940, 3829) contain fine gold and telluride grains, along with pyrite and chalcopyrite. Slabs and slivers of host rocks enclosed in vein material are either weakly foliated or completely unfoliated. In a sample from Main Break-hosted vein from the Lake Shore property (east of former Lake Shore shaft 5), mineralized quartz encloses foliated streaks of hydrothermal sericite. Slivers of chlorite seams that presently mark the main slip surface of the '04 Break and subsidiary faults in Macassa have not been seen enclosed by the gold-bearing quartz veins. Breccia veins and vein intervals consist of angular, unrotated clasts of host rocks cemented by white quartz. In some veins, rock fragments are surrounded by a thin (0.5-1 mm) dark rim of fine molybdenite-graphite aggregate. Most break-associated gold-bearing veins underwent weak to strong fracturing and, locally, cataclasis. Cataclastic breccia of white vein quartz cemented by dark grey gangue material occurs in the Main Break-hosted vein on the Discovery outcrop and in the Teck-Hughes #1 vein. In the Teck-Hughes #1 vein, this dark grey cement consists of fine-grained quartz-sericite aggregate (sericite > quartz) with finely dispersed opaque matter (possibly graphite and/or molybdenite). Gold and tellurides are present both in quartz fragments and (mostly) in the dark quartz-sericite matrix indicating that the brecciation overlapped with mineralization (Photo 45). In stope 4938 at the Macassa Mine, fractured gold-bearing quartz is cemented by a barren, post-ore quartz-chlorite aggregate, reflecting post-mineralization movements along the '04 Break.

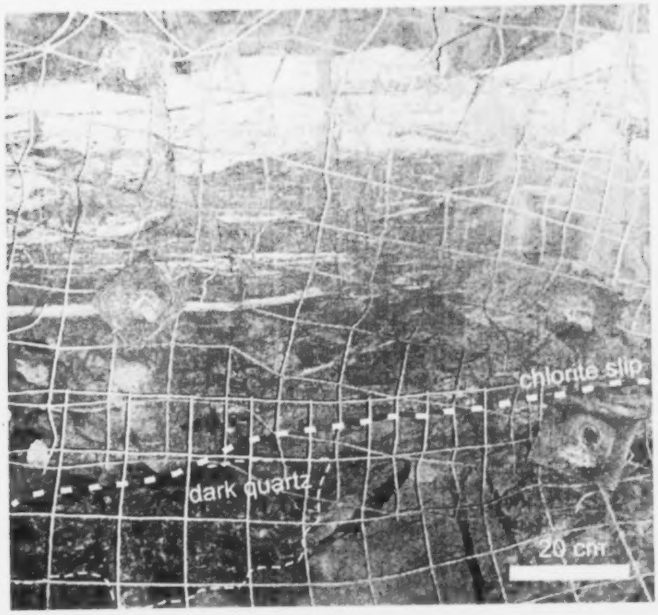

Photo 40. Gold-bearing quartz veins associated with the '04 Break; back of stope 4940, Macassa Mine, west is on the left-hand side. Planar vein 0.5-1 m south of the main chloritic slip of the '04 Break and irregular pod of dark quartz along the slip. Both are gold-bearing (samples 4940-1 and 4940-3, listed in Appendix A are, respectively, from the planar vein and the irregular quartz pod).

Photo 41. Foliation north of a gold-bearing vein hosted by the Main Break (Discovery outcrop, facing east).

Photo 42. Cataclastic band (C) along the margin of the gold-bearing vein (Discovery outcrop, facing north). Pen magnet (approximately 12 cm) for scale.

The break-associated auriferous veins are characterized by massive, banded and breccia textures, which typically alternate along and across the strike of a single vein. Massive portions of veins consist of uniform white quartz filling. Banded to laminated texture is defined by irregular bands of darker quartz, sharp slip surfaces coated with fine molybdenite and graphite (?), and 0.5 to 3 cm thick slivers of host rocks oriented parallel to vein walls. Also characteristic is the presence of stylolites approximately parallel to the vein boundaries (Photos 43 and 44), with approximately horizontal, northwest-southeast-oriented teeth (cones). Length of stylolite teeth varies from millimetres to 1-1.5 cm. Stylolites are marked by dark films of fine molybdenite-graphite material and locally (e.g., stopes 4940, 3829) contain fine gold and telluride grains, along with pyrite and chalcopyrite. Slabs and slivers of host rocks enclosed in vein material are either weakly foliated or completely unfoliated. In a sample from Main Break-hosted vein from the Lake Shore property (east of former Lake Shore shaft 5), mineralized quartz encloses foliated streaks of hydrothermal sericite. Slivers of chlorite seams that presently mark the main slip surface of the '04 Break and subsidiary faults in Macassa have not been seen enclosed by the gold-bearing quartz veins. Breccia veins and vein intervals consist of angular, unrotated clasts of host rocks cemented by white quartz. In some veins, rock fragments are surrounded by a thin (0.5-1 mm) dark rim of fine molybdenite-graphite aggregate. Most break-associated gold-bearing veins underwent weak to strong fracturing and, locally, cataclasis. Cataclastic breccia of white vein quartz cemented by dark grey gangue material occurs in the Main Break-hosted vein on the Discovery outcrop and in the Teck-Hughes #1 vein. In the Teck-Hughes #1 vein, this dark grey cement consists of fine-grained quartz-sericite aggregate (sericite > quartz) with finely dispersed opaque matter (possibly graphite and/or molybdenite). Gold and tellurides are present both in quartz fragments and (mostly) in the dark quartz-sericite matrix indicating that the brecciation overlapped with mineralization (Photo 45). In stope 4938 at the Macassa Mine, fractured gold-bearing quartz is cemented by a barren, post-ore quartz-chlorite aggregate, reflecting post-mineralization movements along the '04 Break.

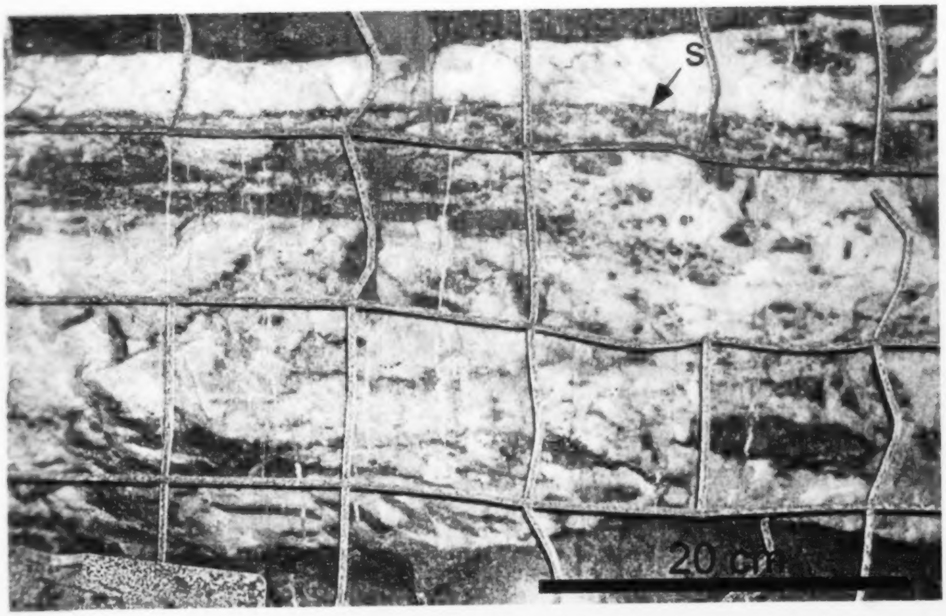

Photo 43. Typical textural appearance of a steeply (roughly 70°) dipping vein associated with the '04 Break (stope 4940, Macassa Mine). Slabs and angular fragments of host rocks are cemented by quartz; dark stylolite surface (marked "s") is parallel to vein walls.

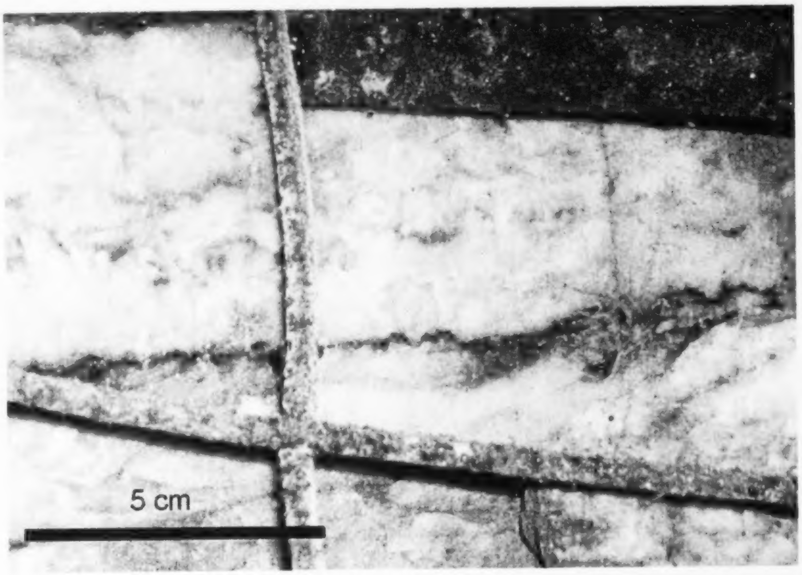

Photo 44. Close-up view of a stylolite in a break-associated vein ('04 Break, stope 4940, Macassa Mine).

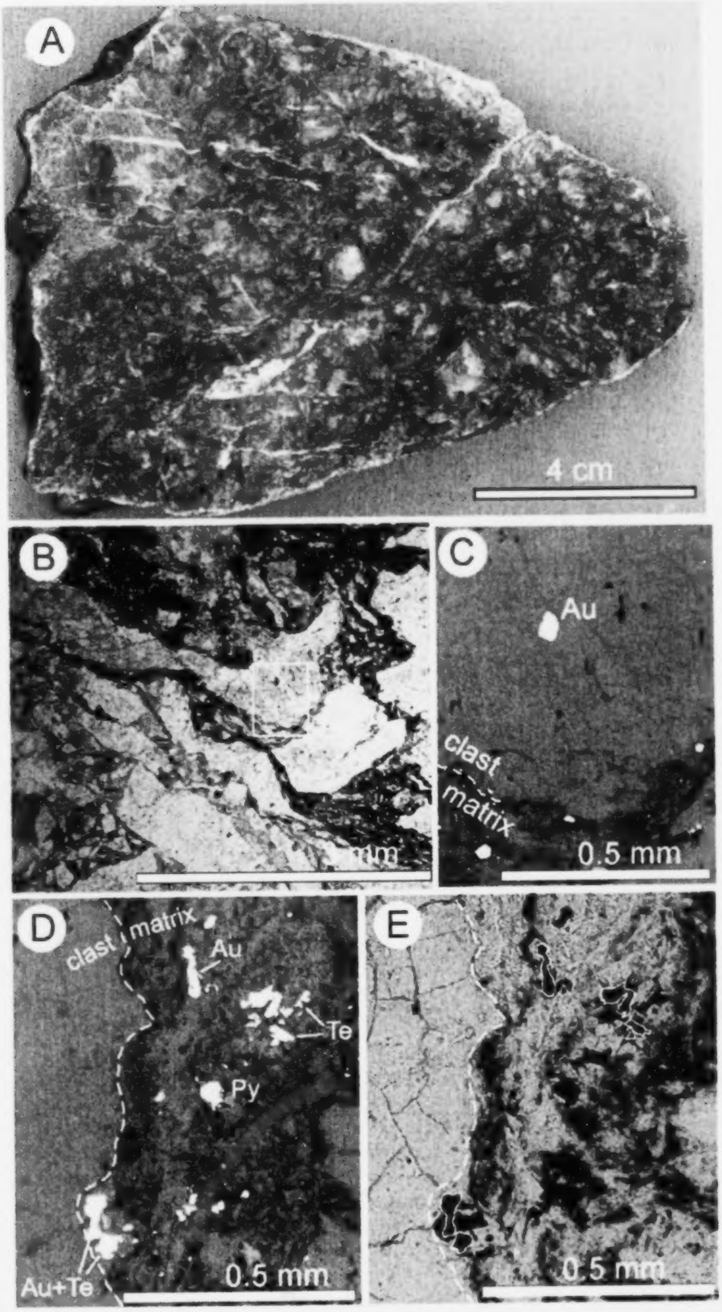

Photo 45. Cataclasized quartz from Teck-Hughes #1 vein. A) polished slab: angular fragments of quartz (light colored) and, more rare, of host syenite porphyry are cemented by dark grey quartz-sericite aggregate (sericite >50%). B-E) photomicrographs (B and E, transmitted plane-polarized light; C and D, reflected light). Gold (Au) and tellurides (Te) (0.01-0.02 mm) occur in quartz clasts (C) and (more frequently) in sericite-rich cementing aggregate (D and E), indicating that cataclasis overlapped with mineralization. Dark coloration of the cementing aggregate is largely due to the presence of very fine opaque, non-reflective particles, possibly molybdenite and graphite (or carbon). Geochemical data for this sample (sample 1254-2) are listed in Appendix A. In surface exposure of the #1 vein, dark cataclasized quartz represented by this sample is volumetrically subordinate to white quartz with wall rock clasts.

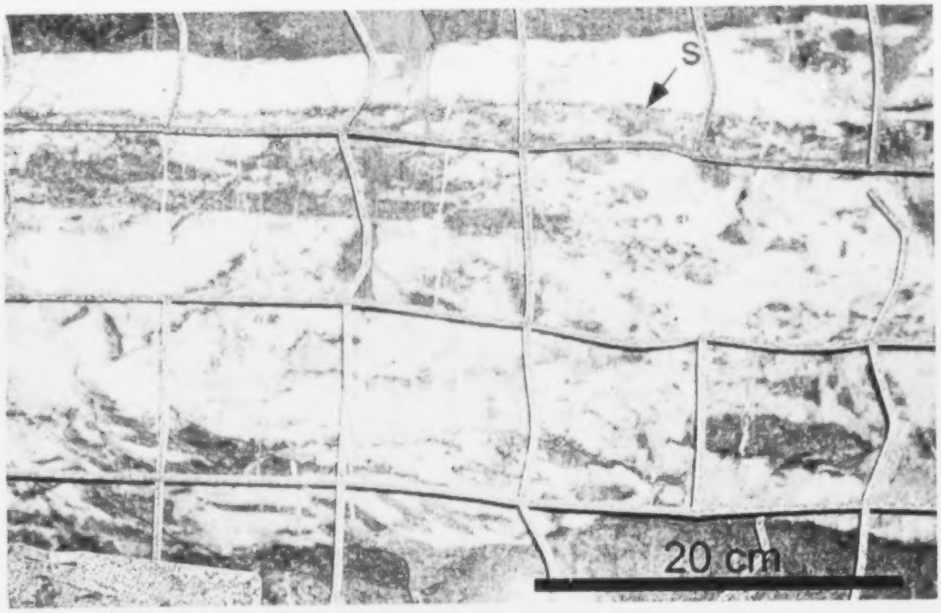

Photo 43. Typical textural appearance of a steeply (roughly 70°) dipping vein associated with the '04 Break (stope 4940, Macassa Mine). Slabs and angular fragments of host rocks are cemented by quartz; dark stylolite surface (marked "s") is parallel to vein walls.

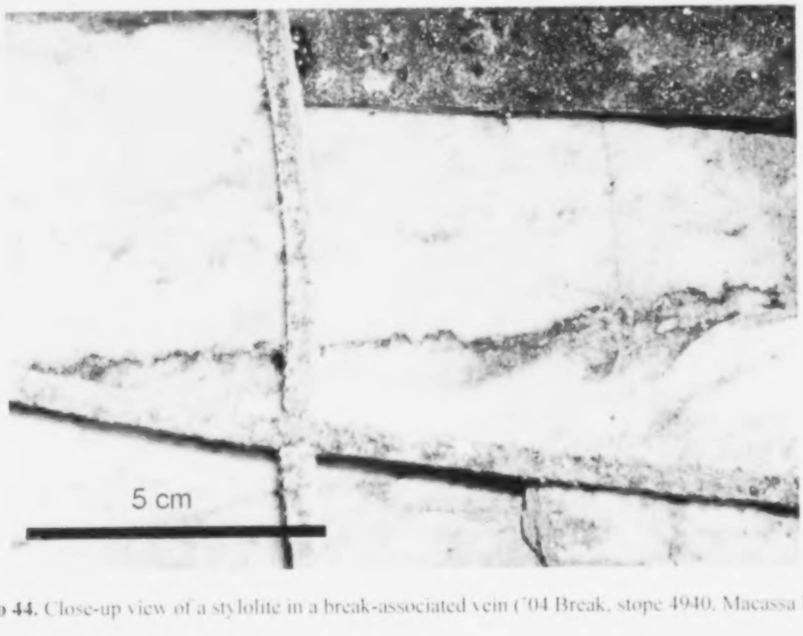

Photo 44. Close-up view of a stylolite in a break-associated vein ('04 Break, stope 4940, Macassa Mine).

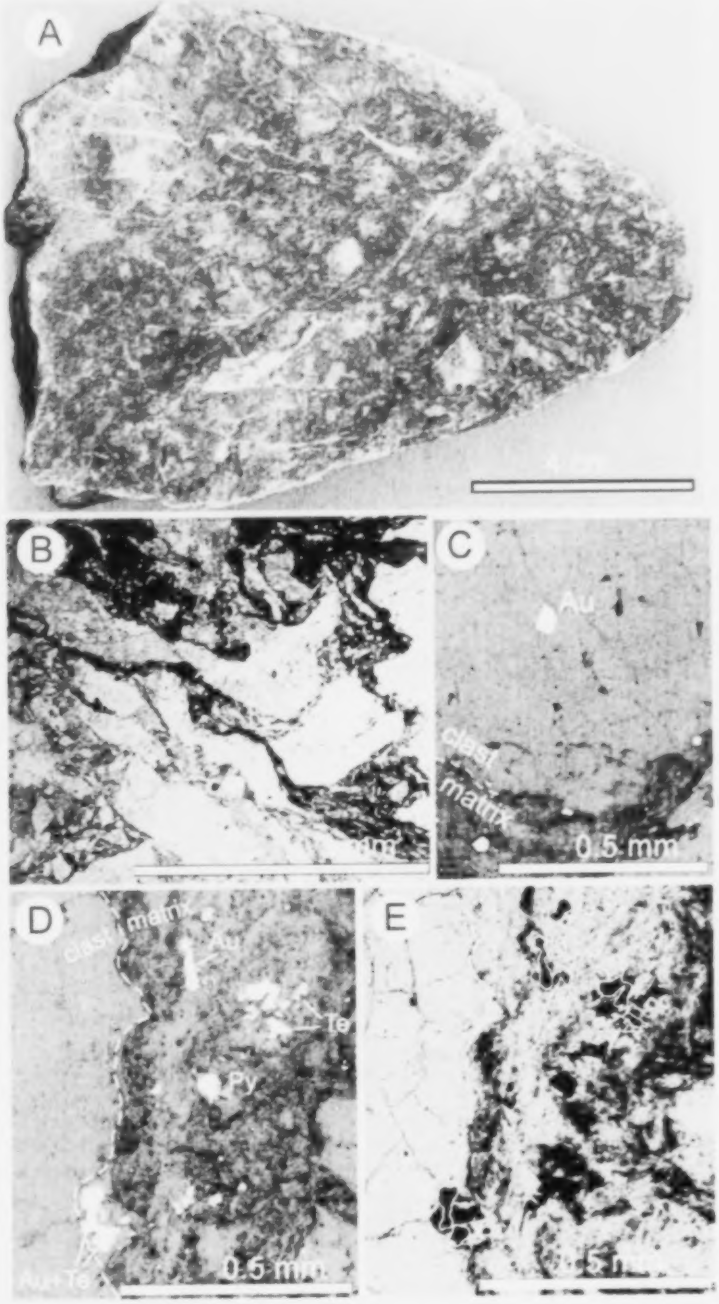

Photo 45. Cataclasized quartz from Teck-Hughes #1 vein. A) polished slab: angular fragments of quartz (light colored) and, more rare, of host syenite porphyry are cemented by dark grey quartz-sericite aggregate (sericite ~50%). B-E) photomicrographs (B and E, transmitted plane-polarized light; C and D, reflected light). Gold (Au) and tellurides (Te) (0.01-0.02 mm) occur in quartz clasts (C) and (more frequently) in sericite-rich cementing aggregate (D and E), indicating that cataclasis overlapped with mineralization. Dark coloration of the cementing aggregate is largely due to the presence of very fine opaque, non-reflective particles, possibly molybdenite and graphite (or carbon). Geochemical data for this sample (sample 1254-2) are listed in Appendix A. In surface exposure of the #1 vein, dark cataclasized quartz represented by this sample is volumetrically subordinate to white quartz with wall rock clasts.

Hanging-wall veins exhibit a variety of orientations: from shallow (10-35°) to steep (60°-70°) south dipping, and some veins in a wedge-shaped block between the 04' and No. 6 breaks dip steeply (60-70°) north. Thickness of individual veins varies from 5-7 cm to 0.5-1.0 m. The steeply north- and south-dipping hanging-wall veins are associated with minor subsidiary fault structures and are overall similar to break-related veins. In fact, for veins located close (e.g., within about 5 m) to the '04 Break, classification into "break" or "hanging wall" category is arbitrary.

Shallowly south-dipping (10-40°) hanging-wall veins tend to become steeper towards the north, as they converge with the '04 Break (Still 2001; M. Sutton, Kirkland Lake Gold Inc., personal communication, 2004). The flatter portions of these veins also tend to have higher gold grade (Still 2001). Details of localization of individual veins vary. Moderately to shallowly dipping veins hosted by tuffs are generally bedding-parallel (e.g., stopes 4713, 4512, 5030). In stope 4744, a gently (about 30°) south-dipping vein is hosted by a mafic syenite sill intruding tuffs. The vein is located close to the contact of the sill, and is approximately parallel to it. The largest of the observed shallowly to moderately dipping veins, 4206-S3, strikes 055° to 100° and dips about 30-35° south; it is hosted entirely by mafic syenite, and is spatially associated with a small fault that dips 30° to 60° south (Photo 46). The fault (and probably the vein) appears to become steeper towards the south (near the southern wall of the stope).

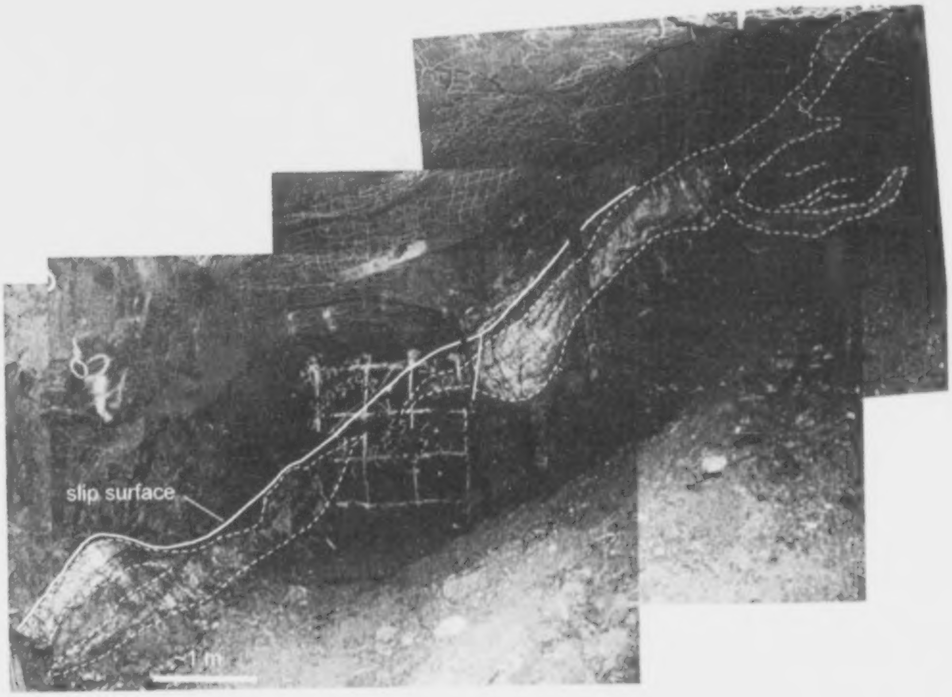

Photo 46. Vein 4206-S3 (Macassa Mine). Cross-section view facing approximately west. Vein is spatially associated with a small fault that typically dips about 30-40° south but steepens to 55-60° (S) near the southern wall. The vein is hosted by mafic syenite.

It should be noted that even veins that are approximately concordant to bedding or lithological contacts tend to be spatially associated with minor faults or slips, i.e., it is more appropriate to consider these veins as controlled by tectonically re-activated surfaces. For example, in stope 5030, a vein striking about 115-120° and dipping about 20° (southwest) is hosted by tuffs and is associated with two sharp bedding-parallel slips. A graphite-molybdenite-coated slip surface in a footwall of the vein contains approximately dip-parallel striations. The vein consists of concordant (i.e., bedding- and slip-parallel) banded or breccia intervals and discordant breccia pockets (Photo 47). The geometry of the latter can be interpreted as dilational jogs formed during reverse (southwest over northeast) movements along bedding-parallel slips.

Texturally, steeply and shallowly dipping hanging-wall veins are similar to steep, break-associated veins. Massive, banded and breccia textures alternate along and across strike of individual veins. Boundary-parallel sharp stylolites were observed both in steeply (roughly 60°, stope 4229-5) and more shallowly (30-45°, stope 4512) south-dipping hanging wall veins. In a moderately dipping (30-45°) vein in stope 4512, stylolite teeth are oriented near horizontal, at about 45° to vein boundaries and stylolite planes. Perhaps slightly unusual is a banded texture of vein 4206-S3, where bands of white and dark quartz, and breccia layers make up a crudely layered crustiform-like banding (Photo 48). Similar to break-associated veins, shallowly and steeply dipping hanging-wall veins are commonly fractured. In some gold-rich segments of the 4206-S3 vein gold and telluride mineralization is associated with late fracture filling along irregular network (Photo 49A,B).

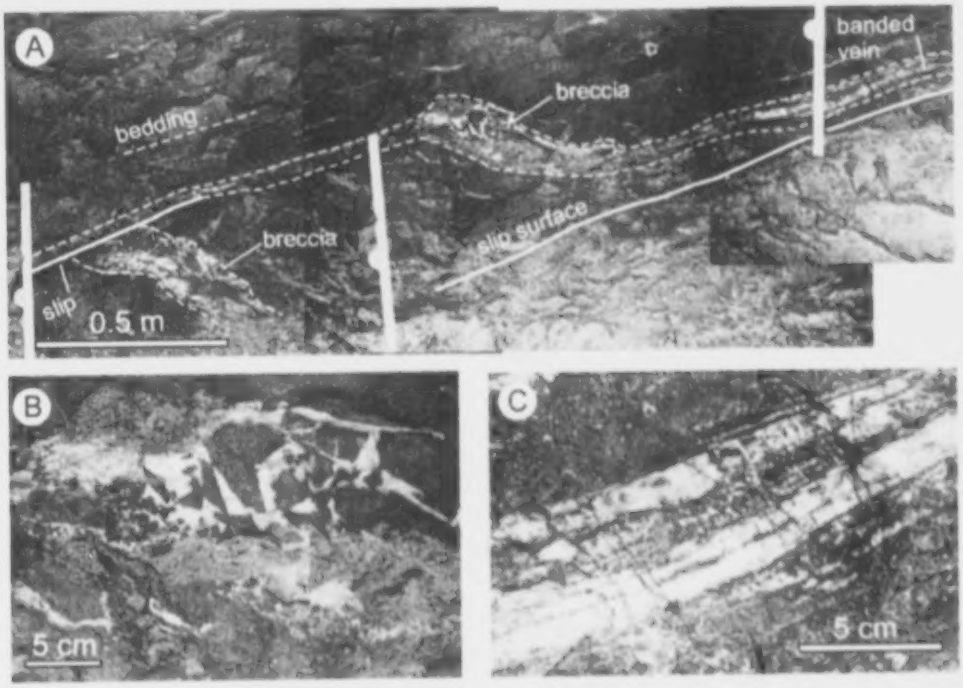

Photo 47. Bedding-parallel vein in tuffs (stope 5030, Macassa Mine, cross-section view, west-southwest is on the left-hand side). Breccia pockets discordant to bedding may have formed as dilational jogs during reverse motion along slip planes. B) close-up view of a breccia interval: angular wall rock clasts cemented by white quartz. C) banded texture defined by dark fractures and bands.

Hanging-wall veins exhibit a variety of orientations: from shallow (10-35°) to steep (60°-70°) south dipping, and some veins in a wedge-shaped block between the 04' and No. 6 breaks dip steeply (60-70°) north. Thickness of individual veins varies from 5-7 cm to 0.5-1.0 m. The steeply north- and south-dipping hanging-wall veins are associated with minor subsidiary fault structures and are overall similar to break-related veins. In fact, for veins located close (e.g., within about 5 m) to the '04 Break, classification into "break" or "hanging wall" category is arbitrary.

Shallowly south-dipping (10-40°) hanging-wall veins tend to become steeper towards the north, as they converge with the '04 Break (Still 2001; M. Sutton, Kirkland Lake Gold Inc., personal communication, 2004). The flatter portions of these veins also tend to have higher gold grade (Still 2001). Details of localization of individual veins vary. Moderately to shallowly dipping veins hosted by tuffs are generally bedding-parallel (e.g., stopes 4713, 4512, 5030). In stope 4744, a gently (about 30°) south-dipping vein is hosted by a mafic syenite sill intruding tuffs. The vein is located close to the contact of the sill, and is approximately parallel to it. The largest of the observed shallowly to moderately dipping veins, 4206-S3, strikes 055° to 100° and dips about 30-35° south; it is hosted entirely by mafic syenite, and is spatially associated with a small fault that dips 30° to 60° south (Photo 46). The fault (and probably the vein) appears to become steeper towards the south (near the southern wall of the stope).

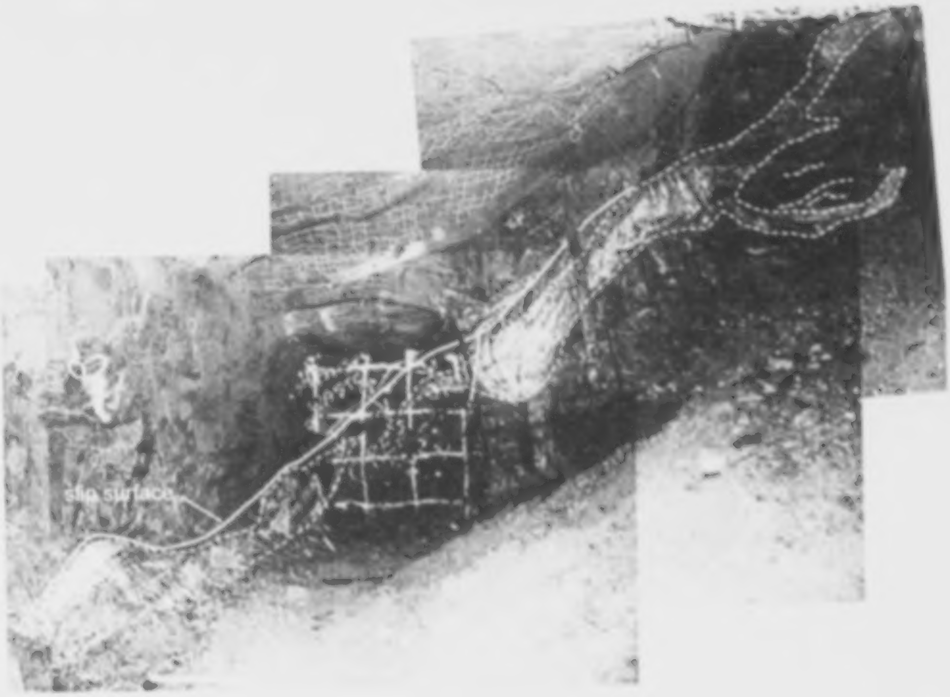

Photo 46. Vein 4206-S3 (Macassa Mine). Crosssection view facing approximately west. Vein is spatially associated with a small fault that typically dips about 30-40° south but steepens to 55-60° (S) near the southern wall. The vein is hosted by mafic syenite.

It should be noted that even veins that are approximately concordant to bedding or lithological contacts tend to be spatially associated with minor faults or slips, i.e., it is more appropriate to consider these veins as controlled by tectonically re-activated surfaces. For example, in stope 5030, a vein striking about 115-120° and dipping about 20° (southwest) is hosted by tuffs and is associated with two sharp bedding-parallel slips. A graphite-molybdenite-coated slip surface in a footwall of the vein contains approximately dip-parallel striations. The vein consists of concordant (i.e., bedding- and slip-parallel) banded or breccia intervals and discordant breccia pockets (Photo 47). The geometry of the latter can be interpreted as dilational jogs formed during reverse (southwest over northeast) movements along bedding-parallel slips.

Texturally, steeply and shallowly dipping hanging-wall veins are similar to steep, break-associated veins. Massive, banded and breccia textures alternate along and across strike of individual veins. Boundary-parallel sharp stylolites were observed both in steeply (roughly 60°, stope 4229-5) and more shallowly (30-45°, stope 4512) south-dipping hanging wall veins. In a moderately dipping (30-45°) vein in stope 4512, stylolite teeth are oriented near horizontal, at about 45° to vein boundaries and stylolite planes. Perhaps slightly unusual is a banded texture of vein 4206-S3, where bands of white and dark quartz, and breccia layers make up a crudely layered crustiform-like banding (Photo 48). Similar to break-associated veins, shallowly and steeply dipping hanging-wall veins are commonly fractured. In some gold-rich segments of the 4206-S3 vein gold and telluride mineralization is associated with late fracture filling along irregular network (Photo 49A,B).

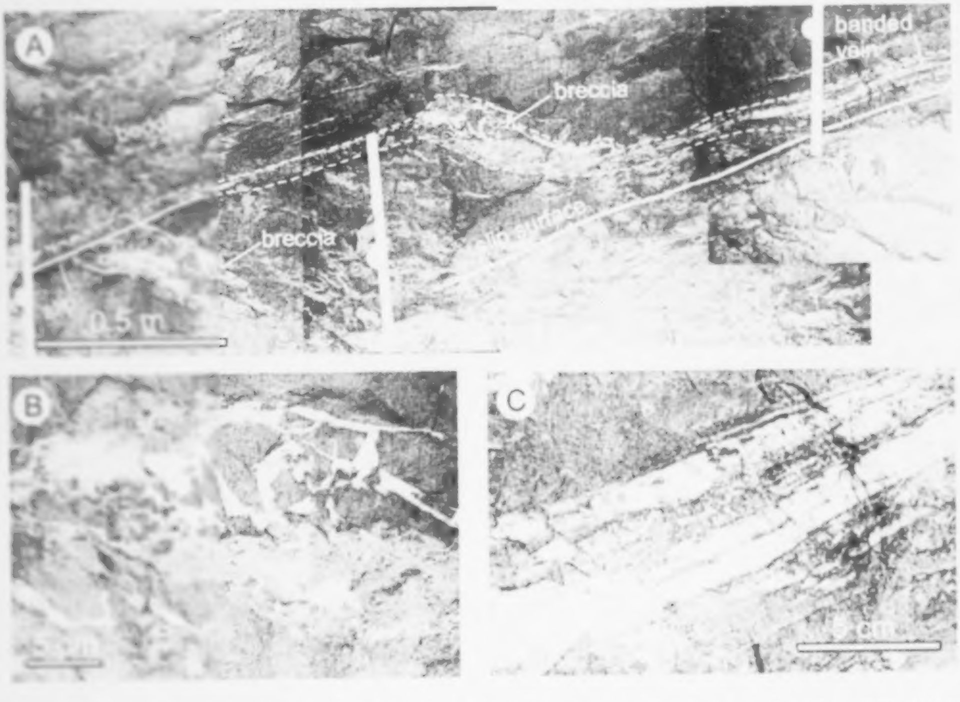

Photo 47. Bedding-parallel vein in tuffs (stope 5030, Macassa Mine, cross-section view, west-southwest is on the left-hand side) Breccia pockets discordant to bedding may have formed as dilational jogs during reverse motion along slip planes. B) close-up view of a breccia interval: angular wall rock clasts cemented by white quartz. C) banded texture defined by dark fractures and bands.

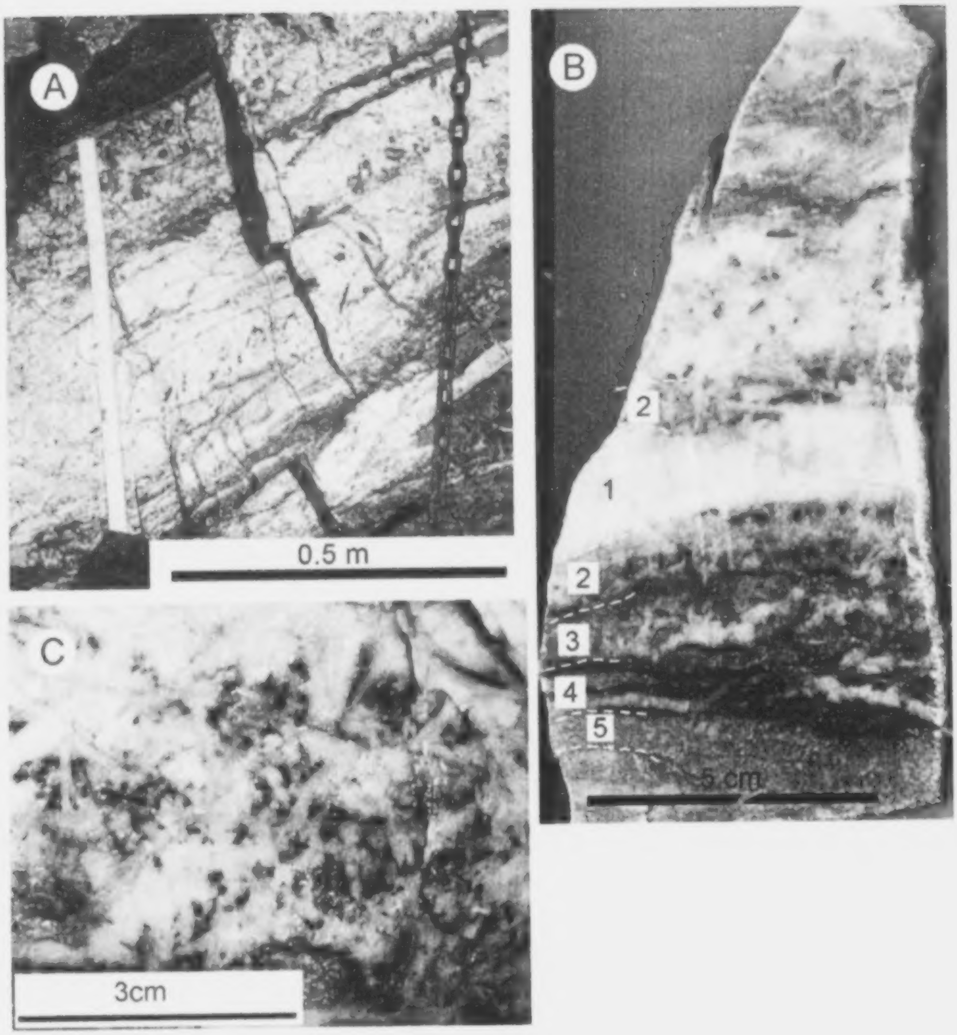

Photo 48. A) Close-up view of vein 4206-S3. Crude banding defined by layers and bands of darker and lighter quartz, slabs and angular fragments of host mafic syenite. B) polished slab from the same part of the vein, showing crustiform-like layering. 1, massive white quartz; 2, randomly oriented prismatic quartz crystals (0.5-1.5 cm long) enclosed in darker matrix that (based on microscopic observations) consists of fine-grained (0.05-0.1 mm) quartz with minor feldspar, sericite, carbonate, and fine opaque "dust" (0.01-0.02 mm); 3, same as 2, but also includes angular mafic syenite clasts; 4, dark grey fine-grained quartz (0.05 mm) with approximately 50% opaque non-reflective particles, and minor feldspar, carbonate, and sericite; 5, sliver of strongly sulphidized (pyrite) mafic syenite. C) a close-up view illustrating characteristic relationships of white and dark quartz in the same part of the vein. Dark fine-grained quartz encloses randomly oriented coarse prismatic quartz crystals or fills intersticies between them.

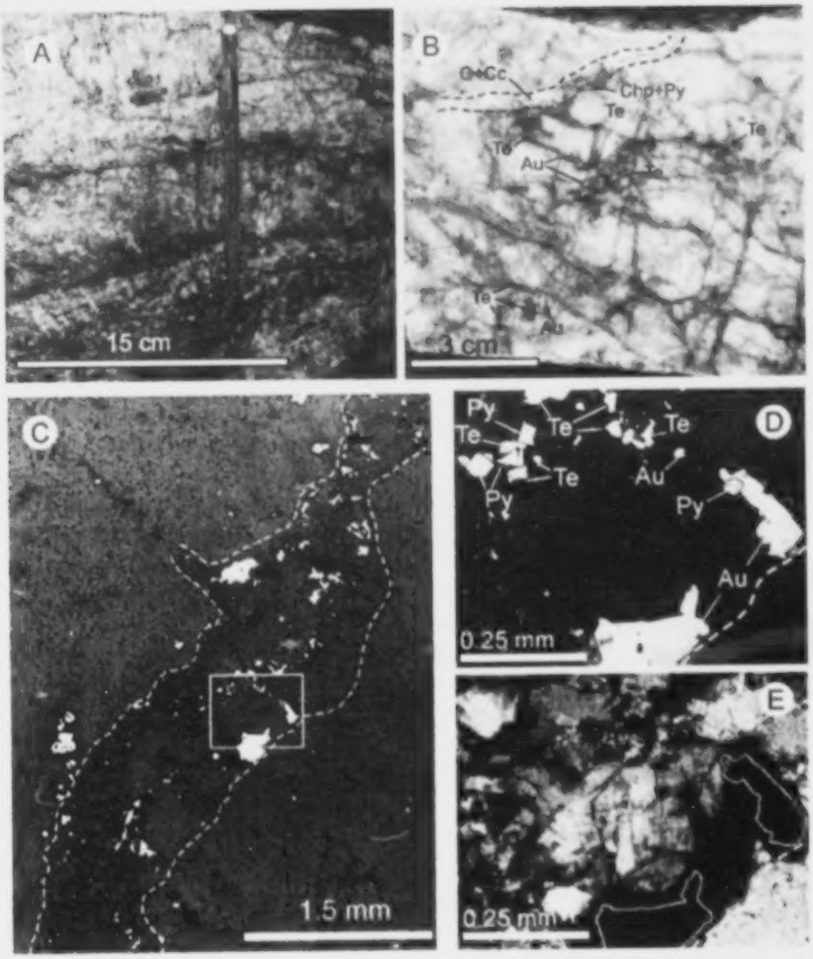

Photo 49. Fracturing and late vein filling in vein 4206-S3 (area corresponding to left-hand bottom part of Photo 46). A) general view of strongly fractured quartz, with late filling aggregate along fractures. B) polished slab from the same area. Gold (Au) and tellurides (Te) tend to occur along the late fractures filled with dull greenish grey (dark on the photo) fine-grained material. Under the microscope, this late vein filling consists of fine-grained quartz, feldspar (most probably K-feldspar), carbonate, and sericite. Note also late quartz-carbonate veinlet (Q-Cc) with pyrite and chalcopyrite (Chp+Py). C) photomicrograph (reflected light) of one of the dark veinlets from photo B. Note concentration of metallic minerals (pyrite, gold and tellurides) in the veinlet (rectangle marks the area of photos D and E). D-E) photomicrographs (respectively, refected light and transmitted light, cross nicols), representing magnified veiws of the rectangular area from photo C. Metallic minerals include gold (Au), tellurides (altaite, Te), and pyrite (Py). Gold is intergrown with feldspar (E, centre of the photo) that shows grid-like twinning characteristic of K-feldspar.

Classifying gold-bearing veins of the Kirkland Lake camp in conventional "fault-fill vein vs. extensional vein" nomenclature (e.g., Robert and Poulsen 2001) is not simple, primarily because of lack of discrete, texturally distinct vein populations. However, it is reasonably clear that steeply (≥ 60°) dipping veins associated with the Main Break, the '04 Break, and similarly oriented hanging-wall veins should be classified as fault-fill veins, based on their close association with and generally parallel orientation to faults, as well as on locally developed vein-parallel foliation in the immediate wall rocks (e.g., Photo 41).

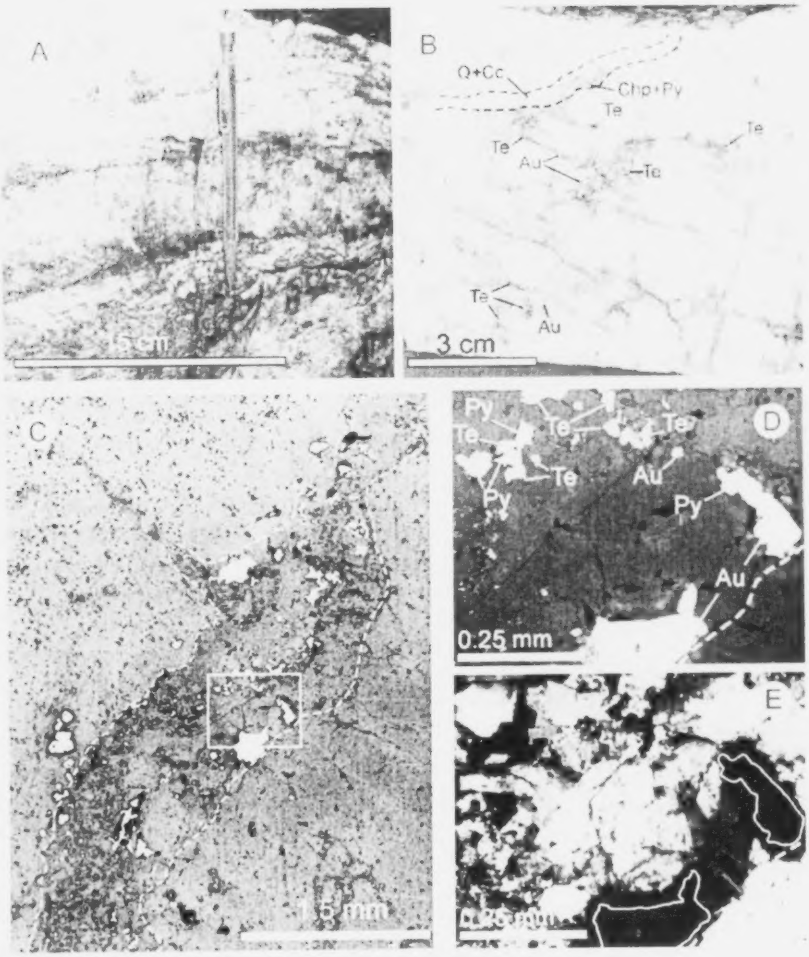

Photo 49. Fracturing and late vein filling in vein 4206-S3 (area corresponding to left-hand bottom part of Photo 46). A) general view of strongly fractured quartz, with late filling aggregate along fractures. B) polished slab from the same area. Gold (Au) and tellurides (Te) tend to occur along the late fractures filled with dull greenish grey (dark on the photo) fine-grained material. Under the microscope, this late vein filling consists of fine-grained quartz, feldspar (most probably K-feldspar), carbonate, and sericite. Note also late quartz-carbonate veinlet (Q-Cc) with pyrite and chalcopyrite (Chp+Py). C) photomicrograph (reflected light) of one of the dark veinlets from photo B. Note concentration of metallic minerals (pyrite, gold and tellurides) in the veinlet (rectangle marks the area of photos D and E). D-E) photomicrographs (respectively, refected light and transmitted light, cross nicols), representing magnified veiws of the rectangular area from photo C. Metallic minerals include gold (Au), tellurides (altaite, Te), and pyrite (Py). Gold is intergrown with feldspar (E, centre of the photo) that shows grid-like twinning characteristic of K-feldspar.

Classifying gold-bearing veins of the Kirkland Lake camp in conventional "fault-fill vein vs. extensional vein" nomenclature (e.g., Robert and Poulsen 2001) is not simple, primarily because of lack of discrete, texturally distinct vein populations. However, it is reasonably clear that steeply (>60°) dipping veins associated with the Main Break, the '04 Break, and similarly oriented hanging-wall veins should be classified as fault-fill veins, based on their close association with and generally parallel orientation to faults, as well as on locally developed vein-parallel foliation in the immediate wall rocks (e.g., Photo 41).

Previously, Thomson et al. (1950) interpreted moderately (about 45°) south-dipping subsidiary veins as extensional veins in the hanging wall of the Main Break reverse fault. The relatively shallowly dipping hanging-wall veins observed at the Macassa Mine in this project, and thus, probably similarly oriented veins at other mines, are unlikely to be extensional. Near-horizontal orientation is expected for extensional veins associated with steep reverse faults (e.g., Robert and Poulsen 2001), whereas at Macassa, many of the veins that are considered shallowly dipping, dip approximately 30-45° south. An even steeper dip angle (roughly 55°-60°) is characteristic of the Teck-Hughes "E" vein that can be remotely observed in a steep wall of a small open pit (Photo 50). There is little or no textural distinction between shallow and steep veins, and textures diagnostic only of extensional veins such as mineral fibres orthogonal to vein walls are not found. Many of the observed veins are spatially associated with and are parallel to minor subsidiary faults (e.g., 4206-S3, "E" vein, Photos 46 and 50), or are controlled by re-activated pre-existing surfaces, such as bedding planes (e.g., 4512, 4713, 5030), or intrusive contacts (4744). Features resembling dilational jogs associated with reverse movement along bedding-parallel slip planes were observed in vein in stope 5030. Although extensional opening mechanism may have played a role locally, it appears more appropriate to interpret gently to moderately dipping (roughly 30-45°) hanging-wall veins as fault-fill veins associated with minor subsidiary structures and reactivated bedding planes and lithological contacts.

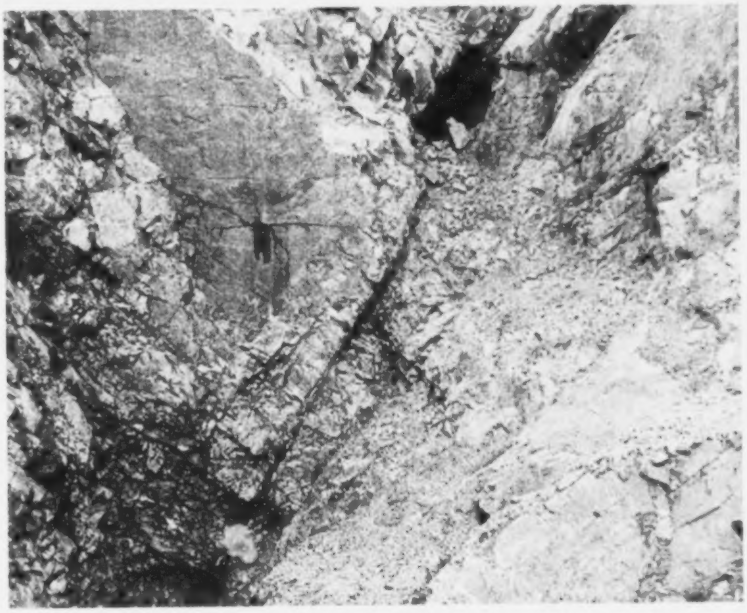

Photo 50. Remote view of the Teck-Hughes "E" vein in the proximal hanging wall of the Main Break (looking to the west, old stope on the top is about 1.5 m wide). The vein is hosted by a sharp, most likely brittle, fault or fracture that dips about 55° south (centre of the photo).

METALLIC MINERALS

The mineralogy of Kirkland Lake ores is described in detail by Todd (1928) and Thomson et al. (1950), and only macroscopic observations and pilot microscopic study of 15 samples were done in this project. Gold is accompanied by tellurides (altaite, calaverite, petzite, and coloradoite; Todd 1928; Thomson et al. 1950). Other metallic minerals include pyrite, chalcopyrite, minor sphalerite and very rare arsenopyrite.

Among tellurides, altaite is the most abundant. Milling investigations of two bulk ore samples from the Lake Shore Mine showed that gold-bearing tellurides account on average for 11-19% of the total gold (Thomson et al. 1950). As discussed in the section on geochemistry of gold-bearing veins, relative proportions of native gold vs. telluride gold probably range broadly. Although some gold is associated with pyrite in altered host rocks (Thomson et al. 1950), economically significant gold mineralization is related to gold and tellurides contained in quartz veins.

VEIN-FILLING TYPES

In all veins examined in this study, multiple generations of quartz distinguished by various shades of grey are present. Previously, Todd (1928) and Thomson et al. (1950) documented early white, and later darker generations of quartz. Dark quartz was identified as being better mineralized than the "practically barren" white quartz (Todd 1928, p.67).

A brief petrographic study of quartz vein samples shows that the white quartz that constitutes the bulk of vein fillings is medium to coarse crystalline. Quartz crystals are largely anhedral, and less commonly subhedral to euhedral. The most common grain size is 1-3 mm, and some euhedral to subhedral prismatic crystals are up to 10-20 mm long. Abundant fluid inclusions, including 3-phase aqueous-carbonic, are hosted by the quartz crystals. Orientation of large euhedral-subhedral prismatic crystals is either random, or at high angles to vein walls. Interstices between prismatic crystals are commonly filled with finer-grained darker quartz, and some prismatic quartz crystals are enclosed in the darker quartz matrix (see below). The high-angle orientation of quartz crystals to vein walls, although not equally well-defined, was observed in practically all types of veins (e.g., '04 Break-associated steep veins 4940 and 3829; steep Tech Hughes #1 vein, steeply north-dipping hanging-wall vein 4528; shallowly to moderately south-dipping hanging-wall veins 4206-S3 and 4512). In some breccia veins, wall-rock fragments are overgrown by radiating prismatic quartz crystals.

The darker (grey to almost black) vein filling consists of distinctly finer (0.01-0.1 mm) quartz (Photo 51) accompanied by variable amounts of sericite, carbonate and feldspar (e.g., 4206-S3). The variably intense dark coloration appears to be largely due to the presence of fine opaque particles or clots (0.01-0.05 mm, Photo 51 B, D). Their presence in the fine-grained aggregate and absence in the coarse quartz crystals is particularly well seen in transmitted light with the conoscopic condenser lens that makes fluid inclusions in large "white" quartz crystals invisible. In polished thin sections, these opaque particles are non-reflective (Photo 51B,C,D). They may represent molybdenite or graphite flakes that are too small and are not sufficiently polished to be reflective, or they may consist of a non-crystalline carbonaceous substance, perhaps amorphous carbon. Very fine (0.005-0.01 mm) brown titanite (?) was seen in the dark fine-grained quartz in samples from vein 4206-S3.

The relationships between the dark vein fill and the coarser white quartz vary. In the cataclastic parts of Teck-Hughes #1 vein, fine-grained (0.01-0.02 mm) dark quartz-sericite (sericite > 50%) aggregate cements angular fragments (0.3-1.5 cm) of lighter quartz (Photo 45). Gold and tellurides (0.01-0.02 mm) are present mainly in the dark sericite-rich matrix, and less frequently, in quartz fragments.

In vein 4206-S3, grey to dark grey, fine-grained (0.03-0.1 mm) quartz with minor K-feldspar (?), sericite, carbonate and variably abundant opaque particles forms discrete bands (2-5 mm) and occurs as matrix enclosing randomly oriented white subhedral prismatic (0.5-1.5 cm long) quartz crystals, or filling interstices between them (Photos 48, 51). The dark quartz occurs in multiple concordant bands parallel to vein contacts, and the relative abundance of dark and white vein fillings defines a characteristic crude layering, along with the abundance of host rock fragments (Photo 48B,C). In other veins (e.g., 4528, 4506, 3829), the darker aggregate of fine quartz, subordinate carbonate, sericite, and opaque particles similarly forms a matrix that encloses larger prismatic white quartz crystals oriented randomly or at high angles to vein walls.Very fine-grained gold, tellurides and pyrite occur in the dark fine-grained vein filling aggregate (Photo 51C,F). The material of an irregular-shaped grey quartz pod along the '04 Break at Macassa stope 4940 (Photo 40, bottom part) consists almost entirely of very fine-grained (0.01-0.05 mm) quartz, with subordinate coarser (0.1-0.5 mm), typically strained, anhedral quartz grains, patches of carbonate, sericite flakes, and some opaque grains.

A distinct vein filling type is documented in vein 4206-S3 where macroscopically visible gold and tellurides are associated with a network of thin (1-3 mm) greenish grey to dark grey fracture-fill veinlets (Photo 49). Under the microscope, these veinlets consist of fine (0.02-0.1 mm) quartz, relatively abundant feldspar (optically identified as K-feldspar, based on characteristic grid-like twinning pattern, Photo 49E), carbonate and sericite. Very fine-grained (0.002-0.01 mm) titanite (?), and non-reflective opaque particles similar to those described earlier are also present. Gold and tellurides occur both within these veinlets and in proximity to them, along fractures in white quartz. Petrographic (optical) identifications show that feldspar may actually be more abundant than quartz in these late veinlets.

The occurrence of the dark, fine-grained quartz as a matrix enclosing coarser white quartz crystals, and concordant layering of dark and white quartz within individual veins (e.g., vein 4206-S3, Photo 48), imply that the dark quartz is unlikely to constitute a discrete generation that entirely postdated the white quartz. More probably, the fine grained dark quartz was deposited multiple times, perhaps during episodes of relatively rapid precipitation, alternating with periods of more slow, unrestricted growth of coarser quartz crystals. Such variations in the precipitation regime may be related to fault-valve mechanism, in which fault slip, brecciation, and associated pressure drops induced quartz precipitation. Presently available data are insufficient to confirm this possibility, and the origin of vein-filling types deserves further investigation because of its potential implications for gold deposition processes. The presence of gold and tellurides in the dark fine-grained vein-filling aggregate indicates that events or mechanisms that controlled precipitation of the dark quartz could also have triggered gold deposition.

The presence of euhedral-subhedral prismatic quartz crystals oriented randomly or at high angles to vein walls and enclosed in the darker fine-grained quartz matrix indicates unrestricted growth of prismatic quartz in fluid-filled cavities that were later filled with finer-grained quartz. This assemblage, along with prismatic quartz crystals radiating from angular wall-rock clasts, constitutes an open-space-filling texture. Although the occurrence of open-space-filling textures in fault-fill veins is generally atypical, they have been documented at several gold deposits (e.g., Hagemann et al.1992; Robert and Brown 1986; Boullier and Robert 1992). Such textures are particularly common at relatively shallow (i.e., epizonal, Hagemann and Cassidy 2000) systems, due to low effective confining pressure (e.g., Hagemann et al. 1992). The presence of open-space-filling textures in variably oriented veins of the Kirkland Lake gold deposit, and the association of veins with largely brittle faults imply that hydrothermal activity occurred at relatively shallow crustal levels. Fluid pressure may have played an important role in the opening of both shallowly and steeply dipping veins, which can at least partially explain textural similarities between the two vein types.

Post-Ore Veining

Non-auriferous post-ore veins occur along the ore-controlling faults (the Main Break and the '04 Break) and major post-ore faults. The post-ore veins either cut across or are parallel to auriferous quartz veins. They generally consist of translucent quartz and pink or white carbonate, commonly with films and bands of dark green chlorite along vein selvages, and locally with coarse (3-5 mm) rosettes of chlorite within veins. Some veins contain clots and patches of pyrite and chalcopyrite. Late, post-ore barite and gypsum (selenite) veinlets are also common.

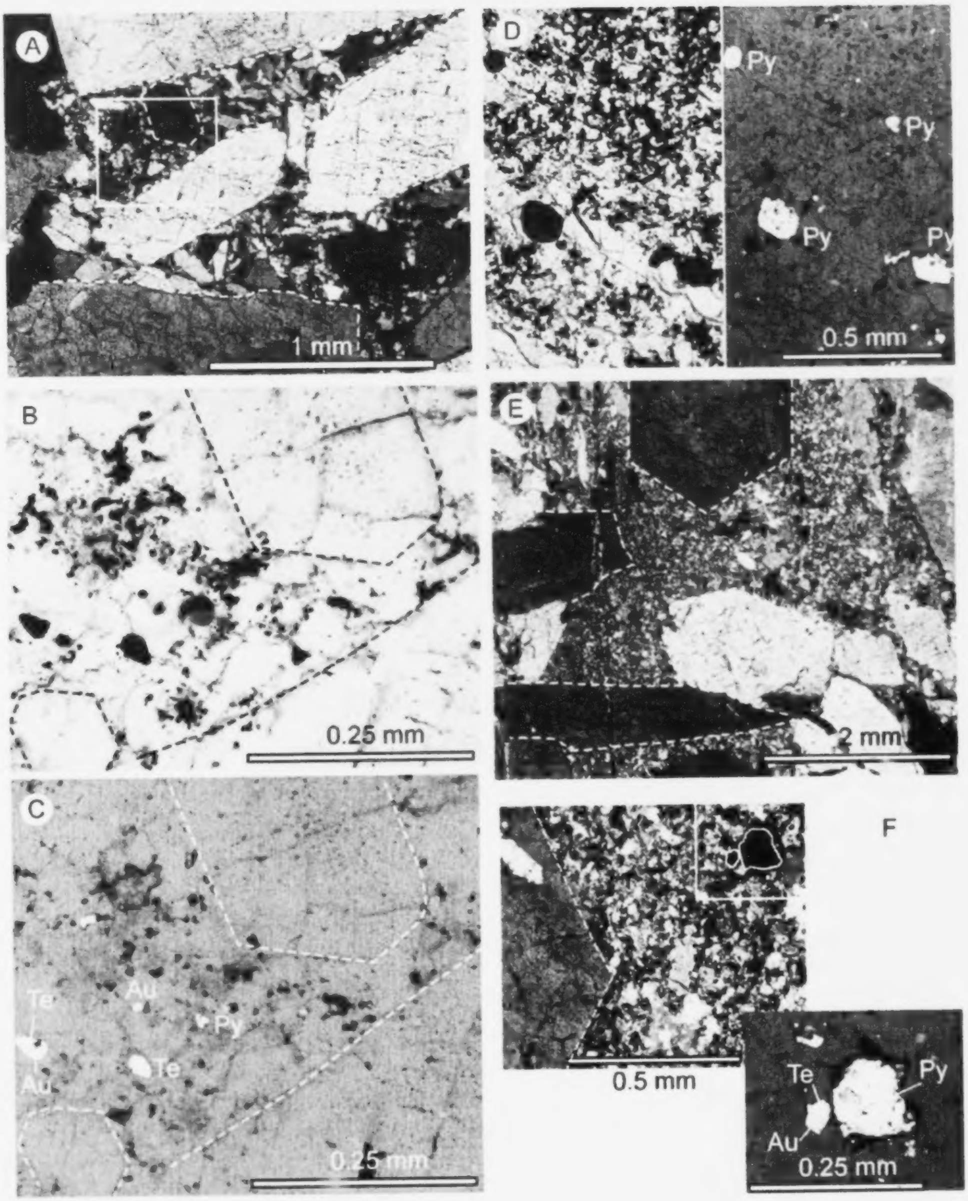

Photo 51. Photomicrographs illustrating vein filling types in gold-bearing quartz veins. Photos A-D depict vein 4206-S3, material from layers marked "2" and "4" on Photo 48B; photos E and F are of vein 4506. A) Fine-grained quartz (dark matrix on Photo 48B, layers marked "2", and on Photo 48C) filling intersticial spaces between coarser euhedral prismatic quartz crystals (white on Photos 48B-C). Transmitted light, cross nicols. B) Enlarged view of a rectangular area of photo A, large euhedral quartz crystals are outlined by dashed lines, note presence of opaque "dust" in fine-grained quartz aggregate (transmitted plane-polarized light). C) The same area as in B, reflected light. Very fine-grained gold (Au) and altaite (Te) occurring in the fine-grained quartz aggregate; opaque "dust" visible on photo B is non-reflective. D) (left-hand: plane polarized transmitted light; right-hand: reflected light) dark fine-grained quartz (from layer marked "4" on Photo 48B) with approximately 50% opaque non-reflective particles. E and F, vein 4506. E) fine-grained matrix consisting of quartz, sericite, carbonate, and possibly subordinate feldspar, enclosing euhedral prismatic quartz crystals (outlined by dashed line). Note variable orientation of euhedral quartz crystals. F) enlarged view of the fine-grained matrix containing gold (Au) and altaite (Te), along with pyrite (lower right-hand). Larger euhedral quartz crystal is outlined by dashed line.

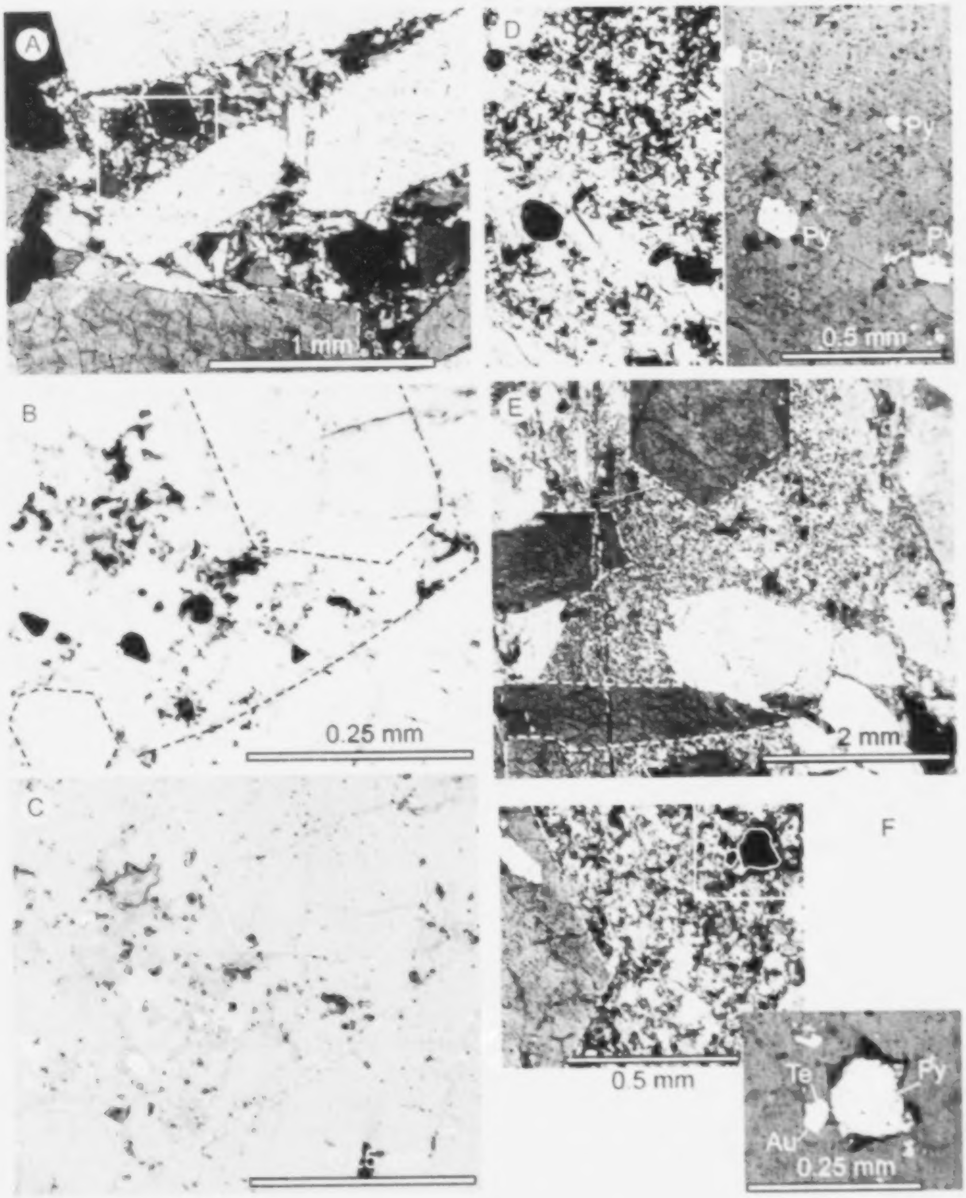

Photo 51. Photomicrographs illustrating vein filling types in gold-bearing quartz veins. Photos A-D depict vein 4206-S3, material from layers marked "2" and "4" on Photo 48B; photos E and F are of vein 4506. A) Fine-grained quartz (dark matrix on Photo 48B, layers marked "2", and on Photo 48C) filling intersticial spaces between coarser euhedral prismatic quartz crystals (white on Photos 48B-C). Transmitted light, cross nicols. B) Enlarged view of a rectangular area of photo A, large euhedral quartz crystals are outlined by dashed lines, note presence of opaque "dust" in fine-grained quartz aggregate (transmitted plane-polarized light). C) The same area as in B, reflected light. Very fine-grained gold (Au) and altaite (Te) occurring in the fine-grained quartz aggregate; opaque "dust" visible on photo B is non-reflective. D) (left-hand: plane polarized transmitted light; right-hand: reflected light) dark fine-grained quartz (from layer marked "4" on Photo 48B) with approximately 50% opaque non-reflective particles. E and F, vein 4506. E) fine-grained matrix consisting of quartz, sericite, carbonate, and possibly subordinate feldspar, enclosing euhedral prismatic quartz crystals (outlined by dashed line). Note variable orientation of euhedral quartz crystals. F) enlarged view of the fine-grained matrix containing gold (Au) and altaite (Te), along with pyrite (lower right-hand). Larger euhedral quartz crystal is outlined by dashed line.

Wall Rock Alteration

Macroscopic observations at the Macassa Mine show that hydrothermal alteration associated with gold-bearing quartz veins includes variable but generally moderate carbonatization, minor sericitization, and local silicification. Rocks in immediate proximity to gold-bearing quartz veins and wall-rock clasts within the veins invariably contain disseminated pyrite. Red coloration of syenitic rocks and some varieties of tuffs is due to very fine dust of hematite, especially in K-feldspars, however it is not completely clear whether this hematitization is directly related to gold mineralization. Preliminary microscopic observations of quartz vein samples show that hydrothermal K-feldspar, replacing primary magmatic K-feldspar, may be present in mafic syenite in proximity to veins, as well as in mafic syenite fragments enclosed in vein matrix. In the central part of the Kirkland Lake camp (Lake Shore, Wright-Hargreaves, and Teck-Hughes mines), veins are locally accompanied by rather strong wall-rock sericitization. Several lines of evidence suggest that this sericitization is closely related to gold mineralization. Within veins, sericite is commonly associated with gold. In a cataclasized part of the Teck-Hughes #1 vein, the sericite-rich matrix hosts gold and telluride grains (Photo 45D,E). In a gold-bearing quartz sample from the Lake Shore property (sample LS, Appendix A), fragments of strongly sericitized syenite porphyry and monomineral sericitic streaks are enclosed in quartz vein matrix, and some sericite streaks contain gold and tellurides. On the Mud Break ouctcrop, a relatively thick and intense sericite alteration halo is symmetrically distributed on both sides of a thin quartz veinlet (Photo 38B). Previously, Thomson et al. (1950, e.g, p.122) also described sericitic alteration in the central part of the camp as closely related to gold mineralization.

Patches (2-5 cm) of bright green mica, possibly a vanadium-rich variety (roscoelite), were observed in sericitized and silicified syenite porphyries within the Mud Break mineralized zone. As discussed in a section on geochemistry of gold mineralization, elevated V values in some gold-bearing samples from other locations in the Kirkland Lake camp may also indicate the presence of vanadium mica.

Strong carbonatization in cataclastic bands along the Main and '04 breaks is equally present in mineralized and unmineralized fault segments, and probably is largely unrelated to mineralization (see Thomson et al. 1950). Data in Kerrich and Watson (1984) show the addition of CO_2 along breaks not accompanied by elevated gold values, whereas no significant CO_2 addition is observed along some gold-bearing veins. This similarly indicates that although strong carbonatization occurred along major faults, it probably was not an essential part of the mineralizing process. Also, intensive chloritization (dark green chlorite) along fault slips, characteristic of the Macassa Mine, appears to be unrelated to gold mineralization, for the following reasons. Dark green chlorite is clearly not a major component of mineralized quartz veins. Apart from locally present chloritized pyroxene in mafic syenites, there is no pronounced bulk chloritization of host rocks along mineralized veins and of rock fragments incorporated into the veins. If chlorite is present in veins, it always texturally postdates mineralized quartz, that is, it coats fractures or occurs in selvages of crosscutting late barren quartz-carbonate veinlets (e.g., Teck-Hughes vein #1). None of the observed mineralized banded veins containing wall-rock slivers, probably incorporated through the crack-seal mechanism, actually contains fragments of chloritic gouge or chloritized slip bands. On the contrary, in late, barren, quartz-carbonate veins and veinlets, dark green chlorite is commonly present as films in selvages and, in places, as rosettes within the veins (e.g., stope 4247, Macassa Mine). Thus, intense chloritization along fault slips is probably associated with a late post-mineralization hydrothermal event. Hicks and Hattori (1988) documented the same post-dating nature of chloritic gouge with respect to the auriferous North vein in the central part of the camp.

Sense of Movement Along the Kirkland Lake Fault and '04 Break

Features potentially indicating the sense of movement along ore-controlling faults include oblique internal foliation in fault zones (the Main Break at surface and '04 Break in stope 4528 MCF) and striations on chloritic slip surfaces of the Main Break and '04 Break. Striations on chloritic slips reflect post-ore movements, because intensive chloritization along fault postdated gold mineralization. Relatively shallow-plunging striations probably record post-diabase strike-slip movements (see below).

Oblique foliation within sericitic deformation bands along the Main Break on the Lake Shore property, indicative of reverse-dextral slip, could reflect syn-mineralization movements. Sericitization is related to formation of gold-bearing veins, and foliation of sericitic deformation bands may be broadly synchronous with mineralization, although post-mineralization origin is also possible. The weakly developed oblique foliation in the '04 Break (stope 4528 MCF), compatible with reverse slip, may reflect pre-, syn- or post-mineralization movements.

Previously published estimates on the magnitude of the slip movements along the faults are based on analyses of displaced markers. These estimates suggest reverse (south side up) sense of movement on the Main Break. Using the tuff-conglomerate contact on the the Teck-Hughes and Kirkland Lake Gold properties, Todd (1928) estimated a vertical movement of 610 m. Hopkins (1940) analyzed the shape of the syenite intrusion at the Kirkland Lake and Macassa mines and proposed a 17° clockwise (facing north) rotational movement of the hanging wall, with the pivotal point located at about 1000 m below the surface near the western boundary of the Wright-Hargreaves Mine. Thomson et al. (1950) summarized displacement data for various markers across the camp: a pipe-like syenite body at Macassa, Kirkland Lake Gold, and Teck-Hughes (about 450 m, reverse); small quartz-feldspar porphyry intrusions at Lake Shore (400-490 m, reverse); and the syenite porphyry-sandstone contact at the Toburn Mine (about 105 m, reverse). Thomson et al. (1950) concluded that the Main Break had a rotational reverse movement, with increasingly larger displacement in the west, and this movement pre-dated mineralization. Late displacements of diabase dikes are invariably strike-slip sinistral, reaching 25-30 m at Teck-Hughes and Lake Shore, roughly 0.75 m at the eastern part of Macassa, and about 2.5 m at Toburn (Thomson et al. 1950). Shallowly plunging striations on chlorite-coated slip planes of the Main Break and '04 Break are probably related to these post-diabase movements.

Kinematic indicators documented in the present study are in general agreement with previously documented predominantly reverse movements. The inferred dextral component can also be reconciled with these previous studies given the complex geometry of most markers. It is also possible that reverse-dextral movements occurred during some short episodes, whereas the overall displacement was largely reverse (south over north). The presence of an oblique reverse-dextral-slip foliation in sericitic bands also provides information on the relative timing of fault movements and mineralization. Sericitization accompanied gold mineralization, and thus the movements were not entirerely pre-ore as proposed by Thomson et al. (1950) but must have overlapped with or posdated mineralization.

Narrows Break Mineralization

Considerable confusion exists over the location of a structure called "Narrows Break" (Lackey 1990, p.74). The name is currently applied to mineralization exposed in a stripped area about 360 m north-northwest of the former Kirkland Lake Gold Main shaft and roughly 340 m north of the Main Break (S. Carmichael, Kirkland Lake Gold Inc., personal communication, 2004; Figure 33). The same gold occurrence is named "Powderhouse Shear Zone" by Lackey (1990).

Mineralization occurs as a zone of sheeted veinlets and pervasive iron-carbonatization and sulphidation (pyrite) localized at the southern contact of an augite syenite sill intruded in Timiskaming sandstones and reworked tuffs. Timiskaming rocks strike about 085°-095° (locally to about 110°-120°), dip 50-60° (30-40° in places) south (Figure 34). Steep discrete northeast-trending cleavage S4 intersects bedding from about 30° counterclockwise to almost orthogonally (Figure 34). Southwest-plunging folds with axial planar S4 are relatively rare and generally poorly developed. No major ore-controlling fault-like structure is observed in the stripped area. The 1-2 m wide, roughly 35 m long, northeast-trending (about 050°) assay-defined ore zone marked for bulk sampling by Kirkland Lake Gold Inc. geologists roughly corresponds to a swarm of thin (1 to 10 mm) sheeted carbonate-quartz veinlets hosted by carbonatized and sulphidized coarse- to medium-grained sandstones (Photo 52) and mafic syenites (near the northeastern end). Similar veinlets are also observed in other parts of the stripped outcrop. Within the ore zone, most veinlets strike 030°-050° and dip steeply southeast (Figure 34). The veinlets are typically zoned: carbonate lines the veinlet walls and quartz fills the center of the veinlets. Individual quartz and carbonate crystals are commonly oriented at high angles to veinlet walls. Gold, occasionally macroscopically visible, occurs along veinlet selvages (Photo 53), and may also be present in the sulphidized host rocks. Average gold grades of the ore zone are relatively low, on the order of 0.15 ounces per ton over 5 feet (about 5 g/t over 1.5 m) (M. Sutton, Kirkland Lake Gold Inc., personal communication, 2004), although 2 grab samples from the sheeted veinlet zone returned 60 and 90 g/t Au (Appendix A). Veinlets (in the ore zone and throughout the stripped outcrop) show variable relationships with S4. Some veinlets are hosted by cleavage planes, others crosscut them, and some are folded with axial planar S4. This indicates broad temporal overlap between veining and D4 deformation. The Narrows Break mineralized zone differs from typical Kirkland Lake gold mineralization by its lack of large veins, distinctly higher proportion of carbonate in vein material, stronger wall-rock carbonatization, and lack of tellurides and molybdenite.

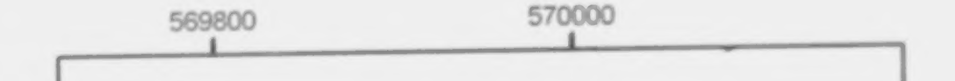

Figure 33. Location of the Narrows Break stripping and mineralized zone.

D Zone

The D zone was recently discovered by Kirkland Lake Gold Inc. in the Macassa shaft #3 area at a depth of 970-1050 m, and is presently considered one of the most promising exploration targets at the Macassa Mine. The zone strikes 010-020° and dips about 45° east. In summer-early fall 2004, drifting on the 3400-foot level of Macassa Mine was following the unmineralized to weakly mineralized portion of the structure, but the high-grade interval was not reached by the end of the 2004 field season. In the drift, the unmineralized to weakly mineralized part of the D zone is represented by a sharp slip surface in weakly strained conglomerates. Northeast-plunging (025-035°/25°) and approximately dip-parallel slickensides were observed in two locations. The slip surface is coated by chlorite and accompanied by a 0.4-0.5 m wide bleached zone with disseminated pyrite. A 1-1.5 m wide swarm of thin (1-2 cm) quartz-carbonate veinlets occurs in the immediate footwall of the structure. These veinlets are somewhat similar to those observed on the Narrows Break stripping: white carbonate lines the walls and quartz fills central parts. According to the mine geologists, these veinlets are only weakly auriferous, and thus are probably not representative of the predominant mineralization style of the high-grade D zone. A steeply dipping, northeast-trending (030°-040°/70°) foliation, which probably corresponds to S4, is defined by rather weak pebble flattening in the conglomerates. The zone appears to crosscut the foliation, although this relationship is not diagnostic, primarily because of weak development of the fabric.

Intramineral Dikes

Still (2001) described felsic green dikes crosscutting gold-bearing veins, containing quartz fragments, and locally mineralized, with grab sample Au values reaching approximately 18 g/t. In the present study, dikes occurring in immediate proximity to gold-bearing veins were observed at the Macassa Mine (Photos 54 and 55). Direct contacts between the dikes and quartz veins are common, but in most cases cannot be interpreted in terms of the relative timing of the emplacement of the dikes and quartz veins. Dikes and veins are approximately parallel and are hosted by the same fractures. Contacts are in most cases sharp, and virtually all dikes are strongly sericitized, carbonatized, contain disseminated pyrite and show elevated gold values (e.g., 30-135 ppb in samples collected in this study, Appendix A). Relatively unaltered (note low CO_2 of sample 4528D, Appendix A), 0.2 to 0.7 m thick dike occurs along the north-dipping gold-bearing vein in stope 4528 MCF (eastern part, Photo 55). Splintery injections of dike microapophyses into vein quartz, and quartz fragments (0.3-1 cm) enclosed entirely in the matrix of the dike are seen in samples collected from this stope (Photo 56). In addition to that, the angular fragments of host mafic syenites enclosed in quartz are strongly sulphidized, whereas the dike along the vein contact, and dike microapopophyses injecting quartz, show weak or no sulphidation. These relationships imply that the emplacement of the dike postdated at least some phases of vein formation. This confirms the intramineral nature of the dikes (Still 2001). In addition to these dikes, texturally and compositionally identical planar intrusions were documented at several locations at surface. As shown below, the dikes are petrographically and geochemically distinct from the other intrusions and constitute a separate magmatic phase. The following section provides a brief description of these small planar intrusions that are for descriptive purposes termed "intramineral dikes".

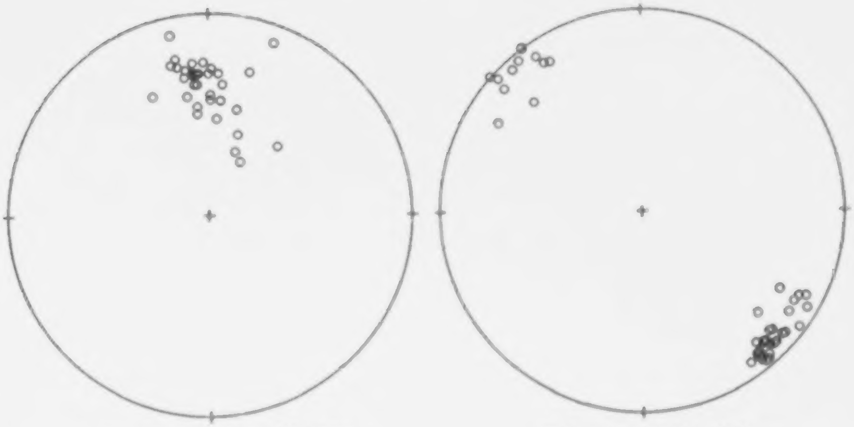

Poles to bedding (N=33)

Poles to S4 (N=38)

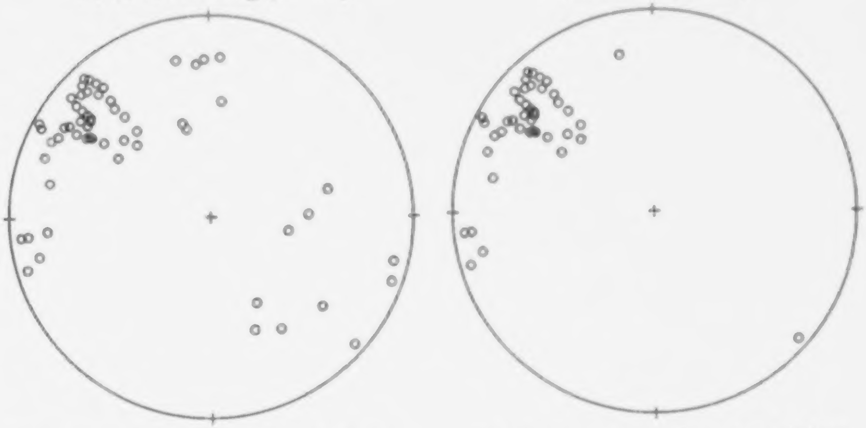

Poles to quartz-carbonate veinlets
(entire Narrows Break stripping, N=59)

Poles to quartz-carbonate veinlets
(assay-defined ore zone, N=43)

Figure 34. Stereonet plots for the Narrows Break stripped outcrop: bedding, S4 and quartz-carbonate veinlets (right-hand bottom plot corresponds to the assay-defined ore body marked for bulk sampling by Kirkland Gold Inc. geologists).

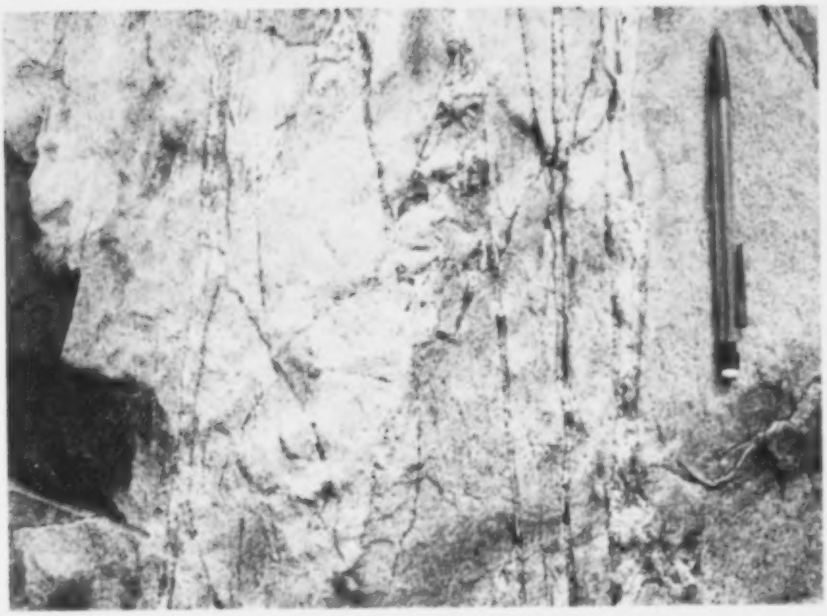

Photo 52. Narrows Break mineralized zone: sheeted carbonate-quartz veinlets in carbonatized and sulphidized Timiskaming sandstones. Pencil (15 cm) for scale.

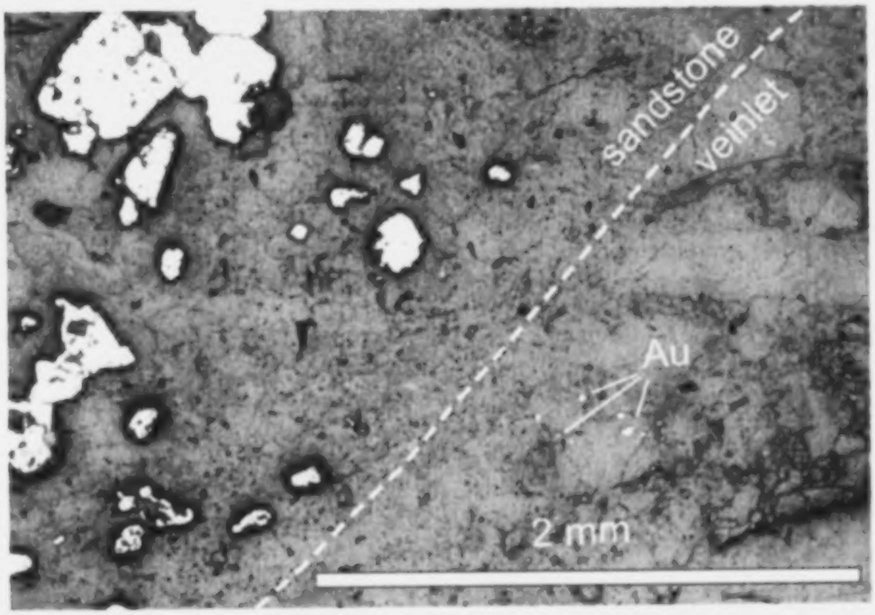

Photo 53. Reflected light photomicrograph of a mineralized veinlet from Narrows Break mineralized zone. Gold (Au) occurs near the veinlet wall. Bright reflective grains in sandstone are pyrite.

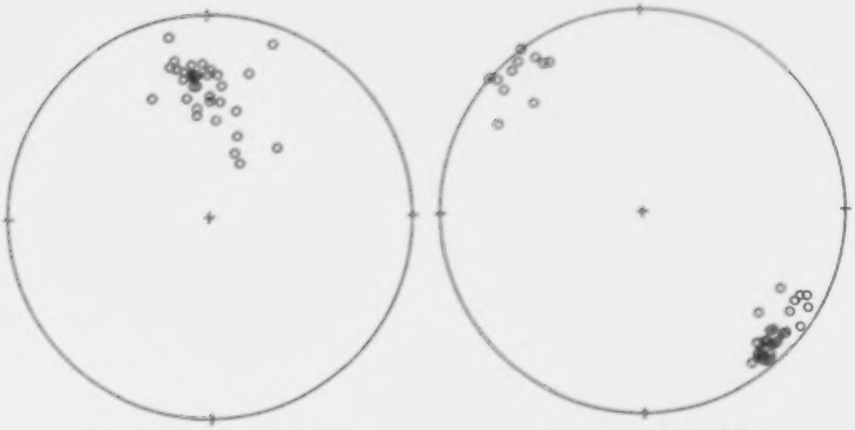

Poles to bedding (N=33)

Poles to S4 (N=38)

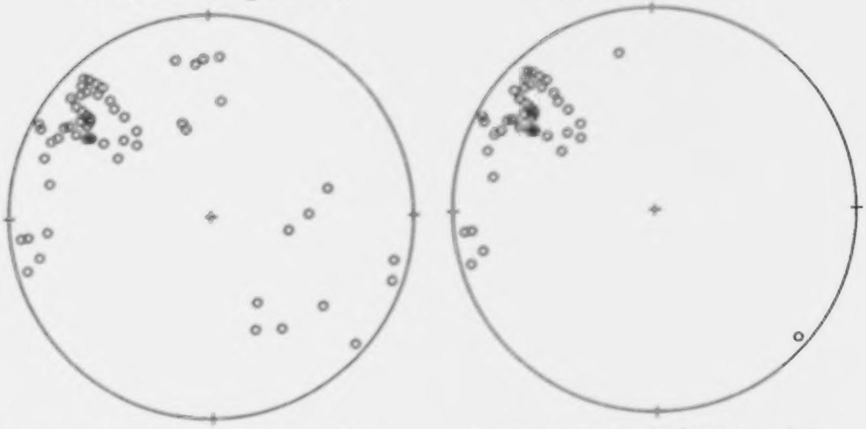

Poles to quartz-carbonate veinlets
(entire Narrows Break stripping, N=59)

Poles to quartz-carbonate veinlets
(assay-defined ore zone, N=43)

Figure 34. Stereonet plots for the Narrows Break stripped outcrop: bedding, S4 and quartz-carbonate veinlets (right-hand bottom plot corresponds to the assay-defined ore body marked for bulk sampling by Kirkland Gold Inc. geologists).

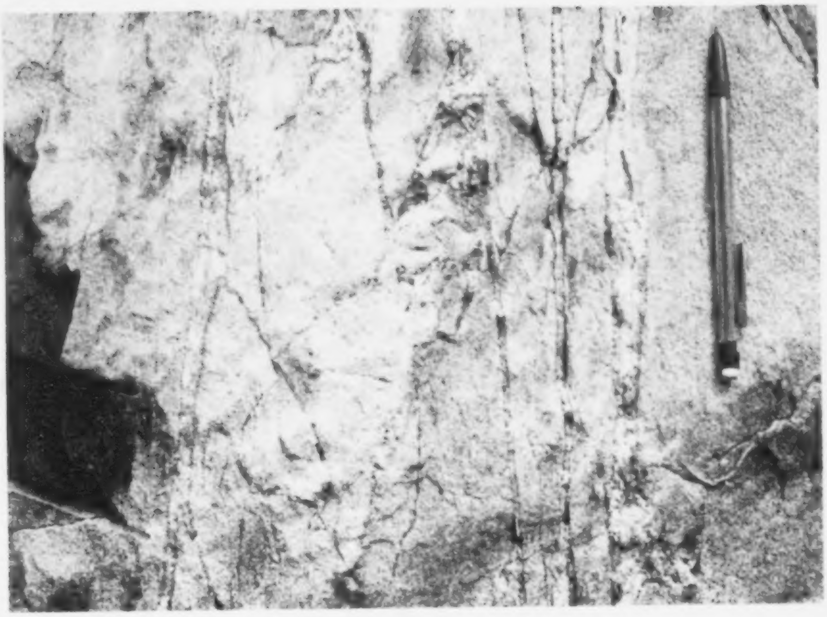

Photo 52. Narrows Break mineralized zone: sheeted carbonate-quartz veinlets in carbonatized and sulphidized Timiskaming sandstones. Pencil (15 cm) for scale.

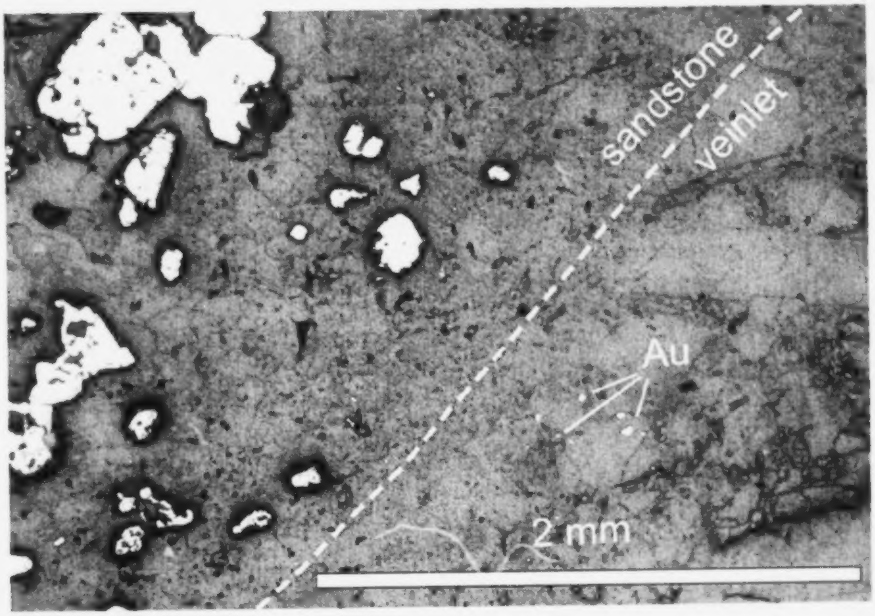

Photo 53. Reflected light photomicrograph of a mineralized veinlet from Narrows Break mineralized zone. Gold (Au) occurs near the veinlet wall. Bright reflective grains in sandstone are pyrite.

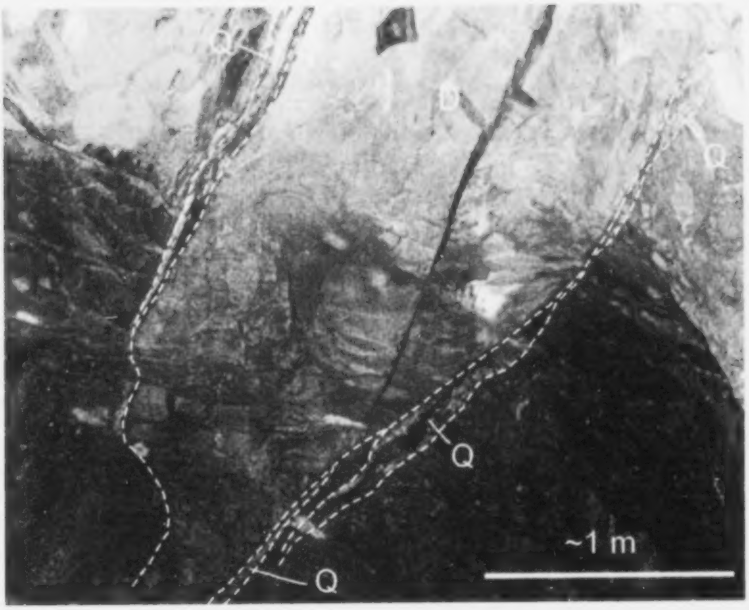

Photo 54. Dike (D) and gold-bearing quartz veins (Q) in stope 4529, Macassa Mine (cross section view, facing west).

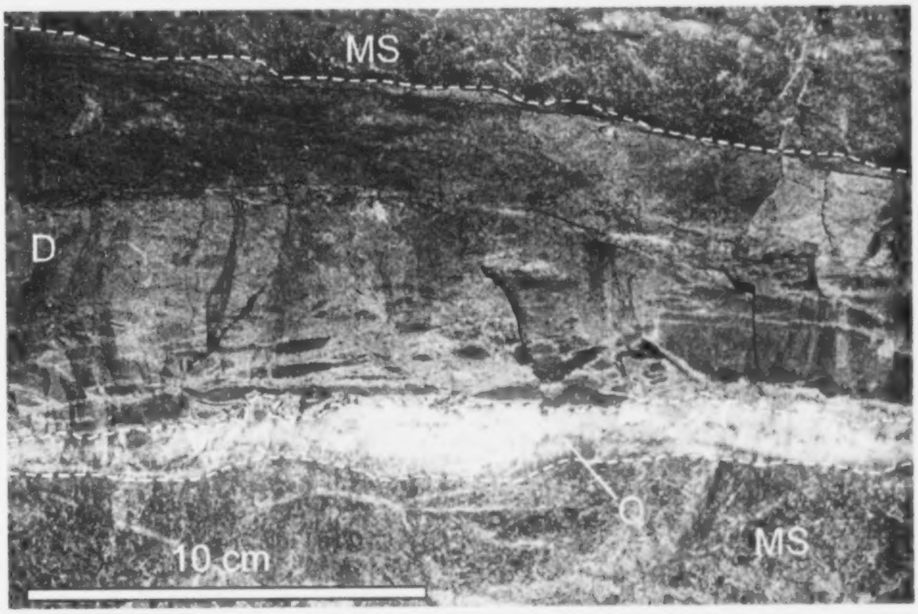

Photo 55. Dike on the back of stope 4528, Macassa Mine. Dike has a sharp jagged contact with the vein and there is no sulphidation of the dike along the contact.

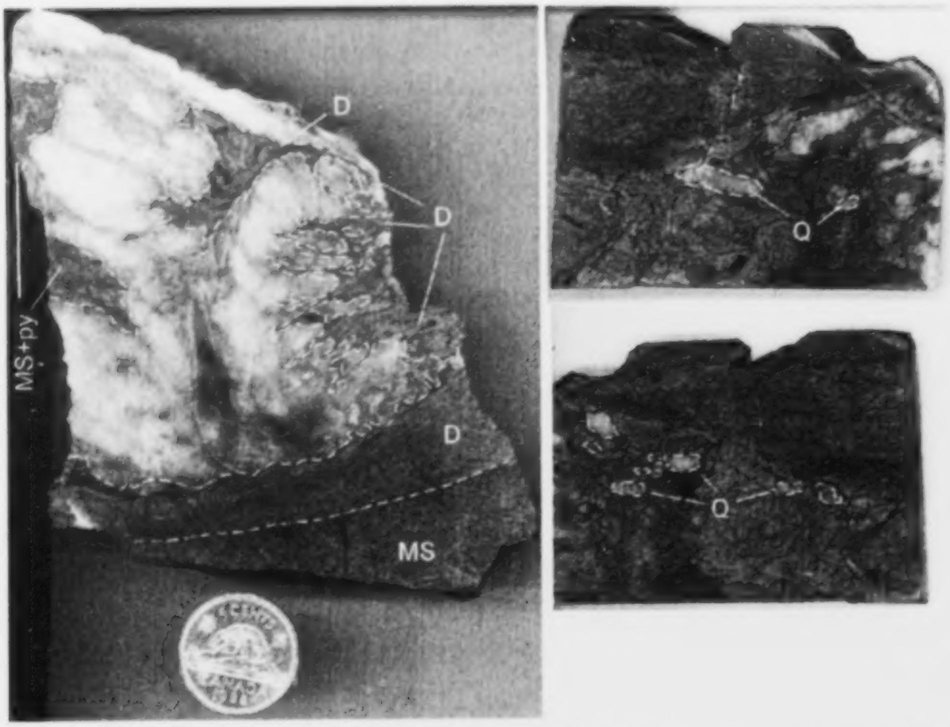

Photo 56. Cut sample of the dike-vein contact from stope 4528 (Macassa Mine). Left column: splintery injections of dike material (D) into the quartz vein: fragments of mafic syenites enclosed in the vein (left-hand side) are strongly sulphidized (MS+py) whereas 1-3 mm thick dike injections do not show sulphidation. Right column: fragments of vein quartz (Q) entirely enclosed in the dike matrix. Sample courtesy of D. Quick, Kirkland Lake Gold Inc. The same dike is shown in Photo 55.

The thickness of most intramineral dikes examined underground at the Macassa Mine varies from 0.3 to about 1.5 m, and unusually thin (2-5 cm) dikes occur in places. Their overall orientation is approximately parallel to the '04 Break, however, local abrupt changes in orientation are common. Altered rocks are typically light grey with variable subtle tints. The relatively unaltered dike from stope 4528 MCF east, is green to dirty greyish green. Macroscopically, dikes exposed in underground workings are either aphanitic or contain small (0.5-2 mm) dull light green flakes of altered mica (?) and, more rarely, light green prismatic pseudomorphs (2-3 mm). Contacts with wall rocks are sharp and frequently have irregular outlines. Immediate endocontacts of dikes are marked by thin (1-3 mm) light-colored rims, probably chilled margins.

Dikes exposed at surface outcrops vary in thickness from a few centimetres to 1-1.5 m. Apart from weathering, they are similar to those observed underground. Thin (2-10 cm) dikes commonly show abrupt changes of orientation. Contacts are sharp and often splintery, with thin microapophyses penetrating wall rocks; angular xenoliths of immediate host rocks are common (Photo 57). Macroscopically, the rocks are largely aphanitic; in one location (station 004VOI1518), dikes contain relatively coarse (roughly 2 mm) possibly xenocrystic biotite grains. Most of the dikes exposed at surface are carbonatized to a variable extent.

In thin section, the least-altered intramineral dikes (e.g., sample 004VOI1518-2) contain 10-20% thin biotite flakes (0.25-0.5 mm) and relatively sparse rounded or ovoid grains (0.25-0.4 mm) completely replaced by fine-grained feldspar. Some dikes also contain relatively coarse (1-2 mm) euhedral prismatic

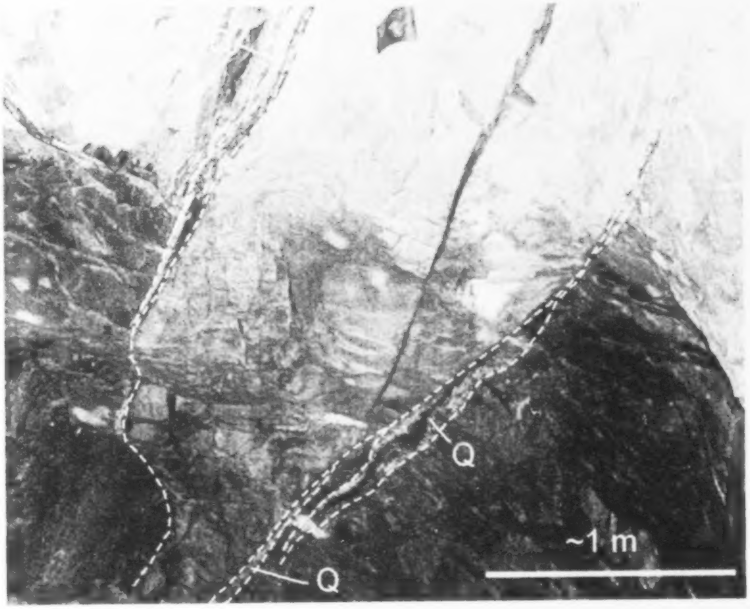

Photo 54. Dike (D) and gold-bearing quartz veins (Q) in stope 4529. Macassa Mine (cross section view, facing west).

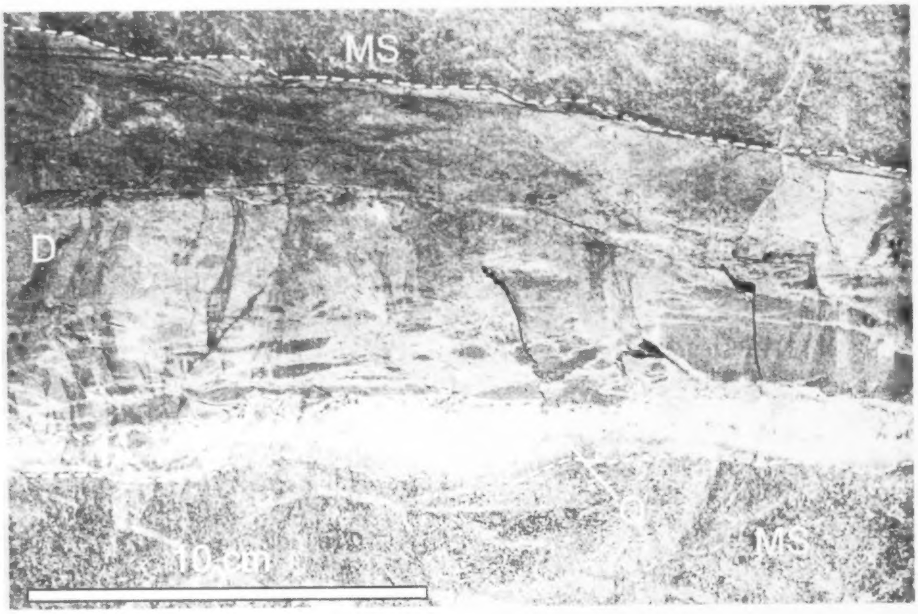

Photo 55. Dike on the back of stope 4528. Macassa Mine. Dike has a sharp jagged contact with the vein and there is no sulphidation of the dike along the contact.

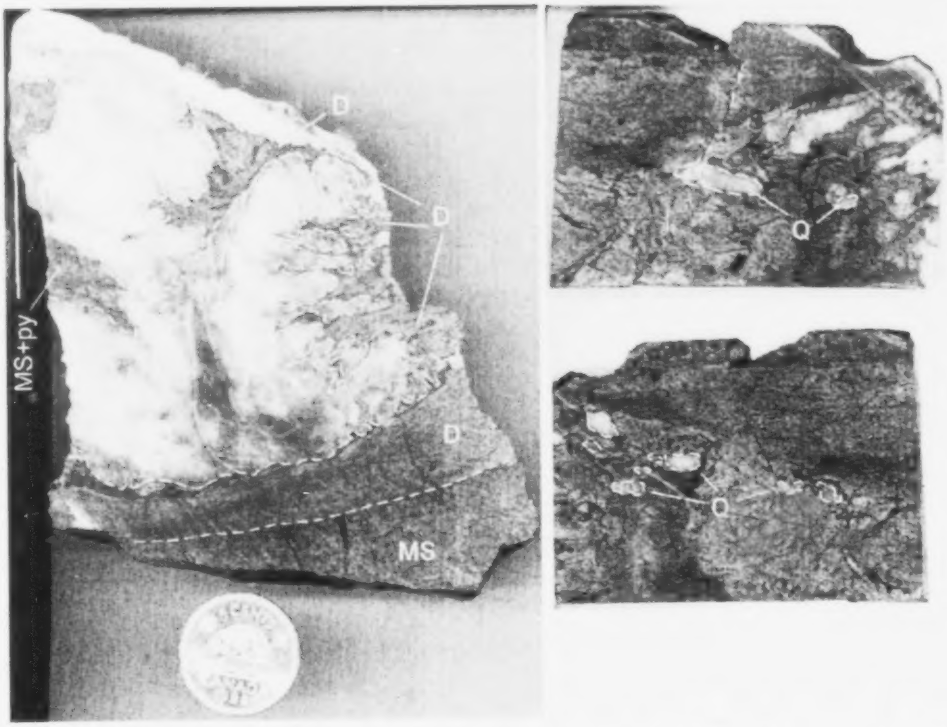

Photo 56. Cut sample of the dike-vein contact from stope 4528 (Macassa Mine). Left column: splintery injections of dike material (D) into the quartz vein; fragments of mafic syenites enclosed in the vein (left-hand side) are strongly sulphidized (MS+py) whereas 1-3 mm thick dike injections do not show sulphidation. Right column: fragments of vein quartz (Q) entirely enclosed in the dike matrix. Sample courtesy of D. Quick, Kirkland Lake Gold Inc. The same dike is shown in Photo 55.

The thickness of most intramineral dikes examined underground at the Macassa Mine varies from 0.3 to about 1.5 m, and unusually thin (2-5 cm) dikes occur in places. Their overall orientation is approximately parallel to the '04 Break, however, local abrupt changes in orientation are common. Altered rocks are typically light grey with variable subtle tints. The relatively unaltered dike from stope 4528 MCF east, is green to dirty greyish green. Macroscopically, dikes exposed in underground workings are either aphanitic or contain small (0.5-2 mm) dull light green flakes of altered mica (?) and, more rarely, light green prismatic pseudomorphs (2-3 mm). Contacts with wall rocks are sharp and frequently have irregular outlines. Immediate endocontacts of dikes are marked by thin (1-3 mm) light-colored rims, probably chilled margins.

Dikes exposed at surface outcrops vary in thickness from a few centimetres to 1-1.5 m. Apart from weathering, they are similar to those observed underground. Thin (2-10 cm) dikes commonly show abrupt changes of orientation. Contacts are sharp and often splintery, with thin microapophyses penetrating wall rocks; angular xenoliths of immediate host rocks are common (Photo 57). Macroscopically, the rocks are largely aphanitic; in one location (station 004VOI1518), dikes contain relatively coarse (roughly 2 mm) possibly xenocrystic biotite grains. Most of the dikes exposed at surface are carbonatized to a variable extent.

In thin section, the least-altered intramineral dikes (e.g., sample 004VOI1518-2) contain 10-20% thin biotite flakes (0.25-0.5 mm) and relatively sparse rounded or ovoid grains (0.25-0.4 mm) completely replaced by fine-grained feldspar. Some dikes also contain relatively coarse (1-2 mm) euhedral prismatic pseudomorphs of carbonate, chlorite, sericite, ±epidote and secondary acicular amphibole (?). Most likely, these represent altered mafic phenocrysts, perhaps pyroxene. Coarser (1-2 mm) biotite grains present in some dikes are likely xenocrystic as they show signs of resorption. Similar mineral constituents (fine mica flakes, rounded to ovoid feldspar pseudomorphs and euhedral prismatic pseudomorphs), although strongly to completely carbonate-sericite-altered, are recognized in thin sections of intramineral dikes from underground workings.

Geochemical data for 9 samples of intramineral dikes, both from surface outcrops and underground workings, are listed in Appendix A. The whole-rock (total alkali versus silica) composition of these dikes corresponds to trachybasalt to phonotephrite (Figure 35). The rocks are definitely alkalic, although total alkali content and relative proportions of K_2O and Na_2O vary, probably due to alteration. A roughly 10% K_2O content combined with rather low Na_2O in the least altered sample (004VOI1518-2) shows that the dikes probably belong to the potassic rather than sodic type of alkalic rocks. Binary plots of immobile elements and element ratios (Figures 36 and 37) show good clustering and distinct (compared to other intrusive rock types) trace element systematics for these dike samples. This supports macroscopic and petrographic observations, suggesting that the intramineral dikes from underground workings and surface outcrops belong to one coherent group that is distinct both from major intrusive phases and coarse lamprophyre dikes and sills. Primitive-mantle-normalized plots (Figure 38) of intramineral dikes share key similarities with corresponding data of major intrusive phases, including strongly fractionated REE and well-pronounced Nb, Ti, and Sc lows. Most of these features are universally typical for Timiskaming volcanic rocks and related plutons (e.g., Ben Othman et al. 1990), thus, on a big scale, the intramineral dikes probably represent the same magmatic cycle as stratified Timiskaming volcanic rocks and related intrusions.

Most (5 of 6) intramineral dikes observed on surface outcrops are moderately to strongly foliated (S4). Conflicting relationships between the dikes and S4 are observed on outcrop 004VOI1518 (568572E 5333147N, Figure 39, Photo 58), where the folded (F4) bedding-parallel contact of syenite porphyry and tuff is crosscut at high angle by two intramineral dikes that are parallel to axial planar S4. The larger (1-1.5 m wide) dike is pervasively foliated, whereas the smaller (3-5 cm) dike, which changes orientation from axial planar-parallel to bedding-parallel, does not contain foliation. Apart from a difference in intensity of deformation, the dikes are similar petrographically and geochemically (in immobile element systematics). Crosscutting relationships of dikes and the fold (F4), combined with the presence of S4 foliation in one dike and lack thereof in the other, implies that emplacement of the dikes overlapped in time with D4 deformation, and the thin dike largely postdated D4 folding and shortening.

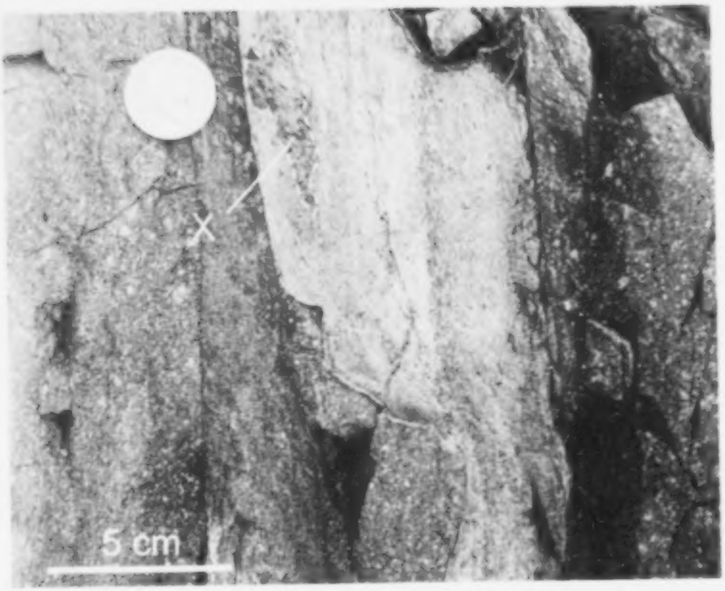

Photo 57. Surface exposure of an intramineral dike, a close-up view (Macassa property, trench on the north-south powerline, south of the Goldthorpe road; station 004VOI1745, 568593E 5332584N). A 3-10 cm thick dike crosscutting syenite porphyry and containing wall rock xenoliths (X).

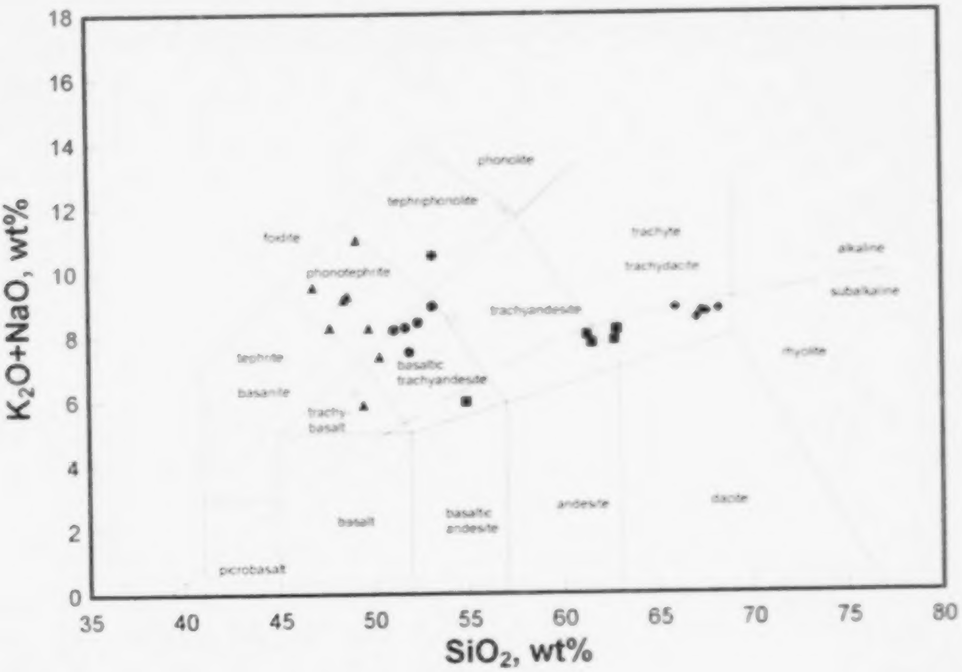

Figure 35. Total alkali vs. silica (Le Bas et al. 1986; Irvine and Baragar 1971) plots of intrusive rocks of the Kirkland Lake camp. Filled diamonds, feldspar-rich syenite porphyries; squares, sparsely porphyritic syenite porphyries; filled circles, mafic syenites; open diamonds, syenites; open circle, trachyandesite (west of the Amikougami Creek fault); filled triangles, intramineral dikes; open triangle, coarse biotite lamprophyre.

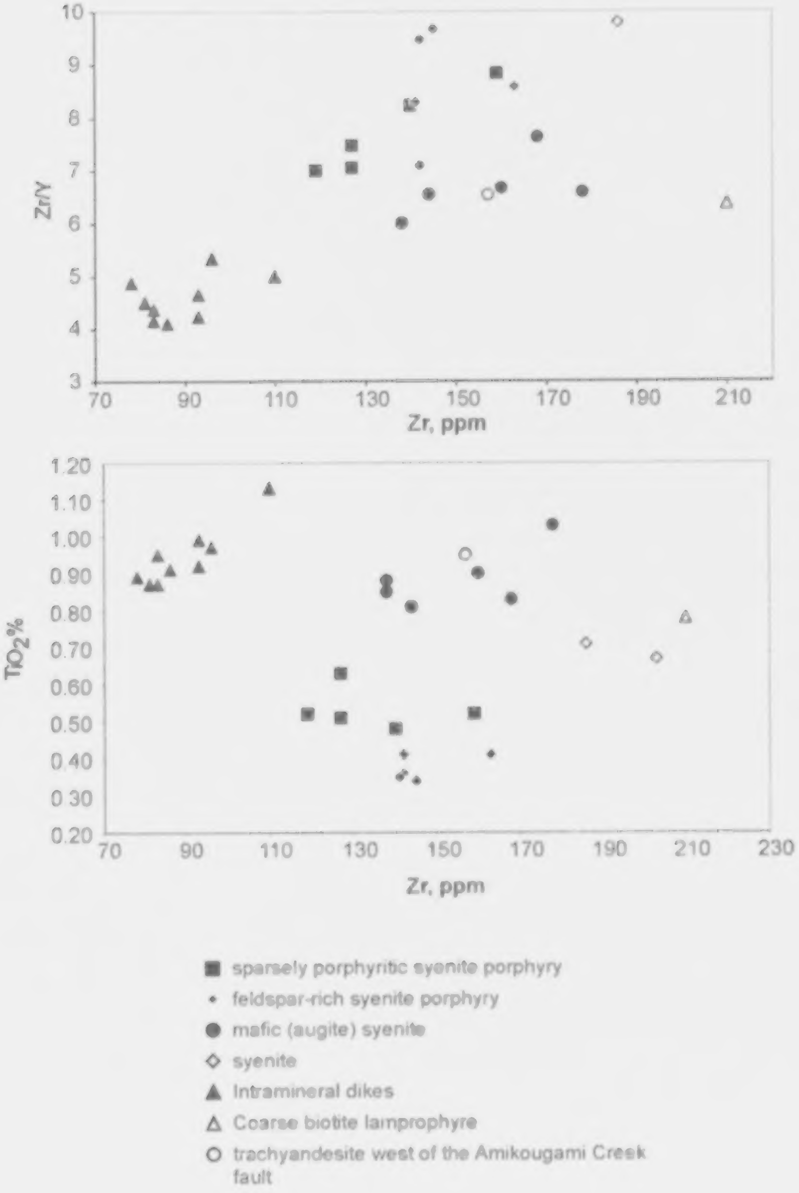

Figure 36. Zr vs. Zr/Y and Zr vs. TiO_2 plots for intrusive rocks of the Kirkland Lake camp.

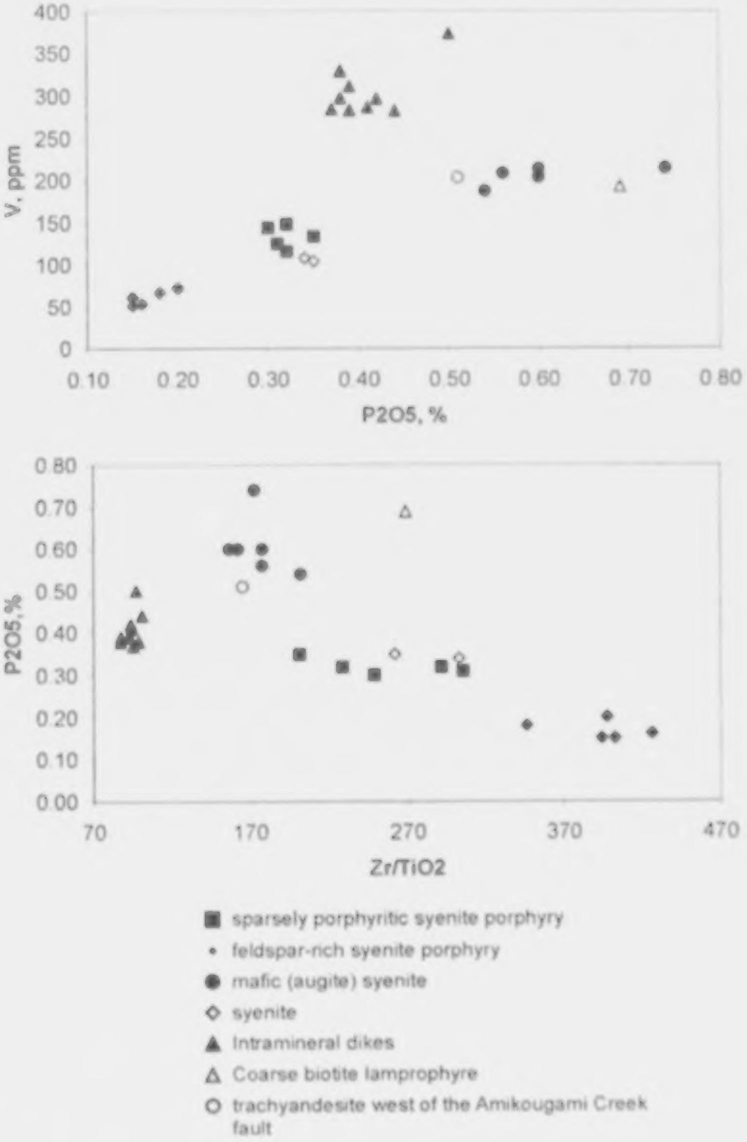

Figure 37. P_2O_5 vs. V and Zr/TiO_2 vs. P_2O_5 plots for intrusive rocks of the Kirkland Lake camp.

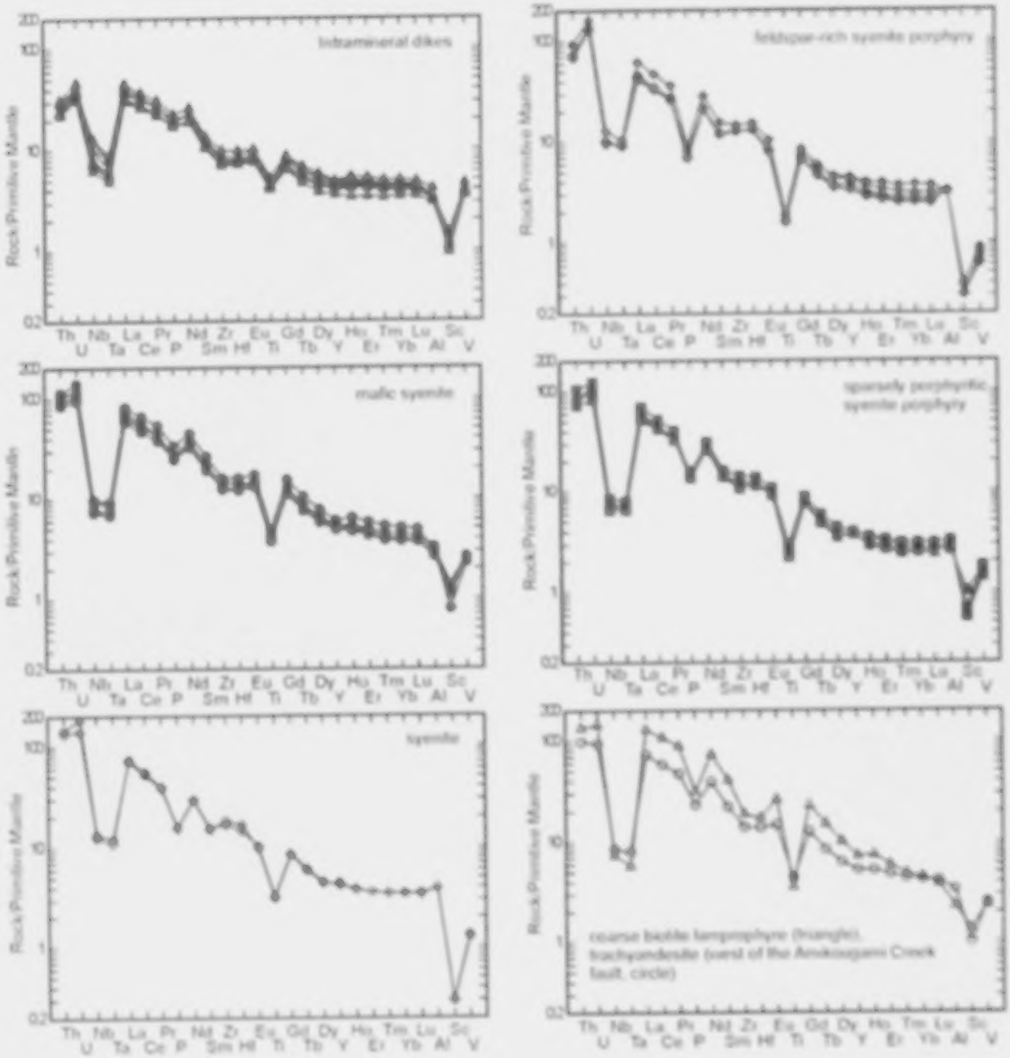

Figure 38. Primitive-mantle-normalized trace element plots for intrusive rocks of the Kirkland Lake camp. Primitive mantle values are from Sun and McDonough (1989).

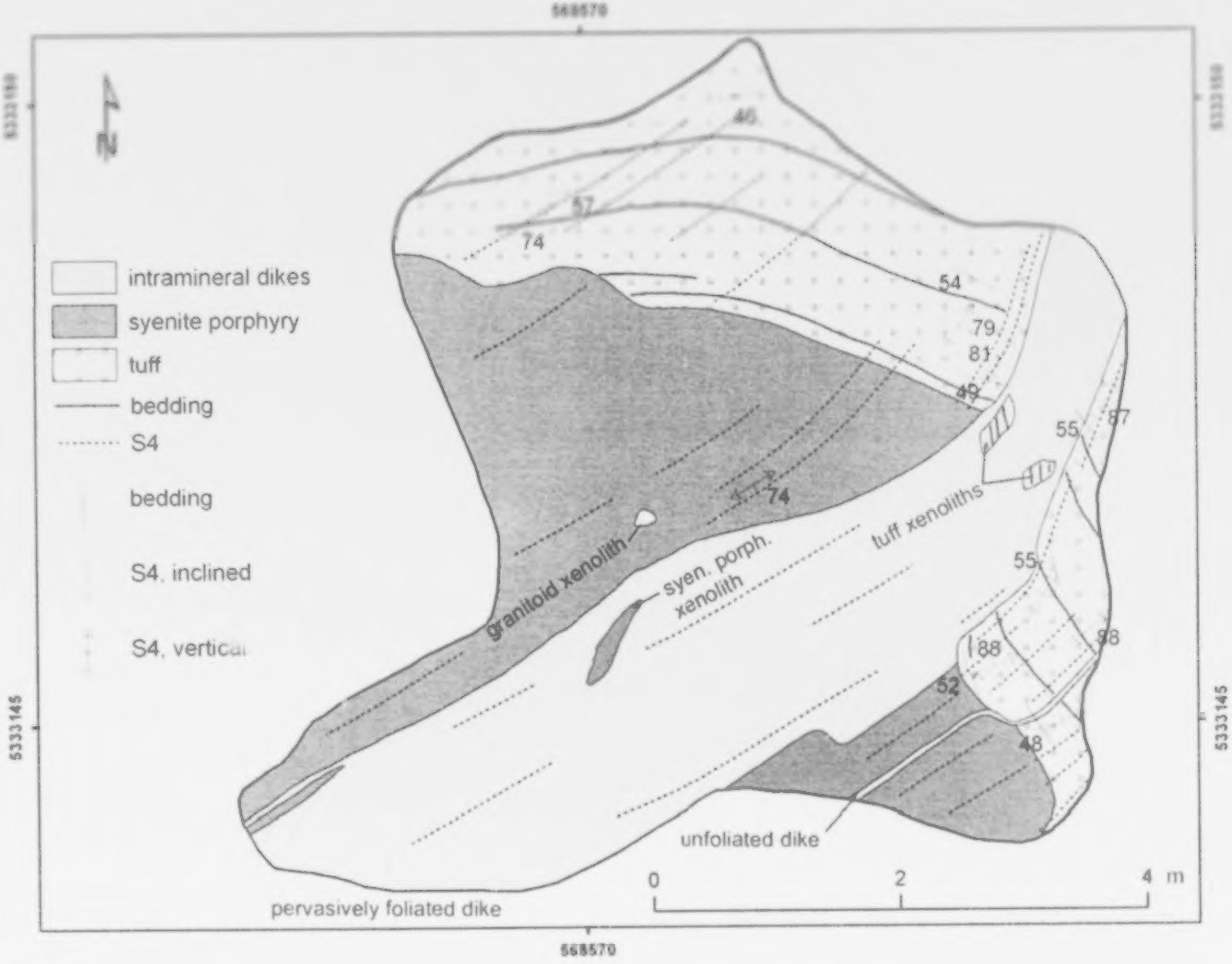
568570
5333150
5333150
N
intramineral dikes
syenite porphyry
tuff
bedding
S4
bedding
S4, inclined
S4, vertical
46
57
74
54
79
81
49
55
87
74
tuff xenoliths
granitoid xenolith
syen. porph. xenolith
55
88
88
52
48
unfoliated dike
5333145
5333145
0
2
4 m
pervasively foliated dike
568570

Figure 39. Geological plan of the outcrop 004VOI1518 (568572E 5333147N). See also Photo 58.

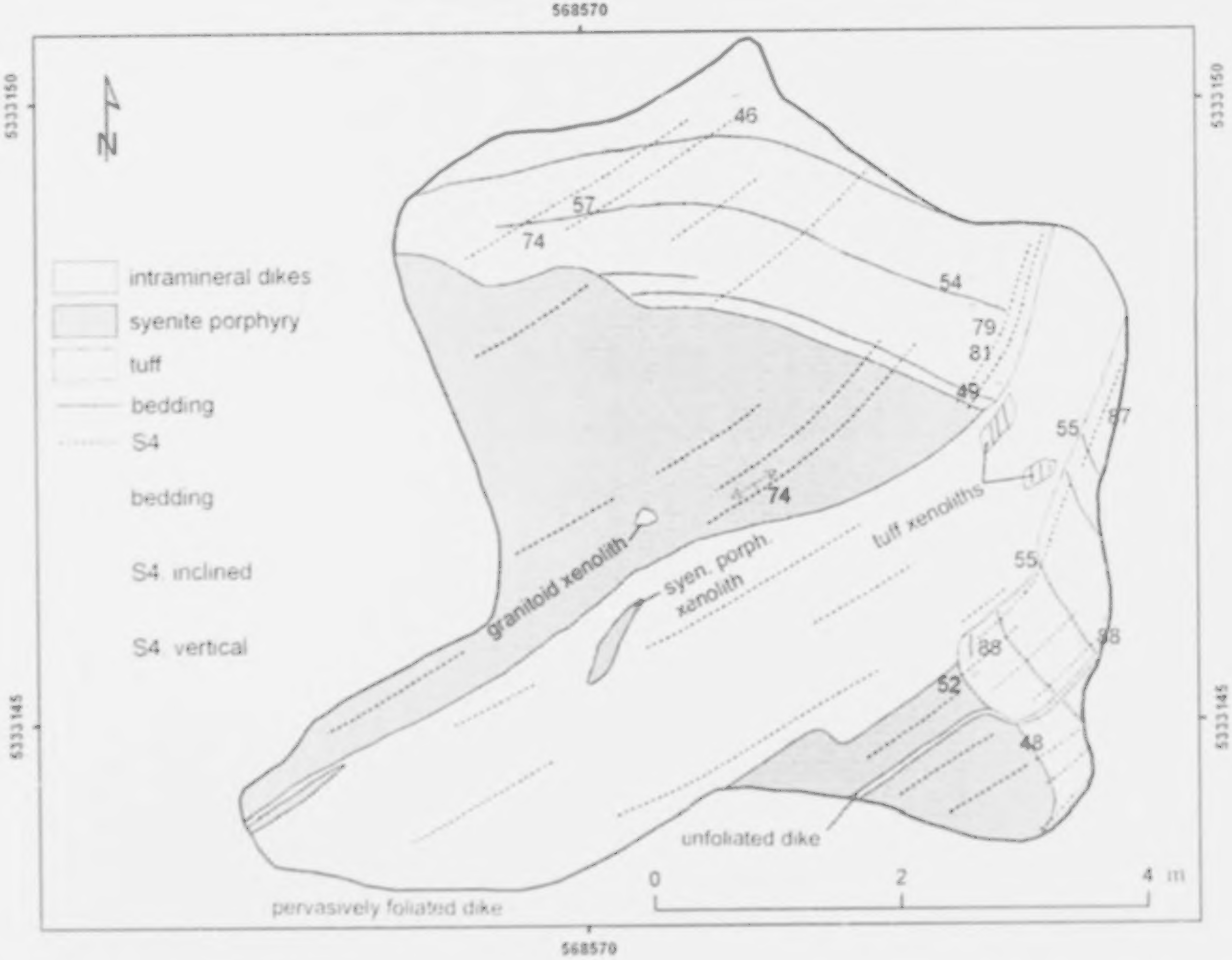
568570
5333150
5333145
N
intramineral dikes
syenite porphyry
tuff
bedding
S4
bedding
S4 inclined
S4 vertical
46
57
74
54
79
81
49
55
87
74
tuff xenoliths
granitoid xenolith
syen. porph. xenolith
55
88
98
52
48
unfoliated dike
pervasively foliated dike
0
2
4 m

Figure 39. Geological plan of the outcrop 004VO11518 (568572E 5333147N). See also Photo 58

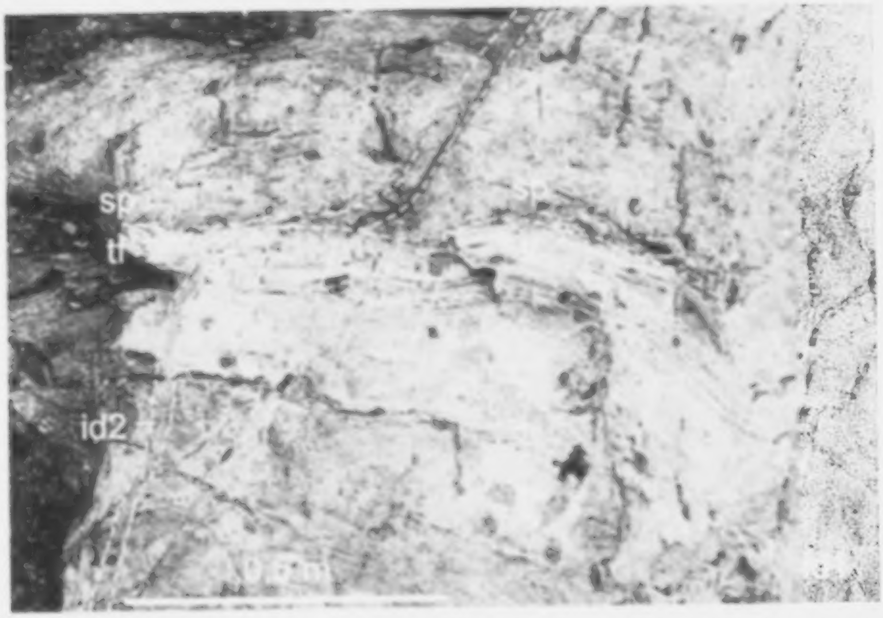

Photo 58. Portion of outcrop 004VOI1518 (area corresponding to the lower right-hand side of Figure 39), looking southwest. Fragment of a folded contact of tuffs (tf) and syenite porphyries (sp) transected at high angle by axial planar S4 cleavage (solid lines). Two S4-parallel intramineral dikes crosscut syenite porphyries and tuffs. The dike on the right-hand side (id1) is pervasively foliated, whereas the thin dike on the left-hand side (a short segment of which is hosted by the tuff-syenite contact plane) is unfoliated. Emplacement of the second dike (small) most probably largely postdated D4 folding.

Relative Timing of Deformation and Mineralization

The exact relative timing of Kirkland Lake gold mineralization and deformation events is not entirely clear. Apparent temporal overlap between the emplacement of the intramineral dikes and D4 (documented at outcrop 004VOI1518) suggests that the formation of the gold-bearing veins at the Macassa Mine could have, at least partially, overlapped with D4. As most intramineral dikes exposed at surface are foliated (S4), gold-bearing quartz veins possibly formed early during D4 and were later deformed.

Syn-mineralization stylolites that host gold and telluride grains in northeast-trending, steeply dipping quartz veins (e.g., stope 4940) are parallel to the regional S4 orientation. The alignment of stylolite teeth approximates the orientation of greatest principal stress (Davis and Reynolds 1996, p.443-444). Horizontal (northwest-southeast) orientation of stylolite teeth in auriferous veins indicates that the veins experienced northwest-southeast shortening (cf. Boullier and Robert 1992), and the occurrence of gold and tellurides along stylolite surfaces suggests that this shortening probably overlapped with mineralization. The orientation of S4 corresponds to the same shortening direction, implying that mineralization could have formed broadly synchronous with D4.

Syn-mineralization cataclasis of the Teck-Hughes #1 vein hosted by a subsidiary north splay of the Main Break (Todd 1928) shows that mineralization was accompanied by movements along host fault structures. The inferred reverse-dextral (south side up and to the west) slip along the primary ore-controlling structure, the Main Break, is also kinematically compatible with regional northwest-southeast

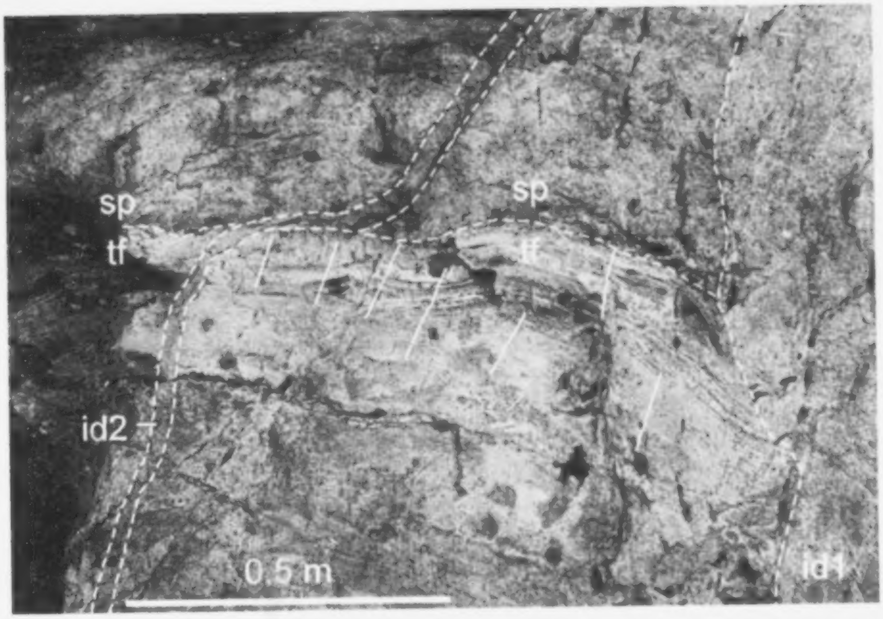

Photo 58. Portion of outcrop 004VOI1518 (area corresponding to the lower right-hand side of Figure 39), looking southwest. Fragment of a folded contact of tuffs (tf) and syenite porphyries (sp) transected at high angle by axial planar S4 cleavage (solid lines). Two S4-parallel intramineral dikes crosscut syenite porphyries and tuffs. The dike on the right-hand side (id1) is pervasively foliated, whereas the thin dike on the left-hand side (a short segment of which is hosted by the tuff-syenite contact plane) is unfoliated. Emplacement of the second dike (small) most probably largely postdated D4 folding.

Relative Timing of Deformation and Mineralization

The exact relative timing of Kirkland Lake gold mineralization and deformation events is not entirely clear. Apparent temporal overlap between the emplacement of the intramineral dikes and D4 (documented at outcrop 004VOI1518) suggests that the formation of the gold-bearing veins at the Macassa Mine could have, at least partially, overlapped with D4. As most intramineral dikes exposed at surface are foliated (S4), gold-bearing quartz veins possibly formed early during D4 and were later deformed.

Syn-mineralization stylolites that host gold and telluride grains in northeast-trending, steeply dipping quartz veins (e.g., stope 4940) are parallel to the regional S4 orientation. The alignment of stylolite teeth approximates the orientation of greatest principal stress (Davis and Reynolds 1996, p.443-444). Horizontal (northwest-southeast) orientation of stylolite teeth in auriferous veins indicates that the veins experienced northwest-southeast shortening (cf. Boullier and Robert 1992), and the occurrence of gold and tellurides along stylolite surfaces suggests that this shortening probably overlapped with mineralization. The orientation of S4 corresponds to the same shortening direction, implying that mineralization could have formed broadly synchronous with D4.

Syn-mineralization cataclasis of the Teck-Hughes #1 vein hosted by a subsidiary north splay of the Main Break (Todd 1928) shows that mineralization was accompanied by movements along host fault structures. The inferred reverse-dextral (south side up and to the west) slip along the primary ore-controlling structure, the Main Break, is also kinematically compatible with regional northwest-southeast shortening characteristic of D4. Based on the above summarized evidence, we suggest that the high-grade gold-bearing veins of the Kirkland Lake deposit could have formed relatively early in the D4 event, and have been partially overprinted by continuing deformation. Mineralization was accompanied by reverse-dextral to reverse movements along the Main Break. Sheeted veinlets of the Narrows Break mineralized zone show conflicting relationships with the S4 cleavage, and thus their formation was broadly synchronous with D4.

Amikougami Creek Fault

Gold mineralization at the Macassa Mine and Kirkland Lake camp in general ends against the post-ore Amikougami Creek fault (Map P.3558, back pocket). West of the fault, only a few isolated gold occurrences have been discovered so far. The sense and magnitude of the displacement along the Amikougami Creek fault are still poorly understood. Previous mapping (Thomson 1945) shows roughly 270 m apparent sinistral (west side south) offset of the Main Break along the fault. (As discussed earlier in this report, there are at least 2 and possibly 3 parallel fault structures east of the of the Amikougami Creek fault and it is not obvious which of the 2 or 3 was located west of it.) Underground exploration at the Macassa Mine revealed roughly 120 m of apparent sinistral displacement of the '04 Break, assuming that the east-northeast-striking structure encountered on the west side of the Amikougami Creek fault is the western continuation of the '04 Break. Exploration drifting on the 4750-foot level at Macassa traced this east-northeast-trending structure for up to 427 m, but no ore was found along the structure (Still 2001). As this structure is unmineralized, whereas mineralization along the '04 Break extends vertically for 980 m from the 3825 to 7050-foot levels, the east-striking structure on the west side of the fault may not be the continuation of the '04 Break but is rather a parallel, unmineralized, fault (Still 2001). Determining the slip movement along the Amikougami Creek fault is therefore extremely important for discovering further 04 Break mineralization west of this fault.

The Amikougami Creek fault was examined underground on the 4750-foot level of the Macassa Mine. The fault strikes 340° and dips 70-75° east. It is a 1.3 m wide zone of chloritic gouge and breccia. Two thin (10 and 5-7 cm) diabase dikes are hosted by the fault. A syn-faulting foliation along the west margin of the fault zone is oriented clockwise to the fault walls, suggesting strike-slip sinistral (west side south) displacement. Fault-parallel striations plunge 10° north, which is consistent with subhorizontal strike-slip movement along the fault. At surface, the apparent displacement of mappable markers (e.g., from north to south: Timiskaming unconformity, syenite-porphyry intrusion, south tuff-conglomerate contact near the railroad turn, dikes of syenite porphyry, conglomerate-tuff contact southwest of Macassa shaft 3) is sinistral, but magnitude varies from about 90 to about 200 m, probably in part due to the uncertainty in positioning of most marker contacts. Data in Lackey (1990) show a roughly 200 m apparent sinistral displacement of a diabase dike located by drilling north of railroad turn at the Amikougami Creek crossing (the dike is not shown on Map P.3558), indicating a largely post-diabase timing of displacement.

Lackey (1990) analyzed marker displacement in the area north the Amikougami Creek railway crossing. He used specific stratigraphic units in the tuff package, a mafic syenite body, a diabase dike, and the '04 Break as markers. The tuff unit shows apparent dextral displacement, whereas both the diabase dike and the '04 Break show a left-lateral shift. The pattern was resolved through 800 m vertical (west side down) and 295 m horizontal sinistral movements. We agree with Still (2001) in that this large vertical offset is questionable. The big vertical component is largely a consequence of an assumed dextral displacement of tuff marker units. This dextral displacement disagrees with the opposite, sinistral shift of several other markers (see above), and, most importantly, of the tuff (north)-conglomerate (south) contact in the same area. The tuff-conglomerate contact is more distinct, and probably more reliable than lithologic markers within the tuff package. The discrepancy in apparent slip direction indicates that marker horizons within the tuff package may have been correlated incorrectly across the fault. To date, there is no unequivocal evidence supporting large vertical movements on the Amikougami Creek fault. The available structural data support the latest strike-slip sinistral movement, however the possibility of earlier vertical movements should not be disregarded, and this critical fault displacement requires revision. Analysis of geological markers with different dip angles can help answering the question on whether only strike-slip movements or a combination of strike slip and vertical movements took place. However, at present, positioning of the potential markers in proximity to the fault is not sufficiently precise for such analysis. A review of existing drilling and ground magnetic data should be done to help in selecting reliable and precisely positioned markers. Among possible candidates are (from north to south): Timiskaming unconformity, tuff-conglomerate contact near the railroad Amikougami Creek crossing, 80-100 m wide syenite porphyry dike or sill immediately north of Macassa shaft #3, and a conglomerate-tuff contact southwest of Macassa shaft #3.

U-Pb and Re-Os Geochronology

Geochronological studies were done to determine the age of Kirkland Lake gold mineralization and assist in establishing relationships between hydrothermal activity, deformation, and magmatism. We attempted to date an ore-hosting syenite porphyry (feldspar-rich variety in classification of this report), two intramineral dikes and mineralized veins using the U-Pb and Re-Os methods. The U-Pb (Thermal Ionization Mass Spectroscopy, TIMS) and Re-Os analyses were done, respectively, at the Jack Satterly Geochronological Laboratory at the University of Toronto, and at the Radiogenic Isotope Facility at the University of Alberta. In-situ Sensitive High Resolution Ion Microprobe (SHRIMP) analysis of zircons was completed at the Geological Survey of Canada laboratory in Ottawa. Analytical techniques of U-Pb and Re-Os methods are discussed in Ayer et al. (2005), and Selby and Creaser (2004), respectively. The syenite porphyry sample (03JAA0006-geochronological sample, 004VOI1947-1-matching geochemical sample) was collected from the outcrop of the Main Break mineralization on the former Wright-Hargreaves property (Discovery outcrop, station 004VOI1947 of the present project). Samples of intramineral dikes are from stope 4529 (Macassa Mine, between the 4250 and 4500-foot levels) and surface outcrop 004VOI1518 (the large, foliated dike in Figure 39). Geochemical analyses of 3 samples are listed in Appendix A under sample names 004VOI1947-1 (syenite porphyry), 4529 (intramineral dike from stope 4529), and 004VOI1518-1 (intramineral dike from the surface outcrop). Three molybdenite-bearing samples are from active stopes of the Macassa Mine (stopes 4744, 4247-3, and 5030), and one (Tegren Gracie claim, the 5400-foot level, Macassa Mine) was contributed by the OGS Resident Geologist office in Kirkland Lake. Results of geochronological analyses are summarized below.

Evaluation of mineral concentrates from the 2 intramineral dike samples revealed an absence of mineral phases suitable for the U-Pb analysis. U-Pb dating of zircons from syenite porphyry returned complex results. TIMS ages of 5 single-grain fractions vary from 2700 to 2690 Ma (2700.2 ± 2.9 Ma, 2700.6 ± 4.4 Ma, 2694.4 ± 7.4 Ma, 2689.6 ± 4.7 Ma, 2689.7 ± 41.3 Ma; Figure 40). The youngest identifiable population is ca. 2690 Ma, which obviously indicates zircon inheritance, since Timiskaming clastic rocks that host syenite intrusions in the Kirkland Lake camp are younger than 2680 Ma (Corfu et al. 1991). The 12 in-situ SHRIMP dates form a near continuous range from about 2723 Ma to about 2675 Ma, accompanied by two outlying younger ages, 2649 Ma and 2642 Ma (Figure 41). One in-situ date (2673.5 ± 6.1 Ma) falls into a "geologically expected" range, but the textural setting of this spot age is uncertain. Overall, the data do not provide a reliable magmatic age. The two youngest in-situ SHRIMP ages likely reflect some metamorphic or hydrothermal zircon growth. Although the possibility of young magmatic ages cannot be completely discarded, it appears generally improbable: the youngest age comes from a diffuse overgrowth rim that does not show typical "magmatic" oscillatory zoning.

In summary, our U-Pb analyses have not produced definitive data on the age of the syenite porphyry and maximum age of Kirkland Lake mineralization, primarily due to the zircon inheritance problem. Although certainly disappointing, this result is not completely unexpected: constant presence of xenoliths is a diagnostic feature of Kirkland Lake syenite porphyries, and it can explain the abundance of inherited zircon. Future U-Pb studies may be able to overcome this problem by analyzing exceedingly larger number of zircon fractions and conducting more detailed in-situ (SHRIMP) analyses. Dating geologically older intrusive phases (mafic syenite and especially syenite) should also be considered.

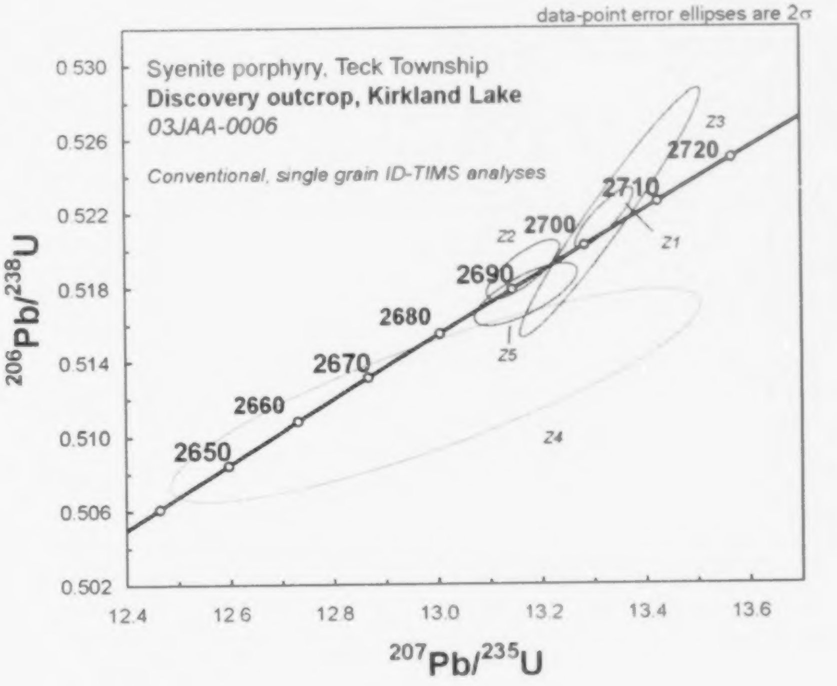

Figure 40. Concordia plot for the U-Pb TIMS (zircon) analysis of the syenite porphyry sample.

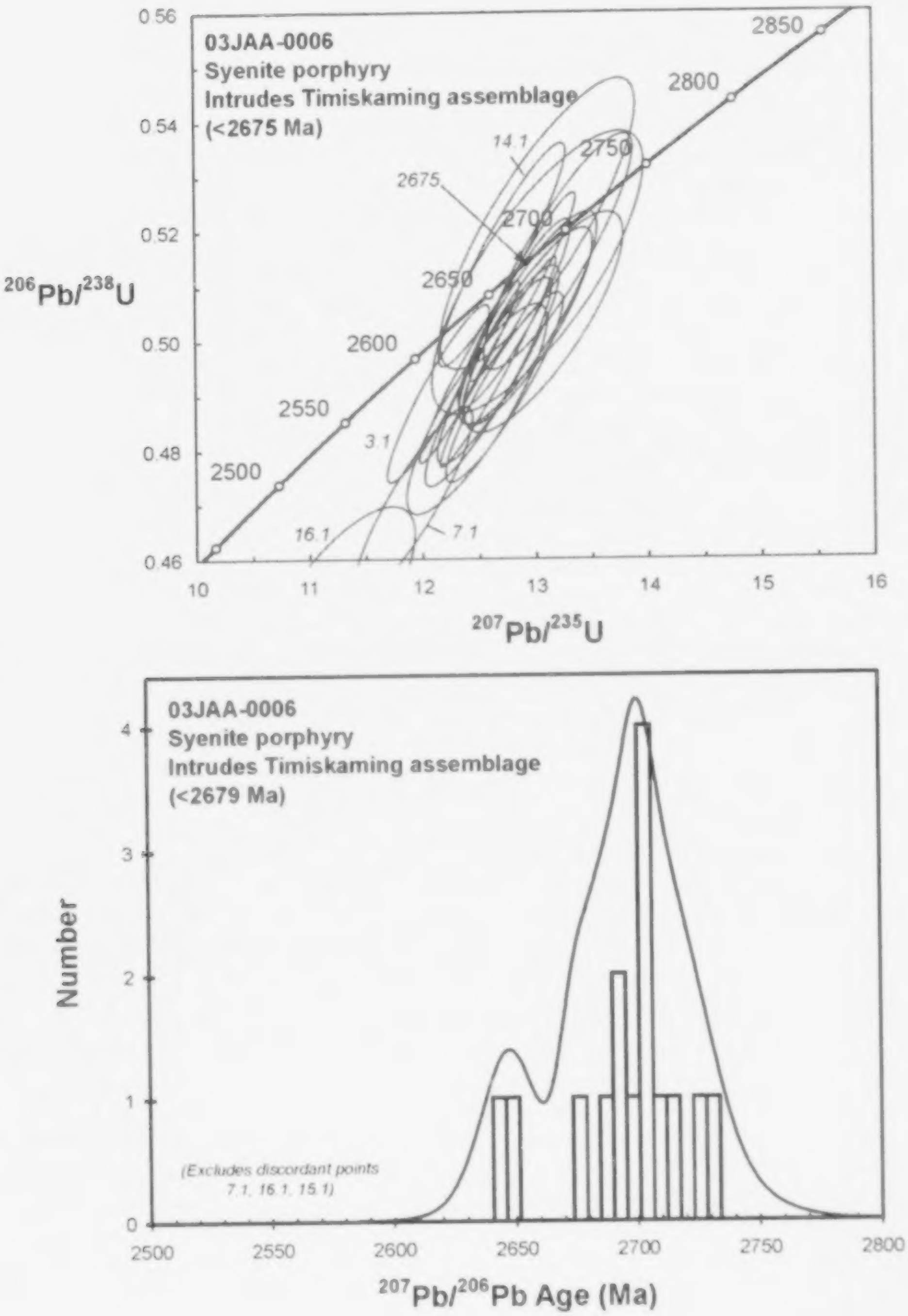

Figure 41. Results of in-situ (SHRIMP) analyses of the syenite porphyry sample: concordia plot (top) and distribution of in-situ ages (bottom).

Table 2. Summary of the Re-Os analytical data.

Sample	weight (g)	Re ppm	± 2σ	^{187}Os ppb	± 2 σ	Model age	± 2 σ	+/- 2 σ inc λ
Samples analyzed in full from large mineral separates								
4744 piece "A"	0.21250	0.544	0.001	15.60	0.03	2677	8	12
4744 piece "A"	0.27619	0.529	0.001	15.09	0.03	2666	8	11
Both 4744 analyses taken from a single drilled mineral separate of 0.50g								
Tegren Gracie	0.19986	0.675	0.002	19.50	0.03	2696	7	11
Tegren Gracie	0.27619	0.679	0.002	19.60	0.03	2694	7	11
Both Tegren Gracie analyses taken from a single drilled mineral separate of 0.48g								
5030 piece"A"	0.10506	0.714	0.002	22.50	0.04	2976	8	13
5030 piece"A"	0.19309	0.724	0.002	22.75	0.03	2927	8	12
5030 piece"A"	0.32835	0.698	0.002	22.31	0.03	2977	8	12
All 5030 analyses taken from a single drilled mineral separate of 0.71g								
Samples analyzed in full from small mineral separates								
4247-3 piece "A"	0.04322	0.765	0.002	22.74	0.03	2773	7	11
4247-3 piece "B"	0.05351	0.900	0.002	26.11	0.04	2710	7	11
Both 4247 analyses taken from single drilled mineral separates comprising the entire analysis weight								

Preliminary Re-Os results available at the time of report submission are summarized in Table 2. Of 4 model Re-Os ages, 3 are older than Timiskaming clastic rocks and cannot be geologically meaningful. Two of these ages are also not internally reproducible: aliquots of the same samples do not agree within 2σ errors. Two aliquots of sample 4744 produced internally consistent ages of 2666±12 Ma and 2677±11 Ma that comply with available broad geologic constraints. Separation of more molybdenite material from this sample is presently underway, and additional analysis in the near future may produce more certain results and allow better geologic assessment of Re-Os ages of this and other samples.

Although these Re-Os results are still preliminary, the complexity of the data is obvious, and this complexity most likely stems from chemical and crystallographic properties of molybdenite samples. All analyzed samples returned very low Re contents, which in other studies yielded poorly reproducible Re-Os dates (Selby and Creaser 2004). XRD analyses of samples 4744 and 5030 show that molybdenites belong to the 3R polytype. Virtually all existing Re-Os age dates are generated from the other, 2H polytype, that is far more typical for hydrothermal systems. Re-Os systematics of the 3R molybdenite have not been rigorously studied, and may potentially be very different from the better understood 2H systematics.

In summary, the results of U-Pb and Re-Os dating received to date do not provide independent constraints on the timing of gold mineralization. Zircon inheritance is clearly a major factor complicating the U-Pb dating. Additional Re-Os analysis of sample 4744 may bring a more precise result and help explain the meaning of other, anomalously old, ages.

Geochemistry of Kirkland Lake Gold-Bearing Veins

Geochemical data for auriferous quartz vein samples and brief characteristics of analyzed material are listed in Appendix A. Kirkland Lake gold veins are characterized by high Te, Mo, Pb, Ag (although for most samples with Au >50 g/t, Au/Ag ratios exceed 10), sporadically high Cu and normally low As. The most salient feature is the high tellurium content that exceeds gold values in all samples and shows well-defined positive correlation with gold (Figure 42). Previously published analyses of bulk ore samples from Lake Shore and Kirkland Lake Gold mines (Todd 1928; Thomson et al. 1950) show similar gold-tellurium relationships, confirming that the geochemical data presented here is representative of Kirkland Lake mineralization in general. Good gold-tellurium correlation indicates that presence of tellurides is the essential feature of Kirkland Lake gold mineralization, and that gold and tellurides most probably precipitated simultaneously through the same depositional mechanism.

Elevated Pb values in gold-bearing samples is largely due to the presence of altaite (PbTe). Altaite is the most abundant tellurium mineral in Kirkland Lake gold veins (Todd 1928; Thomson et al. 1950), and it also hosts practically all the lead, since galena is either absent or occurs in insignificant amounts, mainly as a post-ore mineral (Todd 1928; Thomson et al. 1950). Gold is present in native form or as tellurides: calaverite ($AuAgTe_2$) and rarer petzite (Ag_3AuTe_2) (Todd 1928; Thomson et al. 1950). Non gold-bearing tellurides, other than altaite, are rare (Todd 1928; Thomson et al. 1950). Assuming that all lead occurs in altaite, and the remaining tellurium is combined with gold and silver in calaverite, it is possible to estimate the proportions of native gold and telluride gold from chemical data (cf. Todd 1928, p.71). The ternary plot in Figure 43 demonstrates relative molecular proportions of combined gold and silver, tellurium and lead, and inferred modes of gold occurrence. Relatively high Pb/Te ratio of 4 samples (3 of which are low grade: Au ≤ 17 ppm) indicates that all tellurium occurs as altaite, and in 2 of these samples, the Pb/Te ratio significantly exceeds 1, implying the presence of galena. In all other samples, molecular proportions of tellurium exceed those of lead, indicating the presence of gold tellurides. Relative proportions of native and telluride gold vary significantly; 2 samples contain enough tellurium to bound all contained gold and silver in calaverite. There is no obvious relationship between gold grade and proportions of native vs. telluride gold, and no distinct spatial variations of Au-Pb-Te proportions, although the dataset is probably too small to reveal such trends. High molybdenum contents that are clearly related to the presence of molybdenite show no identifiable correlation to gold values.

Another interesting feature is the elevated vanadium content in sample 1254-2. This sample consists of cataclasized quartz cemented by dark-grey quartz-sericite matrix that hosts most gold and telluride grains. The presence of syenite porphyry clasts cannot explain the 350 ppm vanadium content (vanadium in this variety of syenite porphyry ranges from 50 to 75 ppm). Vanadium-bearing mica may be present in the mica-rich cement of the mineralized cataclasite. Previously, Kerrich and Watson (1984) reported V contents of up to 518 and 1716 ppm for the mafic syenite breccia ore at the Macassa Mine. These values significantly exceed vanadium contents in unaltered mafic syenites (e.g., 180-220 ppm, appendix A) and may also indicate the presence of vanadium-bearing mica in the ore. In this study, patches of bright green mica, macroscopically strongly resembling vanadium mica, roscoelite, were observed in altered syenite porphyries along the Mud Break. Microprobe analysis is needed to confirm the presence of vanadium mica in the hydrothermal assemblage of Kirkland Lake mineralization. Roscoelite is common for alkaline epithermal gold systems (e.g., Jensen and Barton 2000), and thus the presence of vanadium-rich mica in

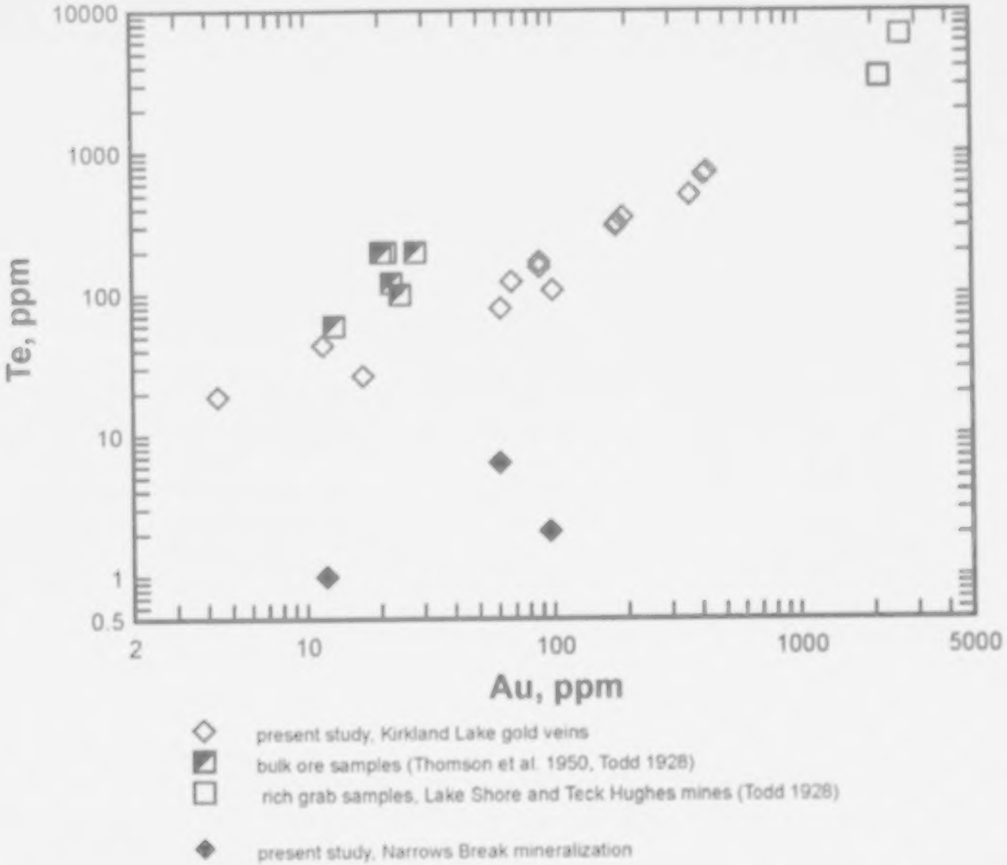

Figure 42. Au vs. Te plot for veins of the Kirkland Lake deposit and Narrows Break mineralized zone. Includes data for samples from this study (listed in Appendix A) and previously published data on bulk ore samples and gold-rich grab samples (Kirkland Lake Gold, Teck-Hughes and Lake Shore mines). Samples from Kirkland Lake gold veins of present study and grab samples of Todd (1928) show well-defined correlation of Au and Te and Au/Te<1. Bulk ore samples show similar relationships, a slight deviation from the trend is probably due to low resoulution of Te analyses in bulk samples (for most bulk samples Te is reported in %, to two decimals). Narrows Break mineralization is characterized by much lower Te values.

Kirkland Lake gold veins and alteration halos may provide important information on the genesis of mineralization.

The geochemistry of the Narrows Break mineralization differs from that of Kirkland Lake gold veins primarily by the lack of elevated Te (Figure 42), Mo, and Pb. This geochemical signature combined with already mentioned very different mineralization style (sheeted veinlets with abundant carbonate, stronger wall-rock carbonatization), suggests that the Narrows Break mineralized zone probably represents a separate mineralized system unrelated to Kirkland Lake mineralization.

Figures 44, 45, and 46 compare Kirkland Lake gold mineralization with other gold occurrences described earlier in this report. Kirkland Lake gold veins differ from all other mineralized zones by high Te (Te>Au), Mo, and low As. Te is also elevated in the Upper Canada L zone, however Te contents of the L zone are lower than in Kirkland Lake ores, and no gold tellurides, only altaite, have been identified at Upper Canada. Other differences between the two deposits include higher As content and lower Au/Ag ratios of the Upper Canada mineralization. Apart from trace elements, another already mentioned important difference is the less intensive bulk wall-rock carbonatization at Kirkland Lake. The reason for this is not completely clear at present: available fluid inclusion data (although very fragmental) suggest presence of CO_2 – rich fluids in Kirkland Lake hydrothermal system (e.g., Watson 1984, p.184-188), and carbonic inclusions in mineralized quartz were also observed in this study.

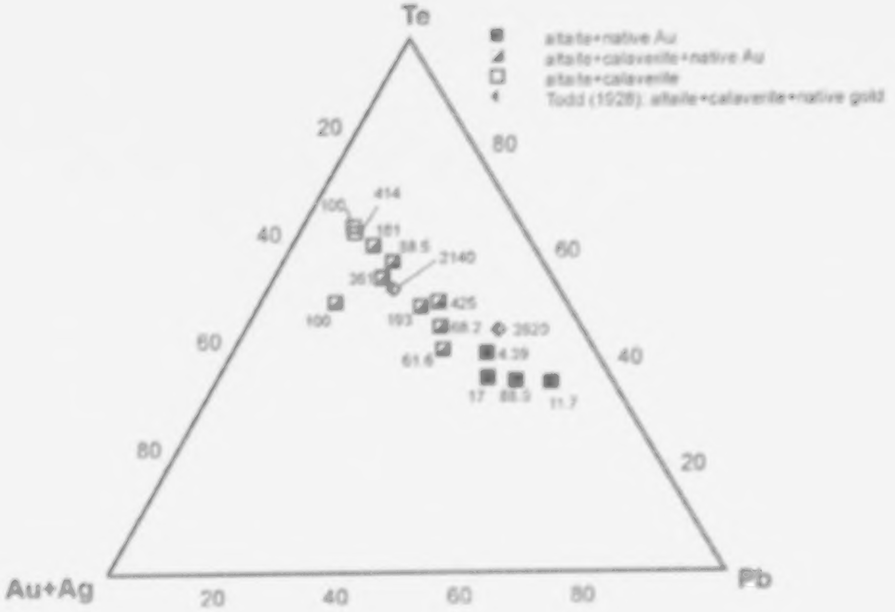

Figure 43. Ternary plot of molecular proportions of combined Au and Ag, Te, and Pb and probable mode of occurrence of gold. Te is assumed to combine with all contained Pb to form altaite (PbTe, the most abundant telluride in Kirkland Lake ores). The remaining Te is expected to form calaverite ($AuAgTe_2$), and the "excess" Au-Ag is assumed to be present in native form. Square and diamond symbols depict data of this study, and of Todd (1928), respectively. Filled symbols show samples in which amounts of Te are sufficient only to form altaite (or even insufficient to match all contained Pb), and thus all Au is likely to be present in native form. Half-filled symbols correspond to samples in which relative element proportions "allow" formation of altaite, calaverite, and presence of native Au. Open squares depict samples in which amounts of Te are sufficiently high to bind all contained Pb in altaite and all Au-Ag in calaverite (i.e., no native gold is present under above listed assumptions). Numbers depict Au (g/t). The apparent trend from the Pb apex to the Au+Ag-Te line corresponds to a general increase in the "telluride Au/native Au" ratio. The plot indicates that in virtually all (except 1) samples with Au > 50 g/t, Au tellurides are likely to be present, relative proportion of native and telluride Au ranges broadly and does not appear to be related to the gold grade.

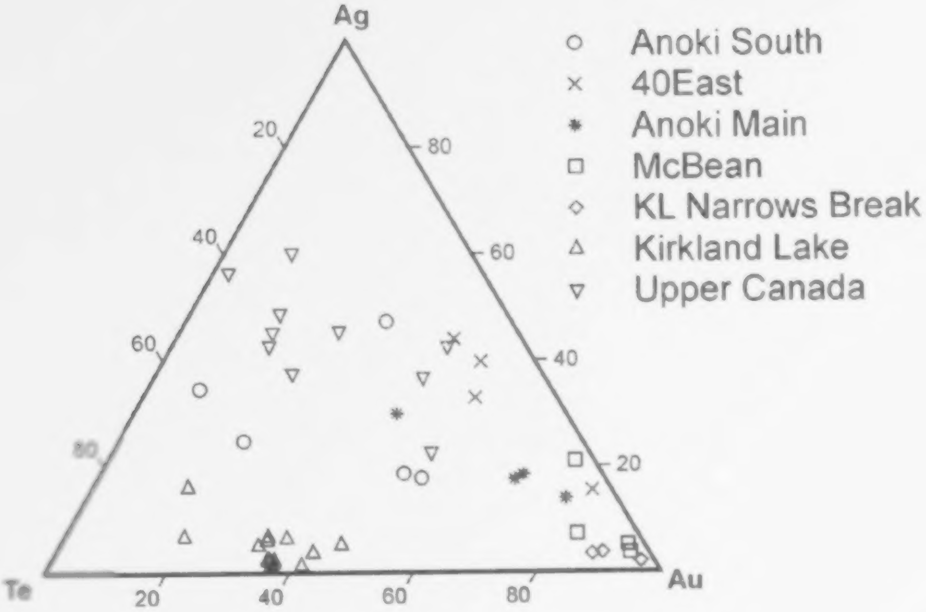

Figure 44. Au-Ag-Te ternary plot (wt%) for samples of Kirkland Lake gold veins, Narrows Break mineralization, and mineralized zones of the Gauthier Township transect.

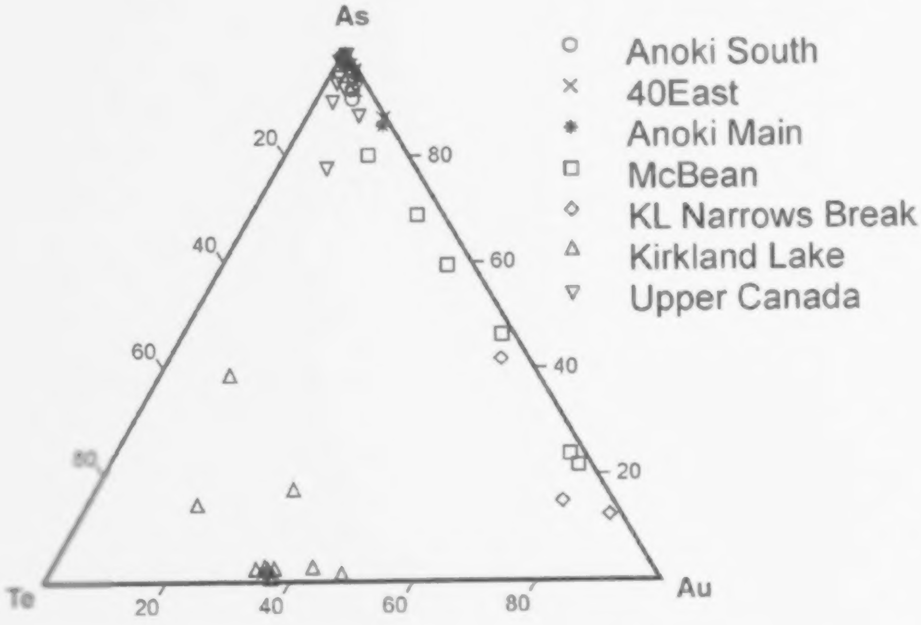

Figure 45. Au-As-Te ternary plot (wt%) for samples of Kirkland Lake gold veins, Narrows Break mineralization, and mineralized zones of the Gauthier Township transect.

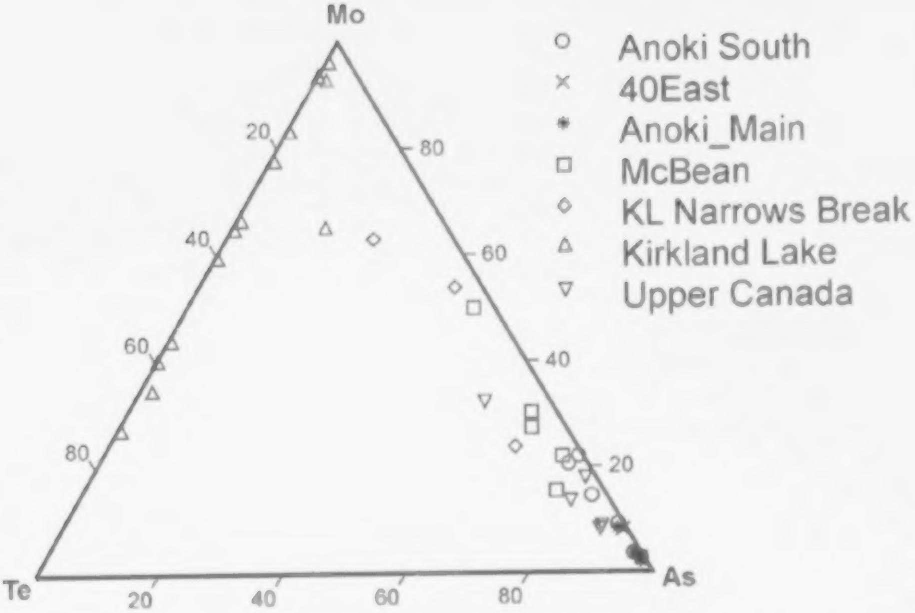

Figure 46. Te-Mo-As ternary plot (wt%) for samples of Kirkland Lake gold veins, Narrows Break mineralization, and mineralized zones of Gauthier Township transect.

Origin of Kirkland Lake Gold Mineralization

The origin of gold mineralization in the Kirkland Lake deposit was discussed in several publications, including Watson (1984), Kerrich and Watson (1984), Cameron and Hattori (1987), Robert and Poulsen (1997), and most recently in the Society of Economic Geologists Thayer Lindsley Lecture by Robert (2004). Watson (1984) and Kerrich and Watson (1984) proposed that Kirkland Lake mineralization was formed from 350-460°C fluids of crustal, probably metamorphic, origin, with a possible contribution of magmatic fluids. This was followed by downward penetration of oxidizing, sulphate-bearing, and relatively low-temperature (<200°C waning to approximately 50°C) marine or meteoric fluids (Kerrich and Watson 1984). Cameron and Hattori (1987) documented evidence for oxidized fluids, such as the constant ^{34}S depletion of sulphides, presence of sulphates in veins and hematite in alteration halos, and proposed magmatic (oxidized felsic magma) fluid source. They also interpreted the syenitic intrusions as "slightly older" than mineralization and suggested that fluids were likely derived from magma at depth. Robert and Poulsen (1997) indicated that the Kirkland Lake vein array was formed in a late reverse-fault system overprinting folded Timiskaming rocks, i.e., it was emplaced in a setting similar to that of the Dome and Pamour deposits in Timmins. Robert (2001) introduced a new syenite-associated disseminated gold deposit group. These deposits tend to cluster along major faults and comprise variably developed quartz stockworks in intensely altered (albite and K-feldspar) wall rocks. The deposits are intimately associated with Timiskaming-age monzonitic to syenitic porphyry intrusions near the base of erosional remnants of Timiskaming-type sedimentary rocks. Mineralization was emplaced between 2682 Ma and 2672 Ma (i.e., broadly contemporaneous with Timiskaming sedimentation) and overprinted by regional fabric-forming deformation (Robert 2001). More recently, Robert (2004) classified the Kirkland Lake deposit as belonging to this group. In his interpretation, Robert (2004) proposed that the mineralization was formed from fluids derived from the syenitic intrusive complex, it pre-dated D2, and was overprinted by subsequent deformation.

In agreement with the interpretations of Cameron and Hattori (1987) and Robert (2004), a very distinctive metal assemblage of Kirkland Lake veins strongly suggests that Kirkland Lake gold mineralization is genetically unrelated to other gold occurrences described in this report. As discussed below, Kirkland Lake high-grade gold veins were probably formed from compositionally distinct fluids derived from a different source than the fluids that deposited gold along the Larder Lake–Cadillac deformation zone and its splays. It is difficult to envision a mechanism that could generate the telluride- and molybdenite-rich mineralization that we see in Kirkland Lake veins from the same fluid that produced the typical low Te-Mo mineralization of the Larder Lake–Cadillac gold occurrences. Strong correlation of gold and tellurium suggests that both were deposited synchronously, and there was no superposition of discrete gold- and tellurium-rich mineralizing pulses. Synchronous introduction of gold and tellurium is also supported by the close mineralogical association of native gold and tellurides. The possibility that the distinct metal inventory of Kirkland Lake veins is not fluid source-related but instead reflects host rock signature inherited through fluid-rock interactions at the final stages of fluid migration, cannot be completely discarded but appears improbable. There is no evidence for volumetrically significant fluid-wall rock exchange, as the alteration halos directly associated with Kirkland Lake veins are relatively small. Besides, mineralization is hosted by geochemically variable rocks (e.g., mafic syenite, syenite porphyry, tuff, conglomerate), however no chemical or mineralogical zoning reflecting the host lithologies has been noticed to date. Thus, most probably, geochemistry of Kirkland Lake mineralization reflects the fluid chemistry, which was originally different from that of gold-bearing fluids that migrated and deposited gold in the Larder Lake–Cadillac deformation zone and its immediate splays. Consequently, the Kirkland Lake gold deposit is unlikely to be part of the regional hydrothermal system associated with the Larder Lake–Cadillac deformation zone.

Amongst all potential fluid sources, derivation of the fluids from alkaline magmas appears most likely. The Kirkland Lake gold deposit shares strong analogies with epithermal-style gold deposits associated with alkaline magmatism (Jensen and Barton 2000). The best known Phanerozoic deposits of this group are Emperor (Fiji) and Cripple Creek (Colorado, USA; Jensen and Barton 2000). Several key geological parameters of the Kirkland Lake deposit are typical for epithermal-style systems related to alkaline magmatism. These include high-grade (low base-metal) veins, high Au/Ag ratios, high tellurium contents (e.g., Te>Au at Kirkland Lake), presence of gold tellurides, common presence of molybdenite, K-metasomatism (e.g., sericitization at Kirkland Lake), and spatial association of mineralization with the multi-phase alkaline igneous complex. In addition, there are less pronounced or less well established features of the Kirkland Lake mineralization that are also common to alkaline-related epithermal systems, such as the occurrence of vanadium mica, and presence of sulphates, hematite, and possibly magnetite (e.g., Cameron and Hattori 1987; Watson and Kerrich 1984). Strong structural control of gold-bearing veins is also common for epithermal-style deposits related to alkaline magmatism (Jensen and Barton 2000).

The main weakness of the magmatic fluid model is the absence of causative plutons. Presently available data are insufficient to link mineralization to any specific intrusive phase. The U-Pb and Re-Os analyses of this project have not produced reliable geochronological constraints on the relative timing of magmatism and mineralization. Structural relationships indicate that mineralization post-dated the emplacement and crystallization of the syenite porphyry (i.e., the latest phase of the composite alkalic stock), since the gold-bearing Main Break crosscuts and displaces the syenite porphyry intrusion. Hicks and Hattori (1988) reported that gold-related alteration overprints syngenetic syenite porphyry alteration, and thus genetic relationships between mineralization and syenite porphyries that are presently exposed at surface are unlikely. This, however, does not rule out the possibility of a magmatic origin for the gold-bearing fluids: the mineralizing fluids could have been derived from a distal magmatic source at depth as suggested by Cameron and Hattori (1987). The occurrence of alkaline intramineral dikes confirmed by this study indicates that alkaline magmatism had not ended by the time of gold mineralization, an active magmatic chamber existed at depth and could have served as a fluid source.

Based on a) the relative chronology of gold-bearing quartz veins, intramineral dikes and deformational fabrics, b) the presence of S4-parallel syn-mineralization stylolites in gold-bearing veins, c) syn-mineralization cataclasis in gold veins indicative of syn-mineralization fault movements, and d) the compatibility of the inferred reverse-dextral movement on the Main Break with the northwest-southeast compression direction of D4, we propose that the mineralization could have formed relatively early in the D4 event. Syn-D4 timing of gold mineralization does not preclude the alkalic magmatic fluid source, because at present there is no evidence that would qualify the alkalic magmatism as entirely pre-deformational. For example, two large alkalic plutons in the area, the Lebel Stock and the Murdock Creek pluton, are interpreted as syn-D2 (Wilkinson et al. 1999); it is also possible that magmatism partly overlapped with D4.

The style and composition of the quartz-carbonate sheeted-veinlet mineralized zone of the Narrows Break differ from those of typical Kirkland Lake gold veins and is overall more similar to the gold occurrences along the Larder Lake–Cadillac deformation zone. Most probably, the Narrows Break represents a separate hydrothermal system. Documented structural relationships indicate that the Narrows Break mineralization was formed broadly synchronous with D4.

Summary

DEFORMATION HISTORY

We identify 3 post-Timiskaming fabric-forming deformation events, which occurred after an early syn- to post-Timiskaming deformation that did not generate deformational fabrics. This early (non fabric-forming) deformation is marked by bedding reversals in Timiskaming turbidites. The maximum age of turbidites (2677.7 ± 3.1 Ma) constrains the maximum age of this deformation event. The earliest fabric-forming event, D2, is related to oblique dextral reverse movements along the Larder Lake–Cadillac deformation zone (documented in Gauthier Township) and characterized by penetrative S2 foliation. This deformation is overall compatible with north-south shortening as previously suggested by Wilkinson et al. (1999), however, we do not find evidence for sinistral movements along northeast-trending segments of the Larder Lake–Cadillac deformation zone. D3 corresponds to an east-west shortening event that locally produced a north-trending S3 foliation. D4 is related to northwest-southeast shortening and manifested by a regional steep northeast-trending foliation. The occurrence of an east-west shortening event (D3) between D2 and D4 does not support previous interpretations of a prolonged progressive deformation from D2 to D4 (e.g., Toogood and Hodgson 1986).

GOLD MINERALIZATION

Hodgson and Hamilton (1989) linked the formation of gold deposits of the Kirkland Lake–Larder Lake area to the final stages of D4 (D2 under the original authors' nomenclature), and implied a single regional fluid source for gold mineralization. Our results suggest that gold mineralization is associated with D2 and D4, and it probably involved more than one fluid source.

Gold-bearing veins along the brittle to brittle-ductile Kirkland Lake fault (Main Break) were formed at relatively shallow crustal levels, probably simultaneously with reverse-dextral to reverse movement on the Main Break. Mineralization was likely emplaced early during D4. The distinct metal inventory (Te>Au, Mo, Pb, Ag, high Au/Ag, low As) of Kirkland Lake mineralization indicates a separate fluid source, different from gold deposits and occurrences clustering along the Larder Lake–Cadillac deformation zone and its splays. Based on presently available data, a deep alkaline magmatic fluid source (magmatic chamber or intrusion at depth) appears most probable. The interpretation of Kirkland Lake as a stand-alone hydrothermal system probably related to alkalic magmatism and unrelated to gold mineralization along the Larder Lake–Cadillac deformation zone agrees with the interpretation of Robert (2004). However, the syn-D4 timing of mineralization proposed in this report differs from the pre-D2 timing suggested by Robert (2004). The Narrows Break mineralized zone located about 350 m north of the Main Break differs in style, geochemistry, and alteration from typical Kirkland Lake gold veins and most likely represents a separate hydrothermal system. Relationships between S4 and sheeted veinlets of the Narrows Break mineralized zone indicate that they were formed during D4.

Gold mineralization in Gauthier Township represents a separate and older hydrothermal event than that of the Kirkland Lake gold lodes. Mineralization at the Upper Canada Mine occurs in a high-strain ductile deformation zone that probably represents a splay of the Larder Lake–Cadillac deformation zone. Although hydrothermal activity spanned 3 deformation phases (D2, D3, and D4), gold was introduced relatively early, during D2, and was accompanied by strong bulk carbonatization. Subsequent deformation and, possibly, hydrothermal activity overprinted gold mineralization. The effect of this overprint on key geological and economical parameters of gold mineralization is unclear.

Gold occurrences of the Anoki and McBean properties are localized within or in the immediate proximity of the first-order Larder Lake–Cadillac deformation zone. Gold occurs in sulphidized Fe-tholeiite flows (Anoki Main zone), in quartz stockworks within carbonate- and carbonate-fuchsite-altered ultramafic rocks ("green carbonate", McBean and Anoki Deep zones), in quartz-sulphide zones hosted by Timiskaming clastic rocks and locally associated with feldspar-phyric dikes (40 East zone), and in quartz veining with sulphides in cherty to graphitic exhalite horizons enclosed in basalts (Anoki South). In all cases mineralization is accompanied by strong carbonatization. Drill cores from the McBean zone show that mineralization and alteration are most likely synchronous with the development of D2 fabrics. Mineralized zones at the Anoki and McBean properties are part of a regionally extensive hydrothermal system that affected a roughly 20 km long segment of the Larder Lake–Cadillac deformation zone from the Kerr Addison-Chesterville gold deposit (east) to the Anoki occurrences (west). Other similar gold deposits include the Cheminis and Omega deposits in McVittie Township. Most gold production and reserves are from sulphide-rich replacement ores in mafic (mostly tholeiitic) volcanic rocks, whereas native-gold-bearing quartz stockworks in carbonate-fuchsite-altered meta-ultramafic rocks ("green carbonate ore") are second in importance. Gold deposits and occurrences along the Larder Lake–Cadillac and Upper Canada deformation zones are probably related because they have similar geochemical signatures and similar ore zone plunges roughly parallel to L2. The Upper Canada deformation zone is a splay of the Larder Lake–Cadillac deformation zone, and as both structures are syn-D2, they were likely hydraulically connected during the introduction of gold-bearing fluids along these structures.

Acknowledgements

We thank Queenston Mining Inc. and Kirkland Lake Gold Inc. for granting access to their properties, surface and underground workings, and drill core, and for contributing private geological data that were extensively used in this project. Kirkland Lake Gold Inc. provided logistical support for underground work of the first author. Geologists Dale Alexander, Frank Ploeger of Queenston Mining Inc., Mike Sutton, Stewart Carmichael, Ken Rattee, Duncan Quick and Cory Dupuis of Kirkland Lake Gold Inc., and

Chris Pegg (consultant) are thanked for their time and sharing their knowledge of geology and gold mineralization of the Kirkland Lake camp and Kirkland Lake–Larder Lake gold area. We aslo thank Erle Boyce, Eric Marion, and Michael Leahy for allowing access to outcrops on their properties. Strong interest in the project from geologists and prospectors of the Kirkland Lake–Larder Lake area is gratefully acknowledged. The first author was capably assisted in the field by Jennifer Cardamone and Patrick Johnson in 2003, and Natasha Lallier in 2004. Ms. Lallier also actively participated in preparing digital data for geological map P.3558. The project was supported by the Discover Abitibi Initiative, a regional cluster economic development project based on geoscientific investigations of the western Abitibi greenstone belt. The initiative is centred on the Kirkland Lake and Timmins mining camps and directed by local stakeholders. FedNor, Northern Ontario Heritage Fund Corporation and private sector investors provided the funding for the initiative.

References

Ayer, J., Amelin, Y., Corfu, F., Kamo, S., Ketchum, J., Kwok, K. and Trowell, N. 2002. Evolution of the southern Abitibi greenstone belt based on U-Pb geochronology; autochthonous volcanic construction followed by plutonism, regional deformation and sedimentation; Precambrian Research, v.115, p.63-95.

Ayer, J.A., Thurston, P.C., Dube, B., Gibson, H.L., Hamilton, M., Hathaway, B., Hocker, S., Houle, M., Hudak, G., Ispolatov, V., Lafrance, B., Lesher, C.M., MacDonald, P.J., Peloquin, A.S., Piercey, S.J., Reed, L.E. and Thompson, P.H. 2005. Overview of results from the greenstone architecture project: Discover Abitibi Initiative; Ontario Geological Survey, Open File Report 6154.

Bell, C.C. 1987. Ore petrography, carbonate alteration and geochemistry of the McBean Mine, Larder Lake, Ontario; unpublished B.Sc. thesis, McMaster University, Hamilton, Ontario, 92p.

Ben Othman, D., Arndt, N.T., White, W.M. and Jochum, K.P. 1990. Geochemistry and age of Timiskaming alkali volcanics and the Otto syenite stock, Abitibi, Ontario; Canadian Journal of Earth Sciences, v.27, p.1304-1311.

Berthe, D., Choukroune, P. and Jegouzo, P. 1979. Orthogneiss, mylonite and non coaxial deformation of granites; the example of South Armorican shear zone; Journal of Structural Geology, v.1, p.31-42.

Böhlke, J.K. 1988. Carbonate-sulfide equilibria and 'stratabound' disseminated epigenetic gold mineralization: a proposal based on examples from Alleghany, California, U.S.A; Applied Geochemistry, v.3, p.499-516.

Boullier, A.-M. and Robert, F. 1992. Palaeoseismic events recorded in Archaean gold-quartz vein networks, Val d'Or, Abitibi, Quebec, Canada; Journal of Structural Geology, v.14, p.161-179.

Bragg, J.G. 1967. Upper Canada Mine; Northwestern Quebec-northern Ontario, C.I.M.M. centennial field excursion, 1967, p.88-91.

Cameron, E.M. and Hattori, K. 1987. Archean gold mineralization and oxidized hydrothermal fluids; Economic Geology and the Bulletin of the Society of Economic Geologists, v.82, p.1177-1191.

Card, K.D. 1990. A review of the Superior Province of the Canadian Shield, a product of Archean accretion; Precambrian Research, v.48, p.99-156.

Charlewood, G.H. 1964. Geology of deep developments on the main ore zone at Kirkland Lake; Ontario Department of Mines, Geological Circular No.11, 49p.

Clark, R.J.M. and Bonner, R. 1987. Gold mineralization associated with Archean stratabound sulphides in the Cheminis Deposit near Larder Lake, Ontario; CIM Bulletin 1974, v.80, p.45-50.

Corfu, F. 1993. The evolution of the southern Abitibi greenstone belt in light of precise U-Pb geochronology; Economic Geology and the Bulletin of the Society of Economic Geologists, v.88, p.1323-1340.

Corfu, F., Jackson, S.J. and Sutcliffe, R.H. 1991. U-Pb ages and tectonic significance of late Archean alkalic magmatism and nonmarine sedimentation: Timiskaming Group, southern Abitibi belt, Ontario; Canadian Journal of Earth Sciences, v.28, p.489-503.

Davis, G.H and Reynolds, S.J. 1996. Structural geology of rocks and regions; John Wiley & Sons, Inc., 776p.

Eisenlohr, B.N., Groves, D. and Partington, G.A. 1989. Crustal-scale shear zones and their significance to Archaean gold mineralization in Western Australia; Mineralium Deposita, v.24, p.1-8.

Gosselin, P. and Dube, B. 2005. Gold deposits of Canada: distribution, geological parameters and gold content; Geological Survey of Canada, Open File 4896, 105p.

Hagemann, S.G. and Cassidy, K.F. 2000. Archean orogenic lode gold deposits; Reviews in Economic Geology, v.13, p.9-68.

Hagemann, S.G., Groves, D.I., Ridley, J.R. and Vearncombe, J.R. 1992. The Archean lode gold deposits at Wiluna, Western Australia: high-level brittle-style mineralization in a strike-slip regime; Economic Geology and the Bulletin of the Society of Economic Geologists, v.87, p.1022-1053.

Hamilton, J.V. 1986. The structure and stratigraphic setting of gold mineralization in the vicinity of Larder Lake, southcentral Abitibi greenstone belt, northeastern Ontario; unpublished M.Sc thesis, Queen's University, Kingston, Ontario, 156p.

Hamilton, J.V. and Hodgson, C.J. 1984. Structural geology and gold mineralization in the Larder-Lake deformation zone; Ontario Geological Survey, Miscellaneous Paper 119, p.220-225.

Hattori, K. and Levesque, G.S. 1989. Hydrothermal activity in the Kirkland Lake intrusive complex; Ontario Geological Survey, Miscellaneous Paper 143, p.59-67.

Hicks, K.D. and Hattori, K. 1988. Magmatic-hydrothermal and wall rock alteration petrology at the Lake Shore gold deposit, Kirkland Lake, Ontario; Ontario Geological Survey, Miscellaneous Paper 140, p.192-204.

Hodgson, C.J. and Hamilton, J.V. 1989. Gold mineralization in the Abitibi greenstone belt: end-stage result of Archean collisional tectonics?; p.86-100 *in* Keays, R.R., Ramsay, R.H. and Groves, D.I., eds., The geology of gold deposits: the perspective in 1988, Economic Geology Monograph 6.

Hodgson, C.J., Hamilton, J.V. and Guimond, R.P. 1991. Relationship between gold deposits and the tectonic framework of the Abitibi greenstone belt in the Kirkland Lake–Larder Lake area; Ontario Geological Survey, Open File Report 5782, 60p.

Hopkins, H. 1940. Faulting at the Wright-Hargreaves mines, with notes on ground movements; Canadian Institute of Mining and Metallurgy Transactions, v.43, p.685-707.

Hopkins, H. 1949. Structure at Kirkland Lake, Ontario, Canada; Geological Society of America Bulletin, v.60, p.909-922.

Hyde, R.S. 1978. Sedimentology, volcanology, stratigraphy, and tectonic setting of the Archean Timiskaming Group, Abitibi greenstone belt, northeastern Ontario, Canada; unpublished Ph.D. thesis, McMaster University, Hamilton, Ontario, 422p.

Hyde, R.S. 1980. Sedimentary facies in the Archean Timiskaming Group and their tectonic implications, Abitibi greenstone belt, northeastern Ontario, Canada; Precambrian Research, v.12, p.161-195.

Irvine, T.N. and Baragar, W.R.A. 1971. A guide to the chemical classification of the common volcanic rocks; Canadian Journal of Earth Sciences, v.8, p.523-548.

Jackson, S.L. 1995. Larder Lake area; Ontario Geological Survey, Map 2628, scale 1:50 000.

Jackson, S.L. and Fyon, A. 1991. The western Abitibi Subprovince in Ontario; p.405-482 *in* Geology of Ontario, Ontario Geological Survey, Special Volume 4, Part 1.

Jensen, E.P. and Barton, M.D. 2000. Gold deposits related to alkaline magmatism; Reviews in Economic Geology, v.13, p.279-314.

Jensen, L.S. 1976. A new cation plot for classifying subalkalic volcanic rocks; Ontario Department of Mines, Miscellaneous Paper 66, p.22.

Jolly, W.T. 1978. Metamorphic history of the Archean Abitibi Belt; Geological Survey of Canada Paper, v.78-10, p.63-78.

Kerrich, R. and Watson, G.P. 1984. The Macassa Mine Archean lode gold deposit, Kirkland Lake, Ontario: geology, patterns of alteration, and hydrothermal regimes; Economic Geology and the Bulletin of the Society of Economic Geologists, v.79, p.1104-1130.

Kishida, A. and Kerrich, R. 1987. Hydrothermal alteration zoning and gold concentration at the Kerr-Addison Archean lode gold deposit, Kirkland Lake, Ontario; Economic Geology and the Bulletin of the Society of Economic Geologists, v.82, p.649-690.

Lackey, T.N., Jr. 1990. Alkaline tuffs at Kirkland Lake, Ontario; unpublished M.Sc. thesis, Queen's University, Kingston, Ontario, 451p.

Le Bas, M.J., Le Maitre, R.W., Streckeisen, A. and Zanettin, B.A. 1986. Chemical classification of volcanic rocks based on the total alkali-silica diagram; Journal of Petrology, v.27, p.745-750.

Legault, M.I. and Hattori, K. 1994a. Late Archaean geological development recorded in the Timiskaming Group sedimentary rocks, Kirkland Lake area, Abitibi greenstone belt, Canada; Precambrian Research, v.68, p.23-42.

Legault, M.I. and Hattori, K. 1994b. Provenance of igneous clasts in conglomerates of the Archaean Timiskaming Group, Kirkland Lake area, Abitibi greenstone belt, Canada; Canadian Journal of Earth Sciences, v.31, p.1749-1762.

Lister, G.S. and Snoke, A.W. 1984. S-C mylonites; Journal of Structural Geology, v.6, p.617-638.

MacLean, A. 1944. Township of Lebel, District of Timiskaming, Ontario; Ontario Department of Mines, Map 53a, scale 1:12 000.

McCuaig, T.C. and Kerrich, R. 1998. P-T-t-deformation-fluid characteristics of lode gold deposits: evidence from alteration systematics; Ore Geology Reviews, v.12, p.381-454.

Mueller, W., Donaldson, J.A. and Doucet, P. 1994. Volcanic and tectono-plutonic influences on sedimentation in the Archaean Kirkland Basin, Abitibi greenstone belt, Canada; Precambrian Research, v.68, p.201-230.

Neumayr, P. and Hagemann, S.G. 2002. Hydrothermal fluid evolution within the Cadillac tectonic zone, Abitibi greenstone belt, Canada: relationship to auriferous fluids in adjacent second- and third-order shear zone; Economic Geology and the Bulletin of the Society of Economic Geologists, v.97, p.1203-1225.

Oliver, N.H.S., Ord, A., Valenta, R.K. and Upton, P. 2001. Deformation, fluid flow, and ore genesis in heterogeneous rocks, with examples and numerical models from the Mount Isa district, Australia; Reviews in Economic Geology, v.14, p.51-73.

Ontario Geological Survey 2002. Ontario airborne geophysical surveys, magnetic and electromagnetic data, grid, vector and profile data, Kirkland Lake area; Ontario Geological Survey, Geophysical Data Set 1102 Revised.

Ontario Geological Survey 2004. Ontario airborne geophysical surveys, magnetic data, grid data (ASCII format) and vector data, Kirkland Lake–Larder Lake area; Ontario Geological Survey, Geophysical Data Set 1053a.

Phillips, G.N., Groves, D.I. and Martyn, J.E. 1984. An epigenetic origin for Archean banded iron-formation-hosted gold deposits; Economic Geology and the Bulletin of the Society of Economic Geologists, v.79, p.162-171.

Platt, J.P. 1984. Secondary cleavages in ductile shear zones; Journal of Structural Geology, v.6, p.439-442.

Poulsen, K.H., Robert, F. and Dube, B. 2000. Geological classification of Canadian gold deposits; Geological Survey of Canada Bulletin 540, 106p.

Queenston Mining Inc., 1996. Annual report, 14p.

Queenston Mining Inc. 2002. Annual report, 20p.

Queenston Mining Inc. 2003. Annual report, 24p.

Ridler, R. 2001. Technical report on Kirkland Lake mineral properties (Macassa Mine, Kirkland Lake Gold, Teck-Hughes, Lake Shore, Wright-Hargreaves) located in Kirkland Lake, Ontario, Canada for Foxpoint Resources Ltd. (posted at www.klgold.com, downloaded in spring 2004), 64p.

Ridley, J., Mikucki, E.J. and Groves, D.I. 1996. Archean lode-gold deposits: fluid flow and chemical evolution in vertically extensive hydrothermal systems; Ore Geology Reviews, v.10, p.279-293.

Robert, F. 1989. Internal structure of the Cadillac tectonic zone southeast of Val d'Or, Abitibi greenstone belt, Québec; Canadian Journal of Earth Sciences, v.26, p.2661-2675.

Robert, F. 1990. Structural setting and control of gold-quartz veins of the Val d'Or area, southeastern Abitibi subprovince; p.167-210 *in* Ho, S.E., Robert, F. and Groves, D., eds., Gold and base-metal mineralization in the Abitibi subprovince, Canada, with emphasis on the Quebec segment - Short course notes: Geology Department (Key Centre) and University Extension, The University of Western Australia, Publication no. 24.

Robert, F. 2001. Syenite-associated disseminated gold deposits in the Abitibi greenstone belt, Canada; Mineralium Deposita, v.36, p.503-516.

Robert, F. 2004. Giant Gold Deposits of the Abitibi Greenstone Belt and Related Models; SEG Thayer Lindsley Lecture at Laurentian University (Sudbury, Ontario, Canada), December 17, 2004.

Robert, F. and Brown, A.C. 1986. Archean gold-bearing quartz veins at the Sigma Mine, Abitibi greenstone belt, Québec: Part 1, geologic relations and formation of the vein system; Economic Geology and the Bulletin of the Society of Economic Geologists, v.81, p.578-592.

Robert, F. and Poulsen, K.H. 1997. World-class Archaean gold deposits in Canada: an overview; Australian Journal of Earth Sciences, v.44, p.329-351.

Robert, F. and Poulsen, K.H. 2001. Vein formation and deformation in greenstone gold deposits; Reviews in Economic Geology, v.14, p.111-155.

Ropchan, J.C. 2000. Petrographic and geochemical studies of the alteration zones associated with gold mineralization at the Holloway Mine, southwestern Abitibi greenstone belt, Canada; unpublished M.Sc. thesis, University of Ottawa, Ottawa, Ontario, 151p.

Ropchan, J.R., Luinstra, B., Fowler, A.D., Benn, K., Ayer, J., Berger, B., Dahn, R., Labine, R. and Amelin, Y. 2002. Host-rock and structural controls on the nature and timing of gold mineralization at the Holloway Mine, Abitibi Subprovince, Ontario; Economic Geology and the Bulletin of the Society of Economic Geologists, v.97, p.291-309.

Selby, D. and Creaser, R.A. 2004. Macroscale NTIMS and microscale LA-MC-ICP-MS Re-Os isotopic analysis of molybdenite: Testing spatial restrictions for reliable Re-Os age determinations, and implications for the decoupling of Re and Os within molybdenite; Geochimica et Cosmochimica Acta, v.68, p.3897-3908.

Smith, J.P., Spooner, E.T.C., Broughton, D.W. and Ploeger, F.R. 1993. Archean Au-Ag-(W) quartz vein/disseminated mineralisation within the Larder Lake–Cadillac Break, Kerr Addison-Chesterville System, Northeast Ontario, Canada, Ontario Geoscience Research Grant Program, Grant No. 364; Ontario Geological Survey, Open File Report 5831, 310p.

Stevenson, D.B., Broughton, D.W., Cruji, D.R., Masson, M.W. and Parry, S.E. 1995. Geology and exploration history of the Amalgamated Kirkland Deposit, Kirkland Lake, Ontario; Exploration and Mining Geology, v.4, p.187-196.

Still, A.C. 2001. Structural setting and controls of gold mineralization at the Macassa Mine, Kirkland Lake, Ontario; unpublished M.Sc. thesis, Queen's University, Kingston, Ontario, 151p.

Sun, S.S. and McDonough, W.F. 1989. Chemical and isotopic systematics of oceanic basalts: implications for mantle composition and processes; p.313-345 *in* Saunders, A.D. and Norry, M.J., eds., Magmatism in the ocean basins, Geological Society Special Publications, v.42.

Thomson, J.E. 1941. Geology of McGarry and McVittie Townships, Larder Lake Area; Ontario Department of Mines, Annual Report, v.50, pt.7, p.1-99.

Thomson, J.E. 1945. Township of Teck, District of Timiskaming, Ontario; Ontario Department of Mines, Map 1945-1, scale 1:12 000.

Thomson, J.E. 1950. Geology of Teck Township and the Kenogami Lake area, Kirkland Lake gold belt; Ontario Department of Mines, Annual Report, v.57, pt.5, p.1-53.

Thomson, J.E., Charlewood, G.H., Griffin, K., Hawley, J.E., Hopkins, H., MacIntosh, C.G., Ogryzlo, S.P., Perry, O.S. and Ward, W. 1950. Geology of the main ore zone at Kirkland Lake; Ontario Department of Mines, Annual Report, v.57, pt.5, p.54-188.

Thomson, J.E. and Griffis, A.T. 1941. Geology of Gauthier Township, East Kirkland Lake area; Ontario Department of Mines, Annual Report, v.50, pt.8, 29p.

Todd, E.W. 1928. Kirkland Lake gold area (a detailed study of the central zone and vicinity); Ontario Department of Mines, Annual Report, v.37, pt.2, 176p.

Toogood, D.J. 1986a. McBean Mine and Kirkland Lake–Larder Lake Break; p.48-49 *in* Pirie, J. and Downes, M.J., eds., Gold '86 Excursion Guidebook, Toronto, GOLD '86.

Toogood, D.J. 1986b. Regional geology of the Abitibi belt in the vicinity of the Kirkland Lake–Larder Lake gold camps; p.46-47 *in* Pirie, J. and Downes, M.J., eds., Gold '86 Excursion Guidebook, Toronto, GOLD '86.

Toogood, D.J. 1989. The Upper Canada Mine, an Archean shear-hosted lode gold deposit; Queenston Mining Inc., internal report, p.1-57. (Accessible at the MNDM library, Sudbury, Ontario.)

Toogood, D.J. and Hodgson, C.J. 1985. A structural investigation between Kirkland Lake and Larder Lake gold camps; *Ontario Geological Survey, Miscellaneous Paper 127, p.200-205.*

Toogood, D.J. and Hodgson, C.J. 1986. Relationship between gold deposits and the tectonic framework of the Abitibi greenstone belt in the Kirkland Lake–Larder Lake area; Ontario Geological Survey, Miscellaneous Paper 130, p.79-86.

Tully, D.W. 1963. The geology of the Upper Canada Mine; Proceedings of the Geological Association of Canada, v.15, p.61-86.

Ward, W., Charlewood, G.H., Griffin, K., Hopkins, H., Ogryzlo, S.P. and Perry, D.S. 1948. The gold mines of Kirkland Lake (Ontario), Structural geology of Canadian ore deposits; Canadian Institute of Mining and Metallurgy, symposium volume, p.644-653.

Warwick, M. 1981. Gold mineralisation of the flow ores at Kerr Addison Mine; unpublished B.Sc. thesis, University of Western Ontario, London, Ontario, 101p.

Watson, G.P. 1984. Ore types and fluid regimes: Macassa gold mine, Kirkland Lake; unpublished Ph.D. thesis, University of Western Ontario, London, Ontario, 341p.

Watson, G.P. and Kerrich, R. 1983. Macassa Mine, Kirkland Lake: production history, geology, gold ore types and hydrothermal regimes; Ontario Geological Survey, Miscellaneous Paper 110, p.56-74.

Wilkinson, L. 1993. Post-Timiskaming structural history of the Larder Lake–Cadillac Deformation Zone, southwestern Abitibi belt, Ontario; unpublished M.Sc. thesis, University of Toronto, Toronto, Ontario, 162p.

Wilkinson, L., Cruden, A.R. and Krogh, T.E. 1999. Timing and kinematics of post-Timiskaming deformation within the Larder Lake–Cadillac deformation zone, southwest Abitibi greenstone belt, Ontario, Canada; Canadian Journal of Earth Sciences, v.36, p.627-647.

This page left blank intentionally

Appendix A

Geochemical Data

This appendix consists of 6 tables: tables A.1 and A.2 contain lithogeochemical data intended for protolith characterization (major elements, REE, HFSE, etc.); tables A.3, A.4, and A.5 contain pathfinder trace element and major element (A.5) data for mineralized samples. Table A.6 contains brief descriptions of mineralized samples. Data for Upper Canada Mine samples are listed in tables A.1 and A.4 (with some overlap). Negative values correspond to values below detection limits.

Abbreviations:

Geolabs – Geoscience Laboratories, Ontario Ministry of Northern Development and Mines
Actlabs – Activation Laboratories Ltd (Ancaster, Ontario)
XRF – X-ray fluorescence
IRC – infra-red absorption
ICP-MS – closed beaker solution, inductively coupled plasma mass-spectrometry
H. ICP-MS – proprietary digestion, ICP-MS analysis
ICP-AES – closed beaker solution, inductively coupled plasma atomic emission spectroscopy
MS-AHT – hydride, inductively coupled plasma mass-spectrometry
MS-IAT – fire assay with ICP-MS finish
ICP-OES – four acid solution, inductively coupled plasma optical emission spectrometry
INAA – instrumental neutron activation analysis
Fire, grav. – fire assay with gravimetric finish
AAS-Flame – beaker solution, atomic absorption spectroscopy

Unit codes:

Alkalic Intrusives	13
Alkalic Volcanics	5
Felsic to Intermediate Intrusive	12
Mafic Intrusive	10
Mafic Volcanic	2
Temiskaming Sediments	8
Ultramafic Volcanic	1

Table A.1. Analytical results for samples from first field season (2003), Gauthier Township: major and trace element geochemistry, analyses by Geolabs.

			sample id		003VOB0012-1	003VOB0109-2	AN03-35-431.5	AN03-52-539
			sample type		surface	surface	drill core	drill core
			drill hole/station		003VOB0012	003VOB0109	AN03-35	AN03-52
			depth, ft				431.5	539
			Township		Gauthier	Gauthier	Gauthier	Gauthier
			unit_code		1	1	1	1
			rock type		ultramafic metavolcanic (carbonate-fuchsite schist)	ultramafic metavolcanic (carbonate-fuchsite schist)	ultramafic metavolcanic (talc-chlorite schist)	ultramafic metavolcanic (talc-chlorite schist)
			UTM_NAD83_E		589349	589837	586374.38	586420.53
			UTM_NAD83_N		5330656	5329817	5331367.21	5331307.92
laboratory	method	det limit	units					
Geolabs	XRF	0.01	%	SiO2	30.78	25.12	39.98	44.53
Geolabs	XRF	0.01	%	TiO2	0.23	0.30	0.33	0.29
Geolabs	XRF	0.01	%	Al2O3	4.71	5.70	5.77	5.45
Geolabs	XRF	0.01	%	Fe2O3	8.12	8.90	9.67	10.09
Geolabs	XRF	0.01	%	MnO	0.13	0.14	0.22	0.11
Geolabs	XRF	0.01	%	MgO	20.18	21.21	24.33	25.93
Geolabs	XRF	0.01	%	CaO	5.35	4.23	6.58	3.37
Geolabs	XRF	0.01	%	Na2O	0.05	0.05	0.03	0.03
Geolabs	XRF	0.01	%	K2O	1.15	2.17	0.20	0.13
Geolabs	XRF	0.01	%	P2O5	0.01	0.01	0.03	0.01
Geolabs	XRF	0.05	%	LOI	27.73	30.41	11.96	8.39
			%	Total	98.46	98.23	99.08	98.35
Geolabs	ICP-MS	0.07	ppm	Ce	1.87	1.98	4.24	1.89
Geolabs	ICP-MS	0.007	ppm	Cs	2.868	1.132	1.759	1.429
Geolabs	ICP-MS	0.008	ppm	Dy	1.049	1.022	1.313	0.836
Geolabs	ICP-MS	0.008	ppm	Er	0.678	0.696	0.773	0.54
Geolabs	ICP-MS	0.005	ppm	Eu	0.214	0.2	0.279	0.235
Geolabs	ICP-MS	0.009	ppm	Gd	0.887	0.796	1.158	0.676
Geolabs	ICP-MS	0.1	ppm	Hf	0.4	0.5	0.6	0.4
Geolabs	ICP-MS	0.003	ppm	Ho	0.225	0.237	0.274	0.18
Geolabs	ICP-MS	0.02	ppm	La	0.73	0.82	1.74	1.16
Geolabs	ICP-MS	0.003	ppm	Lu	0.097	0.103	0.116	0.085
Geolabs	ICP-MS	0.2	ppm	Nb	0.4	0.5	0.7	0.3
Geolabs	ICP-MS	0.03	ppm	Nd	1.57	1.53	2.9	1.25
Geolabs	ICP-MS	0.006	ppm	Pr	0.306	0.31	0.632	0.253
Geolabs	ICP-MS	0.05	ppm	Rb	42.18	54.32	9.52	7.03
Geolabs	ICP-MS	0.01	ppm	Sm	0.56	0.53	0.82	0.45
Geolabs	ICP-MS	0.5	ppm	Sr	326.3	310.9	303.7	105.2
Geolabs	ICP-MS	0.17	ppm	Ta	-0.17	-0.17	-0.17	-0.17
Geolabs	ICP-MS	0.003	ppm	Tb	0.155	0.144	0.205	0.121
Geolabs	ICP-MS	0.06	ppm	Th	0.1	0.1	0.23	0.09
Geolabs	ICP-MS	0.003	ppm	Tm	0.098	0.106	0.114	0.083
Geolabs	ICP-MS	0.007	ppm	U	0.03	0.08	0.112	0.069
Geolabs	ICP-MS	0.02	ppm	Y	5.93	6.09	7.5	4.49
Geolabs	ICP-MS	0.01	ppm	Yb	0.9	0.69	0.74	0.57
Geolabs	ICP-MS	0.1	ppm	Ba	100.819	75.138	863.709	9.747
Geolabs	ICP-AES	0.1	ppm	Be	0.23	0.43	0.19	0.14
Geolabs	ICP-AES	1	ppm	Co	76	76	82	97
Geolabs	ICP-AES	3	ppm	Cu	29	54	47	53
Geolabs	ICP-AES	8	ppm	Mo	-8	-8	-8	-8
Geolabs	ICP-AES	3	ppm	Ni	933	891	1036	1269
Geolabs	ICP-AES	0.3	ppm	Sc	13.1	14.1	15.3	16.2
Geolabs	ICP-AES	0.6	ppm	V	82.6	93.7	78.4	95.7
Geolabs	ICP-AES	2	ppm	W	10	7	-2	-2
Geolabs	ICP-AES	2	ppm	Zn	81	65	86	117
Geolabs	XRF	4	ppm	Cr_XRF	1993	2821	2532	2319
Geolabs	XRF	4	ppm	V_XRF				
Geolabs	XRF	3	ppm	Zr_XRF	11	20	34	17
Geolabs	XRF	2	ppm	Nb_XRF				
Geolabs	IRC	0.03	%	CO2	25.3	26.2		
Geolabs	IRC	0.01	%	S	0.03	-0.03		

Table A.1. (cont'd)

			sample id		003VOI0083-1	003VOI0664-1	003VOI0671-1	003VOI0679-1
			sample type		surface	surface	surface	surface
			drill hole/station		003VOI0083	003VOI0664	003VOI0671	003VOI0679
			depth, ft					
			Township		Gauthier	Gauthier	Gauthier	Gauthier
			unit_code		2	2	2	2
			rock type		mafic metavolcanic (chlorite schist)	mafic metavolcanic (chlorite schist)	mafic metavolcanic (chlorite schist)	mafic metavolcanic (pillow basalt)
			UTM_NAD83_E		588635	588452	588608	586964
			UTM_NAD83_N		5331143	5331191	5331026	5331210
laboratory	method	det limit	units					
Geolabs	XRF	0.01	%	SiO2	48.52	48.59	50.65	46.89
Geolabs	XRF	0.01	%	TiO2	1.82	1.81	1.75	1.44
Geolabs	XRF	0.01	%	Al2O3	13.15	12.68	12.40	12.97
Geolabs	XRF	0.01	%	Fe2O3	18.76	17.31	14.24	17.36
Geolabs	XRF	0.01	%	MnO	0.19	0.28	0.16	0.28
Geolabs	XRF	0.01	%	MgO	5.14	3.35	3.60	6.61
Geolabs	XRF	0.01	%	CaO	7.53	6.20	5.24	12.22
Geolabs	XRF	0.01	%	Na2O	1.79	3.61	3.42	1.13
Geolabs	XRF	0.01	%	K2O	0.04	0.25	0.13	0.26
Geolabs	XRF	0.01	%	P2O5	0.11	0.13	0.12	0.11
Geolabs	XRF	0.05	%	LOI	4.44	6.92	8.29	1.88
			%	Total	101.50	101.12	100.00	101.14
Geolabs	ICP-MS	0.07	ppm	Ce	14.29	19.97	15.62	18.17
Geolabs	ICP-MS	0.007	ppm	Cs	0.281	0.604	0.312	0.183
Geolabs	ICP-MS	0.008	ppm	Dy	5.459	6.344	5.812	4.827
Geolabs	ICP-MS	0.008	ppm	Er	3.514	4.131	3.879	2.88
Geolabs	ICP-MS	0.005	ppm	Eu	1.21	1.386	1.269	1.362
Geolabs	ICP-MS	0.009	ppm	Gd	4.763	5.578	5.087	4.796
Geolabs	ICP-MS	0.1	ppm	Hf	2.3	3	3.1	2.8
Geolabs	ICP-MS	0.003	ppm	Ho	1.164	1.385	1.275	1.022
Geolabs	ICP-MS	0.02	ppm	La	5.59	7.96	5.7	6.73
Geolabs	ICP-MS	0.003	ppm	Lu	0.534	0.624	0.578	0.403
Geolabs	ICP-MS	0.2	ppm	Nb	3.4	4.5	4.6	5.5
Geolabs	ICP-MS	0.03	ppm	Nd	11.46	14.69	12.17	14.23
Geolabs	ICP-MS	0.006	ppm	Pr	2.259	2.992	2.436	2.889
Geolabs	ICP-MS	0.05	ppm	Rb	0.65	5.05	2.92	2.57
Geolabs	ICP-MS	0.01	ppm	Sm	3.6	4.3	3.77	4.05
Geolabs	ICP-MS	0.5	ppm	Sr	149.7	111.9	79.7	290.6
Geolabs	ICP-MS	0.17	ppm	Ta	0.24	0.31	0.27	0.37
Geolabs	ICP-MS	0.003	ppm	Tb	0.821	0.967	0.882	0.805
Geolabs	ICP-MS	0.06	ppm	Th	0.43	0.56	0.55	0.56
Geolabs	ICP-MS	0.003	ppm	Tm	0.519	0.633	0.579	0.421
Geolabs	ICP-MS	0.007	ppm	U	0.146	0.151	0.146	0.158
Geolabs	ICP-MS	0.02	ppm	Y	29.19	34.99	31.94	25.53
Geolabs	ICP-MS	0.01	ppm	Yb	3.4	4.15	3.8	2.68
Geolabs	ICP-MS	0.1	ppm	Ba	19.761	59.971	24.866	59.734
Geolabs	ICP-AES	0.1	ppm	Be	0.26	0.37	0.25	0.4
Geolabs	ICP-AES	1	ppm	Co	51	38	36	59
Geolabs	ICP-AES	3	ppm	Cu	57	32	81	2663
Geolabs	ICP-AES	8	ppm	Mo	-8	-8	-8	-8
Geolabs	ICP-AES	3	ppm	Ni	77	30	42	113
Geolabs	ICP-AES	0.3	ppm	Sc	37.9	35.1	32.5	23.6
Geolabs	ICP-AES	0.6	ppm	V	706	462	363.1	250.4
Geolabs	ICP-AES	2	ppm	W	3	-2	6	-2
Geolabs	ICP-AES	2	ppm	Zn	148	103	125	297
Geolabs	XRF	4	ppm	Cr_XRF	56	30	40	103
Geolabs	XRF	4	ppm	V_XRF	706	462		
Geolabs	XRF	3	ppm	Zr_XRF	81	105	106	109
Geolabs	XRF	2	ppm	Ni_XRF				
Geolabs	IRC	0.03	%	CO2			6.37	
Geolabs	IRC	0.01	%	S			0.08	

Table A.1. (cont'd)

			sample id		003VOI0679-3	003VOI0128-1	003VOI0168-1	003VOI0278-1
			sample type		surface	surface	surface	surface
			drill hole/station		003VOI0679	003VOI0128	003VOI0168	003VOI0278
			depth, ft					
			Township		Gauthier	Gauthier	Gauthier	Gauthier
			unit_code		2	5	5	5
			rock type		mafic metavolcanic (pillow basalt)	feldspar-amphibole-phyric lava	feldspar-phyric lava	amphibole-phyric lava
			UTM_NAD83_E		586947	585558	585982	587310
			UTM_NAD83_N		5331214	5332812	5332541	5333290
laboratory	method	det limit	units					
Geolabs	XRF	0.01	%	SiO2	48.04	54.83	56.96	48.03
Geolabs	XRF	0.01	%	TiO2	1.41	0.55	0.46	0.94
Geolabs	XRF	0.01	%	Al2O3	13.40	15.91	15.80	13.89
Geolabs	XRF	0.01	%	Fe2O3	15.73	7.43	5.54	9.94
Geolabs	XRF	0.01	%	MnO	0.22	0.16	0.12	0.17
Geolabs	XRF	0.01	%	MgO	4.86	4.16	3.04	6.55
Geolabs	XRF	0.01	%	CaO	6.89	5.75	3.91	9.77
Geolabs	XRF	0.01	%	Na2O	3.85	4.87	5.25	3.78
Geolabs	XRF	0.01	%	K2O	0.39	3.84	3.82	2.86
Geolabs	XRF	0.01	%	P2O5	0.10	0.29	0.22	0.52
Geolabs	XRF	0.05	%	LOI	6.57	1.73	4.41	3.73
			%	Total	101.46	99.51	99.54	100.16
Geolabs	ICP-MS	0.07	ppm	Ce	16.69	106.3	92.21	155.75
Geolabs	ICP-MS	0.007	ppm	Cs	0.483	1.441	2.987	21.131
Geolabs	ICP-MS	0.008	ppm	Dy	4.558	3.706	3.422	5.67
Geolabs	ICP-MS	0.008	ppm	Er	2.775	1.996	1.893	2.584
Geolabs	ICP-MS	0.005	ppm	Eu	1.37	1.902	1.679	3.576
Geolabs	ICP-MS	0.009	ppm	Gd	4.545	5.408	5.036	10.267
Geolabs	ICP-MS	0.1	ppm	Hf	2.6	4.1	4.5	4.1
Geolabs	ICP-MS	0.003	ppm	Ho	0.955	0.71	0.656	0.992
Geolabs	ICP-MS	0.02	ppm	La	6.04	54.12	48.34	75.65
Geolabs	ICP-MS	0.003	ppm	Lu	0.388	0.306	0.299	0.327
Geolabs	ICP-MS	0.2	ppm	Nb	5.3	7.2	6.7	4.8
Geolabs	ICP-MS	0.03	ppm	Nd	13.05	45.91	38.3	78.72
Geolabs	ICP-MS	0.006	ppm	Pr	2.621	12.437	10.504	19.596
Geolabs	ICP-MS	0.05	ppm	Rb	6.72	88.16	86.12	150.764
Geolabs	ICP-MS	0.01	ppm	Sm	3.79	7.48	6.78	14.28
Geolabs	ICP-MS	0.5	ppm	Sr	163.4	1567.351	1071.4	2067.224
Geolabs	ICP-MS	0.17	ppm	Ta	0.36	0.41	0.42	0.27
Geolabs	ICP-MS	0.003	ppm	Tb	0.765	0.687	0.655	1.2
Geolabs	ICP-MS	0.06	ppm	Th	0.55	10.46	11.73	11.38
Geolabs	ICP-MS	0.003	ppm	Tm	0.398	0.3	0.285	0.355
Geolabs	ICP-MS	0.007	ppm	U	0.16	3.049	3.637	3.345
Geolabs	ICP-MS	0.02	ppm	Y	24.59	19.29	18.8	26.34
Geolabs	ICP-MS	0.01	ppm	Yb	2.62	1.99	1.91	2.27
Geolabs	ICP-MS	0.1	ppm	Ba	95.816	1745.584	1639.446	1763.542
Geolabs	ICP-AES	0.1	ppm	Be	0.44	1.69	1.48	1.24
Geolabs	ICP-AES	1	ppm	Co	48	21	18	33
Geolabs	ICP-AES	3	ppm	Cu	279	709	88	248
Geolabs	ICP-AES	8	ppm	Mo	-8	-8	-8	-8
Geolabs	ICP-AES	3	ppm	Ni	61	43	34	57
Geolabs	ICP-AES	0.3	ppm	Sc	16.3	14.8	9.5	22.9
Geolabs	ICP-AES	0.6	ppm	V	219.8	157.4	95.7	223.9
Geolabs	ICP-AES	2	ppm	W	-2	-2	7	3
Geolabs	ICP-AES	2	ppm	Zn	128	133	101	122
Geolabs	XRF	4	ppm	Cr_XRF	22	140	132	210
Geolabs	XRF	4	ppm	V_XRF				
Geolabs	XRF	3	ppm	Zr_XRF	100	237	218	258
Geolabs	XRF	2	ppm	Ni_XRF				
Geolabs	IRC	0.03	%	CO2				
Geolabs	IRC	0.01	%	S				

Table A.1. (cont'd)

			sample id		003VOI0289-1	003VOI0349-1	003VOI0385-1	003VOI0422-1
			sample type		surface	surface	surface	surface
			drill hole/station		003VOI0289	003VOI0349	003VOI0385	003VOI0422
			depth, ft					
			Township		Gauthier	Gauthier	Gauthier	Gauthier
			unit_code		5	5	5	5
			rock type		feldspar-phyric lava	volcaniclastic breccia	aphyric lava (?)	feldspar-phyric lava
			UTM_NAD83_E		587236	588444	588254	587842
			UTM_NAD83_N		5333449	5331798	5332643	5332221
laboratory	method	det limit	units					
Geolabs	XRF	0.01	%	SiO2	60.19	58.57	47.64	54.24
Geolabs	XRF	0.01	%	TiO2	0.43	0.52	0.78	0.52
Geolabs	XRF	0.01	%	Al2O3	15.09	14.10	14.78	15.15
Geolabs	XRF	0.01	%	Fe2O3	5.22	6.30	8.63	6.51
Geolabs	XRF	0.01	%	MnO	0.09	0.11	0.13	0.13
Geolabs	XRF	0.01	%	MgO	2.80	4.59	5.73	3.08
Geolabs	XRF	0.01	%	CaO	3.69	3.70	6.23	5.23
Geolabs	XRF	0.01	%	Na2O	5.12	5.19	3.48	5.01
Geolabs	XRF	0.01	%	K2O	3.83	1.29	5.75	4.22
Geolabs	XRF	0.01	%	P2O5	0.20	0.21	0.65	0.37
Geolabs	XRF	0.05	%	LOI	2.75	4.95	5.30	4.72
			%	Total	99.42	99.53	99.09	99.19
Geolabs	ICP-MS	0.07	ppm	Ce	79.07	74.15	214.161	132.97
Geolabs	ICP-MS	0.007	ppm	Cs	2.495	0.951	38.539	3.069
Geolabs	ICP-MS	0.008	ppm	Dy	2.99	2.684	5.864	4.294
Geolabs	ICP-MS	0.008	ppm	Er	1.578	1.402	2.54	2.091
Geolabs	ICP-MS	0.005	ppm	Eu	1.64	1.578	3.964	2.567
Geolabs	ICP-MS	0.009	ppm	Gd	4.694	4.414	11.564	7.479
Geolabs	ICP-MS	0.1	ppm	Hf	4	3.2	4.8	5
Geolabs	ICP-MS	0.003	ppm	Ho	0.559	0.518	1	0.767
Geolabs	ICP-MS	0.02	ppm	La	40.52	35.74	106.268	66.24
Geolabs	ICP-MS	0.003	ppm	Lu	0.233	0.191	0.308	0.293
Geolabs	ICP-MS	0.2	ppm	Nb	5.5	4.2	7.2	7.2
Geolabs	ICP-MS	0.03	ppm	Nd	35.72	35.09	96.92	61.87
Geolabs	ICP-MS	0.006	ppm	Pr	9.363	8.971	25.4	15.926
Geolabs	ICP-MS	0.05	ppm	Rb	91.78	19.19	213.629	107.98
Geolabs	ICP-MS	0.01	ppm	Sm	6.28	6	16.56	10.54
Geolabs	ICP-MS	0.5	ppm	Sr	882.9	564	1889.182	1381.321
Geolabs	ICP-MS	0.17	ppm	Ta	0.32	0.26	0.38	0.37
Geolabs	ICP-MS	0.003	ppm	Tb	0.579	0.533	1.306	0.898
Geolabs	ICP-MS	0.06	ppm	Th	7.62	5.03	19.72	12.37
Geolabs	ICP-MS	0.003	ppm	Tm	0.226	0.196	0.339	0.291
Geolabs	ICP-MS	0.007	ppm	U	2.438	1.458	4.525	3.589
Geolabs	ICP-MS	0.02	ppm	Y	15.31	13.99	26.41	21
Geolabs	ICP-MS	0.01	ppm	Yb	1.51	1.3	2.13	1.95
Geolabs	ICP-MS	0.1	ppm	Ba	1847.874	2046.009	2384.114	2143.996
Geolabs	ICP-AES	0.1	ppm	Be	1.39	0.77	2.32	1.64
Geolabs	ICP-AES	1	ppm	Co	16	29	30	20
Geolabs	ICP-AES	3	ppm	Cu	361	68	99	278
Geolabs	ICP-AES	8	ppm	Mo	-8	-8	-8	-8
Geolabs	ICP-AES	3	ppm	Ni	36	173	48	27
Geolabs	ICP-AES	0.3	ppm	Sc	11.2	12.9	17	11.6
Geolabs	ICP-AES	0.6	ppm	V	96.6	105	183.8	124.1
Geolabs	ICP-AES	2	ppm	W	4	4	-2	-2
Geolabs	ICP-AES	2	ppm	Zn	87	98	117	112
Geolabs	XRF	4	ppm	Cr_XRF	106	468	154	87
Geolabs	XRF	4	ppm	V_XRF				
Geolabs	XRF	3	ppm	Zr_XRF	182	132	296	241
Geolabs	XRF	2	ppm	Ni_XRF				
Geolabs	IRC	0.03	%	CO2				
Geolabs	IRC	0.01	%	S				

Table A.1. (cont'd)

			sample id		003VCB0429-1	003VCB0440-1	003VCB0482-1	003VOI0612-1
			sample type		surface	surface	surface	surface
			drill hole/station		003VCB0429	003VCB0440	003VCB0482	003VOI0612
			depth, ft					
			Township		Gauthier	Gauthier	Gauthier	Gauthier
			unit_code		5	5	5	5
			rock type		pyroxene-phyric lava	pseudoleucite-phyric lava (?)	mafic-phyric lava	tuff (Upper Canada "L-NW" stripping)
			UTM_NAD83_E		587657	587629	589016	586201.98
			UTM_NAD83_N		5332418	5332262	5332583	5332346.26
laboratory	method	det limit	units					
Geolabs	XRF	0.01	%	SiO2	45.34	43.68	47.39	49.37
Geolabs	XRF	0.01	%	TiO2	1.25	1.02	0.84	0.61
Geolabs	XRF	0.01	%	Al2O3	9.28	13.33	13.71	13.24
Geolabs	XRF	0.01	%	Fe2O3	11.53	9.36	9.45	6.80
Geolabs	XRF	0.01	%	MnO	0.25	0.23	0.14	0.37
Geolabs	XRF	0.01	%	MgO	9.80	8.28	7.22	4.64
Geolabs	XRF	0.01	%	CaO	11.58	7.92	6.85	8.28
Geolabs	XRF	0.01	%	Na2O	1.32	4.34	2.69	2.66
Geolabs	XRF	0.01	%	K2O	3.96	4.37	4.92	3.26
Geolabs	XRF	0.01	%	P2O5	0.72	0.84	0.68	0.35
Geolabs	XRF	0.05	%	LOI	1.51	6.72	5.12	9.44
			%	Total	96.54	97.89	99.02	99.03
Geolabs	ICP-MS	0.07	ppm	Ce	499.315	553.689	214.565	98.09
Geolabs	ICP-MS	0.007	ppm	Cs	35.912	24.091	60.087	4.967
Geolabs	ICP-MS	0.008	ppm	Dy	14.136	13.679	6.563	4.227
Geolabs	ICP-MS	0.008	ppm	Er	5.011	5.306	2.651	2.046
Geolabs	ICP-MS	0.005	ppm	Eu	10.308	9.35	4.513	2.326
Geolabs	ICP-MS	0.009	ppm	Gd	29.844	27.593	13.224	7.066
Geolabs	ICP-MS	0.1	ppm	Hf	15.3	16.8	5	3.7
Geolabs	ICP-MS	0.003	ppm	Ho	2.198	2.213	1.074	0.756
Geolabs	ICP-MS	0.02	ppm	La	224.249	239.784	105.239	47.85
Geolabs	ICP-MS	0.003	ppm	Lu	0.471	0.511	0.311	0.288
Geolabs	ICP-MS	0.2	ppm	Nb	23.3	27.6	7	5.1
Geolabs	ICP-MS	0.03	ppm	Nd	232.995	225.922	102.47	48.64
Geolabs	ICP-MS	0.006	ppm	Pr	58.864	60.358	26.369	12.01
Geolabs	ICP-MS	0.05	ppm	Rb	252.232	304.538	166.778	103.45
Geolabs	ICP-MS	0.01	ppm	Sm	41.237	38.705	18.06	9.22
Geolabs	ICP-MS	0.5	ppm	Sr	4599.582	3509.592	2267.678	1505.791
Geolabs	ICP-MS	0.17	ppm	Ta	0.79	1	0.36	0.32
Geolabs	ICP-MS	0.003	ppm	Tb	3.3	3.103	1.489	0.856
Geolabs	ICP-MS	0.06	ppm	Th	36.04	50.96	15.44	8.55
Geolabs	ICP-MS	0.003	ppm	Tm	0.656	0.645	0.344	0.291
Geolabs	ICP-MS	0.007	ppm	U	10.671	12.232	2.658	2.548
Geolabs	ICP-MS	0.02	ppm	Y	61.32	61.69	29	20.66
Geolabs	ICP-MS	0.01	ppm	Yb	3.71	3.97	2.2	1.94
Geolabs	ICP-MS	0.1	ppm	Ba	9236.906	6463.139	2886.952	992.446
Geolabs	ICP-AES	0.1	ppm	Be	6.14	7.4	1.77	1.01
Geolabs	ICP-AES	1	ppm	Co	43	24	33	28
Geolabs	ICP-AES	2	ppm	Cu	508	168	136	86
Geolabs	ICP-AES	8	ppm	Mo	-8	-8	-8	-8
Geolabs	ICP-AES	3	ppm	Ni	126	59	46	45
Geolabs	ICP-AES	0.3	ppm	Sc	22.3	16.3	19.6	17.5
Geolabs	ICP-AES	0.6	ppm	V	231.1	270.7	192.6	147
Geolabs	ICP-AES	2	ppm	W	-2	-2	-2	-2
Geolabs	ICP-AES	2	ppm	Zn	235	232	118	217
Geolabs	XRF	4	ppm	Cr_XRF	518	172	162	263
Geolabs	XRF	4	ppm	Y_XRF				
Geolabs	XRF	3	ppm	Zr_XRF	904	876	300	187
Geolabs	XRF	2	ppm	Nb_XRF				
Geolabs	IRC	0.03	%	CO2				
Geolabs	IRC	0.01	%	S				

Table A.1. (cont'd)

			sample id		10-1	11-1	12-1	13-1
			sample type		surface	surface	surface	surface
			drill hole/station					
			depth, ft					
			Township		Gauthier	Gauthier	Gauthier	Gauthier
			unit_code		5	5	5	5
			rock type		qtz-sericite-carbonate schist (altered tuff?; Upper Canada "L"stripping)	qtz-sericite-carbonate schist (altered tuff?; Upper Canada "L"stripping)	qtz-sericite-carbonate schist (altered tuff?; Upper Canada "L"stripping)	qtz-sericite-carbonate-altered tuff (Upper Canada "L"stripping)
			UTM_NAD83_E		586409.93	586407.45	586404.94	586400.39
			UTM_NAD83_N		5332380.21	5332380.21	5332379.84	5332380.15
laboratory	method	det limit	units					
Geolabs	XRF	0.01	%	SiO2	45.20	48.30	49.08	60.60
Geolabs	XRF	0.01	%	TiO2	0.46	0.55	0.66	0.56
Geolabs	XRF	0.01	%	Al2O3	11.43	13.76	15.26	15.53
Geolabs	XRF	0.01	%	Fe2O3	5.28	6.14	6.73	6.31
Geolabs	XRF	0.01	%	MnO	0.29	0.25	0.22	0.09
Geolabs	XRF	0.01	%	MgO	5.40	4.14	3.46	1.67
Geolabs	XRF	0.01	%	CaO	9.83	7.12	6.55	1.75
Geolabs	XRF	0.01	%	Na2O	0.71	0.47	1.08	1.94
Geolabs	XRF	0.01	%	K2O	5.72	7.71	6.00	5.12
Geolabs	XRF	0.01	%	P2O5	0.25	0.28	0.34	0.27
Geolabs	XRF	0.05	%	LOI	12.97	8.11	9.38	5.20
			%	Total	97.54	96.83	98.76	99.04
Geolabs	ICP-MS	0.07	ppm	Ce	61.98	85.58	92.84	87.21
Geolabs	ICP-MS	0.007	ppm	Cs	4.021	4.887	7.24	6.188
Geolabs	ICP-MS	0.008	ppm	Dy	3.034	3.586	4.08	3.511
Geolabs	ICP-MS	0.008	ppm	Er	1.61	1.864	2.146	1.867
Geolabs	ICP-MS	0.005	ppm	Eu	1.422	1.865	2.14	1.845
Geolabs	ICP-MS	0.009	ppm	Gd	4.369	5.548	6.225	5.334
Geolabs	ICP-MS	0.1	ppm	Hf	2.8	3.3	3.8	3.9
Geolabs	ICP-MS	0.003	ppm	Ho	0.569	0.669	0.771	0.671
Geolabs	ICP-MS	0.02	ppm	La	30.27	42.63	45.61	44.35
Geolabs	ICP-MS	0.003	ppm	Lu	0.228	0.264	0.303	0.274
Geolabs	ICP-MS	0.2	ppm	Nb	3.9	4.6	5.3	5.3
Geolabs	ICP-MS	0.03	ppm	Nd	28.86	39.76	43.68	39.5
Geolabs	ICP-MS	0.006	ppm	Pr	7.347	10.274	11.17	10.187
Geolabs	ICP-MS	0.05	ppm	Rb	156.53	191.497	213.209	182.087
Geolabs	ICP-MS	0.01	ppm	Sm	5.35	7.23	8.05	7.08
Geolabs	ICP-MS	0.5	ppm	Sr	1251.832	944.7	1128.1	467.6
Geolabs	ICP-MS	0.17	ppm	Ta	0.24	0.27	0.32	0.34
Geolabs	ICP-MS	0.003	ppm	Tb	0.557	0.679	0.781	0.667
Geolabs	ICP-MS	0.06	ppm	Th	5.81	7.2	8.4	8.86
Geolabs	ICP-MS	0.003	ppm	Tm	0.228	0.269	0.311	0.271
Geolabs	ICP-MS	0.007	ppm	U	1.723	1.939	2.26	2.69
Geolabs	ICP-MS	0.02	ppm	Y	15.82	18.1	20.84	17.57
Geolabs	ICP-MS	0.01	ppm	Yb	1.52	1.77	2.04	1.79
Geolabs	ICP-MS	0.1	ppm	Ba	1588.478	1159.175	1807.284	912.391
Geolabs	ICP-AES	0.1	ppm	Be	0.9	1.13	1.58	1.66
Geolabs	ICP-AES	1	ppm	Co	18	21	21	18
Geolabs	ICP-AES	3	ppm	Cu	99	90	81	56
Geolabs	ICP-AES	8	ppm	Mo	-8	-8	-8	-8
Geolabs	ICP-AES	3	ppm	Ni	19	20	21	20
Geolabs	ICP-AES	0.3	ppm	Sc	11.3	12.4	15.4	11.3
Geolabs	ICP-AES	0.6	ppm	V	138.8	175.8	171.2	135.1
Geolabs	ICP-AES	2	ppm	W	23	23	31	349
Geolabs	ICP-AES	2	ppm	Zn	70	64	79	46
Geolabs	XRF	4	ppm	Cr_XRF	88	85	112	105
Geolabs	XRF	4	ppm	V_XRF				
Geolabs	XRF	3	ppm	Zr_XRF	150	155	179	163
Geolabs	XRF	2	ppm	Ni_XRF				
Geolabs	IRC	0.03	%	CO2	13	9.45	8.51	2.1
Geolabs	IRC	0.01	%	S	1.41	2.55	1.39	3.09

Table A.1. (cont'd)

			sample id		3-3	7-1	7-2	7-3
			sample type		surface	surface	surface	surface
			drill hole/station					
			depth, ft					
			Township		Gauthier	Gauthier	Gauthier	Gauthier
			unit_code		5	5	5	5
			rock type		qtz-sericite-carbonate-altered tuff (Upper Canada "L" stripping)	qtz-sericite-carbonate schist (altered tuff?; Upper Canada "L" stripping)	qtz-sericite-carbonate-altered tuff (Upper Canada "L" stripping)	qtz-sericite-carbonate-altered tuff (Upper Canada "L" stripping)
			UTM_NAD83_E		586435.34	586419.24	586418.86	586418.14
			UTM_NAD83_N		5332391.13	5332384.05	5332384.99	5332387.15
laboratory	method	det limit	units					
Geolabs	XRF	0.01	%	SiO2	64.88	55.36	56.07	54.13
Geolabs	XRF	0.01	%	TiO2	0.31	0.65	0.53	0.69
Geolabs	XRF	0.01	%	Al2O3	13.72	15.56	12.33	15.51
Geolabs	XRF	0.01	%	Fe2O3	3.54	7.23	7.37	7.70
Geolabs	XRF	0.01	%	MnO	0.12	0.08	0.16	0.17
Geolabs	XRF	0.01	%	MgO	0.99	1.60	3.32	2.07
Geolabs	XRF	0.01	%	CaO	1.91	2.11	4.56	3.18
Geolabs	XRF	0.01	%	Na2O	1.26	0.06	0.06	0.82
Geolabs	XRF	0.01	%	K2O	10.09	9.48	6.12	8.04
Geolabs	XRF	0.01	%	P2O5	0.24	0.31	0.25	0.36
Geolabs	XRF	0.05	%	LOI	2.37	6.03	6.21	6.05
			%	Total	99.40	98.47	96.98	98.74
Geolabs	ICP-MS	0.07	ppm	Ce	54.4	100.5	82.48	96
Geolabs	ICP-MS	0.007	ppm	Cs	4.022	5.509	4.697	5.69
Geolabs	ICP-MS	0.008	ppm	Dy	2.272	4.111	3.66	4.135
Geolabs	ICP-MS	0.008	ppm	Er	1.111	2.277	1.933	2.177
Geolabs	ICP-MS	0.005	ppm	Eu	1.254	2.108	1.876	2.076
Geolabs	ICP-MS	0.009	ppm	Gd	3.615	6.433	5.311	6.307
Geolabs	ICP-MS	0.1	ppm	Hf	2.6	4.7	3.2	4
Geolabs	ICP-MS	0.003	ppm	Ho	0.411	0.788	0.694	0.777
Geolabs	ICP-MS	0.02	ppm	La	27.26	49.45	41.08	46.67
Geolabs	ICP-MS	0.003	ppm	Lu	0.158	0.337	0.274	0.31
Geolabs	ICP-MS	0.2	ppm	Nb	3.2	6.5	4.4	5.4
Geolabs	ICP-MS	0.03	ppm	Nd	25.29	46.55	38.26	45.36
Geolabs	ICP-MS	0.006	ppm	Pr	6.359	12.049	9.733	11.638
Geolabs	ICP-MS	0.05	ppm	Rb	186.79	229.251	183.834	210.487
Geolabs	ICP-MS	0.01	ppm	Sm	4.52	8.23	6.94	8.21
Geolabs	ICP-MS	0.5	ppm	Sr	579.6	356.5	661.3	581.8
Geolabs	ICP-MS	0.17	ppm	Ta	0.22	0.4	0.28	0.33
Geolabs	ICP-MS	0.003	ppm	Tb	0.452	0.79	0.698	0.801
Geolabs	ICP-MS	0.06	ppm	Th	5.55	11.12	7.25	8.63
Geolabs	ICP-MS	0.003	ppm	Tm	0.16	0.333	0.281	0.318
Geolabs	ICP-MS	0.007	ppm	U	1.692	3.381	2.615	2.516
Geolabs	ICP-MS	0.02	ppm	Y	11.31	22.75	20.43	21.4
Geolabs	ICP-MS	0.01	ppm	Yb	1.08	2.21	1.8	2.07
Geolabs	ICP-MS	0.1	ppm	Ba	3079.472	1354.369	491.094	409.011
Geolabs	ICP-AES	0.1	ppm	Be	0.28	1.73	1.79	1.53
Geolabs	ICP-AES	1	ppm	Co	12	23	19	25
Geolabs	ICP-AES	3	ppm	Cu	84	56	39	81
Geolabs	ICP-AES	8	ppm	Mo	9	-8	24	-8
Geolabs	ICP-AES	3	ppm	Ni	14	22	22	22
Geolabs	ICP-AES	0.3	ppm	Sc	8.1	14.1	12.3	15
Geolabs	ICP-AES	0.6	ppm	V	43.8	188	251.3	175
Geolabs	ICP-AES	2	ppm	W	9	18	15	21
Geolabs	ICP-AES	2	ppm	Zn	30	46	55	57
Geolabs	XRF	4	ppm	Cr_XRF	45	104	107	109
Geolabs	XRF	4	ppm	V_XRF				
Geolabs	XRF	3	ppm	Zr_XRF	111	188	143	165
Geolabs	XRF	2	ppm	Ni_XRF				
Geolabs	IRC	0.03	%	CO2	2.47	2.65	6.03	4
Geolabs	IRC	0.01	%	S	1.78	4.77	4.45	4.16

Table A.1. (cont'd)

			sample id		8-1	9-1	AN03-38-903.5	AN03-49-1276.6
			sample type		surface	surface	drill core	drill core
			drill hole/station				AN03-38	AN03-49
			depth, ft				903.5	1276.6
			Township		Gauthier	Gauthier	Gauthier	Gauthier
			unit_code		5	5	5	5
			rock type		qtz-sericite-(carbonate)-altered tuff (Upper Canada "L" stripping)	qtz-sericite-altered tuff (Upper Canada "L" stripping)	tuff	lava or tuff
			UTM_NAD83_E		586412.12	586412.09	586973.63	586344
			UTM_NAD83_N		5332388.29	5332382.72	5331250.48	5331277
laboratory	method	det limit	units					
Geolabs	XRF	0.01	%	SiO2	61.60	63.93	49.54	49.79
Geolabs	XRF	0.01	%	TiO2	0.60	0.54	0.54	1.01
Geolabs	XRF	0.01	%	Al2O3	16.86	16.56	12.55	13.93
Geolabs	XRF	0.01	%	Fe2O3	5.97	5.03	7.52	10.01
Geolabs	XRF	0.01	%	MnO	0.05	0.01	0.17	0.16
Geolabs	XRF	0.01	%	MgO	1.52	1.18	4.72	5.65
Geolabs	XRF	0.01	%	CaO	0.82	0.42	7.46	7.58
Geolabs	XRF	0.01	%	Na2O	0.06	0.20	4.00	2.56
Geolabs	XRF	0.01	%	K2O	6.47	7.14	1.88	5.92
Geolabs	XRF	0.01	%	P2O5	0.31	0.26	0.27	0.81
Geolabs	XRF	0.05	%	LOI	5.20	4.72	10.23	1.78
			%	Total	99.48	99.99	98.88	99.20
Geolabs	ICP-MS	0.07	ppm	Ce	102.35	90.26	70.65	295.635
Geolabs	ICP-MS	0.007	ppm	Cs	6.895	5.924	1.942	8.581
Geolabs	ICP-MS	0.008	ppm	Dy	4.203	3.383	4.091	8.434
Geolabs	ICP-MS	0.008	ppm	Er	2.317	1.739	2.251	3.568
Geolabs	ICP-MS	0.005	ppm	Eu	2.078	1.782	1.719	5.94
Geolabs	ICP-MS	0.009	ppm	Gd	6.233	5.383	5.666	16.751
Geolabs	ICP-MS	0.1	ppm	Hf	4.3	4.3	3.3	7.9
Geolabs	ICP-MS	0.003	ppm	Ho	0.806	0.611	0.806	1.431
Geolabs	ICP-MS	0.02	ppm	La	51.28	45.77	35.02	142.963
Geolabs	ICP-MS	0.003	ppm	Lu	0.342	0.265	0.339	0.429
Geolabs	ICP-MS	0.2	ppm	Nb	5.9	5.6	4.3	8.6
Geolabs	ICP-MS	0.03	ppm	Nd	46.9	40.6	34.21	142.539
Geolabs	ICP-MS	0.006	ppm	Pr	11.948	10.648	8.468	36.188
Geolabs	ICP-MS	0.05	ppm	Rb	218.331	219.514	57.52	150.542
Geolabs	ICP-MS	0.01	ppm	Sm	8.26	7.41	6.66	24.39
Geolabs	ICP-MS	0.5	ppm	Sr	145.3	161.5	823.9	2805.418
Geolabs	ICP-MS	0.17	ppm	Ta	0.37	0.36	0.36	0.39
Geolabs	ICP-MS	0.003	ppm	Tb	0.805	0.652	0.757	1.903
Geolabs	ICP-MS	0.06	ppm	Th	9.66	9.24	6.42	22.06
Geolabs	ICP-MS	0.003	ppm	Tm	0.342	0.254	0.33	0.477
Geolabs	ICP-MS	0.007	ppm	U	3.378	3.978	1.74	5.1
Geolabs	ICP-MS	0.02	ppm	Y	23.14	16.3	22.15	39.29
Geolabs	ICP-MS	0.01	ppm	Yb	2.29	1.73	2.22	3.07
Geolabs	ICP-MS	0.1	ppm	Ba	1052.175	655.31	2360.183	2677.556
Geolabs	ICP-AES	0.1	ppm	Be	2.9	2.35	0.98	2.05
Geolabs	ICP-AES	1	ppm	Co	20	17	24	32
Geolabs	ICP-AES	3	ppm	Cu	74	41	59	182
Geolabs	ICP-AES	8	ppm	Mo	34	-8	-8	-8
Geolabs	ICP-AES	3	ppm	Ni	22	19	35	40
Geolabs	ICP-AES	0.3	ppm	Sc	13.3	10.9	16.5	19.7
Geolabs	ICP-AES	0.6	ppm	V	154.8	160.9	120.9	235.9
Geolabs	ICP-AES	2	ppm	W	8	11	-2	-2
Geolabs	ICP-AES	2	ppm	Zn	1102	66	86	136
Geolabs	XRF	4	ppm	Cr_XRF	113	99	126	99
Geolabs	XRF	4	ppm	V_XRF				
Geolabs	XRF	3	ppm	Zr_XRF	163	161	145	432
Geolabs	XRF	2	ppm	Ni_XRF				
Geolabs	IRC	0.03	%	CO2	0.65	0.13		
Geolabs	IRC	0.01	%	S	3.56	3.26		

Table A.1. (cont'd)

			sample id		AN03-57-891.1	AN97-09-2449.5	L4-2	003VOI0543-1
			sample type		drill core	drill core	surface	surface
			drill hole/station		AN03-57	AN97-09		003VOI0543
			depth, ft		891.1	2449.5		
			Township		Gauthier	Gauthier	Gauthier	Gauthier
			unit_code		5	5	5	8
			rock type		lava	breccia	qtz-sericite-carbonate-altered tuff	sandstone-siltstone
			UTM_NAD83_E		586759.81	586049.16	586383.48	589358
			UTM_NAD83_N		5331383.85	5331112.58	5332344.94	5331803
laboratory	method	det limit	units					
Geolabs	XRF	0.01	%	SiO2	52.06	44.96	61.51	61.87
Geolabs	XRF	0.01	%	TiO2	0.74	1.07	0.36	0.57
Geolabs	XRF	0.01	%	Al2O3	14.87	15.41	15.13	16.30
Geolabs	XRF	0.01	%	Fe2O3	7.87	11.89	4.32	4.93
Geolabs	XRF	0.01	%	MnO	0.16	0.19	0.09	0.06
Geolabs	XRF	0.01	%	MgO	3.31	6.90	2.29	2.39
Geolabs	XRF	0.01	%	CaO	6.18	9.25	2.65	2.18
Geolabs	XRF	0.01	%	Na2O	5.76	3.52	1.71	3.86
Geolabs	XRF	0.01	%	K2O	3.32	2.13	5.59	2.60
Geolabs	XRF	0.01	%	P2O5	0.44	0.53	0.16	0.19
Geolabs	XRF	0.05	%	LOI	5.36	5.10	4.94	4.62
			%	Total	100.07	100.94	98.75	99.58
Geolabs	ICP-MS	0.07	ppm	Ce	134.45	163.67	77.23	66.67
Geolabs	ICP-MS	0.007	ppm	Cs	10.274	4.275	4.454	5.376
Geolabs	ICP-MS	0.008	ppm	Dy	5.853	5.307	2.285	2.636
Geolabs	ICP-MS	0.008	ppm	Er	2.686	2.382	1.125	1.357
Geolabs	ICP-MS	0.005	ppm	Eu	3.31	3.302	1.417	1.332
Geolabs	ICP-MS	0.009	ppm	Gd	9.754	9.556	3.859	3.972
Geolabs	ICP-MS	0.1	ppm	Hf	4.1	4.9	4.2	4.6
Geolabs	ICP-MS	0.003	ppm	Ho	1.025	0.924	0.421	0.491
Geolabs	ICP-MS	0.02	ppm	La	61.85	80.92	38.59	31.62
Geolabs	ICP-MS	0.003	ppm	Lu	0.333	0.299	0.162	0.192
Geolabs	ICP-MS	0.2	ppm	Nb	5.2	7.3	5.7	5.6
Geolabs	ICP-MS	0.03	ppm	Nd	68.15	76.12	32.6	30.48
Geolabs	ICP-MS	0.006	ppm	Pr	16.997	19.601	8.871	8.012
Geolabs	ICP-MS	0.05	ppm	Rb	152.097	82.74	167.048	86.21
Geolabs	ICP-MS	0.01	ppm	Sm	12.67	13.22	5.53	5.22
Geolabs	ICP-MS	0.5	ppm	Sr	1326.732	1492.307	478.2	418.4
Geolabs	ICP-MS	0.17	ppm	Ta	0.28	0.41	0.32	0.4
Geolabs	ICP-MS	0.003	ppm	Tb	1.183	1.13	0.473	0.496
Geolabs	ICP-MS	0.06	ppm	Th	9.76	12.68	9.29	6.99
Geolabs	ICP-MS	0.003	ppm	Tm	0.375	0.324	0.163	0.193
Geolabs	ICP-MS	0.007	ppm	U	2.189	5.937	3.509	2.113
Geolabs	ICP-MS	0.02	ppm	Y	28.32	25.37	11.65	12.98
Geolabs	ICP-MS	0.01	ppm	Yb	2.39	2.07	1.08	1.26
Geolabs	ICP-MS	0.1	ppm	Ba	1429.382	1424.862	1152.416	775.785
Geolabs	ICP-AES	0.1	ppm	Be	1.25	1.41	1.72	0.97
Geolabs	ICP-AES	1	ppm	Co	29	24	13	20
Geolabs	ICP-AES	3	ppm	Cu	231	353	20	48
Geolabs	ICP-AES	8	ppm	Mo	-8	-8	-8	-8
Geolabs	ICP-AES	3	ppm	Ni	36	30	27	70
Geolabs	ICP-AES	0.3	ppm	Sc	20.7	13	5.5	10.9
Geolabs	ICP-AES	0.6	ppm	V	217.5	148.7	58.1	93.8
Geolabs	ICP-AES	2	ppm	W	-2	-2	-2	-2
Geolabs	ICP-AES	2	ppm	Zn	120	129	31	66
Geolabs	XRF	4	ppm	Cr_XRF	109	62	117	283
Geolabs	XRF	4	ppm	V_XRF				
Geolabs	XRF	3	ppm	Zr_XRF	201	309	164	164
Geolabs	XRF	2	ppm	Ni_XRF				
Geolabs	IRC	0.03	%	CO2			3.53	
Geolabs	IRC	0.01	%	S			2.84	

Table A.1. (cont'd)

			sample id		003VOI0570-1	AN03-38-1214.5	AN03-38-527.5	MB96-8A-132
			sample type		surface	drill core	drill core	drill core
			drill hole/station		003VOI0570	AN03-38	AN03-38	MB96-8A
			depth, ft			1214.5	527.5	132
			Township		Gauthier	Gauthier	Gauthier	Gauthier
			unit_code		8	8	8	10
			rock type		sandstone-siltstone	sandstone	sandstone	gabbro
			UTM_NAD83_E		589218	586973.63	586973.63	587844
			UTM_NAD83_N		5331819	5331250.48	5331250.48	5330759
laboratory	method	det limit	units					
Geolabs	XRF	0.01	%	SiO2	63.68	61.25	60.04	41.48
Geolabs	XRF	0.01	%	TiO2	0.53	0.65	0.65	1.47
Geolabs	XRF	0.01	%	Al2O3	15.27	13.09	12.91	9.13
Geolabs	XRF	0.01	%	Fe2O3	5.30	6.45	6.68	16.33
Geolabs	XRF	0.01	%	MnO	0.07	0.11	0.12	0.20
Geolabs	XRF	0.01	%	MgO	3.10	3.58	4.11	11.89
Geolabs	XRF	0.01	%	CaO	2.26	3.77	3.78	12.42
Geolabs	XRF	0.01	%	Na2O	4.03	4.69	4.58	2.05
Geolabs	XRF	0.01	%	K2O	2.31	1.20	0.88	1.10
Geolabs	XRF	0.01	%	P2O5	0.17	0.14	0.16	0.08
Geolabs	XRF	0.05	%	LOI	3.35	5.67	6.64	2.47
			%	Total	100.08	100.61	100.54	98.62
Geolabs	ICP-MS	0.07	ppm	Ce	61.84	51.02	46.04	108.42
Geolabs	ICP-MS	0.007	ppm	Cs	5.534	0.606	0.835	3.346
Geolabs	ICP-MS	0.008	ppm	Dy	2.307	3.038	3.001	5.161
Geolabs	ICP-MS	0.008	ppm	Er	1.226	1.698	1.716	2.528
Geolabs	ICP-MS	0.005	ppm	Eu	1.168	1.258	1.163	3.135
Geolabs	ICP-MS	0.009	ppm	Gd	3.498	3.833	3.693	8.713
Geolabs	ICP-MS	0.1	ppm	Hf	3.7	2.9	2.8	1.5
Geolabs	ICP-MS	0.003	ppm	Ho	0.447	0.61	0.601	0.949
Geolabs	ICP-MS	0.02	ppm	La	30.83	24.24	21.54	45.66
Geolabs	ICP-MS	0.003	ppm	Lu	0.18	0.252	0.238	0.314
Geolabs	ICP-MS	0.2	ppm	Nb	5.2	4	4	3.4
Geolabs	ICP-MS	0.03	ppm	Nd	27.46	24.85	22.14	65.23
Geolabs	ICP-MS	0.006	ppm	Pr	7.275	6.148	5.563	15.002
Geolabs	ICP-MS	0.05	ppm	Rb	74.68	25.05	24.43	55.94
Geolabs	ICP-MS	0.01	ppm	Sm	4.64	4.56	4.24	12.01
Geolabs	ICP-MS	0.5	ppm	Sr	474.7	436.9	304.9	1789.71
Geolabs	ICP-MS	0.17	ppm	Ta	0.38	0.3	0.75	-0.17
Geolabs	ICP-MS	0.003	ppm	Tb	0.449	0.532	0.53	1.034
Geolabs	ICP-MS	0.06	ppm	Th	6.41	3.83	3.63	0.82
Geolabs	ICP-MS	0.003	ppm	Tm	0.179	0.25	0.245	0.351
Geolabs	ICP-MS	0.007	ppm	U	2.172	1.177	1.07	0.251
Geolabs	ICP-MS	0.02	ppm	Y	12.11	16.05	16.25	25.62
Geolabs	ICP-MS	0.01	ppm	Yb	1.17	1.61	1.62	2.16
Geolabs	ICP-MS	0.1	ppm	Ba	823.626	438.354	295.222	602.347
Geolabs	ICP-AES	0.1	ppm	Be	0.95	0.6	0.55	0.69
Geolabs	ICP-AES	1	ppm	Co	23	27	28	36
Geolabs	ICP-AES	3	ppm	Cu	43	58	49	232
Geolabs	ICP-AES	8	ppm	Mo	-8	-8	-8	-8
Geolabs	ICP-AES	3	ppm	Ni	69	110	104	51
Geolabs	ICP-AES	0.3	ppm	Sc	10.6	15.5	13.6	23
Geolabs	ICP-AES	0.6	ppm	V	87.7	127.2	112.7	254.3
Geolabs	ICP-AES	2	ppm	W	4	-2	-2	-2
Geolabs	ICP-AES	2	ppm	Zn	86	87	73	157
Geolabs	XRF	4	ppm	Cr_XRF	254	342	295	164
Geolabs	XRF	4	ppm	V_XRF				
Geolabs	XRF	3	ppm	Zr_XRF	158	120	115	113
Geolabs	XRF	2	ppm	Ni_XRF				
Geolabs	IRC	0.03	%	CO2				
Geolabs	IRC	0.01	%	S				

Table A.1. (cont'd)

			sample id		MB96-8B-126.5	MB97-19-1207.4	003VOI0106-1	003VOI0115-2
			sample type		drill core	drill core	surface	surface
			drill hole/station		MB96-8B	MB97-19	003VOI0106	003VOI0115
			depth, ft		126.5	1207.4		
			Township		Gauthier	Gauthier	Gauthier	Gauthier
			unit_code		10	10	12	12
			rock type		gabbro	altered gabbro (?)	feldspar porphyry	feldspar porphyry
			UTM_NAD83_E		587819	588119	589850	589682
			UTM_NAD83_N		5330769	5330595	5329763	5329910
laboratory	method	det.limit	units					
Geolabs	XRF	0.01	%	SiO2	48.77	53.38	68.51	59.47
Geolabs	XRF	0.01	%	TiO2	0.97	0.68	0.14	0.31
Geolabs	XRF	0.01	%	Al2O3	14.18	13.53	15.80	16.27
Geolabs	XRF	0.01	%	Fe2O3	10.04	8.18	1.45	2.92
Geolabs	XRF	0.01	%	MnO	0.16	0.14	0.02	0.04
Geolabs	XRF	0.01	%	MgO	5.26	6.92	0.37	1.68
Geolabs	XRF	0.01	%	CaO	8.80	6.70	0.96	3.38
Geolabs	XRF	0.01	%	Na2O	5.82	5.23	9.43	9.90
Geolabs	XRF	0.01	%	K2O	3.13	2.36	0.83	0.31
Geolabs	XRF	0.01	%	P2O5	0.49	0.20	0.08	0.14
Geolabs	XRF	0.05	%	LOI	1.37	2.49	1.27	3.58
			%	Total	98.99	99.81	98.85	98.00
Geolabs	ICP-MS	0.07	ppm	Ce	49.02	70.92	13.31	46.16
Geolabs	ICP-MS	0.007	ppm	Cs	1.111	1.674	0.126	0.125
Geolabs	ICP-MS	0.008	ppm	Dy	4.42	3.196	0.462	1.082
Geolabs	ICP-MS	0.008	ppm	Er	2.221	1.721	0.175	0.458
Geolabs	ICP-MS	0.005	ppm	Eu	2.227	1.634	0.453	0.979
Geolabs	ICP-MS	0.009	ppm	Gd	6.975	4.733	1.13	2.377
Geolabs	ICP-MS	0.1	ppm	Hf	2.6	3	2.5	3.1
Geolabs	ICP-MS	0.003	ppm	Ho	0.819	0.607	0.069	0.184
Geolabs	ICP-MS	0.02	ppm	La	16.03	32.7	5.08	21.75
Geolabs	ICP-MS	0.003	ppm	Lu	0.267	0.247	0.019	0.058
Geolabs	ICP-MS	0.2	ppm	Nb	2.9	2.9	1.8	1.8
Geolabs	ICP-MS	0.03	ppm	Nd	39.02	37	8.61	22.9
Geolabs	ICP-MS	0.006	ppm	Pr	7.965	8.979	1.945	5.753
Geolabs	ICP-MS	0.05	ppm	Rb	17.4	46.26	10.42	4.22
Geolabs	ICP-MS	0.01	ppm	Sm	8.62	6.51	1.67	3.99
Geolabs	ICP-MS	0.5	ppm	Sr	445.2	657.5	417.7	473.5
Geolabs	ICP-MS	0.17	ppm	Ta	0.17	0.22	-0.17	0.17
Geolabs	ICP-MS	0.003	ppm	Tb	0.867	0.604	0.111	0.243
Geolabs	ICP-MS	0.06	ppm	Th	1.03	4.46	0.95	2.96
Geolabs	ICP-MS	0.003	ppm	Tm	0.301	0.256	0.022	0.062
Geolabs	ICP-MS	0.007	ppm	U	0.381	1.321	1.03	1.161
Geolabs	ICP-MS	0.02	ppm	Y	21.45	16.7	2.11	5.03
Geolabs	ICP-MS	0.01	ppm	Yb	1.88	1.63	0.14	0.41
Geolabs	ICP-MS	0.1	ppm	Ba	356.909	729.494	1301.705	188.309
Geolabs	ICP-AES	0.1	ppm	Be	0.53	0.79	1.54	0.57
Geolabs	ICP-AES	1	ppm	Co	52	32	4	10
Geolabs	ICP-AES	3	ppm	Cu	38	206	8	16
Geolabs	ICP-AES	8	ppm	Mo	-8	-8	-8	-8
Geolabs	ICP-AES	3	ppm	Ni	76	79	6	36
Geolabs	ICP-AES	0.3	ppm	Sc	47.4	16.4	0.9	3.1
Geolabs	ICP-AES	0.6	ppm	V	493	165.9	8.2	25.6
Geolabs	ICP-AES	2	ppm	W	-2	-2	3	5
Geolabs	ICP-AES	2	ppm	Zn	136	103	9	34
Geolabs	XRF	4	ppm	Cr_XRF	233	395	-4	74
Geolabs	XRF	4	ppm	V_XRF	493			
Geolabs	XRF	3	ppm	Zr_XRF	84	124	86	115
Geolabs	XRF	2	ppm	Ni_XRF				
Geolabs	IRC	0.03	%	CO2				
Geolabs	IRC	0.01	%	S				

Table A.1. (cont'd)

			sample id		003VOI0016-1	003VOI0066-2	003VOI0163-2	003VOI0305-1
			sample type		surface	surface	surface	surface
			drill hole/station		003VOI0016	003VOI0066	003VOI0163	003VOI0305
			depth, ft					
			Township		Gauthier	Gauthier	Gauthier	Gauthier
			unit_code		13	13	13	13
			rock type		diorite	syenite porphyry	feldspar-amphibole-phyric trachyandesite (intrusion)	red feldspar-phyric trachyte (intrusion)
			UTM_NAD83_E		586498	589382	585972	587531
			UTM_NAD83_N		5331159	5330332	5332966	5333123
laboratory	method	det.limit	units					
Geolabs	XRF	0.01	%	SiO2	52.21	54.62	52.47	59.34
Geolabs	XRF	0.01	%	TiO2	0.71	0.90	0.71	0.39
Geolabs	XRF	0.01	%	Al2O3	14.44	13.39	14.56	17.15
Geolabs	XRF	0.01	%	Fe2O3	11.47	8.41	11.46	4.32
Geolabs	XRF	0.01	%	MnO	0.18	0.13	0.18	0.08
Geolabs	XRF	0.01	%	MgO	7.32	2.14	7.35	1.07
Geolabs	XRF	0.01	%	CaO	7.93	4.21	7.88	2.38
Geolabs	XRF	0.01	%	Na2O	3.40	2.71	3.41	7.14
Geolabs	XRF	0.01	%	K2O	1.21	7.20	1.19	4.84
Geolabs	XRF	0.01	%	P2O5	0.06	0.71	0.06	0.17
Geolabs	XRF	0.05	%	LOI	2.30	4.56	2.33	2.29
			%	Total	101.23	98.98	101.60	99.17
Geolabs	ICP-MS	0.07	ppm	Ce	11	264.246	90.79	84.24
Geolabs	ICP-MS	0.007	ppm	Cs	0.982	0.931	1.21	1.58
Geolabs	ICP-MS	0.008	ppm	Dy	2.572	17.013	4.338	2.499
Geolabs	ICP-MS	0.008	ppm	Er	1.636	7.2	2.278	1.482
Geolabs	ICP-MS	0.005	ppm	Eu	0.715	7.289	2.192	1.306
Geolabs	ICP-MS	0.009	ppm	Gd	2.381	23.412	6.678	3.592
Geolabs	ICP-MS	0.1	ppm	Hf	1.5	8.7	4.1	4.1
Geolabs	ICP-MS	0.003	ppm	Ho	0.561	2.954	0.836	0.488
Geolabs	ICP-MS	0.02	ppm	La	4.47	126.903	44.69	45.93
Geolabs	ICP-MS	0.003	ppm	Lu	0.234	0.735	0.314	0.251
Geolabs	ICP-MS	0.2	ppm	Nb	1.7	12.5	5.8	6.1
Geolabs	ICP-MS	0.03	ppm	Nd	7.25	132.599	44.93	32.22
Geolabs	ICP-MS	0.006	ppm	Pr	1.608	33.309	11.314	9.178
Geolabs	ICP-MS	0.05	ppm	Rb	31.67	88.93	93.19	103.69
Geolabs	ICP-MS	0.01	ppm	Sm	2	26.44	8.39	4.99
Geolabs	ICP-MS	0.5	ppm	Sr	294.4	2027.705	1001.2	441.9
Geolabs	ICP-MS	0.17	ppm	Ta	-0.17	0.69	0.36	0.36
Geolabs	ICP-MS	0.003	ppm	Tb	0.409	3.26	0.836	0.462
Geolabs	ICP-MS	0.06	ppm	Th	0.5	16.11	7.9	10.44
Geolabs	ICP-MS	0.003	ppm	Tm	0.237	0.906	0.32	0.228
Geolabs	ICP-MS	0.007	ppm	U	0.136	5.761	1.898	3.135
Geolabs	ICP-MS	0.02	ppm	Y	14.78	76.6	22.08	14
Geolabs	ICP-MS	0.01	ppm	Yb	1.61	5.43	2.07	1.6
Geolabs	ICP-MS	0.1	ppm	Ba	235.58	4739.466	1539.835	1173.425
Geolabs	ICP-AES	0.1	ppm	Be	0.21	1.88	1.14	0.72
Geolabs	ICP-AES	1	ppm	Co	44	7	18	11
Geolabs	ICP-AES	3	ppm	Cu	361	29	1687	539
Geolabs	ICP-AES	8	ppm	Mo	-8	-8	-8	-8
Geolabs	ICP-AES	3	ppm	Ni	73	27	49	14
Geolabs	ICP-AES	0.3	ppm	Sc	25.8	16	18.7	4.1
Geolabs	ICP-AES	0.6	ppm	V	188.2	178.9	168.9	61.9
Geolabs	ICP-AES	2	ppm	W	6	13	-2	11
Geolabs	ICP-AES	2	ppm	Zn	153	70	194	64
Geolabs	XRF	4	ppm	Cr_XRF	254	20	170	13
Geolabs	XRF	4	ppm	V_XRF				
Geolabs	XRF	3	ppm	Zr_XRF	64	394	203	190
Geolabs	XRF	2	ppm	Ni_XRF				
Geolabs	IRC	0.03	%	CO2				
Geolabs	IRC	0.01	%	S				

Table A.1. (cont'd)

			sample id		003VOI0526-1	AN03-39-75	AN03-43-157.4	AN03-53-227.5
			sample type		surface	drill core	drill core	drill core
			drill hole/station		003VOI0526	AN03-39	AN03-43	AN03-53
			depth, ft			75	157.4	227.5
			Township		Gauthier	Gauthier	Gauthier	Gauthier
			unit_code		13	13	13	13
			rock type		feldspar-phyric syenite porphyry (Upper Canada "LW" stripping)	lamprophyre (dike or sill)	syenite (dike or sill)	syenite
			UTM_NAD83_E		586276.1	586915.23	586591.4	586517
			UTM_NAD83_N		5332274.83	5331044.81	5331463.66	5331416
laboratory	method	det limit	units					
Geolabs	XRF	0.01	%	SiO2	60.91	43.02	46.39	52.22
Geolabs	XRF	0.01	%	TiO2	0.36	0.82	0.86	0.93
Geolabs	XRF	0.01	%	Al2O3	15.77	9.66	12.49	16.17
Geolabs	XRF	0.01	%	Fe2O3	4.09	9.73	9.79	8.38
Geolabs	XRF	0.01	%	MnO	0.10	0.16	0.18	0.12
Geolabs	XRF	0.01	%	MgO	1.82	13.05	5.70	4.37
Geolabs	XRF	0.01	%	CaO	3.02	7.92	8.31	4.31
Geolabs	XRF	0.01	%	Na2O	2.68	2.41	4.77	7.59
Geolabs	XRF	0.01	%	K2O	4.64	4.91	2.61	2.35
Geolabs	XRF	0.01	%	P2O5	0.15	0.58	0.65	0.34
Geolabs	XRF	0.05	%	LOI	5.03	4.12	7.64	2.94
			%	Total	98.58	96.38	99.38	99.71
Geolabs	ICP-MS	0.07	ppm	Ce	77.57	136.01	132.28	57.22
Geolabs	ICP-MS	0.007	ppm	Cs	6.632	9.322	7.928	9.646
Geolabs	ICP-MS	0.008	ppm	Dy	2.36	6.584	6.515	4.311
Geolabs	ICP-MS	0.008	ppm	Er	1.248	2.76	3.243	2.377
Geolabs	ICP-MS	0.005	ppm	Eu	1.445	3.603	3.346	1.834
Geolabs	ICP-MS	0.009	ppm	Gd	3.884	11.253	10.165	5.95
Geolabs	ICP-MS	0.1	ppm	Hf	4.3	5.1	4.6	3.5
Geolabs	ICP-MS	0.003	ppm	Ho	0.444	1.12	1.214	0.836
Geolabs	ICP-MS	0.02	ppm	La	40.81	59.9	61.66	26.96
Geolabs	ICP-MS	0.003	ppm	Lu	0.191	0.322	0.446	0.348
Geolabs	ICP-MS	0.2	ppm	Nb	5.9	6.4	8	4.8
Geolabs	ICP-MS	0.03	ppm	Nd	33.02	73.45	67.41	31
Geolabs	ICP-MS	0.006	ppm	Pr	8.82	17.762	16.493	7.218
Geolabs	ICP-MS	0.05	ppm	Rb	172.732	222.018	93.06	71.93
Geolabs	ICP-MS	0.01	ppm	Sm	5.58	13.9	13	6.48
Geolabs	ICP-MS	0.5	ppm	Sr	575.9	875.6	603.5	415.5
Geolabs	ICP-MS	0.17	ppm	Ta	0.34	0.3	0.42	0.31
Geolabs	ICP-MS	0.003	ppm	Tb	0.485	1.375	1.297	0.79
Geolabs	ICP-MS	0.06	ppm	Th	8.81	7.85	10.69	4.65
Geolabs	ICP-MS	0.003	ppm	Tm	0.187	0.365	0.467	0.348
Geolabs	ICP-MS	0.007	ppm	U	3.045	2.475	2.977	1.351
Geolabs	ICP-MS	0.02	ppm	Y	12.9	30.93	32.83	22.84
Geolabs	ICP-MS	0.01	ppm	Yb	1.25	2.26	3	2.28
Geolabs	ICP-MS	0.1	ppm	Ba	1934.305	924.933	2855.635	197.307
Geolabs	ICP-AES	0.1	ppm	Be	1.62	1.79	1.5	0.87
Geolabs	ICP-AES	1	ppm	Co	12	48	27	22
Geolabs	ICP-AES	3	ppm	Cu	13	93	62	107
Geolabs	ICP-AES	8	ppm	Mo	-8	-8	-8	-8
Geolabs	ICP-AES	3	ppm	Ni	18	211	43	26
Geolabs	ICP-AES	0.3	ppm	Sc	5.4	22.1	22.6	16
Geolabs	ICP-AES	0.6	ppm	V	69.3	155.1	204	186.4
Geolabs	ICP-AES	2	ppm	W	-2	-2	-2	-2
Geolabs	ICP-AES	2	ppm	Zn	34	119	108	116
Geolabs	XRF	4	ppm	Cr_XRF	66	1042	122	80
Geolabs	XRF	4	ppm	V_XRF				
Geolabs	XRF	3	ppm	Zr_XRF	165	222	189	138
Geolabs	XRF	2	ppm	Ni_XRF				
Geolabs	IRC	0.03	%	CO2	4.25			
Geolabs	IRC	0.01	%	S	1.02			

Table A.2. Analytical results for samples from second field season (2004), Gauthier and Teck townships: major and trace element geochemistry, analyses by Geolabs and Actlabs.

			sample id		AN03-61-86343	004VOI0695-1	004VOI0696-1	004VOI0710-1
			sample type		drill core	surface	surface	surface
			drill hole/stope		AN03-61	004VOI0695	004VOI0696	004VOI0710
			depth, ft		260			
			Township		Gauthier	Gauthier	Gauthier	Gauthier
			unit_code		2	5	5	5
			rock type		mafic metavolcanic, Anoki Main zone protolith	breccia	amphibole-feldspar phyric lava	amphibole-feldspar phyric lava
			UTM_NAD83_E		586700	590713	590780	590061
			UTM_NAD83_N		5331177	5332873	5332968	5333290
laboratory	method	det.limit	units					
Actlabs	XRF	0.01	%	SiO2	41.92	63.61	57.77	52.5
Actlabs	XRF	0.01	%	TiO2	2.06	0.32	0.52	0.83
Actlabs	XRF	0.01	%	Al2O3	9.81	14.57	14.99	15.83
Actlabs	XRF	0.01	%	Fe2O3	21.33	2.64	6.08	9.3
Actlabs	XRF	0.001	%	MnO	0.277	0.066	0.108	0.159
Actlabs	XRF	0.01	%	MgO	5.45	1.65	3.65	4.86
Actlabs	XRF	0.01	%	CaO	6.73	3.6	4.33	6.65
Actlabs	XRF	0.01	%	Na2O	2.98	4.65	5.38	4.05
Actlabs	XRF	0.01	%	K2O	0.27	3.79	2.25	2.91
Actlabs	XRF	0.01	%	P2O5	0.11	0.18	0.31	0.58
Actlabs	XRF	0.01	%	LOI	9.10	5.10	4.59	2.43
			%	Total	100.04	100.18	99.98	100.10
Geolabs	ICP-MS	0.07	ppm	Ce	24.85	71.21	77.79	124.57
Geolabs	ICP-MS	0.007	ppm	Cs	1.001	3.554	1.336	2.134
Geolabs	ICP-MS	0.008	ppm	Dy	4.513	2.863	2.957	4.592
Geolabs	ICP-MS	0.008	ppm	Er	2.385	1.486	1.57	2.297
Geolabs	ICP-MS	0.005	ppm	Eu	1.58	1.528	1.513	2.684
Geolabs	ICP-MS	0.009	ppm	Gd	5.297	4.414	4.484	7.59
Geolabs	ICP-MS	0.1	ppm	Hf	3	4.3	3.7	4.2
Geolabs	ICP-MS	0.003	ppm	Ho	0.867	0.519	0.561	0.85
Geolabs	ICP-MS	0.02	ppm	La	9.54	34.95	38.95	60.13
Geolabs	ICP-MS	0.003	ppm	Lu	0.289	0.198	0.227	0.312
Geolabs	ICP-MS	0.2	ppm	Nb	7	7.5	5	5.6
Geolabs	ICP-MS	0.03	ppm	Nd	18.47	32.68	35.1	60.1
Geolabs	ICP-MS	0.006	ppm	Pr	3.806	8.515	9.123	15.238
Geolabs	ICP-MS	0.05	ppm	Rb	6.97	97.37	33.42	63.83
Geolabs	ICP-MS	0.01	ppm	Sm	4.89	6	6.14	10.59
Geolabs	ICP-MS	0.5	ppm	Sr	320.5	579.8	601.3	1309.26
Geolabs	ICP-MS	0.17	ppm	Ta	0.43	0.39	0.3	0.28
Geolabs	ICP-MS	0.003	ppm	Tb	0.779	0.563	0.561	0.906
Geolabs	ICP-MS	0.06	ppm	Th	0.74	6.89	6.59	7.8
Geolabs	ICP-MS	0.003	ppm	Tm	0.322	0.203	0.222	0.328
Geolabs	ICP-MS	0.007	ppm	U	0.245	2.964	1.949	1.918
Geolabs	ICP-MS	0.02	ppm	Y	20.86	14.52	14.8	22.42
Geolabs	ICP-MS	0.01	ppm	Yb	2.04	1.35	1.49	2.13
Geolabs	ICP-MS	0.1	ppm	Ba	170.874	2211.88	1695.15	1421.605
Geolabs	ICP-AES	0.1	ppm	Be	0.65	1.42	1	1.29
Geolabs	ICP-AES	1	ppm	Co	68	7	19	26
Geolabs	ICP-AES	3	ppm	Cu	354	14	24	16
Geolabs	ICP-AES	8	ppm	Mo	-8	-8	-8	-8
Geolabs	ICP-AES	3	ppm	Ni	115	28	32	30
Geolabs	ICP-AES	0.3	ppm	Sc	14.5	4.9	12.3	19
Geolabs	ICP-AES	0.6	ppm	V	416	40.3	103.9	168
Geolabs	ICP-AES	2	ppm	W	10	9	4	5
Geolabs	ICP-AES	2	ppm	Zn	168	60	81	109
Actlabs	XRF	5	ppm	Cr_XRF	10	79	96	87
Actlabs	XRF	5	ppm	V_XRF	416	58	135	202
Actlabs	XRF	5	ppm	Zr_XRF	97	152	135	147
Actlabs	XRF	4	ppm	Ni_XRF	112	21	22	17
Actlabs	IRC	0.01	%	CO2	8.03			
Actlabs	IRC	0.01	%	S	0.38			
Geolabs	MS-IAT	6	ppb	Au				
Geolabs	MS-IAT	2	ppb	Pd				
Geolabs	MS-IAT	1	ppb	Pt				

Table A.2. (cont'd)

			sample id		004VOI1182-1	004VOI1935-1	004VOI1884-1	004VOI1277-1
			sample type		surface	surface	surface	surface
			drill hole/stope		004VOI1182	004VOI1935	004VOI1884	004VOI1277
			depth, ft					
			Township		Teck	Teck	Teck	Teck
			unit_code		2	2	13	13
			rock type		basalt	basalt	coarse biotite lamprophyre	feldspar-rich syenite porphyry
			UTM_NAD83_E		567014	567668	568366	570351
			UTM_NAD83_N		5332752	5333234	5330956	5333069
laboratory	method	det.limit	units					
Actlabs	XRF	0.01	%	SiO2	48.78	53.2	46.53	64.86
Actlabs	XRF	0.01	%	TiO2	0.72	0.61	0.78	0.36
Actlabs	XRF	0.01	%	Al2O3	16.25	15.13	10.57	14.92
Actlabs	XRF	0.01	%	Fe2O3	9.47	8.77	8.83	3.49
Actlabs	XRF	0.001	%	MnO	0.17	0.143	0.15	0.07
Actlabs	XRF	0.01	%	MgO	8.03	7.8	11.53	1.38
Actlabs	XRF	0.01	%	CaO	11.32	3.6	9.76	2.4
Actlabs	XRF	0.01	%	Na2O	2.13	3.89	1.81	5.25
Actlabs	XRF	0.01	%	K2O	0.67	0.39	4.14	3.11
Actlabs	XRF	0.01	%	P2O5	0.07	0.05	0.69	0.15
Actlabs	XRF	0.01	%	LOI	2.70	6.32	5.28	4.12
			%	Total	100.31	99.90	100.07	100.11
Geolabs	ICP-MS	0.07	ppm	Ce	7.79	3.98	192.14	61
Geolabs	ICP-MS	0.007	ppm	Cs	2.143	0.926	5.951	2.382
Geolabs	ICP-MS	0.008	ppm	Dy	2.59	1.83	7.451	2.541
Geolabs	ICP-MS	0.008	ppm	Er	1.699	1.223	2.836	1.256
Geolabs	ICP-MS	0.005	ppm	Eu	0.608	0.375	4.409	1.335
Geolabs	ICP-MS	0.009	ppm	Gd	2.236	1.437	13.654	3.906
Geolabs	ICP-MS	0.1	ppm	Hf	1.3	1	5.3	4
Geolabs	ICP-MS	0.003	ppm	Ho	0.56	0.407	1.217	0.46
Geolabs	ICP-MS	0.02	ppm	La	3.16	1.49	88.93	30.16
Geolabs	ICP-MS	0.003	ppm	Lu	0.262	0.185	0.284	0.181
Geolabs	ICP-MS	0.2	ppm	Nb	2.2	1.5	5.3	7.4
Geolabs	ICP-MS	0.03	ppm	Nd	5.61	3.24	98.66	28.15
Geolabs	ICP-MS	0.006	ppm	Pr	1.158	0.655	24.58	7.383
Geolabs	ICP-MS	0.05	ppm	Rb	20.01	9.55	137.31	96.04
Geolabs	ICP-MS	0.01	ppm	Sm	1.68	1.11	18.13	5.21
Geolabs	ICP-MS	0.5	ppm	Sr	351.5	113.5	943.4	780.3
Geolabs	ICP-MS	0.17	ppm	Ta	-0.17	-0.17	0.24	0.38
Geolabs	ICP-MS	0.003	ppm	Tb	0.39	0.27	1.633	0.495
Geolabs	ICP-MS	0.06	ppm	Th	0.29	0.21	11.31	6.21
Geolabs	ICP-MS	0.003	ppm	Tm	0.255	0.189	0.356	0.183
Geolabs	ICP-MS	0.007	ppm	U	0.08	0.16	3.063	2.844
Geolabs	ICP-MS	0.02	ppm	Y	14.85	9.51	33.04	12.76
Geolabs	ICP-MS	0.01	ppm	Yb	1.69	1.25	2.17	1.21
Geolabs	ICP-MS	0.1	ppm	Ba	161.579	65.761	1175.869	2190.024
Geolabs	ICP-AES	0.1	ppm	Be	0.17	0.23	1.81	1.77
Geolabs	ICP-AES	1	ppm	Co	37	44	44	6
Geolabs	ICP-AES	3	ppm	Cu	85	138	45	5
Geolabs	ICP-AES	8	ppm	Mo	-8	-8	-8	-8
Geolabs	ICP-AES	3	ppm	Ni	120	133	289	31
Geolabs	ICP-AES	0.3	ppm	Sc	34.1	40.1	22.7	5.3
Geolabs	ICP-AES	0.6	ppm	V	219.8	211.4	160.3	37.4
Geolabs	ICP-AES	2	ppm	W	2	4	-2	8
Geolabs	ICP-AES	2	ppm	Zn	63	84	105	35
Actlabs	XRF	5	ppm	Cr_XRF	288	485	655	51
Actlabs	XRF	5	ppm	V_XRF	232	250	192	51
Actlabs	XRF	5	ppm	Zr_XRF	43	36	210	142
Actlabs	XRF	4	ppm	Ni_XRF	99	118	260	20
Actlabs	IRC	0.01	%	CO2				
Actlabs	IRC	0.01	%	S				
Geolabs	MS-IAT	6	ppb	Au				
Geolabs	MS-IAT	2	ppb	Pd				
Geolabs	MS-IAT	1	ppb	Pt				

Table A.2. (cont'd)

			sample id		004VOI1311-1	004VOI1472-1	004VOI1947-1	004VOI1952-2
			sample type		surface	surface	surface	surface
			drill hole/stope		004VOI1311	004VOI1472	004VOI1947	004VOI1952
			depth, ft					
			Township		Teck	Teck	Teck	Teck
			unit_code		13	13	13	13
			rock type		feldspar-rich syenite porphyry	feldspar-rich syenite porphyry	feldspar-rich syenite porphyry	feldspar-rich syenite porphyry
			UTM_NAD83_E		570249	569897	571986	570359
			UTM_NAD83_N		5333525	5333278	5333897	5333025
laboratory	method	det.limit	units					
Actlabs	XRF	0.01	%	SiO2	65.64	63.38	64.41	64.93
Actlabs	XRF	0.01	%	TiO2	0.35	0.41	0.34	0.41
Actlabs	XRF	0.01	%	Al2O3	14.89	15.05	14.93	14.46
Actlabs	XRF	0.01	%	Fe2O3	3.17	3.93	3.55	3.82
Actlabs	XRF	0.001	%	MnO	0.05	0.068	0.074	0.059
Actlabs	XRF	0.01	%	MgO	1.46	1.8	1.4	1.83
Actlabs	XRF	0.01	%	CaO	2.04	2.78	2.45	2.87
Actlabs	XRF	0.01	%	Na2O	5.24	5.49	5.24	5.19
Actlabs	XRF	0.01	%	K2O	3.22	3.01	3.11	3.06
Actlabs	XRF	0.01	%	P2O5	0.15	0.2	0.16	0.18
Actlabs	XRF	0.01	%	LOI	3.52	4.05	4.03	3.11
			%	Total	99.73	100.17	99.69	99.92
Geolabs	ICP-MS	0.07	ppm	Ce	62.99	83.43	62.24	59.04
Geolabs	ICP-MS	0.007	ppm	Cs	2.248	2.086	2.371	1.478
Geolabs	ICP-MS	0.006	ppm	Dy	2.72	3.177	2.637	3.348
Geolabs	ICP-MS	0.008	ppm	Er	1.398	1.607	1.314	1.869
Geolabs	ICP-MS	0.005	ppm	Eu	1.422	1.739	1.334	1.347
Geolabs	ICP-MS	0.009	ppm	Gd	4.039	4.994	4.015	4.435
Geolabs	ICP-MS	0.1	ppm	Hf	4.1	4.7	4	4.1
Geolabs	ICP-MS	0.003	ppm	Ho	0.513	0.594	0.485	0.647
Geolabs	ICP-MS	0.02	ppm	La	31.6	42.07	30.49	28.69
Geolabs	ICP-MS	0.003	ppm	Lu	0.201	0.229	0.188	0.27
Geolabs	ICP-MS	0.2	ppm	Nb	7	9.2	7.2	6.9
Geolabs	ICP-MS	0.03	ppm	Nd	29.42	38.6	28.17	28.29
Geolabs	ICP-MS	0.006	ppm	Pr	7.634	10.017	7.35	7.122
Geolabs	ICP-MS	0.05	ppm	Rb	100.2	78.56	95.26	68.82
Geolabs	ICP-MS	0.01	ppm	Sm	5.47	6.87	5.27	5.43
Geolabs	ICP-MS	0.5	ppm	Sr	920.2	924.6	738.5	788.2
Geolabs	ICP-MS	0.17	ppm	Ta	0.39	0.43	0.37	0.39
Geolabs	ICP-MS	0.003	ppm	Tb	0.525	0.629	0.515	0.598
Geolabs	ICP-MS	0.06	ppm	Th	6.29	7.89	6.11	5.8
Geolabs	ICP-MS	0.003	ppm	Tm	0.204	0.235	0.189	0.27
Geolabs	ICP-MS	0.007	ppm	U	2.881	3.373	2.729	2.676
Geolabs	ICP-MS	0.02	ppm	Y	14.09	16.51	13.18	17.32
Geolabs	ICP-MS	0.01	ppm	Yb	1.36	1.5	1.26	1.83
Geolabs	ICP-MS	0.1	ppm	Ba	4904.607	3330.815	2289.726	2985.408
Geolabs	ICP-AES	0.1	ppm	Be	1.79	1.79	1.47	1.36
Geolabs	ICP-AES	1	ppm	Co	6	8	9	10
Geolabs	ICP-AES	3	ppm	Cu	-3	8	5	4
Geolabs	ICP-AES	8	ppm	Mo	-8	-8	-8	-8
Geolabs	ICP-AES	3	ppm	Ni	29	31	26	33
Geolabs	ICP-AES	0.3	ppm	Sc	5.1	6.4	5.3	6.6
Geolabs	ICP-AES	0.6	ppm	V	34.7	46.8	36.5	44
Geolabs	ICP-AES	2	ppm	W	10	11	4	7
Geolabs	ICP-AES	2	ppm	Zn	55	58	37	57
Actlabs	XRF	5	ppm	Cr_XRF	70	53	60	76
Actlabs	XRF	5	ppm	V_XRF	61	72	53	67
Actlabs	XRF	5	ppm	Zr_XRF	141	163	145	142
Actlabs	XRF	4	ppm	Ni_XRF	19	21	18	26
Actlabs	IRC	0.01	%	CO2				
Actlabs	IRC	0.01	%	S				
Geolabs	MS-IAT	6	ppb	Au				
Geolabs	MS-IAT	2	ppb	Pd				
Geolabs	MS-IAT	1	ppb	Pt				

Table A.2. (cont'd)

			sample id		4528D	4229-4	4229-5	4529
			sample type		underground	underground	underground	underground
			drill hole/stope		stope 4528	stope 4229 sublevel 4	stope 4229 sublevel 5	4529
			depth, ft					
			Township		Teck	Teck	Teck	Teck
			unit_code		13	13	13	13
			rock type		intramineral dike	intramineral dike	intramineral dike	intramineral dike
			UTM_NAD83_E UTM_NAD83_N					
laboratory	method	det.limit	units					
Actlabs	XRF	0.01	%	SiO2	49.07	40.81	43.15	43.52
Actlabs	XRF	0.01	%	TiO2	1.13	0.89	0.87	0.87
Actlabs	XRF	0.01	%	Al2O3	18.73	13.81	14.76	14.83
Actlabs	XRF	0.01	%	Fe2O3	12.23	9.48	10.25	10.78
Actlabs	XRF	0.001	%	MnO	0.046	0.173	0.207	0.173
Actlabs	XRF	0.01	%	MgO	6.35	4.68	4.06	4
Actlabs	XRF	0.01	%	CaO	1.22	8.63	7.26	6.65
Actlabs	XRF	0.01	%	Na2O	5.46	3.34	3.57	2.6
Actlabs	XRF	0.01	%	K2O	2.27	4.92	4.53	5.64
Actlabs	XRF	0.01	%	P2O5	0.5	0.39	0.39	0.37
Actlabs	XRF	0.01	%	LOI	3.16	12.98	11.32	10.64
			%	Total	100.16	100.11	100.36	100.07
Geolabs	ICP-MS	0.07	ppm	Ce	65.93	47.69	50.04	49.56
Geolabs	ICP-MS	0.007	ppm	Cs	3.069	3.598	6.502	6.967
Geolabs	ICP-MS	0.008	ppm	Dy	4.235	2.801	3.249	3.424
Geolabs	ICP-MS	0.008	ppm	Er	2.495	1.622	2.011	2.079
Geolabs	ICP-MS	0.005	ppm	Eu	1.691	1.268	1.281	1.301
Geolabs	ICP-MS	0.009	ppm	Gd	5.09	3.787	3.735	4.096
Geolabs	ICP-MS	0.1	ppm	Hf	3	2.2	2.2	2.3
Geolabs	ICP-MS	0.003	ppm	Ho	0.874	0.551	0.67	0.706
Geolabs	ICP-MS	0.02	ppm	La	31.15	21.88	22.64	22.92
Geolabs	ICP-MS	0.003	ppm	Lu	0.352	0.254	0.292	0.299
Geolabs	ICP-MS	0.2	ppm	Nb	7.1	5.2	5.6	5.7
Geolabs	ICP-MS	0.03	ppm	Nd	35.12	25.84	25.34	26.31
Geolabs	ICP-MS	0.006	ppm	Pr	8.613	6.177	6.385	6.503
Geolabs	ICP-MS	0.05	ppm	Rb	73.01	166.91	261.71	288.91
Geolabs	ICP-MS	0.01	ppm	Sm	6.04	4.62	4.6	4.78
Geolabs	ICP-MS	0.5	ppm	Sr	132.8	988.1	882.8	887.8
Geolabs	ICP-MS	0.17	ppm	Ta	0.35	0.22	0.23	0.24
Geolabs	ICP-MS	0.003	ppm	Tb	0.733	0.505	0.549	0.585
Geolabs	ICP-MS	0.06	ppm	Th	2.68	1.9	2.01	2.05
Geolabs	ICP-MS	0.003	ppm	Tm	0.364	0.245	0.293	0.304
Geolabs	ICP-MS	0.007	ppm	U	0.977	0.759	0.736	0.724
Geolabs	ICP-MS	0.02	ppm	Y	21.06	13.91	16.93	18.34
Geolabs	ICP-MS	0.01	ppm	Yb	2.4	1.66	1.96	2
Geolabs	ICP-MS	0.1	ppm	Ba	249	707.647	1245.263	993.144
Geolabs	ICP-AES	0.1	ppm	Be	2.12	1.69	2.72	2.54
Geolabs	ICP-AES	1	ppm	Co	32	35	32	20
Geolabs	ICP-AES	3	ppm	Cu	44	33	90	38
Geolabs	ICP-AES	8	ppm	Mo	-8	-8	-8	-8
Geolabs	ICP-AES	3	ppm	Ni	29	27	24	25
Geolabs	ICP-AES	0.3	ppm	Sc	19.3	18.6	16.5	17
Geolabs	ICP-AES	0.5	ppm	V	297.7	238	216.4	219.7
Geolabs	ICP-AES	2	ppm	W	30	14	6	6
Geolabs	ICP-AES	2	ppm	Zn	126	88	71	61
Actlabs	XRF	5	ppm	Cr_XRF	17	21	15	15
Actlabs	XRF	5	ppm	V_XRF	373	311	283	284
Actlabs	XRF	5	ppm	Zr_XRF	110	78	81	83
Actlabs	XRF	4	ppm	Ni_XRF	17	13	6	8
Actlabs	IRC	0.01	%	CO2	0.51	12.28	10.30	9.31
Actlabs	IRC	0.01	%	S	0.31	0.56	0.16	0.19
Geolabs	MS-IAT	6	ppb	Au		34.24	30.28	135.05
Geolabs	MS-IAT	2	ppb	Pd		8.39	7.78	9.04
Geolabs	MS-IAT	1	ppb	Pt		8.95	6.74	7.57

Table A.2. (cont'd)

			sample id		004VOI1322-1	004VOI1518-2	004VOI1518-4	004VOI1745-2
			sample type		surface	surface	surface	surface
			drill hole/stope		004VOI1322	004VOI1518	004VOI1518	004VOI1745
			depth, ft					
			Township		Teck	Teck	Teck	Teck
			unit_code		13	13	13	13
			rock type		intramineral dike	intramineral dike	intramineral dike	intramineral dike
			UTM_NAD83_E		570215	568572	568572	568593
			UTM_NAD83_N		5333798	5333147	5333147	5332584
laboratory	method	det limit	units					
Actlabs	XRF	0.01	%	SiO2	46.83	47.37	44.03	45.77
Actlabs	XRF	0.01	%	TiO2	0.92	0.99	0.91	0.97
Actlabs	XRF	0.01	%	Al2O3	15.7	15.75	14.72	15.68
Actlabs	XRF	0.01	%	Fe2O3	11.65	12.22	11.25	11.34
Actlabs	XRF	0.001	%	MnO	0.157	0.129	0.191	0.145
Actlabs	XRF	0.01	%	MgO	4.34	5.02	4.57	5.06
Actlabs	XRF	0.01	%	CaO	6.3	3.93	8.58	4.92
Actlabs	XRF	0.01	%	Na2O	6.06	0.2	4.5	1.07
Actlabs	XRF	0.01	%	K2O	1.66	10.36	3.09	5.57
Actlabs	XRF	0.01	%	P2O5	0.44	0.42	0.41	0.38
Actlabs	XRF	0.01	%	LOI	6.29	3.96	8.05	9.29
			%	Total	100.34	100.35	100.30	100.20
Geolabs	ICP-MS	0.07	ppm	Ce	60.88	56.4	58.33	48.56
Geolabs	ICP-MS	0.007	ppm	Cs	0.568	5.78	2.3	11.325
Geolabs	ICP-MS	0.008	ppm	Dy	3.47	3.934	3.767	3.289
Geolabs	ICP-MS	0.008	ppm	Er	2.137	2.297	2.197	1.962
Geolabs	ICP-MS	0.005	ppm	Eu	1.29	1.671	1.506	1.334
Geolabs	ICP-MS	0.009	ppm	Gd	4.042	4.833	4.61	3.973
Geolabs	ICP-MS	0.1	ppm	Hf	2.6	2.6	2.4	2.5
Geolabs	ICP-MS	0.003	ppm	Ho	0.733	0.806	0.761	0.685
Geolabs	ICP-MS	0.02	ppm	La	28.75	25.54	26.78	22.54
Geolabs	ICP-MS	0.003	ppm	Lu	0.317	0.33	0.322	0.288
Geolabs	ICP-MS	0.2	ppm	Nb	7.1	9.3	8.8	5
Geolabs	ICP-MS	0.03	ppm	Nd	30.47	30.95	31.11	25.44
Geolabs	ICP-MS	0.006	ppm	Pr	7.683	7.578	7.657	6.283
Geolabs	ICP-MS	0.05	ppm	Rb	23.86	283.4	85.63	300.88
Geolabs	ICP-MS	0.01	ppm	Sm	4.93	5.74	5.4	4.71
Geolabs	ICP-MS	0.5	ppm	Sr	298	898.2	362.1	112.3
Geolabs	ICP-MS	0.17	ppm	Ta	0.27	0.36	0.33	0.22
Geolabs	ICP-MS	0.003	ppm	Tb	0.567	0.685	0.64	0.573
Geolabs	ICP-MS	0.06	ppm	Th	2.57	2.56	2.41	2.13
Geolabs	ICP-MS	0.003	ppm	Tm	0.312	0.333	0.322	0.29
Geolabs	ICP-MS	0.007	ppm	U	0.851	0.848	0.813	0.808
Geolabs	ICP-MS	0.02	ppm	Y	18.38	20.52	19.78	16.13
Geolabs	ICP-MS	0.01	ppm	Yb	2.04	2.17	2.06	1.92
Geolabs	ICP-MS	0.1	ppm	Ba	483.056	2478.521	1001.572	282.215
Geolabs	ICP-AES	0.1	ppm	Be	0.9	2.17	1.73	3.14
Geolabs	ICP-AES	1	ppm	Co	27	28	29	30
Geolabs	ICP-AES	3	ppm	Cu	118	113	107	108
Geolabs	ICP-AES	8	ppm	Mo	-8	-8	-8	-8
Geolabs	ICP-AES	3	ppm	Ni	25	37	30	38
Geolabs	ICP-AES	0.3	ppm	Sc	21	20.9	18.3	25.3
Geolabs	ICP-AES	0.6	ppm	V	238.2	256.7	236.1	252.7
Geolabs	ICP-AES	2	ppm	W	12	9	12	7
Geolabs	ICP-AES	2	ppm	Zn	102	97	103	114
Actlabs	XRF	5	ppm	Cr_XRF	-8	25	12	45
Actlabs	XRF	5	ppm	V_XRF	282	296	286	297
Actlabs	XRF	5	ppm	Zr_XRF	93	93	86	96
Actlabs	XRF	4	ppm	Ni_XRF	7	20	16	21
Actlabs	IRC	0.01	%	CO2				
Actlabs	IRC	0.01	%	S				
Geolabs	MS-IAT	6	ppb	Au				
Geolabs	MS-IAT	2	ppb	Pd				
Geolabs	MS-IAT	1	ppb	Pt				

Table A.2. (cont'd)

			sample id		004VOI1749-1	004VOI1232-1	004VOI1317-3	004VOI1317-1
			sample type		surface	surface	surface	surface
			drill hole/stope		004VOI1749	004VOI1232	004VOI1317	004VOI1317
			depth, ft					
			Township		Teck	Teck	Teck	Teck
			unit_code		13	13	13	13
			rock type		intramineral dike	mafic (augite) syenite	mafic (augite) syenite	mafic (augite) syenite
			UTM_NAD83_E		568556	567762	570143	570143
			UTM_NAD83_N		5332469	5332706	5333588	5333588
laboratory	method	det limit	units					
Actlabs	XRF	0.01	%	SiO2	45.11	49.56	49.37	48.45
Actlabs	XRF	0.01	%	TiO2	0.95	1.03	0.83	0.85
Actlabs	XRF	0.01	%	Al2O3	14.78	14.42	15.11	12.21
Actlabs	XRF	0.01	%	Fe2O3	11.2	10.02	8.35	9.21
Actlabs	XRF	0.001	%	MnO	0.188	0.171	0.123	0.145
Actlabs	XRF	0.01	%	MgO	4.85	7.61	4.23	7.47
Actlabs	XRF	0.01	%	CaO	8.41	5.48	4.57	7.02
Actlabs	XRF	0.01	%	Na2O	3.4	1.5	3.09	3.06
Actlabs	XRF	0.01	%	K2O	1.9	6.44	6.67	4.68
Actlabs	XRF	0.01	%	P2O5	0.38	0.74	0.54	0.6
Actlabs	XRF	0.01	%	LOI	9.13	3.07	7.01	6.70
			%	Total	100.30	100.04	99.90	100.40
Geolabs	ICP-MS	0.07	ppm	Ce	46.95	117.54	100.92	92.2
Geolabs	ICP-MS	0.007	ppm	Cs	3.724	3.951	1.569	15.892
Geolabs	ICP-MS	0.008	ppm	Dy	3.374	5.673	4.22	4.411
Geolabs	ICP-MS	0.008	ppm	Er	2.008	2.755	2.124	2.142
Geolabs	ICP-MS	0.005	ppm	Eu	1.323	2.875	2.218	2.311
Geolabs	ICP-MS	0.009	ppm	Gd	4.016	9.086	6.533	7.122
Geolabs	ICP-MS	0.1	ppm	Hf	2.3	4.9	4.2	3.7
Geolabs	ICP-MS	0.003	ppm	Ho	0.69	1.039	0.774	0.8
Geolabs	ICP-MS	0.02	ppm	La	21.06	56.27	50.59	44.2
Geolabs	ICP-MS	0.003	ppm	Lu	0.287	0.357	0.284	0.276
Geolabs	ICP-MS	0.2	ppm	Nb	4.5	7	7	5.2
Geolabs	ICP-MS	0.03	ppm	Nd	26.14	60.06	48.01	47.26
Geolabs	ICP-MS	0.006	ppm	Pr	6.22	14.887	12.206	11.633
Geolabs	ICP-MS	0.05	ppm	Rb	75.95	125.63	129.94	211.96
Geolabs	ICP-MS	0.01	ppm	Sm	4.8	11.66	8.76	9.2
Geolabs	ICP-MS	0.5	ppm	Sr	641.4	971.4	818	930
Geolabs	ICP-MS	0.17	ppm	Ta	0.2	0.38	0.37	0.28
Geolabs	ICP-MS	0.003	ppm	Tb	0.57	1.12	0.805	0.884
Geolabs	ICP-MS	0.06	ppm	Th	1.94	9.8	9.69	7.53
Geolabs	ICP-MS	0.003	ppm	Tm	0.293	0.386	0.298	0.299
Geolabs	ICP-MS	0.007	ppm	U	0.668	2.371	2.952	2.267
Geolabs	ICP-MS	0.02	ppm	Y	17.37	27.26	20.61	21.15
Geolabs	ICP-MS	0.01	ppm	Yb	1.88	2.47	1.92	1.9
Geolabs	ICP-MS	0.1	ppm	Ba	1261.552	2638.547	2173.702	1833.234
Geolabs	ICP-AES	0.1	ppm	Be	1.38	1.38	1.46	2.12
Geolabs	ICP-AES	1	ppm	Co	30	31	17	29
Geolabs	ICP-AES	3	ppm	Cu	105	75	40	79
Geolabs	ICP-AES	8	ppm	Mo	-8	-8	-8	-8
Geolabs	ICP-AES	3	ppm	Ni	35	106	50	115
Geolabs	ICP-AES	0.3	ppm	Sc	24.9	23.4	13.5	20.1
Geolabs	ICP-AES	0.6	ppm	V	263.8	178.3	155.8	178.4
Geolabs	ICP-AES	2	ppm	W	4	-2	9	7
Geolabs	ICP-AES	2	ppm	Zn	119	129	86	104
Actlabs	XRF	5	ppm	Cr_XRF	42	290	123	281
Actlabs	XRF	5	ppm	V_XRF	329	214	187	213
Actlabs	XRF	5	ppm	Zr_XRF	83	178	168	138
Actlabs	XRF	4	ppm	Ni_XRF	16	86	34	104
Actlabs	IRC	0.01	%	CO2				
Actlabs	IRC	0.01	%	S				
Geolabs	MS-IAT	6	ppb	Au				
Geolabs	MS-IAT	2	ppb	Pd				
Geolabs	MS-IAT	1	ppb	Pt				

Table A.2. (cont'd)

laboratory	method	det.limit	units					
			sample id		004VOI1374-1	004VOI1493-1	004VOI1952-1	004VOI1907-1
			sample type		surface	surface	surface	surface
			drill hole/stope		004VOI1374	004VOI1493	004VOI1952	004VOI1907
			depth, ft					
			Township		Teck	Teck	Teck	Teck
			unit_code		13	13	13	13
			rock type		mafic (augite) syenite	mafic (augite) syenite	mafic (augite) syenite	pyroxene-feldspar-phyric trachyandesite
			UTM_NAD83_E		569961	568736	570359	567637
			UTM_NAD83_N		5333236	5333204	5333025	5329977
Actlabs	XRF	0.01	%	SiO2	49.26	51.07	50.46	52.55
Actlabs	XRF	0.01	%	TiO2	0.81	0.88	0.9	0.95
Actlabs	XRF	0.01	%	Al2O3	12.81	12.89	14.21	15.62
Actlabs	XRF	0.01	%	Fe2O3	8.65	9.55	9.18	9.31
Actlabs	XRF	0.001	%	MnO	0.134	0.144	0.12	0.14
Actlabs	XRF	0.01	%	MgO	7.06	7.89	5.99	4.61
Actlabs	XRF	0.01	%	CaO	6.84	7.97	5.02	4.96
Actlabs	XRF	0.01	%	Na2O	3.53	2.58	3.1	4.61
Actlabs	XRF	0.01	%	K2O	4.39	4.8	5.37	3.67
Actlabs	XRF	0.01	%	P2O5	0.56	0.6	0.6	0.51
Actlabs	XRF	0.01	%	LOI	6.29	1.77	4.78	3.10
			%	Total	100.34	100.14	99.73	100.03
Geolabs	ICP-MS	0.07	ppm	Ce	83.49	94.72	95.77	103.72
Geolabs	ICP-MS	0.007	ppm	Cs	19.561	9.105	18.149	1.676
Geolabs	ICP-MS	0.008	ppm	Dy	4.193	4.593	4.732	4.654
Geolabs	ICP-MS	0.008	ppm	Er	2.048	2.212	2.329	2.304
Geolabs	ICP-MS	0.005	ppm	Eu	2.167	2.511	2.374	2.459
Geolabs	ICP-MS	0.009	ppm	Gd	6.706	7.456	7.283	7.523
Geolabs	ICP-MS	0.1	ppm	Hf	3.8	3.7	4.3	4.3
Geolabs	ICP-MS	0.003	ppm	Ho	0.769	0.827	0.859	0.859
Geolabs	ICP-MS	0.02	ppm	La	40.16	45.74	44.98	50.12
Geolabs	ICP-MS	0.003	ppm	Lu	0.272	0.286	0.311	0.307
Geolabs	ICP-MS	0.2	ppm	Nb	5.5	5.3	6.6	6.1
Geolabs	ICP-MS	0.03	ppm	Nd	43.63	49.83	47.62	52.81
Geolabs	ICP-MS	0.006	ppm	Pr	10.496	12.144	11.822	13.061
Geolabs	ICP-MS	0.05	ppm	Rb	156.64	137.26	193.09	74.89
Geolabs	ICP-MS	0.01	ppm	Sm	8.55	9.63	9.31	9.77
Geolabs	ICP-MS	0.5	ppm	Sr	1028.9	1309.06	973.1	958.3
Geolabs	ICP-MS	0.17	ppm	Ta	0.3	0.29	0.35	0.33
Geolabs	ICP-MS	0.003	ppm	Tb	0.825	0.911	0.925	0.912
Geolabs	ICP-MS	0.06	ppm	Th	7.88	7.29	8.88	8.39
Geolabs	ICP-MS	0.003	ppm	Tm	0.283	0.302	0.327	0.326
Geolabs	ICP-MS	0.007	ppm	U	2.275	1.989	2.475	1.984
Geolabs	ICP-MS	0.02	ppm	Y	20.17	22.24	22.71	23.03
Geolabs	ICP-MS	0.01	ppm	Yb	1.83	1.92	2.16	2.08
Geolabs	ICP-MS	0.1	ppm	Ba	1840.623	2106.537	2336.808	1904.154
Geolabs	ICP-AES	0.1	ppm	Be	1.86	1.77	1.81	1.5
Geolabs	ICP-AES	1	ppm	Co	27	31	30	21
Geolabs	ICP-AES	3	ppm	Cu	82	92	79	70
Geolabs	ICP-AES	8	ppm	Mo	-8	-8	-8	-8
Geolabs	ICP-AES	3	ppm	Ni	110	128	50	39
Geolabs	ICP-AES	0.3	ppm	Sc	18.4	21	18.2	17.2
Geolabs	ICP-AES	0.6	ppm	V	166.9	182.8	172.6	187.4
Geolabs	ICP-AES	2	ppm	W	4	-2	-2	12
Geolabs	ICP-AES	2	ppm	Zn	94	106	115	116
Actlabs	XRF	5	ppm	Cr_XRF	262	285	154	59
Actlabs	XRF	5	ppm	V_XRF	208	203	204	203
Actlabs	XRF	5	ppm	Zr_XRF	144	138	160	157
Actlabs	XRF	4	ppm	Ni_XRF	105	107	38	20
Actlabs	IRC	0.01	%	CO2				
Actlabs	IRC	0.01	%	S				
Geolabs	MS-IAT	6	ppb	Au				
Geolabs	MS-IAT	2	ppb	Pd				
Geolabs	MS-IAT	1	ppb	Pt				

Table A.2. (cont'd)

			sample id		004VOI1155-1	004VOI1320-1	004VOI1518-5	004VOI1555-1
			sample type		surface	surface	surface	surface
			drill hole/stope		004VOI1155	004VOI1320	004VOI1518	004VOI1555
			depth, ft					
			Township		Teck	Teck	Teck	Teck
			unit_code		13	13	13	13
			rock type		sparsely porphyritic syenite porphyry	sparsely porphyritic syenite porphyry	sparsely porphyritic syenite porphyry	sparsely porphyritic syenite porphyry
			UTM_NAD83_E		567271	570245	568572	568578
			UTM_NAD83_N		5332678	5333721	5333147	5332706
laboratory	method	det.limit	units					
Actlabs	XRF	0.01	%	SiO2	53.56	58.45	58.66	59.74
Actlabs	XRF	0.01	%	TiO2	0.63	0.51	0.52	0.48
Actlabs	XRF	0.01	%	Al2O3	12.03	14.31	14.52	14.7
Actlabs	XRF	0.01	%	Fe2O3	7.85	5.74	5.86	5.29
Actlabs	XRF	0.001	%	MnO	0.129	0.09	0.107	0.076
Actlabs	XRF	0.01	%	MgO	10.83	4.34	4.48	3.11
Actlabs	XRF	0.01	%	CaO	6.36	4.03	3.5	4.06
Actlabs	XRF	0.01	%	Na2O	3.08	4.63	4.27	4.41
Actlabs	XRF	0.01	%	K2O	2.72	3.02	3.14	3.07
Actlabs	XRF	0.01	%	P2O5	0.35	0.3	0.32	0.32
Actlabs	XRF	0.01	%	LOI	2.66	4.65	4.34	4.75
			%	Total	100.20	100.07	99.71	100.01
Geolabs	ICP-MS	0.07	ppm	Ce	74.94	76.92	81.05	75.51
Geolabs	ICP-MS	0.007	ppm	Cs	1.464	5.084	4.597	2.687
Geolabs	ICP-MS	0.008	ppm	Dy	3.192	2.79	2.652	2.578
Geolabs	ICP-MS	0.008	ppm	Er	1.517	1.345	1.276	1.269
Geolabs	ICP-MS	0.005	ppm	Eu	1.757	1.587	1.529	1.541
Geolabs	ICP-MS	0.009	ppm	Gd	5.23	4.693	4.445	4.424
Geolabs	ICP-MS	0.1	ppm	Hf	3.5	3.6	3.7	3.7
Geolabs	ICP-MS	0.003	ppm	Ho	0.571	0.5	0.481	0.47
Geolabs	ICP-MS	0.02	ppm	La	35.83	39.02	42.03	38.19
Geolabs	ICP-MS	0.003	ppm	Lu	0.198	0.183	0.178	0.18
Geolabs	ICP-MS	0.2	ppm	Nb	4.7	5	5.1	5.2
Geolabs	ICP-MS	0.03	ppm	Nd	37.29	35.63	36.44	34.9
Geolabs	ICP-MS	0.006	ppm	Pr	9.227	9.259	9.593	9.03
Geolabs	ICP-MS	0.05	ppm	Rb	57.95	90.61	116.7	87.24
Geolabs	ICP-MS	0.01	ppm	Sm	6.8	6.26	6.23	6.18
Geolabs	ICP-MS	0.5	ppm	Sr	604.5	2500.09	2769.22	563
Geolabs	ICP-MS	0.17	ppm	Ta	0.27	0.29	0.3	0.3
Geolabs	ICP-MS	0.003	ppm	Tb	0.63	0.562	0.541	0.522
Geolabs	ICP-MS	0.06	ppm	Th	6.21	6.91	6.88	7.08
Geolabs	ICP-MS	0.003	ppm	Tm	0.209	0.188	0.179	0.182
Geolabs	ICP-MS	0.007	ppm	U	1.749	2.207	2.148	2.343
Geolabs	ICP-MS	0.02	ppm	Y	15.54	13.65	13.13	12.7
Geolabs	ICP-MS	0.01	ppm	Yb	1.36	1.24	1.28	1.21
Geolabs	ICP-MS	0.1	ppm	Ba	1141.337	3772.371	3287.64	1488.489
Geolabs	ICP-AES	0.1	ppm	Be	1.08	1.3	1.56	1.32
Geolabs	ICP-AES	1	ppm	Co	41	18	18	12
Geolabs	ICP-AES	3	ppm	Cu	10	23	54	5
Geolabs	ICP-AES	8	ppm	Mo	-8	-8	-8	-8
Geolabs	ICP-AES	3	ppm	Ni	280	69	73	38
Geolabs	ICP-AES	0.3	ppm	Sc	17.5	11.8	11.6	9.6
Geolabs	ICP-AES	0.6	ppm	V	120.4	95.1	99.8	93.8
Geolabs	ICP-AES	2	ppm	W	7	9	14	7
Geolabs	ICP-AES	2	ppm	Zn	85	69	74	71
Actlabs	XRF	5	ppm	Cr_XRF	670	220	227	112
Actlabs	XRF	5	ppm	V_XRF	134	144	148	116
Actlabs	XRF	5	ppm	Zr_XRF	127	127	119	140
Actlabs	XRF	4	ppm	Ni_XRF	267	63	69	29
Actlabs	IRC	0.01	%	CO2				
Actlabs	IRC	0.01	%	S				
Geolabs	MS-IAT	6	ppb	Au				
Geolabs	MS-IAT	2	ppb	Pd				
Geolabs	MS-IAT	1	ppb	Pt				

Table A.2. (cont'd)

			sample id		004VOI1745-1	004VOI1272-1	004VOI1952-3
			sample type		surface	surface	surface
			drill hole/stope		004VOI1745	004VOI1272	004VOI1952
			depth, ft				
			Township		Teck	Teck	Teck
			unit_code		13	13	13
			rock type		sparsely porphyritic syenite porphyry	syenite	syenite
			UTM_NAD83_E		568593	570274	570359
			UTM_NAD83_N		5332584	5333054	5333025
laboratory	method	det.limit	units				
Actlabs	XRF	0.01	%	SiO2	60.53	53.25	53.94
Actlabs	XRF	0.01	%	TiO2	0.52	0.67	0.71
Actlabs	XRF	0.01	%	Al2O3	15.08	18.02	18.15
Actlabs	XRF	0.01	%	Fe2O3	5.6	4.02	4.39
Actlabs	XRF	0.001	%	MnO	0.075	0.118	0.116
Actlabs	XRF	0.01	%	MgO	3.26	2.09	1.84
Actlabs	XRF	0.01	%	CaO	3.06	3.91	3.67
Actlabs	XRF	0.01	%	Na2O	5.08	3.34	3.96
Actlabs	XRF	0.01	%	K2O	2.8	7.91	7.2
Actlabs	XRF	0.01	%	P2O5	0.31	0.34	0.35
Actlabs	XRF	0.01	%	LOI	3.80	6.34	5.77
			%	Total	100.12	100.01	100.10
Geolabs	ICP-MS	0.07	ppm	Ce	93.8	93.46	99.11
Geolabs	ICP-MS	0.007	ppm	Cs	1.697	4.608	3.238
Geolabs	ICP-MS	0.008	ppm	Dy	3.222	3.233	3.338
Geolabs	ICP-MS	0.008	ppm	Er	1.592	1.712	1.718
Geolabs	ICP-MS	0.005	ppm	Eu	1.811	1.647	1.735
Geolabs	ICP-MS	0.009	ppm	Gd	5.235	4.963	5.114
Geolabs	ICP-MS	0.1	ppm	Hf	4.3	5.1	4.5
Geolabs	ICP-MS	0.003	ppm	Ho	0.589	0.615	0.628
Geolabs	ICP-MS	0.02	ppm	La	48.23	48.74	51.01
Geolabs	ICP-MS	0.003	ppm	Lu	0.227	0.257	0.25
Geolabs	ICP-MS	0.2	ppm	Nb	6.1	9.6	9
Geolabs	ICP-MS	0.03	ppm	Nd	42.02	39.13	40.18
Geolabs	ICP-MS	0.006	ppm	Pr	11.168	10.614	11.056
Geolabs	ICP-MS	0.05	ppm	Rb	57.7	204.18	186.24
Geolabs	ICP-MS	0.01	ppm	Sm	7.22	6.71	6.92
Geolabs	ICP-MS	0.5	ppm	Sr	692.7	431.2	527.9
Geolabs	ICP-MS	0.17	ppm	Ta	0.33	0.5	0.45
Geolabs	ICP-MS	0.003	ppm	Tb	0.626	0.632	0.659
Geolabs	ICP-MS	0.06	ppm	Th	9.01	12.36	11.39
Geolabs	ICP-MS	0.003	ppm	Tm	0.228	0.256	0.257
Geolabs	ICP-MS	0.007	ppm	U	2.578	3.853	2.966
Geolabs	ICP-MS	0.02	ppm	Y	16.19	16.8	17.04
Geolabs	ICP-MS	0.01	ppm	Yb	1.52	1.68	1.7
Geolabs	ICP-MS	0.1	ppm	Ba	1997.892	1484.092	1345.185
Geolabs	ICP-AES	0.1	ppm	Be	1.37	2.02	1.87
Geolabs	ICP-AES	1	ppm	Co	15	4	9
Geolabs	ICP-AES	3	ppm	Cu	34	33	64
Geolabs	ICP-AES	8	ppm	Mo	-8	-8	-8
Geolabs	ICP-AES	3	ppm	Ni	47	21	19
Geolabs	ICP-AES	0.3	ppm	Sc	11	5.2	5
Geolabs	ICP-AES	0.6	ppm	V	99	74	74.1
Geolabs	ICP-AES	2	ppm	W	4	11	6
Geolabs	ICP-AES	2	ppm	Zn	79	63	56
Actlabs	XRF	5	ppm	Cr_XRF	119	61	51
Actlabs	XRF	5	ppm	V_XRF	125	108	104
Actlabs	XRF	5	ppm	Zr_XRF	159	203	186
Actlabs	XRF	4	ppm	Ni_XRF	37	9	7
Actlabs	IRC	0.01	%	CO2			
Actlabs	IRC	0.01	%	S			
Geolabs	MS-IAT	6	ppb	Au			
Geolabs	MS-IAT	2	ppb	Pd			
Geolabs	MS-IAT	1	ppb	Pt			

Table A.3. Analytical results for samples from mineralized zones other than Upper Canada Mine: trace element data, analyses by Actlabs.

			mineralized_zone		Anoki South	Anoki South	Anoki South
			Township		Gauthier	Gauthier	Gauthier
			Sample ID		AN02-20-69314	AN02-20-69315	AN02-21-69664
			sample type		drill core	drill core	drill core
			station/drill hole/stope		AN02-20	AN02-20	AN02-21
			Depth from (ft)		1167	1169	1335
			Depth to (ft)		1169	1171.1	1337.3
			utm_nad83_E		586707.01	586707.01	586689.97
			utm_nad83_N		5330762.29	5330762.29	5330703.87
Laboratory	Method	det. limit	unit				
Actlabs	Fire. grav	0.03	ppm	Au	1.78	1.85	0.48
Actlabs	ICP-OES	0.3	ppm	Ag	0.6	0.7	0.7
Actlabs	ICP-OES	0.3	ppm	Cd	5.5	5.6	4.6
Actlabs	ICP-OES	1	ppm	Cu	288	290	67
Actlabs	ICP-OES	1	ppm	Mn	1207	900	930
Actlabs	ICP-OES	1	ppm	Mo	6	8	3
Actlabs	ICP-OES	1	ppm	Ni	163	149	39
Actlabs	ICP-OES	3	ppm	Pb	133	20	553
Actlabs	ICP-OES	1	ppm	Zn	2010	2319	623
Actlabs	ICP-OES	0.01	%	Al	4.52	3.94	3.67
Actlabs	ICP-OES	1	ppm	Be	2	2	-1
Actlabs	ICP-OES	0.01	%	Ca	2.31	3.11	4.21
Actlabs	ICP-OES	0.01	%	K	3.1	4.23	2.33
Actlabs	ICP-OES	0.01	%	Mg	0.67	0.51	2.49
Actlabs	ICP-OES	0.001	%	P	0.066	0.046	0.028
Actlabs	ICP-OES	1	ppm	Sr	35	33	68
Actlabs	ICP-OES	0.01	%	Ti	0.35	0.37	0.18
Actlabs	ICP-OES	2	ppm	V	217	223	62
Actlabs	ICP-OES	1	ppm	Y	9	8	8
Actlabs	INAA	2	ppb	Au_INAA			
Actlabs	INAA	0.5	ppm	As	34.4	29.8	29.6
Actlabs	INAA	50	ppm	Ba	425	530	230
Actlabs	INAA	0.5	ppm	Br	-0.5	-0.5	-0.5
Actlabs	INAA	1	ppm	Co	49	45	19
Actlabs	INAA	2	ppm	Cr	361	337	66
Actlabs	INAA	1	ppm	Cs	-1	-1	-1
Actlabs	INAA	0.01	%	Fe	5.65	5.44	3.89
Actlabs	INAA	1	ppm	Hf	1	2	2
Actlabs	INAA	1	ppm	Hg	-1	-1	-1
Actlabs	INAA	5	ppb	Ir	-5	-5	-5
Actlabs	INAA	0.01	%	Na	0.07	0.06	0.05
Actlabs	INAA	15	ppm	Rb	79	63	39
Actlabs	INAA	0.1	ppm	Sb	0.8	0.3	0.4
Actlabs	INAA	0.1	ppm	Sc	28.2	25.6	7.2
Actlabs	INAA	0.01	%	Sn	-0.01	-0.01	-0.01
Actlabs	INAA	0.5	ppm	Ta	-0.5	-0.5	0.5
Actlabs	INAA	0.2	ppm	Th	1.2	1	1.1
Actlabs	INAA	0.5	ppm	U	-0.5	-0.5	0.7
Actlabs	INAA	1	ppm	W	13	83	-1
Actlabs	INAA	0.5	ppm	La	10	8.7	10.6
Actlabs	INAA	3	ppm	Ce	21	17	22
Actlabs	INAA	5	ppm	Nd	13	11	10
Actlabs	INAA	0.1	ppm	Sm	2.5	2.3	2
Actlabs	INAA	0.2	ppm	Eu	1	0.8	0.5
Actlabs	INAA	0.5	ppm	Tb	-0.5	-0.5	-0.5
Actlabs	INAA	0.2	ppm	Yb	2.3	1.8	0.9
Actlabs	INAA	0.05	ppm	Lu	0.35	0.29	0.15
Actlabs	H ICP-MS	0.1	ppm	Ge	-0.1	-0.1	-0.1
Actlabs	H ICP-MS	0.1	ppm	Se	3.5	5.9	1.5
Actlabs	H ICP-MS	0.1	ppm	Te	1	1.2	0.3
Actlabs	H ICP-MS	0.1	ppm	Bi	0.9	0.7	-0.1
Actlabs	IRC	0.01	ppm	S	3.95	5.15	0.49
Actlabs	IRC	0.01	ppm	CO2	5.64	5.35	8.25

Table A.3. (cont'd)

			mineralized_zone		Anoki South	Anoki South	Anoki South
			Township		Gauthier	Gauthier	Gauthier
			Sample ID		AN02-21-69666	AN02-21-69667	AN02-21-69674
			sample type		drill core	drill core	drill core
			station/drill hole/stope		AN02-21	AN02-21	AN02-21
			Depth from (ft)		1339	1342	1358.1
			Depth to (ft)		1342	1344.9	1360
			utm_nad83_E		586689.97	586689.97	586689.97
			utm_nad83_N		5330703.87	5330703.87	5330703.87
Laboratory	Method	det. limit	unit				
Actlabs	Fire, grav	0.03	ppm	Au	-0.03	0.41	0.27
Actlabs	ICP-OES	0.3	ppm	Ag	0.3	0.5	1.1
Actlabs	ICP-OES	0.3	ppm	Cd	1.4	3.9	7.3
Actlabs	ICP-OES	1	ppm	Cu	121	222	590
Actlabs	ICP-OES	1	ppm	Mn	1404	1340	249
Actlabs	ICP-OES	1	ppm	Mo	2	33	5
Actlabs	ICP-OES	1	ppm	Ni	82	143	123
Actlabs	ICP-OES	3	ppm	Pb	26	37	166
Actlabs	ICP-OES	1	ppm	Zn	290	1360	3964
Actlabs	ICP-OES	0.01	%	Al	4.14	4.55	2.5
Actlabs	ICP-OES	1	ppm	Be	1	2	-1
Actlabs	ICP-OES	0.01	%	Ca	5.22	4.71	0.8
Actlabs	ICP-OES	0.01	%	K	3.02	3.21	1.95
Actlabs	ICP-OES	0.01	%	Mg	3.08	3.21	0.63
Actlabs	ICP-OES	0.001	%	P	0.045	0.064	0.052
Actlabs	ICP-OES	1	ppm	Sr	133	129	34
Actlabs	ICP-OES	0.01	%	Ti	0.34	0.24	0.12
Actlabs	ICP-OES	2	ppm	V	172	122	71
Actlabs	ICP-OES	1	ppm	Y	6	9	9
Actlabs	INAA	2	ppb	Au_INAA	70		
Actlabs	INAA	0.5	ppm	As	74.8	116	134
Actlabs	INAA	50	ppm	Ba	300	690	315
Actlabs	INAA	0.5	ppm	Br	-0.5	-0.5	-0.5
Actlabs	INAA	1	ppm	Co	32	52	60
Actlabs	INAA	2	ppm	Cr	220	267	106
Actlabs	INAA	1	ppm	Cs	-1	1	-1
Actlabs	INAA	0.01	%	Fe	5.52	6.42	5.39
Actlabs	INAA	1	ppm	Hf	2	2	-1
Actlabs	INAA	1	ppm	Hg	-1	-1	-1
Actlabs	INAA	5	ppb	Ir	-5	-5	-5
Actlabs	INAA	0.01	%	Na	0.8	0.45	0.03
Actlabs	INAA	15	ppm	Rb	60	63	28
Actlabs	INAA	0.1	ppm	Sb	0.6	0.8	1
Actlabs	INAA	0.1	ppm	Sc	20.9	14.6	7.2
Actlabs	INAA	0.01	%	Sn	-0.01	-0.01	-0.01
Actlabs	INAA	0.5	ppm	Ta	-0.5	-0.5	-0.5
Actlabs	INAA	0.2	ppm	Th	1	2.2	0.9
Actlabs	INAA	0.5	ppm	U	-0.5	0.8	0.8
Actlabs	INAA	1	ppm	W	5	7	7
Actlabs	INAA	0.5	ppm	La	7.2	19.9	5.1
Actlabs	INAA	3	ppm	Ce	17	40	12
Actlabs	INAA	5	ppm	Nd	8	23	7
Actlabs	INAA	0.1	ppm	Sm	1.9	3.1	1.4
Actlabs	INAA	0.2	ppm	Eu	0.7	1.1	0.5
Actlabs	INAA	0.5	ppm	Tb	-0.5	0.6	-0.5
Actlabs	INAA	0.2	ppm	Yb	1.7	1.2	0.6
Actlabs	INAA	0.05	ppm	Lu	0.25	0.22	0.12
Actlabs	H. ICP-MS	0.1	ppm	Ge	-0.1	-0.1	-0.1
Actlabs	H. ICP-MS	0.1	ppm	Se	1.9	3.8	7.3
Actlabs	H. ICP-MS	0.1	ppm	Te	0.4	1.1	1.8
Actlabs	H. ICP-MS	0.1	ppm	Bi	0.1	0.9	2.8
Actlabs	IRC	0.01	ppm	S	2.57	5.3	7.15
Actlabs	IRC	0.01	ppm	CO2	9.75	8.61	1.14

Table A.3. (cont'd)

			mineralized_zone		40East	40East	40East
			Township		Gauthier	Gauthier	Gauthier
			Sample ID		AN03-49-57174	AN03-49-57176	AN03-49-57177
			sample type		drill core	drill core	drill core
			station/drill hole/stope		AN03-49	AN03-49	AN03-49
			Depth from (ft)		1012	1018	1021
			Depth to (ft)		1015	1021	1024
			utm_nad83_E		586344	586344	586344
			utm_nad83_N		5331277	5331277	5331277
Laboratory	Method	det. limit	unit				
Actlabs	Fire. grav	0.03	ppm	Au	1.23	0.82	1.17
Actlabs	ICP-OES	0.3	ppm	Ag	1.2	0.5	0.9
Actlabs	ICP-OES	0.3	ppm	Cd	1	1.1	2.7
Actlabs	ICP-OES	1	ppm	Cu	78	29	15
Actlabs	ICP-OES	1	ppm	Mn	907	895	980
Actlabs	ICP-OES	1	ppm	Mo	3	3	3
Actlabs	ICP-OES	1	ppm	Ni	25	20	20
Actlabs	ICP-OES	3	ppm	Pb	147	41	32
Actlabs	ICP-OES	1	ppm	Zn	108	124	641
Actlabs	ICP-OES	0.01	%	Al	4.52	4.2	3.65
Actlabs	ICP-OES	1	ppm	Be	3	2	2
Actlabs	ICP-OES	0.01	%	Ca	3.39	3.82	3.63
Actlabs	ICP-OES	0.01	%	K	4.01	3.78	4.29
Actlabs	ICP-OES	0.01	%	Mg	2	1.96	1.86
Actlabs	ICP-OES	0.001	%	P	0.099	0.126	0.1
Actlabs	ICP-OES	1	ppm	Sr	894	984	793
Actlabs	ICP-OES	0.01	%	Ti	0.24	0.24	0.24
Actlabs	ICP-OES	2	ppm	V	112	99	108
Actlabs	ICP-OES	1	ppm	Y	13	13	11
Actlabs	INAA	2	ppb	Au_INAA			
Actlabs	INAA	0.5	ppm	As	34	34.1	33.4
Actlabs	INAA	50	ppm	Ba	1200	1150	1150
Actlabs	INAA	0.5	ppm	Br	-0.5	-0.5	-0.5
Actlabs	INAA	1	ppm	Co	12	11	13
Actlabs	INAA	2	ppm	Cr	81	104	81
Actlabs	INAA	1	ppm	Cs	2	2	2
Actlabs	INAA	0.01	%	Fe	2.5	2.37	2.75
Actlabs	INAA	1	ppm	Hf	3	2	1
Actlabs	INAA	1	ppm	Hg	-1	-1	-1
Actlabs	INAA	5	ppb	Ir	-5	-5	-5
Actlabs	INAA	0.01	%	Na	1.92	2.32	2.07
Actlabs	INAA	15	ppm	Rb	48	37	49
Actlabs	INAA	0.1	ppm	Sb	1.3	1.4	1.4
Actlabs	INAA	0.1	ppm	Sc	8.9	9.3	10.2
Actlabs	INAA	0.01	%	Sn	-0.01	-0.01	-0.01
Actlabs	INAA	0.5	ppm	Ta	-0.5	1.1	-0.5
Actlabs	INAA	0.2	ppm	Th	5.6	6.4	6.5
Actlabs	INAA	0.5	ppm	U	2.1	1.4	2.9
Actlabs	INAA	1	ppm	W	20	23	16
Actlabs	INAA	0.5	ppm	La	26.2	28.4	30.3
Actlabs	INAA	3	ppm	Ce	43	47	51
Actlabs	INAA	5	ppm	Nd	24	27	27
Actlabs	INAA	0.1	ppm	Sm	3.4	3.9	4.1
Actlabs	INAA	0.2	ppm	Eu	0.9	1	1.1
Actlabs	INAA	0.5	ppm	Tb	-0.5	-0.5	-0.5
Actlabs	INAA	0.2	ppm	Yb	1.1	1.3	1.4
Actlabs	INAA	0.05	ppm	Lu	0.18	0.23	0.22
Actlabs	H. ICP-MS	0.1	ppm	Ge	-0.1	-0.1	-0.1
Actlabs	H. ICP-MS	0.1	ppm	Se	1.5	0.5	0.6
Actlabs	H. ICP-MS	0.1	ppm	Te	0.3	0.2	0.2
Actlabs	H. ICP-MS	0.1	ppm	Bi	1.2	-0.1	0.3
Actlabs	IRC	0.01	ppm	S	1.06	1.21	1.33
Actlabs	IRC	0.01	ppm	CO2	6.67	7.04	7.04

Table A.3. (cont'd)

			mineralized_zone		40East	40East	Anoki_Main
			Township		Gauthier	Gauthier	Gauthier
			Sample ID		AN03-49-57178	AN03-49-57180	AN03-61-86348
			sample type		drill core	drill core	drill core
			station/drill hole/stope		AN03-49	AN03-49	AN03-61
			Depth from (ft)		1024	1030	273.4
			Depth to (ft)		1027	1032	275.7
			utm_nad83_E		586344	586344	586700
			utm_nad83_N		5331277	5331277	5331177
Laboratory	Method	det. limit	unit				
Actlabs	Fire, grav	0.03	ppm	Au	5.28	1.92	4.87
Actlabs	ICP-OES	0.3	ppm	Ag	1	0.8	1.3
Actlabs	ICP-OES	0.3	ppm	Cd	0.6	3.1	0.7
Actlabs	ICP-OES	1	ppm	Cu	28	28	297
Actlabs	ICP-OES	1	ppm	Mn	881	1117	1467
Actlabs	ICP-OES	1	ppm	Mo	1	-1	2
Actlabs	ICP-OES	1	ppm	Ni	20	22	17
Actlabs	ICP-OES	3	ppm	Pb	29	86	23
Actlabs	ICP-OES	1	ppm	Zn	56	767	65
Actlabs	ICP-OES	0.01	%	Al	2.98	3.63	3.63
Actlabs	ICP-OES	1	ppm	Be	2	3	1
Actlabs	ICP-OES	0.01	%	Ca	3.53	4.09	4.02
Actlabs	ICP-OES	0.01	%	K	3.91	4.39	0.31
Actlabs	ICP-OES	0.01	%	Mg	1.75	2.33	2.03
Actlabs	ICP-OES	0.001	%	P	0.098	0.119	0.21
Actlabs	ICP-OES	1	ppm	Sr	831	901	785
Actlabs	ICP-OES	0.01	%	Ti	0.24	0.26	0.63
Actlabs	ICP-OES	2	ppm	V	100	131	92
Actlabs	ICP-OES	1	ppm	Y	8	11	15
Actlabs	INAA	2	ppb	Au_INAA			
Actlabs	INAA	0.5	ppm	As	36.9	32.3	100
Actlabs	INAA	50	ppm	Ba	1200	1400	350
Actlabs	INAA	0.5	ppm	Br	-0.5	-0.5	-0.5
Actlabs	INAA	1	ppm	Co	13	14	-1
Actlabs	INAA	2	ppm	Cr	105	92	26
Actlabs	INAA	1	ppm	Cs	1	2	-1
Actlabs	INAA	0.01	%	Fe	2.77	3.02	8.45
Actlabs	INAA	1	ppm	Hf	1	2	3
Actlabs	INAA	1	ppm	Hg	-1	-1	-1
Actlabs	INAA	5	ppb	Ir	-5	-5	-5
Actlabs	INAA	0.01	%	Na	2.72	2.1	4.18
Actlabs	INAA	15	ppm	Rb	48	102	-15
Actlabs	INAA	0.1	ppm	Sb	1.2	1.3	1.5
Actlabs	INAA	0.1	ppm	Sc	9.8	10.7	7.2
Actlabs	INAA	0.01	%	Sn	-0.01	-0.01	-0.01
Actlabs	INAA	0.5	ppm	Ta	-0.5	1.1	-0.5
Actlabs	INAA	0.2	ppm	Th	6.2	6.8	1.1
Actlabs	INAA	0.5	ppm	U	3.1	2.9	0.9
Actlabs	INAA	1	ppm	W	17	16	31
Actlabs	INAA	0.5	ppm	La	30	29.1	9.4
Actlabs	INAA	3	ppm	Ce	47	52	24
Actlabs	INAA	5	ppm	Nd	24	25	20
Actlabs	INAA	0.1	ppm	Sm	4.3	4	5.3
Actlabs	INAA	0.2	ppm	Eu	0.9	1.1	1.3
Actlabs	INAA	0.5	ppm	Tb	-0.5	-0.5	-0.5
Actlabs	INAA	0.2	ppm	Yb	1.3	1.4	2.2
Actlabs	INAA	0.05	ppm	Lu	0.2	0.24	0.32
Actlabs	H. ICP-MS	0.1	ppm	Ge	-0.1	-0.1	0.1
Actlabs	H. ICP-MS	0.1	ppm	Se	0.5	0.9	3.4
Actlabs	H. ICP-MS	0.1	ppm	Te	0.2	0.8	0.9
Actlabs	H. ICP-MS	0.1	ppm	Bi	-0.1	-0.1	0.7
Actlabs	IRC	0.01	ppm	S	0.84	1.83	7.55
Actlabs	IRC	0.01	ppm	CO2	7.40	7.51	7.70

Table A.3. (cont'd)

			mineralized_zone		Anoki_Main	Anoki_Main	Anoki_Main
			Township		Gauthier	Gauthier	Gauthier
			Sample ID		AN03-61-86350	AN03-61-86356	AN03-61-86358
			sample type		drill core	drill core	drill core
			station/drill hole/stope		AN03-61	AN03-61	AN03-61
			Depth from (ft)		277.5	291	296
			Depth to (ft)		279.2	293	299.1
			utm_nad83_E		586700	586700	586700
			utm_nad83_N		5331177	5331177	5331177
Laboratory	Method	det. limit	unit				
Actlabs	Fire, grav	0.03	ppm	Au	1.71	2.33	6.72
Actlabs	ICP-OES	0.3	ppm	Ag	1.2	0.6	1.2
Actlabs	ICP-OES	0.3	ppm	Cd	1.1	1	1
Actlabs	ICP-OES	1	ppm	Cu	154	185	131
Actlabs	ICP-OES	1	ppm	Mn	1418	1361	1441
Actlabs	ICP-OES	1	ppm	Mo	3	2	4
Actlabs	ICP-OES	1	ppm	Ni	12	5	16
Actlabs	ICP-OES	3	ppm	Pb	21	12	14
Actlabs	ICP-OES	1	ppm	Zn	65	112	86
Actlabs	ICP-OES	0.01	%	Al	3.49	3.73	3.89
Actlabs	ICP-OES	1	ppm	Be	2	3	1
Actlabs	ICP-OES	0.01	%	Ca	4.94	3.55	3.79
Actlabs	ICP-OES	0.01	%	K	0.66	1.3	0.67
Actlabs	ICP-OES	0.01	%	Mg	1.71	1.28	1.77
Actlabs	ICP-OES	0.001	%	P	0.189	0.115	0.136
Actlabs	ICP-OES	1	ppm	Sr	718	740	564
Actlabs	ICP-OES	0.01	%	Ti	0.63	0.56	0.78
Actlabs	ICP-OES	2	ppm	V	92	147	100
Actlabs	ICP-OES	1	ppm	Y	12	16	10
Actlabs	INAA	2	ppb	Au_INAA			
Actlabs	INAA	0.5	ppm	As	83	56.7	44
Actlabs	INAA	50	ppm	Ba	480	1400	310
Actlabs	INAA	0.5	ppm	Br	-0.5	-0.5	-0.5
Actlabs	INAA	1	ppm	Co	32	29	32
Actlabs	INAA	2	ppm	Cr	-5	31	12
Actlabs	INAA	1	ppm	Cs	-1	-1	-1
Actlabs	INAA	0.01	%	Fe	7.17	6.21	7.68
Actlabs	INAA	1	ppm	Hf	1	2	2
Actlabs	INAA	1	ppm	Hg	-1	-1	-1
Actlabs	INAA	5	ppb	Ir	-5	-5	-5
Actlabs	INAA	0.01	%	Na	3.95	3.85	3.9
Actlabs	INAA	15	ppm	Rb	-15	-15	-15
Actlabs	INAA	0.1	ppm	Sb	1.2	1.6	1.2
Actlabs	INAA	0.1	ppm	Sc	7.2	7.3	6.9
Actlabs	INAA	0.01	%	Sn	-0.01	-0.01	-0.01
Actlabs	INAA	0.5	ppm	Ta	-0.5	-0.5	-0.5
Actlabs	INAA	0.2	ppm	Th	1.3	4.5	0.5
Actlabs	INAA	0.5	ppm	U	1.1	1.3	-0.5
Actlabs	INAA	1	ppm	W	17	17	28
Actlabs	INAA	0.5	ppm	La	10.9	28.2	7.7
Actlabs	INAA	3	ppm	Ce	24	56	20
Actlabs	INAA	5	ppm	Nd	20	27	20
Actlabs	INAA	0.1	ppm	Sm	4.8	6.1	4
Actlabs	INAA	0.2	ppm	Eu	1.5	1.6	1.2
Actlabs	INAA	0.5	ppm	Tb	-0.5	-0.5	-0.5
Actlabs	INAA	0.2	ppm	Yb	2	2.4	1.7
Actlabs	INAA	0.05	ppm	Lu	0.29	0.37	0.26
Actlabs	H. ICP-MS	0.1	ppm	Ge	0.1	0.1	-0.1
Actlabs	H. ICP-MS	0.1	ppm	Se	2.6	1.8	3.4
Actlabs	H. ICP-MS	0.1	ppm	Te	1.1	0.5	0.7
Actlabs	H. ICP-MS	0.1	ppm	Bi	0.3	0.3	0.8
Actlabs	IRC	0.01	ppm	S	4.65	5.95	6.75
Actlabs	IRC	0.01	ppm	CO2	10.08	6.71	8.98

Table A.3. (cont'd)

			mineralized_zone		McBean	McBean	McBean
			Township		Gauthier	Gauthier	Gauthier
			Sample ID		MB96-12-42878	MB96-12-42879	MB96-12-42880
			sample type		drill core	drill core	drill core
			station/drill hole/stope		MB96-12	MB96-12	MB96-12
			Depth from (ft)		1457.1	1460	1463
			Depth to (ft)		1460	1463	1464.9
			utm_nad83_E		587871	587871	587871
			utm_nad83_N		5330741	5330741	5330741
Laboratory	Method	det_limit	unit				
Actlabs	Fire, grav	0.03	ppm	Au	14.4	15.5	7.61
Actlabs	ICP-OES	0.3	ppm	Ag	0.8	0.6	2.1
Actlabs	ICP-OES	0.3	ppm	Cd	0.6	0.8	0.4
Actlabs	ICP-OES	1	ppm	Cu	169	201	45
Actlabs	ICP-OES	1	ppm	Mn	649	485	217
Actlabs	ICP-OES	1	ppm	Mo	-1	1	2
Actlabs	ICP-OES	1	ppm	Ni	105	67	50
Actlabs	ICP-OES	3	ppm	Pb	24	19	109
Actlabs	ICP-OES	1	ppm	Zn	46	41	13
Actlabs	ICP-OES	0.01	%	Al	4.65	4.71	2.16
Actlabs	ICP-OES	1	ppm	Be	3	3	1
Actlabs	ICP-OES	0.01	%	Ca	2.63	1.95	1.59
Actlabs	ICP-OES	0.01	%	K	1.96	1.69	0.39
Actlabs	ICP-OES	0.01	%	Mg	3.58	2.25	0.91
Actlabs	ICP-OES	0.001	%	P	0.212	0.245	0.09
Actlabs	ICP-OES	1	ppm	Sr	649	576	367
Actlabs	ICP-OES	0.01	%	Ti	0.35	0.37	0.14
Actlabs	ICP-OES	2	ppm	V	142	125	31
Actlabs	ICP-OES	1	ppm	Y	18	22	12
Actlabs	INAA	2	ppb	Au_INAA			
Actlabs	INAA	0.5	ppm	As	4.1	5	6.8
Actlabs	INAA	50	ppm	Ba	1250	1750	770
Actlabs	INAA	0.5	ppm	Br	-0.5	-0.5	-0.5
Actlabs	INAA	1	ppm	Co	19	17	11
Actlabs	INAA	2	ppm	Cr	161	47	116
Actlabs	INAA	1	ppm	Cs	-1	-1	-1
Actlabs	INAA	0.01	%	Fe	3.34	3.24	1.61
Actlabs	INAA	1	ppm	Hf	4	5	2
Actlabs	INAA	1	ppm	Hg	-1	-1	-1
Actlabs	INAA	5	ppb	Ir	-5	-5	-5
Actlabs	INAA	0.01	%	Na	3.27	3.93	1.6
Actlabs	INAA	15	ppm	Rb	61	-15	23
Actlabs	INAA	0.1	ppm	Sb	0.9	1.1	0.5
Actlabs	INAA	0.1	ppm	Sc	9.8	8.5	3.9
Actlabs	INAA	0.01	%	Sn	-0.01	-0.01	-0.01
Actlabs	INAA	0.5	ppm	Ta	-0.5	-0.5	-0.5
Actlabs	INAA	0.2	ppm	Th	6.2	7.1	3.1
Actlabs	INAA	0.5	ppm	U	1.5	3.4	1.2
Actlabs	INAA	1	ppm	W	16	15	6
Actlabs	INAA	0.5	ppm	La	43.4	54.9	20.2
Actlabs	INAA	3	ppm	Ce	83	104	39
Actlabs	INAA	5	ppm	Nd	44	61	20
Actlabs	INAA	0.1	ppm	Sm	8.8	11.2	4.2
Actlabs	INAA	0.2	ppm	Eu	2.1	2.6	1
Actlabs	INAA	0.5	ppm	Tb	-0.5	-0.5	-0.5
Actlabs	INAA	0.2	ppm	Yb	1.5	1.8	0.7
Actlabs	INAA	0.05	ppm	Lu	0.24	0.25	0.13
Actlabs	H_ICP-MS	0.1	ppm	Ge	0.1	0.1	-0.1
Actlabs	H_ICP-MS	0.1	ppm	Se	1.5	1.6	0.8
Actlabs	H_ICP-MS	0.1	ppm	Te	0.4	0.5	0.3
Actlabs	H_ICP-MS	0.1	ppm	Bi	0.7	1.1	1.2
Actlabs	IRC	0.01	ppm	S	2.31	2.8	1.84
Actlabs	IRC	0.01	ppm	CO2	7.59	4.95	2.53

Table A.3. (cont'd)

			mineralized_zone		McBean	McBean	McBean
			Township		Gauthier	Gauthier	Gauthier
			Sample ID		MB96-12-42907	MB96-12-42910	MB96-12-42915
			sample type		drill core	drill core	drill core
			station/drill hole/stope		MB96-12	MB96-12	MB96-12
			Depth from (ft)		1536	1542.5	1557
			Depth to (ft)		1537.9	1545	1558.9
			utm_nad83_E		587871	587871	587871
			utm_nad83_N		5330741	5330741	5330741
Laboratory	Method	det. limit	unit				
Actlabs	Fire, grav	0.03	ppm	Au	0.82	3.43	2.54
Actlabs	ICP-OES	0.3	ppm	Ag	-0.3	0.3	-0.3
Actlabs	ICP-OES	0.3	ppm	Cd	0.6	-0.3	-0.3
Actlabs	ICP-OES	1	ppm	Cu	113	45	62
Actlabs	ICP-OES	1	ppm	Mn	1052	1188	1088
Actlabs	ICP-OES	1	ppm	Mo	2	6	3
Actlabs	ICP-OES	1	ppm	Ni	130	891	704
Actlabs	ICP-OES	3	ppm	Pb	19	11	10
Actlabs	ICP-OES	1	ppm	Zn	61	57	72
Actlabs	ICP-OES	0.01	%	Al	4.35	1.99	3.23
Actlabs	ICP-OES	1	ppm	Be	2	1	2
Actlabs	ICP-OES	0.01	%	Ca	4.72	4.33	3.36
Actlabs	ICP-OES	0.01	%	K	1.32	1.79	2.23
Actlabs	ICP-OES	0.01	%	Mg	6.81	14.12	12.11
Actlabs	ICP-OES	0.001	%	P	0.309	0.011	0.057
Actlabs	ICP-OES	1	ppm	Sr	1286	510	277
Actlabs	ICP-OES	0.01	%	Ti	0.31	0.15	0.24
Actlabs	ICP-OES	2	ppm	V	132	113	139
Actlabs	ICP-OES	1	ppm	Y	18	3	6
Actlabs	INAA	2	ppb	Au_INAA			
Actlabs	INAA	0.5	ppm	As	4.9	5.6	6.5
Actlabs	INAA	50	ppm	Ba	2250	515	230
Actlabs	INAA	0.5	ppm	Br	-0.5	-0.5	-0.5
Actlabs	INAA	1	ppm	Co	32	61	48
Actlabs	INAA	2	ppm	Cr	359	1560	1190
Actlabs	INAA	1	ppm	Cs	-1	-1	-1
Actlabs	INAA	0.01	%	Fe	4.31	4.84	4.77
Actlabs	INAA	1	ppm	Hf	3	-1	-1
Actlabs	INAA	1	ppm	Hg	-1	1	-1
Actlabs	INAA	5	ppb	Ir	-5	-5	-5
Actlabs	INAA	0.01	%	Na	2.81	0.04	0.99
Actlabs	INAA	15	ppm	Rb	-15	40	48
Actlabs	INAA	0.1	ppm	Sb	1.5	1.6	1.4
Actlabs	INAA	0.1	ppm	Sc	17.4	15.8	16.9
Actlabs	INAA	0.01	%	Sn	-0.01	-0.01	-0.01
Actlabs	INAA	0.5	ppm	Ta	-0.5	-0.5	-0.5
Actlabs	INAA	0.2	ppm	Th	5.4	-0.2	1.5
Actlabs	INAA	0.5	ppm	U	-0.5	0.7	1
Actlabs	INAA	1	ppm	W	13	12	16
Actlabs	INAA	0.5	ppm	La	40.3	1.6	10
Actlabs	INAA	3	ppm	Ce	80	5	21
Actlabs	INAA	5	ppm	Nd	46	-5	13
Actlabs	INAA	0.1	ppm	Sm	8.4	0.7	2.4
Actlabs	INAA	0.2	ppm	Eu	1.9	0.3	0.6
Actlabs	INAA	0.5	ppm	Tb	-0.5	-0.5	-0.5
Actlabs	INAA	0.2	ppm	Yb	1.4	0.6	0.7
Actlabs	INAA	0.05	ppm	Lu	0.24	0.1	0.09
Actlabs	H ICP-MS	0.1	ppm	Ge	0.1	-0.1	-0.1
Actlabs	H ICP-MS	0.1	ppm	Se	1.4	0.4	0.9
Actlabs	H ICP-MS	0.1	ppm	Te	0.4	0.4	0.4
Actlabs	H ICP-MS	0.1	ppm	Bi	3.1	0.4	-0.1
Actlabs	IRC	0.01	ppm	S	0.94	0.29	0.91
Actlabs	IRC	0.01	ppm	CO2	16.12	25.83	20.34

Table A.3. (cont'd)

			mineralized_zone		Kirkland Lake Narrows Break	Kirkland Lake Narrows Break	Kirkland Lake Narrows Break
			Township		Teck	Teck	Teck
			Sample ID		004VOI1520-1	004VOI1522-1	004VOI1523-1
			sample type		surface	surface	surface
			station/drill hole/stope		004VOI1520	004VOI1522	004VOI1523
			Depth from (ft)				
			Depth to (ft)				
			utm_nad83_E		569871	569877	569882
			utm_nad83_N		5333226	5333231	5333238
Laboratory	Method	det. limit	unit				
Actlabs	Fire grav	0.03	ppm	Au	12	60.8	96.7
Actlabs	ICP-OES	0.3	ppm	Ag	0.5	2.4	2
Actlabs	ICP-OES	0.3	ppm	Cd	0.6	1	0.4
Actlabs	ICP-OES	1	ppm	Cu	44	58	79
Actlabs	ICP-OES	1	ppm	Mn	846	142	870
Actlabs	ICP-OES	1	ppm	Mo	12	31	5
Actlabs	ICP-OES	1	ppm	Ni	91	96	93
Actlabs	ICP-OES	3	ppm	Pb	22	45	26
Actlabs	ICP-OES	1	ppm	Zn	65	54	80
Actlabs	ICP-OES	0.01	%	Al	3.17	4.05	3.08
Actlabs	ICP-OES	1	ppm	Be	2	3	2
Actlabs	ICP-OES	0.01	%	Ca	3.53	0.88	4.9
Actlabs	ICP-OES	0.01	%	K	2.82	3.45	7.05
Actlabs	ICP-OES	0.01	%	Mg	2.2	0.85	3.18
Actlabs	ICP-OES	0.001	%	P	0.048	0.032	0.165
Actlabs	ICP-OES	1	ppm	Sr	789	254	825
Actlabs	ICP-OES	0.01	%	Ti	0.3	0.45	0.42
Actlabs	ICP-OES	2	ppm	V	278	585	332
Actlabs	ICP-OES	1	ppm	Y	9	12	15
Actlabs	INAA	2	ppb	Au_INAA			
Actlabs	INAA	0.5	ppm	As	9.3	11.8	13.9
Actlabs	INAA	50	ppm	Ba	770	930	1300
Actlabs	INAA	0.5	ppm	Br	-0.5	-0.5	-0.5
Actlabs	INAA	1	ppm	Co	17	24	25
Actlabs	INAA	2	ppm	Cr	220	258	211
Actlabs	INAA	1	ppm	Cs	1	2	2
Actlabs	INAA	0.01	%	Fe	3.16	5.01	4.24
Actlabs	INAA	1	ppm	Hf	2	4	2
Actlabs	INAA	1	ppm	Hg	-1	-1	-1
Actlabs	INAA	5	ppb	Ir	-5	-5	-5
Actlabs	INAA	0.01	%	Na	2.1	2.94	0.45
Actlabs	INAA	15	ppm	Rb	59	74	77
Actlabs	INAA	0.1	ppm	Sb	1	1.4	0.9
Actlabs	INAA	0.1	ppm	Sc	12.9	8.4	12.8
Actlabs	INAA	0.01	%	Sn	-0.01	-0.03	-0.01
Actlabs	INAA	0.5	ppm	Ta	-0.5	-0.6	-0.5
Actlabs	INAA	0.2	ppm	Th	2	3.6	4.7
Actlabs	INAA	0.5	ppm	U	1.7	-0.7	1.6
Actlabs	INAA	1	ppm	W	7	10	9
Actlabs	INAA	0.5	ppm	La	16.1	49.7	28.9
Actlabs	INAA	3	ppm	Ce	29	80	51
Actlabs	INAA	5	ppm	Nd	18	50	28
Actlabs	INAA	0.1	ppm	Sm	3	7.3	5.2
Actlabs	INAA	0.2	ppm	Eu	0.6	2.1	1.4
Actlabs	INAA	0.5	ppm	Tb	-0.5	-0.5	-0.5
Actlabs	INAA	0.2	ppm	Yb	0.7	-0.2	1.3
Actlabs	INAA	0.05	ppm	Lu	0.11	-0.05	0.23
Actlabs	H ICP-MS	0.1	ppm	Ge	-0.1	0.1	0.2
Actlabs	H ICP-MS	0.1	ppm	Se	0.5	1.4	1.7
Actlabs	H ICP-MS	0.1	ppm	Te	1	6.4	2.1
Actlabs	H ICP-MS	0.1	ppm	Bi	-0.1	-0.1	-0.1
Actlabs	IRC	0.01	ppm	S	1.17	5.35	2.11
Actlabs	IRC	0.01	ppm	CO2	7.07	1.80	8.43

Table A.3. (cont'd)

			mineralized_zone		Kirkland Lake (Macassa)	Kirkland Lake (Macassa)	Kirkland Lake (Macassa)
			Township		Teck	Teck	Teck
			Sample ID		3829	3829-2	3829D
			sample type		underground	underground	underground
			station/drill hole/stope		stope 3829	stope 3829	stope 3829
			Depth from (ft) Depth to (ft)				
			utm_nad83_E utm_nad83_N				
Laboratory	Method	det. limit	unit				
Actlabs	Fire, grav	0.03	ppm	Au	17	4.39	88.5
Actlabs	ICP-OES	0.3	ppm	Ag	3	4.5	14
Actlabs	ICP-OES	0.3	ppm	Cd	-0.3	0.5	-0.3
Actlabs	ICP-OES	1	ppm	Cu	12	82	586
Actlabs	ICP-OES	1	ppm	Mn	281	537	325
Actlabs	ICP-OES	1	ppm	Mo	446	62	2450
Actlabs	ICP-OES	1	ppm	Ni	19	45	29
Actlabs	ICP-OES	3	ppm	Pb	52	31	374
Actlabs	ICP-OES	1	ppm	Zn	8	28	15
Actlabs	ICP-OES	0.01	%	Al	0.79	2.31	0.84
Actlabs	ICP-OES	1	ppm	Be	1	2	-1
Actlabs	ICP-OES	0.01	%	Ca	1.25	2.82	1.24
Actlabs	ICP-OES	0.01	%	K	1.59	4.53	1.58
Actlabs	ICP-OES	0.01	%	Mg	0.69	1.74	0.75
Actlabs	ICP-OES	0.001	%	P	0.004	0.025	0.007
Actlabs	ICP-OES	1	ppm	Sr	904	625	937
Actlabs	ICP-OES	0.01	%	Ti	0.07	0.21	0.06
Actlabs	ICP-OES	2	ppm	V	43	119	42
Actlabs	ICP-OES	1	ppm	Y	3	9	4
Actlabs	INAA	2	ppb	Au_INAA			
Actlabs	INAA	0.5	ppm	As	8.9	14.6	5.4
Actlabs	INAA	50	ppm	Ba	1750	780	1500
Actlabs	INAA	0.5	ppm	Br	1.8	-0.5	-0.5
Actlabs	INAA	1	ppm	Co	5	13	10
Actlabs	INAA	2	ppm	Cr	180	103	176
Actlabs	INAA	1	ppm	Cs	-1	-1	-1
Actlabs	INAA	0.01	%	Fe	1.11	2.11	1.74
Actlabs	INAA	1	ppm	Hf	-1	2	-1
Actlabs	INAA	1	ppm	Hg	-1	-1	2
Actlabs	INAA	5	ppb	Ir	-5	-5	-5
Actlabs	INAA	0.01	%	Na	0.05	0.16	0.03
Actlabs	INAA	15	ppm	Rb	20	68	32
Actlabs	INAA	0.1	ppm	Sb	3.1	6.7	14.1
Actlabs	INAA	0.1	ppm	Sc	1.8	7	1.7
Actlabs	INAA	0.01	%	Sn	-0.01	-0.01	-0.02
Actlabs	INAA	0.5	ppm	Ta	-0.5	-0.5	-0.5
Actlabs	INAA	0.2	ppm	Th	1	2.5	0.9
Actlabs	INAA	0.5	ppm	U	-0.5	0.7	-0.5
Actlabs	INAA	1	ppm	W	3	12	3
Actlabs	INAA	0.5	ppm	La	4.8	15.5	5.3
Actlabs	INAA	3	ppm	Ce	9	30	11
Actlabs	INAA	5	ppm	Nd	-5	17	-5
Actlabs	INAA	0.1	ppm	Sm	1	2.5	1.4
Actlabs	INAA	0.2	ppm	Eu	-0.2	0.6	-0.2
Actlabs	INAA	0.5	ppm	Tb	-0.5	-0.5	-0.5
Actlabs	INAA	0.2	ppm	Yb	-0.2	0.7	-0.2
Actlabs	INAA	0.05	ppm	Lu	-0.05	0.09	-0.05
Actlabs	H. ICP-MS	0.1	ppm	Ge	-0.1	-0.1	-0.1
Actlabs	H. ICP-MS	0.1	ppm	Se	0.7	1.6	2.9
Actlabs	H. ICP-MS	0.1	ppm	Te	26.7	19	170
Actlabs	H. ICP-MS	0.1	ppm	Bi	0.4	-0.1	0.7
Actlabs	IRC	0.01	ppm	S	0.8	2.39	1.93
Actlabs	IRC	0.01	ppm	CO2	2.16	5.42	2.42

Table A.3. (cont'd)

			mineralized_zone		Kirkland Lake (Macassa)	Kirkland Lake (Macassa)	Kirkland Lake (Macassa)
			Township		Teck	Teck	Teck
			Sample ID		4206	4229-5Q	4506
			sample type		underground	underground	underground
			station/drill hole/stope		stope 4206	stope 4229-5	stope 4506
			Depth from (ft) Depth to (ft)				
			utm_nad83_E utm_nad83_N				
Laboratory	Method	det. limit	unit				
Actlabs	Fire. grav	0.03	ppm	Au	88.5	181	183
Actlabs	ICP-OES	0.3	ppm	Ag	6.1	8.4	11.5
Actlabs	ICP-OES	0.3	ppm	Cd	-0.3	0.4	0.4
Actlabs	ICP-OES	1	ppm	Cu	16	69	66
Actlabs	ICP-OES	1	ppm	Mn	221	327	485
Actlabs	ICP-OES	1	ppm	Mo	315	165	250
Actlabs	ICP-OES	1	ppm	Ni	16	43	47
Actlabs	ICP-OES	3	ppm	Pb	77	106	65
Actlabs	ICP-OES	1	ppm	Zn	9	23	26
Actlabs	ICP-OES	0.01	%	Al	0.73	1.43	2.51
Actlabs	ICP-OES	1	ppm	Be	-1	2	2
Actlabs	ICP-OES	0.01	%	Ca	1.05	1.68	2.35
Actlabs	ICP-OES	0.01	%	K	1.23	2.02	4.33
Actlabs	ICP-OES	0.01	%	Mg	0.59	0.97	1.59
Actlabs	ICP-OES	0.001	%	P	0.012	0.036	0.049
Actlabs	ICP-OES	1	ppm	Sr	247	340	228
Actlabs	ICP-OES	0.01	%	Ti	0.06	0.13	0.25
Actlabs	ICP-OES	2	ppm	V	35	102	206
Actlabs	ICP-OES	1	ppm	Y	3	5	12
Actlabs	INAA	2	ppb	Au_INAA			
Actlabs	INAA	0.5	ppm	As	4.8	10.6	4.3
Actlabs	INAA	50	ppm	Ba	260	388	1150
Actlabs	INAA	0.5	ppm	Br	-0.5	-0.5	-0.5
Actlabs	INAA	1	ppm	Co	7	15	19
Actlabs	INAA	2	ppm	Cr	43	195	135
Actlabs	INAA	1	ppm	Cs	-1	-1	2
Actlabs	INAA	0.01	%	Fe	1.1	2.43	3.23
Actlabs	INAA	1	ppm	Hf	-1	-1	3
Actlabs	INAA	1	ppm	Hg	-1	8	-3
Actlabs	INAA	5	ppb	Ir	-5	-5	-5
Actlabs	INAA	0.01	%	Na	0.03	0.08	0.27
Actlabs	INAA	15	ppm	Rb	21	66	81
Actlabs	INAA	0.1	ppm	Sb	2.5	15.5	2.2
Actlabs	INAA	0.1	ppm	Sc	2.1	4.6	7.5
Actlabs	INAA	0.01	%	Sn	-0.03	-0.06	-0.07
Actlabs	INAA	0.5	ppm	Ta	-0.5	-0.5	-0.5
Actlabs	INAA	0.2	ppm	Th	-0.3	-0.6	3
Actlabs	INAA	0.5	ppm	U	-0.7	-1.7	-1.7
Actlabs	INAA	1	ppm	W	5	6	11
Actlabs	INAA	0.5	ppm	La	6.5	9.3	26.2
Actlabs	INAA	3	ppm	Ce	-3	-6	69
Actlabs	INAA	5	ppm	Nd	-5	32	-9
Actlabs	INAA	0.1	ppm	Sm	1.2	1.9	4.7
Actlabs	INAA	0.2	ppm	Eu	0.7	1.3	0.8
Actlabs	INAA	0.5	ppm	Tb	-0.5	-0.5	-0.5
Actlabs	INAA	0.2	ppm	Yb	-0.2	-0.3	-0.2
Actlabs	INAA	0.05	ppm	Lu	-0.05	-0.07	-0.07
Actlabs	H ICP-MS	0.1	ppm	Ge	-0.1	-0.1	-0.1
Actlabs	H ICP-MS	0.1	ppm	Se	0.9	1.1	1.5
Actlabs	H ICP-MS	0.1	ppm	Te	156	305	318
Actlabs	H ICP-MS	0.1	ppm	Bi	1.6	0.2	0.2
Actlabs	IRC	0.01	ppm	S	0.76	1.26	2.37
Actlabs	IRC	0.01	ppm	CO2	1.98	3.08	4.29

Table A.3. (cont'd)

			mineralized_zone		Kirkland Lake (Macassa)	Kirkland Lake (Macassa)	Kirkland Lake (Macassa)
			Township		Teck	Teck	Teck
			Sample ID		4528	4744	4940-1
			sample type		underground	underground	underground
			station/drill hole/stope		stope 4528	stope 4744	stope 4940
			Depth from (ft) Depth to (ft)				
			utm_nad83_E utm_nad83_N				
Laboratory	Method	det. limit	unit				
Actlabs	Fire. grav	0.03	ppm	Au	414	361	193
Actlabs	ICP-OES	0.3	ppm	Ag	26.3	11.8	35.1
Actlabs	ICP-OES	0.3	ppm	Cd	0.4	0.4	-0.3
Actlabs	ICP-OES	1	ppm	Cu	332	45	15
Actlabs	ICP-OES	1	ppm	Mn	522	412	252
Actlabs	ICP-OES	1	ppm	Mo	260	469	513
Actlabs	ICP-OES	1	ppm	Ni	42	44	27
Actlabs	ICP-OES	3	ppm	Pb	160	258	299
Actlabs	ICP-OES	1	ppm	Zn	24	26	5
Actlabs	ICP-OES	0.01	%	Al	1.93	1.92	0.33
Actlabs	ICP-OES	1	ppm	Be	2	2	2
Actlabs	ICP-OES	0.01	%	Ca	2.61	2.04	1.02
Actlabs	ICP-OES	0.01	%	K	3.83	3.34	0.66
Actlabs	ICP-OES	0.01	%	Mg	1.37	1.49	0.54
Actlabs	ICP-OES	0.001	%	P	0.061	0.061	0.004
Actlabs	ICP-OES	1	ppm	Sr	369	504	224
Actlabs	ICP-OES	0.01	%	Ti	0.19	0.19	0.03
Actlabs	ICP-OES	2	ppm	V	107	122	22
Actlabs	ICP-OES	1	ppm	Y	9	8	2
Actlabs	INAA	2	ppb	Au_INAA			
Actlabs	INAA	0.5	ppm	As	8.2	-0.9	5.6
Actlabs	INAA	50	ppm	Ba	505	1200	110
Actlabs	INAA	0.5	ppm	Br	-0.9	-0.8	-0.5
Actlabs	INAA	1	ppm	Co	16	19	6
Actlabs	INAA	2	ppm	Cr	301	86	236
Actlabs	INAA	1	ppm	Cs	-1	5	-1
Actlabs	INAA	0.01	%	Fe	2.3	2.79	1.09
Actlabs	INAA	1	ppm	Hf	-1	4	-1
Actlabs	INAA	1	ppm	Hg	-8	-6	-3
Actlabs	INAA	5	ppb	Ir	-10	-10	-5
Actlabs	INAA	0.01	%	Na	0.08	0.18	0.03
Actlabs	INAA	15	ppm	Rb	39	58	-15
Actlabs	INAA	0.1	ppm	Sb	1.7	3	1.4
Actlabs	INAA	0.1	ppm	Sc	6.5	6.5	1.6
Actlabs	INAA	0.01	%	Sn	-0.17	-0.14	-0.06
Actlabs	INAA	0.5	ppm	Ta	-0.7	-0.7	-0.5
Actlabs	INAA	0.2	ppm	Th	-1.9	-1.6	-0.6
Actlabs	INAA	0.5	ppm	U	-4.6	-3.7	-1.6
Actlabs	INAA	1	ppm	W	8	-1	-1
Actlabs	INAA	0.5	ppm	La	19.6	19.7	2.9
Actlabs	INAA	3	ppm	Ce	-16	-13	-6
Actlabs	INAA	5	ppm	Nd	-22	-20	16
Actlabs	INAA	0.1	ppm	Sm	3.5	3.4	0.6
Actlabs	INAA	0.2	ppm	Eu	-0.3	-0.3	-0.2
Actlabs	INAA	0.5	ppm	Tb	-0.5	0.9	-0.5
Actlabs	INAA	0.2	ppm	Yb	-0.6	-0.6	-0.2
Actlabs	INAA	0.05	ppm	Lu	-0.19	-0.16	-0.07
Actlabs	H ICP-MS	0.1	ppm	Ge	-0.1	-0.1	-0.1
Actlabs	H ICP-MS	0.1	ppm	Se	1.3	1.2	1.3
Actlabs	H ICP-MS	0.1	ppm	Te	698	502	349
Actlabs	H ICP-MS	0.1	ppm	Bi	-0.1	0.5	0.9
Actlabs	IRC	0.01	ppm	S	1.54	1.51	0.51
Actlabs	IRC	0.01	ppm	CO2	3.96	3.59	1.91

Table A.3. (cont'd)

			mineralized_zone		Kirkland Lake (Macassa)	Kirkland Lake (Macassa)	Kirkland Lake (Teck Hughes)
			Township		Teck	Teck	Teck
			Sample ID		4940-3	4512-2	1254-1
			sample type		underground	underground	surface
			station/drill hole/stope		stope 4940	stope 4512	004VOI1254
			Depth from (ft)				
			Depth to (ft)				
			utm_nad83_E				570493
			utm_nad83_N				5333201
Laboratory	Method	det. limit	unit				
Actlabs	Fire, grav	0.03	ppm	Au	100	11.7	61.6
Actlabs	ICP-OES	0.3	ppm	Ag	11.4	4	5.5
Actlabs	ICP-OES	0.3	ppm	Cd	-0.3	-0.3	-0.3
Actlabs	ICP-OES	1	ppm	Cu	73	168	28
Actlabs	ICP-OES	1	ppm	Mn	343	736	422
Actlabs	ICP-OES	1	ppm	Mo	199	1211	284
Actlabs	ICP-OES	1	ppm	Ni	24	9	25
Actlabs	ICP-OES	3	ppm	Pb	42	108	105
Actlabs	ICP-OES	1	ppm	Zn	12	22	15
Actlabs	ICP-OES	0.01	%	Al	0.26	0.88	1.32
Actlabs	ICP-OES	1	ppm	Be	-1	1	-1
Actlabs	ICP-OES	0.01	%	Ca	1.56	2.55	1.47
Actlabs	ICP-OES	0.01	%	K	0.28	1.31	1.94
Actlabs	ICP-OES	0.01	%	Mg	0.9	0.81	0.78
Actlabs	ICP-OES	0.001	%	P	0.012	0.105	0.019
Actlabs	ICP-OES	1	ppm	Sr	394	723	262
Actlabs	ICP-OES	0.01	%	Ti	0.02	0.14	0.05
Actlabs	ICP-OES	2	ppm	V	27	74	67
Actlabs	ICP-OES	1	ppm	Y	2	10	5
Actlabs	INAA	2	ppb	Au_INAA			
Actlabs	INAA	0.5	ppm	As	2.3	9.1	3.4
Actlabs	INAA	50	ppm	Ba	440	670	1850
Actlabs	INAA	0.5	ppm	Br	-0.5	-0.5	1.9
Actlabs	INAA	1	ppm	Co	4	10	5
Actlabs	INAA	2	ppm	Cr	31	168	30
Actlabs	INAA	1	ppm	Cs	-1	-1	1
Actlabs	INAA	0.01	%	Fe	1.05	1.71	1.04
Actlabs	INAA	1	ppm	Hf	1	2	-1
Actlabs	INAA	1	ppm	Hg	-1	-1	-1
Actlabs	INAA	5	ppb	Ir	-5	-5	-5
Actlabs	INAA	0.01	%	Na	0.05	0.18	0.08
Actlabs	INAA	15	ppm	Rb	17	35	41
Actlabs	INAA	0.1	ppm	Sb	0.6	3	4.1
Actlabs	INAA	0.1	ppm	Sc	2	4	1.5
Actlabs	INAA	0.01	%	Sn	-0.04	-0.01	-0.01
Actlabs	INAA	0.5	ppm	Ta	-0.5	-0.5	-0.5
Actlabs	INAA	0.2	ppm	Th	-0.3	4.3	1.7
Actlabs	INAA	0.5	ppm	U	-0.8	-0.5	-0.5
Actlabs	INAA	1	ppm	W	-1	5	4
Actlabs	INAA	0.5	ppm	La	2.8	25	8.9
Actlabs	INAA	3	ppm	Ce	-3	47	15
Actlabs	INAA	5	ppm	Nd	-5	23	-5
Actlabs	INAA	0.1	ppm	Sm	0.8	4.1	1.5
Actlabs	INAA	0.2	ppm	Eu	-0.2	1	0.4
Actlabs	INAA	0.5	ppm	Tb	-0.5	-0.5	-0.5
Actlabs	INAA	0.2	ppm	Yb	-0.2	0.5	0.3
Actlabs	INAA	0.05	ppm	Lu	-0.05	0.1	-0.05
Actlabs	H. ICP-MS	0.1	ppm	Ge	-0.1	-0.1	-0.1
Actlabs	H. ICP-MS	0.1	ppm	Se	0.9	1.3	0.6
Actlabs	H. ICP-MS	0.1	ppm	Te	107	43.5	79.8
Actlabs	H. ICP-MS	0.1	ppm	Bi	0.8	0.8	0.2
Actlabs	IRC	0.01	ppm	S	0.19	1.17	0.41
Actlabs	IRC	0.01	ppm	CO2	2.97	3.59	2.93

Table A.3. (cont'd)

			mineralized_zone		Kirkland Lake (Teck Hughes)	Kirkland Lake (Lake Shore)
			Township		Teck	Teck
			Sample ID		1254-2	LS
			sample type		surface	surface
			station/drill hole/stope		004VOI1254	004VOI1532
			Depth from (ft) Depth to (ft)			
			utm_nad83_E		570493	571031
			utm_nad83_N		5333201	5333353
Laboratory	Method	det. limit	unit			
Actlabs	Fire, grav	0.03	ppm	Au	68.2	425
Actlabs	ICP-OES	0.3	ppm	Ag	13.8	16.6
Actlabs	ICP-OES	0.3	ppm	Cd	0.7	0.3
Actlabs	ICP-OES	1	ppm	Cu	11	28
Actlabs	ICP-OES	1	ppm	Mn	125	111
Actlabs	ICP-OES	1	ppm	Mo	623	489
Actlabs	ICP-OES	1	ppm	Ni	50	21
Actlabs	ICP-OES	3	ppm	Pb	136	670
Actlabs	ICP-OES	1	ppm	Zn	30	43
Actlabs	ICP-OES	0.01	%	Al	3.21	0.94
Actlabs	ICP-OES	1	ppm	Be	3	-1
Actlabs	ICP-OES	0.01	%	Ca	0.5	0.37
Actlabs	ICP-OES	0.01	%	K	3.76	1.14
Actlabs	ICP-OES	0.01	%	Mg	0.67	0.23
Actlabs	ICP-OES	0.001	%	P	0.03	0.015
Actlabs	ICP-OES	1	ppm	Sr	143	251
Actlabs	ICP-OES	0.01	%	Ti	0.13	0.04
Actlabs	ICP-OES	2	ppm	V	350	47
Actlabs	ICP-OES	1	ppm	Y	9	3
Actlabs	INAA	2	ppb	Au_INAA		
Actlabs	INAA	0.5	ppm	As	4.9	4
Actlabs	INAA	50	ppm	Ba	565	1020
Actlabs	INAA	0.5	ppm	Br	-0.5	2.1
Actlabs	INAA	1	ppm	Co	10	4
Actlabs	INAA	2	ppm	Cr	94	84
Actlabs	INAA	1	ppm	Cs	3	-1
Actlabs	INAA	0.01	%	Fe	1.62	0.88
Actlabs	INAA	1	ppm	Hf	2	-1
Actlabs	INAA	1	ppm	Hg	-1	-5
Actlabs	INAA	5	ppb	Ir	-5	-17
Actlabs	INAA	0.01	%	Na	0.04	0.03
Actlabs	INAA	15	ppm	Rb	134	-15
Actlabs	INAA	0.1	ppm	Sb	6.7	11.7
Actlabs	INAA	0.1	ppm	Sc	3.8	0.8
Actlabs	INAA	0.01	%	Sn	-0.02	-0.12
Actlabs	INAA	0.5	ppm	Ta	-0.5	-0.5
Actlabs	INAA	0.2	ppm	Th	3	-1.7
Actlabs	INAA	0.5	ppm	U	-0.5	-4
Actlabs	INAA	1	ppm	W	12	-1
Actlabs	INAA	0.5	ppm	La	23.9	8.5
Actlabs	INAA	3	ppm	Ce	49	69
Actlabs	INAA	5	ppm	Nd	22	-12
Actlabs	INAA	0.1	ppm	Sm	3.5	1
Actlabs	INAA	0.2	ppm	Eu	0.8	-0.2
Actlabs	INAA	0.5	ppm	Tb	0.5	-0.5
Actlabs	INAA	0.2	ppm	Yb	0.5	-0.5
Actlabs	INAA	0.05	ppm	Lu	0.08	-0.19
Actlabs	H ICP-MS	0.1	ppm	Ge	-0.1	-0.1
Actlabs	H ICP-MS	0.1	ppm	Se	1.3	1.5
Actlabs	H ICP-MS	0.1	ppm	Te	123	729
Actlabs	H ICP-MS	0.1	ppm	Bi	0.2	0.3
Actlabs	IRC	0.01	ppm	S	1.05	0.43
Actlabs	IRC	0.01	ppm	CO2	0.88	0.73

Table A.4. Analytical results for mineralized samples from Upper Canada Mine: trace elements, analyses by Geolabs and Actlabs.

			mineralized zone		Upper Canada L zone	Upper Canada L zone	Upper Canada L zone	Upper Canada L zone
			Township		Gauthier	Gauthier	Gauthier	Gauthier
			Sample ID		3-3	7-1	7-2	7-3
			station/drill hole/stope		"L" stripping	"L" stripping	"L" stripping	"L" stripping
			utm nad83 E		586435.34	586419.24	586418.86	586418.14
			utm nad83 N		5332391.13	5332384.05	5332384.99	5332387.2
Laboratory	Method	det. limit	unit					
Geolabs	MS-IAT	6 ppb	ppm	Au	1.33	1.69	4.69	1.19
Actlabs	INAA	2	ppb	Au				
Geolabs	AAS-Flame	2	ppm	Ag	4	3	8	4
Actlabs	ICP-OES	0.3	ppm	Cd				
Geolabs	ICP-AES	3	ppm	Cu	84	56	39	81
Geolabs	XRF	2	ppm	Mo	8	5	27	-2
Geolabs	ICP-AES	3	ppm	Ni	14	22	22	22
Geolabs	XRF	5	ppm	Pb	58	24	32	18
Geolabs	ICP-AES	2	ppm	Zn	30	46	55	57
Geolabs	ICP-AES	0.1	ppm	Be	0.28	1.73	1.79	1.53
Geolabs	ICP-AES	0.7	ppm	Sr	579.6	356.5	661.3	581.8
Geolabs	ICP-AES	0.6	ppm	V	43.8	188	251.3	175
Geolabs	XRF	1	ppm	As	46	48	47	82
Geolabs	ICP-AES	0.8	ppm	Ba	3079.5	1354.4	491.1	409
Geolabs	ICP-AES	1	ppm	Co	12	23	19	25
Geolabs	XRF	4	ppm	Cr	45	104	107	109
Geolabs	ICP-MS	0.05	ppm	Rb	186.79	229.251	183.834	210.487
Geolabs	MS-AHT	0.02	ppm	Sb	3.67	6.95	6.79	6.16
Geolabs	ICP-AES	0.3	ppm	Sc	8.1	14.1	12.3	15
Geolabs	ICP-AES	2	ppm	W	9	18	15	21
Geolabs	IRC	0.01	%	S	1.78	4.77	4.45	4.16
Geolabs	IRC	0.03	%	CO2	2.47	2.65	6.03	4
Actlabs	H. ICP-MS	0.1	ppm	Ge	-0.1	-0.1	-0.1	-0.1
Actlabs	H. ICP-MS	0.1	ppm	Se	2	1.8	2.4	2.7
Actlabs	H. ICP-MS	0.1	ppm	Te	3.5	1.9	8.6	3
Actlabs	H. ICP-MS	0.1	ppm	Bi	2	0.3	0.9	0.5
Geolabs	MS-IAT	2	ppb	Pd	-1	-1	-1	-1
Geolabs	MS-IAT	1	ppb	Pt	-1	1.37	1.98	1.73

Table A.4. (cont'd)

			mineralized zone		Upper Canada L zone	Upper Canada L zone	Upper Canada L zone	Upper Canada L zone
			Township		Gauthier	Gauthier	Gauthier	Gauthier
			Sample ID		8-1	9-1	10-1	11-1
			station/drill hole/stope		"L" stripping	"L" stripping	"L" stripping	"L" stripping
			utm nad83 E		586412.12	586412.09	586409.93	586407.45
			utm nad83 N		5332388.29	5332382.72	5332380.21	5332380.21
Laboratory	Method	det. limit	unit					
Geolabs	MS-IAT	6 ppb	ppm	Au	0.174	0.9	3.55	9.15
Actlabs	INAA	2	ppb	Au				
Geolabs	AAS-Flame	2	ppm	Ag	4	5	3	4
Actlabs	ICP-OES	0.3	ppm	Cd				
Geolabs	ICP-AES	3	ppm	Cu	74	41	99	90
Geolabs	XRF	2	ppm	Mo	35	5	-2	-2
Geolabs	ICP-AES	3	ppm	Ni	22	19	19	20
Geolabs	XRF	5	ppm	Pb	294	34	13	16
Geolabs	ICP-AES	2	ppm	Zn	1102	66	70	64
Geolabs	ICP-AES	0.1	ppm	Be	2.9	2.35	0.9	1.13
Geolabs	ICP-AES	0.7	ppm	Sr	145.3	161.5	1251.8	944.7
Geolabs	ICP-AES	0.6	ppm	V	154.8	160.9	138.8	175.8
Geolabs	XRF	1	ppm	As	154	51	85	99
Geolabs	ICP-AES	0.8	ppm	Ba	1052.2	655.3	1588.5	1159.2
Geolabs	ICP-AES	1	ppm	Co	20	17	18	21
Geolabs	XRF	4	ppm	Cr	113	99	88	85
Geolabs	ICP-MS	0.05	ppm	Rb	218.331	219.514	156.53	191.497
Geolabs	MS-AHT	0.02	ppm	Sb	7.09	6.65	11.14	11.57
Geolabs	ICP-AES	0.3	ppm	Sc	13.3	10.9	11.3	12.4
Geolabs	ICP-AES	2	ppm	W	8	11	23	23
Geolabs	IRC	0.01	%	S	3.56	3.26	1.41	2.55
Geolabs	IRC	0.03	%	CO2	0.65	0.13	13	9.45
Actlabs	H. ICP-MS	0.1	ppm	Ge	0.1	-0.1	-0.1	-0.1
Actlabs	H. ICP-MS	0.1	ppm	Se	11	2.8	0.9	1.3
Actlabs	H. ICP-MS	0.1	ppm	Te	2.9	2.4	1.6	4.5
Actlabs	H. ICP-MS	0.1	ppm	Bi	7.5	0.6	-0.1	0.6
Geolabs	MS-IAT	2	ppb	Pd	6.72	-1	-1	-1
Geolabs	MS-IAT	1	ppb	Pt	23	3.95	-1	1.14

Table A.4. (cont'd)

			mineralized zone		Upper Canada L zone	Upper Canada L zone	Upper Canada	Upper Canada
			Township		Gauthier	Gauthier	Gauthier	Gauthier
			Sample ID		12-1	13-1	003VOI0526-1	L4-2
			station/drill hole/stope		"L" stripping	"L" stripping	003VOI0526	"L4" stripping
			utm nad83 E		586404.94	586400.39	586276.1	586383.48
			utm nad83 N		5332379.84	5332380.15	5332274.83	5332344.94
Laboratory	Method	det. limit	unit					
Geolabs	MS-IAT	6 ppb	ppm	Au	3.15	1.1		
Actlabs	INAA	2	ppb	Au			135	462
Geolabs	AAS-Flame	2	ppm	Ag	3	3	0.3[1]	3.1[1]
Actlabs	ICP-OES	0.3	ppm	Cd			0.6	0.6
Geolabs	ICP-AES	3	ppm	Cu	81	56	13	20
Geolabs	XRF	2	ppm	Mo	-2	-2	-2	-2
Geolabs	ICP-AES	3	ppm	Ni	21	20	18	27
Geolabs	XRF	5	ppm	Pb	17	25	8	18
Geolabs	ICP-AES	2	ppm	Zn	79	46	34	31
Geolabs	ICP-AES	0.1	ppm	Be	1.58	1.66	1.62	1.72
Geolabs	ICP-AES	0.7	ppm	Sr	1128.1	467.6	575.9	478.2
Geolabs	ICP-AES	0.6	ppm	V	171.2	135.1	69.3	58.1
Geolabs	XRF	1	ppm	As	575	225	1798	42
Geolabs	ICP-AES	0.8	ppm	Ba	1807.3	912.4	1934.3	1491.6
Geolabs	ICP-AES	1	ppm	Co	21	18	12	13
Geolabs	XRF	4	ppm	Cr	112	105	66	117
Geolabs	ICP-MS	0.05	ppm	Rb	213.209	182.087	172.732	167.048
Geolabs	MS-AHT	0.02	ppm	Sb	4.31	3.41	3.23	2.53
Geolabs	ICP-AES	0.3	ppm	Sc	15.4	11.3	5.4	5.5
Geolabs	ICP-AES	2	ppm	W	31	349.3	-2	-2
Geolabs	IRC	0.01	%	S	1.39	3.09	1.02	2.84
Geolabs	IRC	0.03	%	CO2	8.51	2.1	4.25	3.53
Actlabs	H. ICP-MS	0.1	ppm	Ge	-0.1	-0.1	-0.1	-0.1
Actlabs	H. ICP-MS	0.1	ppm	Se	1.2	2	0.7	3.1
Actlabs	H. ICP-MS	0.1	ppm	Te	0.9	2.9	1.3	5.1
Actlabs	H. ICP-MS	0.1	ppm	Bi	-0.1	0.3	-0.1	1
Geolabs	MS-IAT	2	ppb	Pd	-1	-1		
Geolabs	MS-IAT	1	ppb	Pt	1.65	4.56		

[1] Analyses carried out by ICP-OES at Actlabs.

Table A.5. Analytical results for selected samples from mineralized zones other than Upper Canada Mine: major and selected trace elements. (Major element data for samples from Upper Canada Mine are listed in Table A.1.)

Laboratory	Actlabs	Actlabs	Actlabs	Actlabs	Actlabs	Actlabs	Actlabs	Actlabs	Actlabs	Actlabs	Actlabs		Actlabs	Actlabs	Actlabs	Actlabs	Actlabs
Method	XRF	XRF	XRF	XRF	XRF	XRF	XRF	XRF	XRF	XRF	XRF		XRF	XRF	XRF	XRF	XRF
det. limit	0.01	0.01	0.01	0.01	0.01	0.01	0.01	0.01	0.01	0.01	0.01		2	5	5	5	4
units	%	%	%	%	%	%	%	%	%	%	%		ppm	ppm	ppm	ppm	ppm
Sample name (mineralized zone)	Al_2O_3	CaO	Fe_2O_3	K_2O	MgO	MnO	Na_2O	P_2O_5	SiO_2	TiO_2	LOI	Total	Y	Zr	V	Cr	Ni
AN02-20-69315 (Anoki South)	14.15	3.98	10.05	4.7	0.88	0.126	0.2	0.11	56.55	0.7	8.70	100.14	21	96	236	422	80
AN03-49-57174 (40 East)	13.3	4.13	4.72	4.16	2.61	0.108	3.46	0.22	59.89	0.4	7.52	100.52	14	119	124	102	14
AN03-49-57178 (40 East)	13.67	4.41	4.62	4.25	2.65	0.112	4.27	0.25	57.57	0.41	7.78	99.99	17	124	116	120	11
AN03-61-86348 (Anoki Main)	13.18	5.15	14.38	0.41	2.89	0.18	6.8	0.47	43.93	1.07	11.78	100.24	27	124	100	21	6
AN03-61-86350 (Anoki Main)	12.61	6.3	12.41	0.89	2.5	0.172	6.29	0.42	45.99	1.06	11.78	100.43	24	116	98	-8	-4
AN03-61-86358 (Anoki Main)	12.87	4.75	14.2	0.77	2.41	0.185	6.59	0.31	44.79	1.26	12.06	100.19	23	116	107	-8	-4
MB96-12-47878 (McBean)	13.9	3.27	5.76	1.91	4.38	0.077	5.39	0.43	55.33	0.53	9.45	100.43	24	189	149	196	78
MB96-12-47879 (McBean)	14.56	2.58	5.4	1.68	2.79	0.062	6.25	0.5	58.38	0.56	7.27	100.03	28	215	134	43	38
MB96-12-42907 (McBean)	11.32	6.29	7.85	1.37	9.05	0.132	4.82	0.71	42.1	0.68	16.05	100.37	22	154	167	469	135
MB96-12-42915 (McBean)	7.78	4.13	8.05	2.09	14.94	0.125	1.52	0.13	39.07	0.38	21.61	99.82	13	53	150	1556	821
004VOI1522-1 (Kirkland Lake Narrows Break)	12.45	1.21	8.1	3.36	1.1	0.028	4.29	0.08	63.36	0.67	5.66	100.31	14	147	550	281	53

Table A.6. Brief descriptions of geochemical samples from mineralized zones.

Deposit/ mineralized zone	Township	Sample ID	Sample type	Station/drill hole/stope	Depth from (ft)	Depth to (ft)	utm_nad83_E	utm_nad83_N	Description of material sampled
Anoki South	Gauthier	AN02-20-69314	drill core	AN02-20	1167	1169	586707.01	5330762.29	altered exhalite, some quartz veining
Anoki South	Gauthier	AN02-20-69315	drill core	AN02-20	1169	1171.1	586707.01	5330762.29	variably altered interflow sedimentary rocks, one quartz veinlet
Anoki South	Gauthier	AN02-21-69664	drill core	AN02-21	1335	1337.3	586689.97	5330703.87	interflow sedimentary rocks, rare quartz veinlets
Anoki South	Gauthier	AN02-21-69666	drill core	AN02-21	1339	1342	586689.97	5330703.87	interflow sedimentary rocks, rare quartz veinlets
Anoki South	Gauthier	AN02-21-69667	drill core	AN02-21	1342	1344.9	586689.97	5330703.87	interflow sedimentary rocks, quartz veinlets, bulk silicification, disseminated pyrite
Anoki South	Gauthier	AN02-21-69674	drill core	AN02-21	1358.1	1360	586689.97	5330703.87	cherty interflow exhalite, pyrite, some quartz veinlets
40 East	Gauthier	AN03-49-57174	drill core	AN03-49	1012	1015	586344	5331277	carbonatized sparsely feldspar-phyric (to aphyric) dike (?), carbonate-quartz veinlets, disseminated pyrite
40 East	Gauthier	AN03-49-57176	drill core	AN03-49	1018	1021	586344	5331277	carbonatized sparsely feldspar-phyric (to aphyric) dike (?), carbonate-quartz veinlets, disseminated pyrite
40 East	Gauthier	AN03-49-57177	drill core	AN03-49	1021	1024	586344	5331277	carbonatized sparsely feldspar-phyric (to aphyric) dike (?), carbonate-quartz veinlets, disseminated pyrite
40East	Gauthier	AN03-49-57178	drill core	AN03-49	1024	1027	586344	5331277	carbonatized sparsely feldspar-phyric (to aphyric) dike (?), carbonate-quartz veinlets, disseminated pyrite
40East	Gauthier	AN03-49-57180	drill core	AN03-49	1030	1032	586344	5331277	carbonatized sparsely feldspar-phyric (to aphyric) dike (?), carbonate-quartz veinlets, disseminated pyrite
Anoki_Main	Gauthier	AN03-61-86348	drill core	AN03-61	273.4	275.7	586700	5331177	quartz-albite-carbonate-pyrite altered basalt, minor or no quartz veining
Anoki_Main	Gauthier	AN03-61-86350	drill core	AN03-61	277.5	279.2	586700	5331177	quartz-albite-carbonate-pyrite altered basalt, minor or no quartz veining
Anoki_Main	Gauthier	AN03-61-86356	drill core	AN03-61	291	293	586700	5331177	quartz-albite-carbonate-pyrite altered basalt, minor or no quartz veining
Anoki_Main	Gauthier	AN03-61-86358	drill core	AN03-61	296	299.1	586700	5331177	quartz-albite-carbonate-pyrite altered basalt, minor or no quartz veining
McBean	Gauthier	MB96-12-42878	drill core	MB96-12	1457.1	1460	587871	5330741	aphyric dike (felsite-type), silicified, pyritized, with quartz veinlets
McBean	Gauthier	MB96-12-42879	drill core	MB96-12	1460	1463	587871	5330741	aphyric dike (felsite-type), silicified, pyritized, with quartz veinlets
McBean	Gauthier	MB96-12-42880	drill core	MB96-12	1463	1464.9	587871	5330741	aphyric dike (felsite-type), silicified, pyritized, with quartz veinlets
McBean	Gauthier	MB96-12-42907	drill core	MB96-12	1536	1537.9	587871	5330741	aphyric dike (?), strongly carbonatized, with disseminated pyrite
McBean	Gauthier	MB96-12-42910	drill core	MB96-12	1542.5	1545	587871	5330741	"green carbonate": quartz veinlets and lenses in carb-fuchsite altered ultramafic rock
McBean	Gauthier	MB96-12-42915	drill core	MB96-12	1557	1558.9	587871	5330741	"green carbonate": quartz veinlets and lenses in carb-fuchsite altered ultramafic rock

Table A.6. (cont'd)

Deposit/ mineralized zone	Township	Sample ID	Sample type	Station/drill hole/stope	Depth from (ft)	Depth to (ft)	utm_nad83_E	utm_nad83_N	Description of material sampled
KL Narrows Break	Teck	004VOI1520-1	surface	004VOI1520			569871	5333226	carbonate-quartz veinlets in coarse sandstone
KL Narrows Break	Teck	004VOI1522-1	surface	004VOI1522			569877	5333231	carbonate-quartz veinlets in coarse sandstone
KL Narrows Break	Teck	004VOI1523-1	surface	004VOI1523			569882	5333238	carbonate-quartz veinlets in augite syenite
Kirkland Lake (Macassa)	Teck	3829	underground	stope 3829					quartz vein associated with '04 Break (full vein width, approx. 10-15 cm)
Kirkland Lake (Macassa)	Teck	3829-2	underground	stope 3829					'04 Break mineralization; veinlet (0.5-1 cm thick) swarm, in silicified and pyritized augite syenite
Kirkland Lake (Macassa)	Teck	3829D	underground	stope 3829					'04 Break mineralization, vein fragment; dark quartz, molybdenite slips
Kirkland Lake (Macassa)	Teck	4206	underground	stope 4206					Moderately (approx. 30°) south-dipping hanging wall vein; full vein width (approx. 30 cm); white, grey and dark grey quartz (4206-S3 vein)
Kirkland Lake (Macassa)	Teck	4229-5Q	underground	stope 4229-5					South dipping (approx. 55-60°) vein in proximal hanging wall of the '04 Break; full vein width (approx. 10 cm; stope 4229, sublevel 5)
Kirkland Lake (Macassa)	Teck	4506	underground	stope 4506					Shallowly (0-20°) south-dipping hanging wall vein; full vein width (approx. 15 cm), quartz and fragments of mafic syenite (approx. 2/3 proportion)
Kirkland Lake (Macassa)	Teck	4528	underground	stope 4528					North-dipping (approx. 60°) vein, hanging wall of the '04 Break; full vein width (approx. 30 cm)
Kirkland Lake (Macassa)	Teck	4744	underground	stope 4744					Shallowly (approx. 20-25°) south dipping hanging wall vein; full vein width (approx. 15 cm), minor mafic syenite material
Kirkland Lake (Macassa)	Teck	4940-1	underground	stope 4940					'04 Break mineralization; full vein width (25-30 cm), largely white quartz, some dark quartz in the axial part
Kirkland Lake (Macassa)	Teck	4940-3	underground	stope 4940					'04 Break mineralization; irregular vein of dark quartz with diffuse contacts; vein fragment: dark fine-grained quartz
Kirkland Lake (Macassa)	Teck	4512-2	underground	stope 4512					South dipping (approx. 45°) hanging wall vein; full vein width (approx. 5-7 cm); mainly white quartz, minor host rock (tuff) material
Kirkland Lake (Teck Hughes)	Teck	1254-1	surface	004VOI1254			570493	5333201	vein fragment, Teck Hughes #1 vein, typical breccia vein: angular porphyry clasts (up to 20%) cemented by white quartz
Kirkland Lake (Teck Hughes)	Teck	1254-2	surface	004VOI1254			570493	5333201	vein fragment; Teck Hughes #1 vein, dark cataclasized quartz

Table A.6. (cont'd)

Deposit/ mineralized zone	Township	Sample ID	Sample type	Station/drill hole/stope	Depth from (ft)	Depth to (ft)	utm_nad83_E	utm_nad83_N	Description of material sampled
Kirkland Lake (Lake Shore)	Teck	LS	surface	004VOI1532			571031	5333353	Lake Shore crown pillar: vein along the Main Break; full vein width (approx. 15-20 cm); fractured quartz with sericitic bands, some host rock fragments, sericitization and molybdenite films in selvages
Upper Canada L zone	Gauthier	3-3	surface	"L" stripping			586435.34	5332391.13	quartz-sericite-carbonate-(+pyrite)-altered tuff
Upper Canada L zone	Gauthier	7-1	surface	"L" stripping			586419.24	5332384.05	quartz-carbonate-sericite schist with pyrite
Upper Canada L zone	Gauthier	7-2	surface	"L" stripping			586418.86	5332384.99	quartz-sericite-carbonate-(+pyrite)-altered tuff
Upper Canada L zone	Gauthier	7-3	surface	"L" stripping			586418.14	5332387.15	quartz-sericite-carbonate-(+pyrite)-altered tuff
Upper Canada L zone	Gauthier	8-1	surface	"L" stripping			586412.12	5332388.29	quartz-carbonate-sericite-(+pyrite)-altered tuff outside mineralized zone
Upper Canada L zone	Gauthier	9-1	surface	"L" stripping			586412.09	5332382.72	quartz-sericite-(+pyrite)-altered tuff
Upper Canada L zone	Gauthier	10-1	surface	"L" stripping			586409.93	5332380.21	quartz-carbonate-sericite schist with pyrite
Upper Canada L zone	Gauthier	11-1	surface	"L" stripping			586407.45	5332380.21	quartz-carbonate-sericite schist with pyrite
Upper Canada L zone	Gauthier	12-1	surface	"L" stripping			586404.94	5332379.84	quartz-carbonate-sericite schist with pyrite
Upper Canada L zone	Gauthier	13-1	surface	"L" stripping			586400.39	5332380.15	quartz-sericite-carbonate-(+pyrite)-altered tuff
Upper Canada	Gauthier	003VOI0526-1	surface	003VOI0526			586276.1	5332274.83	altered syenite-porphyry outside mineralized zone
Upper Canada	Gauthier	L4-2	surface	"L4" stripping			586383.48	5332344.94	quartz-carbonate-sericite-(+pyrite)-altered tuff outside mineralized zone

Metric Conversion Table

Conversion from SI to Imperial			Conversion from Imperial to SI		
SI Unit	*Multiplied by*	*Gives*	*Imperial Unit*	*Multiplied by*	*Gives*
			LENGTH		
1 mm	0.039 37	inches	1 inch	**25.4**	mm
1 cm	0.393 70	inches	1 inch	**2.54**	cm
1 m	3.280 84	feet	1 foot	**0.304 8**	m
1 m	0.049 709	chains	1 chain	20.116 8	m
1 km	0.621 371	miles (statute)	1 mile (statute)	**1.609 344**	km
			AREA		
1 cm^2	0.155 0	square inches	1 square inch	**6.451 6**	cm^2
1 m^2	10.763 9	square feet	1 square foot	**0.092 903 04**	m^2
1 km^2	0.386 10	square miles	1 square mile	2.589 988	km^2
1 ha	2.471 054	acres	1 acre	0.404 685 6	ha
			VOLUME		
1 cm^3	0.061 023	cubic inches	1 cubic inch	**16.387 064**	cm^3
1 m^3	35.314 7	cubic feet	1 cubic foot	0.028 316 85	m^3
1 m^3	1.307 951	cubic yards	1 cubic yard	0.764 554 86	m^3
			CAPACITY		
1 L	1.759 755	pints	1 pint	0.568 261	L
1 L	0.879 877	quarts	1 quart	1.136 522	L
1 L	0.219 969	gallons	1 gallon	**4.546 090**	L
			MASS		
1 g	0.035 273 962	ounces (avdp)	1 ounce (avdp)	28.349 523	g
1 g	0.032 150 747	ounces (troy)	1 ounce (troy)	**31.103 476 8**	g
1 kg	2.204 622 6	pounds (avdp)	1 pound (avdp)	**0.453 592 37**	kg
1 kg	0.001 102 3	tons (short)	1 ton (short)	**907.184 74**	kg
1 t	1.102 311 3	tons (short)	1 ton (short)	**0.907 184 74**	t
1 kg	0.000 984 21	tons (long)	1 ton (long)	**1016.046 908 8**	kg
1 t	0.984 206 5	tons (long)	1 ton (long)	**1.016 046 90**	t
			CONCENTRATION		
1 g/t	0.029 166 6	ounce (troy)/ ton (short)	1 ounce (troy)/ ton (short)	34.285 714 2	g/t
1 g/t	0.583 333 33	pennyweights/ ton (short)	1 pennyweight/ ton (short)	1.714 285 7	g/t

OTHER USEFUL CONVERSION FACTORS

	Multiplied by	
1 ounce (troy) per ton (short)	31.103 477	grams per ton (short)
1 gram per ton (short)	0.032 151	ounces (troy) per ton (short)
1 ounce (troy) per ton (short)	20.0	pennyweights per ton (short)
1 pennyweight per ton (short)	0.05	ounces (troy) per ton (short)

Note: Conversion factors which are in bold type are exact. The conversion factors have been taken from or have been derived from factors given in the Metric Practice Guide for the Canadian Mining and Metallurgical Industries, published by the Mining Association of Canada in co-operation with the Coal Association of Canada.

ISSN 0826-9580
ISBN 0-7794-7792-8